



**Synthesis and Study on Cyclooxygenases Inhibitory Activity of
N-Phenylbenzohydrazide Derivatives**

Watcharin Diloknawarit

**A Thesis Submitted in Partial Fulfillment of the Requirements for the Degree of
Master of Pharmacy in Pharmaceutical Sciences
Prince of Songkla University**

2010

Copyright of Prince of Songkla University

Thesis Title Synthesis and study on cyclooxygenases inhibitory activity of *N*-phenylbenzohydrazide derivatives

Author Miss Watcharin Diloknawarit

Major Program Pharmaceutical Sciences

Major Advisor:

.....
(Asst. Prof. Dr. Chalermkiat Songkram)

Examining Committee:

.....Chairperson
(Assoc. Prof. Dr. Wantana Reanmongkol)

.....
(Asst. Prof. Dr. Chamnan Patarapanich)

.....
(Asst. Prof. Dr. Chalermkiat Songkram)

.....
(Dr. Luelak Lomlim)

The Graduate School, Prince of Songkla University, has approved this thesis as partial fulfillment of the requirements for the Degree of Master of Pharmacy in Pharmaceutical Sciences

.....
(Assoc. Prof. Dr. Krerckchai Thongnoo)

Dean of Graduate School

ชื่อวิทยานิพนธ์ การสังเคราะห์และศึกษาฤทธิ์ยับยั้งเอนไซม์ไซโคลออกซีจีเนสของอนุพันธ์เอน-ฟิ
นิลเบนโซโซไดราไซด์
ผู้เขียน นางสาววัชรินทร์ คิลกนวฤทธิ
สาขาวิชา เกษศาสตร์
ปีการศึกษา 2552

บทคัดย่อ

สารยับยั้งต่อ COX-2 อย่างเลือกจำเพาะเป็นยาต้านการอักเสบที่ไม่ใช่สเตียรอยด์ที่มีพิษต่ำต่อระบบทางเดินอาหาร และจากการยกเลิกการใช้สารกลุ่มนี้บ้างตัวอันเนื่องจากอาการอันไม่พึงประสงค์ต่อระบบหัวใจและหลอดเลือดเมื่อไม่นานมานี้ จึงทำให้มีความจำเป็นในการพัฒนาสารยับยั้งต่อ COX-2 อย่างเลือกจำเพาะที่มีความปลอดภัยที่สูงขึ้น การศึกษาครั้งนี้ผู้วิจัยทำการออกแบบและสังเคราะห์อนุพันธ์เอน-ฟิซิลเบนโซโซไดราไซด์ที่มีส่วนของโครงสร้างเป็นหมู่เมทิลซัลโฟนิลซึ่งเป็นฟาร์มาโคฟอร์ของสารที่มีฤทธิ์ต่อ COX-2 บนตำแหน่งพาราของวงแหวนฟิซิล และมีพันธะเอไมด์ชนิดที่ไม่เป็นวงแหวนมาแทนที่โครงสร้างส่วนวงแหวนกลางของ celecoxib เพื่อนำมาประเมินฤทธิ์ในการยับยั้ง COX สารกลุ่มเอน-ฟิซิลเบนโซโซไดราไซด์จำนวน 12 ชนิด (16-21 และ 27-32) ถูกสังเคราะห์ขึ้นโดยมีร้อยละของการเกิดผลิตภัณฑ์ในช่วงที่ยอมรับได้ (43-99%) คุณสมบัติทางกายภาพและสเปกโทรสโคปิกให้ผลที่สอดคล้องกับโครงสร้างที่ทำการออกแบบไว้ โครงรูปของโมเลกุลในสามมิติของสารกลุ่มเอน-ฟิซิลเบนโซโซไดราไซด์ในสถานะของเหลวและของแข็งถูกทดสอบด้วยเทคนิคโปรตอนนิวเคลียร์แมกเนติกเรโซแนนซ์และเอกซเรย์คริสตัลโลกราฟี จากผลการทดลองพบว่าสาร 16, 27 และ 30 ในสถานะของเหลวมีโครงสร้างของโมเลกุลในสามมิติที่พันธะเอไมด์ชนิดตติยภูมิเป็นแบบซิส ในทางตรงกันข้ามสารประกอบ 16, 19, 27, 29 และ 31 มีโครงสร้างของโมเลกุลในสามมิติเป็นแบบทรานส์ในสถานะของแข็ง ฤทธิ์ในการยับยั้ง COX ของสาร 16-21 และ 27-32 (100 μ M) ให้ฤทธิ์ในการยับยั้ง COX-2 ที่ต่ำถึงปานกลาง (9.5-26.3 %) ซึ่งมีค่าครรชนีความเลือกจำเพาะที่สูงกว่า (1.6-77.9) 10 μ M indomethacin (1.0) ที่เป็นยาอ้างอิง เอน-เบนโซอิล-4-ฟลูออโร-เอน-(4-(เมทิลซัลโฟนิล)ฟิซิล)เบนโซโซไดราไซด์ (32) ให้ฤทธิ์ในการยับยั้ง COX-2 สูงที่สุด (26.3 %) ค่าครรชนีความเลือกจำเพาะที่สูงนี้แสดงให้เห็นว่าส่วนของพารา-เมทิลซัลโฟนิลเอริลจำเป็นสำหรับการยับยั้งต่อ COX-2 การค้นพบนี้แสดงให้เห็นว่าแบบโครงสร้างใหม่ของเอน-ฟิซิลเบนโซโซไดราไซด์อาจถูกพัฒนาต่อเพื่อให้ได้เป็นสารยับยั้งต่อ COX-2

อย่างเลือกจำเพาะตัวใหม่ได้ถึงแม้ว่าความสัมพันธ์ระหว่างโครงสร้างและการออกฤทธิ์ของสารยัง
ไม่มีความชัดเจนและยังต้องการการศึกษาเพิ่มเติมต่อไปในอนาคต

Thesis Title: Synthesis and study on cyclooxygenases inhibitory activity of *N*-phenylbenzohydrazide derivatives

Author: Miss Watcharin Diloknawarit

Major Program: Pharmaceutical Sciences

Academic Year: 2009

ABSTRACT

Selective COX-2 inhibitors possess as NSAIDs with fewer GI toxicity and recently withdrawal some selective COX-2 inhibitors due to their adverse cardiovascular events clearly delineates the need to develop selective COX-2 inhibitors with improved safety profiles. In this investigation, we designed, synthesized and evaluated of COX inhibitory activity of *N*-phenylbenzohydrazide derivatives containing a COX-2 methylsulfonyl pharmacophore at the *para*-position of phenyl ring and possess acyclic amide bond, in place of the central ring template present in celecoxib. Twelve *N*-phenylbenzohydrazides (**16-21** and **27-32**) were able to synthesize in acceptable yields (43-99%). The physical and spectroscopic properties were in accordance with assumed structures. The conformation of *N*-phenylbenzohydrazides in solution state and solid state were examined by ¹H-NMR and X-ray crystallography technique, respectively. The results showed compound **16**, **27** and **30** were existed predominantly in *cis*-conformation at tertiary amide in solution state. In contrary, compound **16**, **19**, **27**, **29** and **31** were existed in *trans*-conformation in solid state. The COX inhibitory results showed compound **16-21** and **27-32** (100 μM) produced a weak to moderate COX-2 inhibition (9.5-26.3 %) with selectivity index values superior (1.6-77.9) to reference drug, 10 μM indomethacin (1.0). *N*-benzoyl-4-fluoro-*N*-(4-(methylsulfonyl)phenyl)benzohydrazide (**32**) gave the highest COX-2 inhibitory activity (26.3%). The higher selectivity index values suggested that the presence of *para*-methylsulfonylaryl moiety is obligatory for COX-2 selectivity. This finding suggested the novel structural motif of *N*-phenylbenzohydrazides might be further developed to be novel selective COX-2 inhibitors even if their SARs are still not explicit and require the further study.

ACKNOWLEDGEMENTS

The completion of this thesis would be quite impossible without the help of many people, whom I would think.

I would like to express my gratitude to my advisor, Assist. Prof. Dr. Chalermkiat Songkram, for his valuable advice and suggestions throughout the course of this work.

I would also like to thank:

The examination committee members of this thesis for their valuable time, Assoc. Prof. Dr. Aya Tanatani, Department of Chemistry, Faculty of Science, Ochanomizu University, Tokyo, Japan, for her helps and encourage during my research in Japan, Professor Dr. Hiroyuki Kegechika, Assist. Prof. Dr. Tomoya Hirano, Dr. Shinya Fujii, and Dr. Syuichi Mori, School of Biomedical Science, Institute of Biomedical and Bioengineering, Tokyo Medical and Dental University, Tokyo, Japan, for their help, valuable technical advice and also their encourage,

Assoc. Prof. Dr. Isao Azumaya, Faculty of Pharmaceutical Sciences at Kagawa Campus, Tokushima Bunri University, Kagawa, Japan, for his valuable time and kind support in X-ray Crystallography experiment,

Academic Excellence Enhancing Program in Pharmaceutical Sciences, Molecular Pharmaceutics Research Unit and Graduate School of Prince of Songkla University for some of financial support in this research,

All staffs of the Department of Pharmaceutical Chemistry and Central Laboratory Unit, for their help in some technical aspects of this thesis,

My parents, my sisters and my brother for their love and understanding, encouragement and supports,

And finally, for my seniors, colleagues and friends who helped me in innumerable ways during these years.

Watcharin Diloknawarit

CONTENTS

	Page
ABSTRACT (in Thai)	iii
ABSTRACT (in English)	v
ACKNOWLEDGEMENTS	vi
CONTENTS	vii
LIST OF TABLES	ix
LIST OF FIGURES	xii
LIST OF ABBREVIATIONS AND SYMBOLS	xx
CHAPTER 1 INTRODUCTION	1
1.1 Background and Rationale	1
1.1.1 Biosynthesis of prostaglandins and prostanoid substances	1
1.1.2 Cyclooxygenase (COX); target of NSAIDs	5
1.1.3 Non-steroidal anti-inflammatory drugs (NSAIDs)	11
1.1.3.1 Mechanism of action	11
1.1.3.2 Classification of NSAIDs	11
1.1.3.2.1 Classical NSAIDs or Non-selective COX inhibitors	12
1.1.3.2.2 Selective COX-2 inhibitors	14
1.1.3.3 NSAIDs in therapeutics	17
1.2 Review of Literature	20
1.3 Objectives of the thesis	25
CHAPTER 2 EXPERIMENT	26
2.1 Materials and Equipments	26
2.1.1 Material and equipments in synthesis and characterization	26
2.1.2 Materials and equipments in determination of biological activity	28

CONTENTS

	Page
2.2 Method	29
2.2.1 Synthesis and characterization	29
2.2.1.1 Synthesis of <i>N</i> '-acyl- <i>N</i> -(4-substituted phenyl)- 4-(methylsulfonyl)benzohydrazides (16-21)	30
2.2.1.2 Synthesis of <i>N</i> '-Acyl-4-substituted- <i>N</i> - [4-(methylsulfonyl)phenyl]benzohydrazides (27-32)	49
2.2.2 Determination of molecular orientation	62
2.2.3.1 ¹ H-NMR	62
2.2.3.2 X-ray crystallography	62
2.2.3 The evaluation of biological activities	63
CHAPTER 3 RESULTS AND DISCUSSIONS	67
3.1 Synthesis and structure characterization	67
3.1.1 Synthesis of <i>N</i> '-acyl- <i>N</i> -(4-substituted phenyl)- 4-(methylsulfonyl)benzohydrazides (16-21)	67
3.1.2 Synthesis of <i>N</i> '-Acyl-4-substituted- <i>N</i> - [4-(methylsulfonyl)phenyl]benzohydrazides (27-32)	95
3.2 Determination in molecular orientation	117
3.2.1 ¹ H-NMR spectra studies	120
3.2.2 X-ray crystallography studies	128
3.3 Determination of biological activities	136
CHAPTER 4 CONCLUSION	143
REFERENCES	146
APPENDIX	152
VITAE	206

LIST OF TABLES

Table		Page
Table 1	Biologic Activities Associated with the Eicosanoids	4
Table 2	Comparisons of COX-1 and COX-2	9
Table 3	Non-selective COX inhibitors classify on the basis of their basic chemical structures and the examples for each category	12
Table 4	COX inhibitory of <i>N</i> -substituted benzanilides (IX , X and XI) compare quantitative of generated PGE ₂ from knockout cell lines COX-1 and COX-2 using radioimmunoassay	24
Table 5	The lists of chemicals and solvents used in synthesis and characterization	27
Table 6	Physical characteristics and melting point of 4-9	70
Table 7	The comparison of IR (KBr) data of 4-9	71
Table 8	The comparison of ¹ H-NMR (500MHz, DMSO- <i>d</i> ₆) data of 4-6	73
Table 9	The comparison of ¹ H-NMR (500MHz, CDCl ₃) data of 7-9	74
Table 10	The stoichiometric amount of all entities and % yield of 10-15	76
Table 11	Physical characteristics and melting point of 10-15	77
Table 12	The comparison of IR (KBr) data of 10-15	78
Table 13	The comparison of ¹ H-NMR (500MHz) data of 10-12	80
Table 14	The comparison of ¹ H-NMR (500MHz) data of 13-15	81
Table 15	The stoichiometric amount of all entities and % yield of 16-21	83
Table 16	Physical characteristics and melting point of 16-21	84
Table 17	The comparison of IR (KBr) data of 16-21	85
Table 18	The comparison of ¹ H-NMR (400MHz) data of 16-18	88
Table 19	The comparison of ¹ H-NMR (400MHz) data of 19-21	89
Table 20	The comparison of ¹³ C-NMR (400MHz) data of 16-18	91
Table 21	The comparison of ¹³ C-NMR (400MHz) data of 19-21	92
Table 22	The high resolution mass spectrometric results of 16-21	93

LIST OF TABLES

Table		Page
Table 23	The elemental analysis data of 16-21	94
Table 24	Physical characteristics and melting point of 22-24	99
Table 25	The comparison of IR (KBr) spectra data of 22-24	100
Table 26	The comparison of ¹ H-NMR (500MHz) data of 22-24	101
Table 27	Physical characteristics and melting point of 25-26	103
Table 28	The comparison of IR (KBr) data of 25-26	104
Table 29	The comparison of ¹ H-NMR (500MHz, DMSO- <i>d</i> ₆) data of 25-26	105
Table 30	The stoichiometric amount of all entities and % yield of 27-32	106
Table 31	Physical characteristics and melting point of 27-32	107
Table 32	The comparison of IR (KBr) data of 27-32	108
Table 33	The comparison of ¹ H-NMR (400MHz, CDCl ₃) data of 27-29	110
Table 34	The comparison of ¹ H-NMR (400MHz, CDCl ₃) data of 30-32	111
Table 35	The comparison of ¹³ C-NMR (400MHz, CDCl ₃) data of 27-29	112
Table 36	The comparison of ¹³ C-NMR (400MHz, CDCl ₃) data of 30-32	113
Table 37	The high resolution mass spectrometric results of 27-32	114
Table 38	The elemental analysis data of 27-32	115
Table 39	Total yield of twelve desired <i>N</i> -phenylbenzohydrazides (16-21 and 27-32)	116
Table 40	¹ H-NMR spectral data of PCB02 and PCB04	122
Table 41	¹ H-NMR spectral data of PCB02, PCB04, 16 and 19	123
Table 42	¹ H-NMR spectral data of PCA02 and PCA04	127
Table 43	¹ H-NMR spectral data of PCA02, PCA04, 27 and 30	127
Table 44	Torsion angle of R-N-C(=O)-R (°), N-C bond length (Å) and sum of three valence angles around N (°) of compound 16 , 19 , 27 , 29 and 31	129
Table 45	Crystal structure data and details of structure refinement for compounds 16 , 19 , 27 , 29 and 31	130

LIST OF TABLES

Table		Page
Table 46	The related intermolecular bonds and its distance (Å) of crystal packing of compounds 16, 19, 27, 29 and 31	132
Table 47	COX inhibitory activity of compounds 16-21 and 27-32 using colorimetric COX (ovine) inhibitory screening assay	139

LIST OF FIGURES

Figure		Page
Figure 1	COX and 5-LOX pathway	3
Figure 2	Role of COX-1 and COX-2	6
Figure 3	Reaction mechanism for COX enzymes. The COX reaction is peroxide-dependent and requires that the heme group at the peroxidase site undergo a two-electron oxidation. A tyrosyl (Tyr) radical is generated from the POX reaction and initiates the COX reaction, which then becomes autocatalytic in the presence of substrate, until radical induced inactivation occurs.	7
Figure 4	Structural representation of the murine COX-2 dimer	8
Figure 5	Solvent accessible surfaces in COX-1 and COX-2	10
Figure 6	The example of non-selective COX inhibitors	14
Figure 7	The example of modified known NSAIDs to improve COX-2 selectivity	15
Figure 8	The example of diaryl- or aryl-heteroaryl-ethers (sulfonanilide inhibitors)	16
Figure 9	The example of vicinal diaryl heterocycles inhibitors	17
Figure 10	Three main structural features of celecoxib	21
Figure 11	Compounds were reported as selective COX-2 inhibitors	22
Figure 12	Conformation of celecoxib analogue, SC-558, in active site of murine COX-2	23
Figure 13	Conformation of benzanilide (<i>cis</i>) and <i>N</i> -methylbenzanilide (<i>trans</i>)	23
Figure 14	Compare structure of <i>N</i> -phenylbenzohydrazides and celecoxib	25
Figure 15	Structure of targeted <i>N</i> -phenylbenzohydrazide derivatives	29
Figure 16	IR spectrum (KBr) of <i>N</i> '-phenylacetohydrazide (4)	153
Figure 17	¹ H-NMR (500MHz, DMSO- <i>d</i> ₆) spectrum of <i>N</i> '-phenylacetohydrazide (4)	153
Figure 18	IR spectrum (KBr) of <i>N</i> '- <i>p</i> -tolylacetohydrazide (5)	154
Figure 19	¹ H-NMR (500MHz, DMSO- <i>d</i> ₆) spectrum of <i>N</i> '- <i>p</i> -tolylacetohydrazide (5)	154
Figure 20	IR spectrum (KBr) of <i>N</i> '-(4-fluorophenyl)acetohydrazide (6)	155

LIST OF FIGURES

Figure		Page
Figure 21	¹ H-NMR (500MHz, DMSO- <i>d</i> ₆) spectrum of <i>N</i> -(4-fluorophenyl)acetohydrazide (6)	155
Figure 22	IR spectrum (KBr) of <i>N</i> -phenylbenzohydrazide (7)	156
Figure 23	¹ H-NMR (500MHz, CDCl ₃) spectrum of <i>N</i> -phenylbenzohydrazide (7)	156
Figure 24	IR spectrum (KBr) of <i>N</i> - <i>p</i> -tolylbenzohydrazide (8)	157
Figure 25	¹ H-NMR (500MHz, CDCl ₃) spectrum of <i>N</i> - <i>p</i> -tolylbenzohydrazide (8)	157
Figure 26	IR spectrum (KBr) of <i>N</i> -(4-fluorophenyl)benzohydrazide (9)	158
Figure 27	¹ H-NMR (500MHz, CDCl ₃) spectrum of <i>N</i> -(4-fluorophenyl)benzohydrazide (9)	158
Figure 28	IR spectrum (KBr) of <i>N</i> -acetyl-4-(methylthio)- <i>N</i> -phenylbenzohydrazide (10)	159
Figure 29	¹ H-NMR (500MHz, CDCl ₃) spectrum of <i>N</i> -acetyl-4-(methylthio)- <i>N</i> -phenylbenzo hydrazide (10)	159
Figure 30	IR spectrum (KBr) of <i>N</i> -acetyl-4-(methylthio)- <i>N</i> - <i>p</i> -tolylbenzohydrazide (11)	160
Figure 31	¹ H-NMR (400MHz, Acetone- <i>d</i> ₆) spectrum of <i>N</i> -acetyl-4-(methylthio)- <i>N</i> - <i>p</i> -tolyl benzohydrazide (11)	160
Figure 32	IR spectrum (KBr) of <i>N</i> -acetyl- <i>N</i> -(4-fluorophenyl)-4-(methylthio)benzohydrazide (12)	161
Figure 33	¹ H-NMR (400MHz, CDCl ₃) spectrum of <i>N</i> -acetyl- <i>N</i> -(4-fluorophenyl)-4-(methylthio) benzohydrazide (12)	161
Figure 34	IR spectrum (KBr) of <i>N</i> -benzoyl-4-(methylthio)- <i>N</i> -phenylbenzohydrazide (13)	162
Figure 35	¹ H-NMR (400MHz, Acetone- <i>d</i> ₆) spectrum of <i>N</i> -benzoyl-4-(methylthio)- <i>N</i> -phenyl benzohydrazide (13)	162
Figure 36	IR spectrum (KBr) of <i>N</i> -benzoyl-4-(methylthio)- <i>N</i> - <i>p</i> -tolylbenzohydrazide (14)	163

LIST OF FIGURES

Figure		Page
Figure 37	¹ H-NMR (400MHz, CDCl ₃) spectrum of <i>N</i> '-benzoyl-4-(methylthio)- <i>N</i> - <i>p</i> -tolylbenzo hydrazide (14)	163
Figure 38	IR spectrum (KBr) of <i>N</i> '-benzoyl- <i>N</i> -(4-fluorophenyl)-4-(methylthio)benzohydrazide (15)	164
Figure 39	¹ H-NMR (400MHz, CDCl ₃) spectrum of <i>N</i> '-benzoyl- <i>N</i> -(4-fluorophenyl)-4-(methyl thio)benzohydrazide (15)	164
Figure 40	IR spectrum (KBr) of <i>N</i> '-acetyl-4-(methylsulfonyl)- <i>N</i> -phenylbenzohydrazide (16)	165
Figure 41	¹ H-NMR (400MHz, DMSO- <i>d</i> ₆ , 90 °C) spectrum of <i>N</i> '-acetyl-4-(methylsulfonyl)- <i>N</i> -phenylbenzohydrazide (16)	182
Figure 42	¹³ C-NMR (400MHz, DMSO- <i>d</i> ₆ , 90 °C) spectrum of <i>N</i> '-acetyl-4-(methylsulfonyl)- <i>N</i> -phenylbenzohydrazide (16)	183
Figure 43	The mass (HR-MS; ESI) spectrum of <i>N</i> '-acetyl-4-(methylsulfonyl)- <i>N</i> -phenylbenzo- hydrazide (16)	165
Figure 44	IR spectrum (KBr) of <i>N</i> '-acetyl-4-(methylsulfonyl)- <i>N</i> - <i>p</i> -tolylbenzohydrazide (17)	166
Figure 45	¹ H-NMR (400MHz, CDCl ₃ , 52 °C) spectrum of <i>N</i> '-acetyl-4-(methylsulfonyl)- <i>N</i> - <i>p</i> -tolylbenzohydrazide (17)	184
Figure 46	¹³ C-NMR (400MHz, CDCl ₃ , 52 °C) spectrum of <i>N</i> '-acetyl-4-(methylsulfonyl)- <i>N</i> - <i>p</i> -tolylbenzohydrazide (17)	185
Figure 47	The mass (HR-MS; ESI) spectrum of <i>N</i> '-acetyl-4-(methylsulfonyl)- <i>N</i> - <i>p</i> -tolylbenzo- hydrazide (17)	166
Figure 48	IR spectrum (KBr) of <i>N</i> '-acetyl- <i>N</i> -(4-fluorophenyl)-4-(methylsulfonyl)benzo- hydrazide (18)	167

LIST OF FIGURES

Figure		Page
Figure 49	¹ H-NMR (400MHz, DMSO- <i>d</i> ₆ , 90 °C) spectrum of <i>N</i> -acetyl- <i>N</i> -(4-fluorophenyl)-4-(methylsulfonyl)benzohydrazide (18)	186
Figure 50	¹³ C-NMR (400MHz, DMSO- <i>d</i> ₆ , 90 °C) spectrum of <i>N</i> -acetyl- <i>N</i> -(4-fluorophenyl)-4-(methylsulfonyl)benzohydrazide (18)	187
Figure 51	The mass (HR-MS; ESI) spectrum of <i>N</i> -acetyl- <i>N</i> -(4-fluorophenyl)-4-(methylsulfonyl)benzohydrazide (18)	167
Figure 52	IR spectrum (KBr) of <i>N</i> -benzoyl-4-(methylsulfonyl)- <i>N</i> -phenylbenzohydrazide (19)	168
Figure 53	¹ H-NMR (400MHz, DMSO- <i>d</i> ₆ , 90 °C) spectrum of <i>N</i> -benzoyl-4-(methylsulfonyl)- <i>N</i> -phenylbenzohydrazide (19)	188
Figure 54	¹³ C-NMR (400MHz, DMSO- <i>d</i> ₆ , 90 °C) spectrum of <i>N</i> -benzoyl-4-(methylsulfonyl)- <i>N</i> -phenylbenzohydrazide (19)	189
Figure 55	The mass (HR-MS; ESI) spectrum of <i>N</i> -benzoyl-4-(methylsulfonyl)- <i>N</i> -phenylbenzohydrazide (19)	168
Figure 56	IR spectrum (KBr) of <i>N</i> -benzoyl-4-(methylsulfonyl)- <i>N</i> - <i>p</i> -tolylbenzohydrazide (20)	169
Figure 57	¹ H-NMR (400MHz, CDCl ₃ , 50 °C) spectrum of <i>N</i> -benzoyl-4-(methylsulfonyl)- <i>N</i> - <i>p</i> -tolylbenzohydrazide (20)	190
Figure 58	¹³ C-NMR (400MHz, CDCl ₃ , 50 °C) spectrum of <i>N</i> -benzoyl-4-(methylsulfonyl)- <i>N</i> - <i>p</i> -tolylbenzohydrazide (20)	191
Figure 59	The mass (HR-MS; ESI) spectrum of <i>N</i> -benzoyl-4-(methylsulfonyl)- <i>N</i> - <i>p</i> -tolylbenzohydrazide (20)	169
Figure 60	IR spectrum (KBr) of <i>N</i> -benzoyl- <i>N</i> -(4-fluorophenyl)-4-(methylsulfonyl)benzohydrazide (21)	170

LIST OF FIGURES

Figure		Page
Figure 61	¹ H-NMR (400MHz, CDCl ₃ , 50 °C) spectrum of <i>N</i> '-benzoyl- <i>N</i> -(4-fluorophenyl)-4-(methylsulfonyl)benzohydrazide (21)	192
Figure 62	¹³ C-NMR (400MHz, CDCl ₃ , 50 °C) spectrum of <i>N</i> '-benzoyl- <i>N</i> -(4-fluorophenyl)-4-(methylsulfonyl)benzohydrazide (21)	193
Figure 63	The mass (HR-MS; ESI) spectrum of <i>N</i> '-benzoyl- <i>N</i> -(4-fluorophenyl)-4-(methylsulfonyl)benzohydrazide (21)	170
Figure 64	IR spectrum (KBr) of 4-bromothioanisole (22)	171
Figure 65	¹ H-NMR (500MHz, CDCl ₃) spectrum of 4-bromothioanisole (22)	171
Figure 66	IR spectrum (KBr) of 4-bromomethylsulfone (23)	172
Figure 67	¹ H-NMR (500MHz, CDCl ₃) spectrum of 4-bromomethylsulfone (23)	172
Figure 68	IR spectrum (KBr) of (4-(methylsulfonyl)phenyl)hydrazine (24)	173
Figure 69	¹ H-NMR(500MHz, DMSO- <i>d</i> ₆)spectrum of (4-(methylsulfonyl)phenyl)hydrazine (24)	173
Figure 70	IR spectrum (KBr) of <i>N</i> '-(4-(methylsulfonyl)phenyl)acetohydrazide (25)	174
Figure 71	¹ H-NMR (500MHz, DMSO- <i>d</i> ₆) spectrum of <i>N</i> '-(4-(methylsulfonyl)phenyl)aceto hydrazide (25)	174
Figure 72	IR spectrum (KBr) of <i>N</i> '-(4-(methylsulfonyl)phenyl)benzohydrazide (26)	175
Figure 73	¹ H-NMR (500MHz, DMSO- <i>d</i> ₆) spectrum of <i>N</i> '-(4-(methylsulfonyl)phenyl)benzohydrazide (26)	175
Figure 74	IR spectrum (KBr) of <i>N</i> '-acetyl- <i>N</i> -(4-(methylsulfonyl)phenyl)benzohydrazide (27)	176
Figure 75	¹ H-NMR (400MHz, CDCl ₃) spectrum of <i>N</i> '-acetyl- <i>N</i> -(4-(methylsulfonyl)phenyl)benzohydrazide (27)	194
Figure 76	¹³ C-NMR (400MHz, CDCl ₃) spectrum of <i>N</i> '-acetyl- <i>N</i> -(4-(methylsulfonyl)phenyl)benzohydrazide (27)	195

LIST OF FIGURES

Figure		Page
Figure 77	The mass (HR-MS; ESI) spectrum of <i>N</i> '-acetyl- <i>N</i> -(4-(methylsulfonyl)phenyl)benzo hydrazide (27)	176
Figure 78	IR spectrum (KBr) of <i>N</i> '-acetyl-4-methyl- <i>N</i> -(4-(methylsulfonyl)phenyl)benzo- hydrazide (28)	177
Figure 79	¹ H-NMR (400MHz, CDCl ₃) spectrum of <i>N</i> '-acetyl-4-methyl- <i>N</i> -(4-(methylsulfonyl)phenyl)benzohydrazide (28)	196
Figure 80	¹³ C-NMR (400MHz, CDCl ₃) spectrum of <i>N</i> '-acetyl-4-methyl- <i>N</i> -(4-(methylsulfonyl)phenyl)benzohydrazide (28)	197
Figure 81	The mass (HR-MS; ESI) spectrum of <i>N</i> '-acetyl-4-methyl- <i>N</i> -(4-(methylsulfonyl) phenyl)benzohydrazide (28)	177
Figure 82	IR spectrum (KBr) of <i>N</i> '-acetyl-4-fluoro- <i>N</i> -(4-(methylsulfonyl)phenyl)benzo- hydrazide (29)	178
Figure 83	¹ H-NMR (400MHz, CDCl ₃) spectrum of <i>N</i> '-acetyl-4-fluoro- <i>N</i> -(4-(methylsulfonyl)phenyl)benzohydrazide (29)	198
Figure 84	¹³ C-NMR (400MHz, CDCl ₃) spectrum of <i>N</i> '-acetyl-4-fluoro- <i>N</i> -(4-(methylsulfonyl)phenyl)benzohydrazide (29)	199
Figure 85	The mass (HR-MS; ESI) spectrum of <i>N</i> '-acetyl-4-fluoro- <i>N</i> -(4-(methylsulfonyl) phenyl)benzohydrazide (29)	178
Figure 86	IR spectrum (KBr) of <i>N</i> '-benzoyl- <i>N</i> -(4-(methylsulfonyl)phenyl)benzohydrazide (30)	179
Figure 87	¹ H-NMR (400MHz, CDCl ₃) spectrum of <i>N</i> '-benzoyl- <i>N</i> -(4-(methylsulfonyl)phenyl)benzohydrazide (30)	200
Figure 88	¹³ C-NMR (400MHz, CDCl ₃) spectrum of <i>N</i> '-benzoyl- <i>N</i> -(4-(methylsulfonyl)phenyl)benzohydrazide (30)	201

LIST OF FIGURES

Figure		Page
Figure 89	The mass (HR-MS; ESI) spectrum of <i>N</i> -benzoyl- <i>N</i> -(4-(methylsulfonyl)phenyl) benzohydrazide (30)	179
Figure 90	IR spectrum (KBr) of <i>N</i> -benzoyl-4-methyl- <i>N</i> -(4-(methylsulfonyl)phenyl)benzo- hydrazide (31)	180
Figure 91	¹ H-NMR (400MHz, CDCl ₃) spectrum of <i>N</i> -benzoyl-4-methyl- <i>N</i> -(4-(methylsulfonyl)phenyl)benzohydrazide (31)	202
Figure 92	¹³ C-NMR (400MHz, CDCl ₃) spectrum of <i>N</i> -benzoyl-4-methyl- <i>N</i> -(4-(methylsulfonyl)phenyl)benzohydrazide (31)	203
Figure 93	The mass (HR-MS; ESI) spectrum of <i>N</i> -benzoyl-4-methyl- <i>N</i> -(4-(methylsulfonyl) phenyl)benzohydrazide (31)	180
Figure 94	IR spectrum (KBr) of <i>N</i> -benzoyl-4-fluoro- <i>N</i> -(4-(methylsulfonyl)phenyl)benzo- hydrazide (32)	181
Figure 95	¹ H-NMR (400MHz, CDCl ₃) spectrum of <i>N</i> -benzoyl-4-fluoro- <i>N</i> -(4-(methylsulfonyl)phenyl)benzohydrazide (32)	204
Figure 96	¹³ C-NMR (400MHz, CDCl ₃) spectrum of <i>N</i> -benzoyl-4-fluoro- <i>N</i> -(4-(methylsulfonyl)phenyl)benzohydrazide (32)	205
Figure 97	The mass (HR-MS; ESI) spectrum of <i>N</i> -benzoyl-4-fluoro- <i>N</i> -(4-(methylsulfonyl) phenyl)benzohydrazide (32)	181
Figure 98	The oxidation of TMPD in colorimetric determination of peroxidase component in COXs	64
Figure 99	The sample plate setting up 96-wells plate	65
Figure 100	The comparison of ¹ H-NMR (400MHz, DMSO- <i>d</i> ₆) spectrum when operated at 30 °C, 50 °C, 70 °C and 90 °C (from below to top) of compound	86

LIST OF FIGURES

Figure		Page
Figure 101	Planar conformation of acetamide based on C-N bond resonance	118
Figure 102	The possibility conformers of synthesized <i>N</i> -phenyl benzohydrazide derivatives (16-21 and 27-32): (c, c), (c, t), (t, c) and (t, t)	118
Figure 103	Conformation of benzanilide (<i>cis</i>) and <i>N</i> -methylbenzanilide (<i>trans</i>)	119
Figure 104	The energy relationships of conformers of acetanilide and <i>N</i> -methylacetanilide	120
Figure 105	¹ H-NMR signals of 19 in aromatic region at 30 °C, 50 °C, 70 °C and 90 °C	121
Figure 106	The temperature dependence of ¹ H-NMR (from 25 °C to -20 °C) signals of 16 in aromatic region and <i>N-H</i> proton region	124
Figure 107	Possible minor conformation of 16 when N-N bond rotated and allowed <i>N-H</i> to locate in anisotropic area of carbonyl of tertiary amide	124
Figure 108	The preference conformer, major and minor conformers of compound 16 at each temperature (25 °C, 0 °C, -10 °C and -20 °C)	125
Figure 109	The ORTEP drawings of compounds 16 , 19 , 27 , 29 and 31	131
Figure 110	A unit cell (left column) and the crystal packings with related intermolecular bonds (right column) of compound 16 , 19 and 27	133
Figure 111	A unit cell (left column) and the crystal packings with related intermolecular bonds (right column) of compound 29 and 31	134
Figure 112	Amide conformational switching by acid of <i>N</i> -(3,5-bis(dimethylamino)phenyl)- <i>N</i> -methylacetamide	135
Figure 113	The conversion of arachidonic acid to PGH ₂	137
Figure 114	The oxidation of TMPD in colorimetric determination of peroxidase component in COX	138
Figure 115	% inhibition to COX-1 and COX-2 of 100 μM 16-21 and 27-32 compare with 10 μM indomethacin (Indo)	140

LIST OF ABBREVIATIONS AND SYMBOLS

δ	Chemical shift
ν_{\max}	maximum wave number
AA	arachidonic acid
AD	Alzheimer's disease
APC	Adenoma Prevention with Celecoxib trial
APPROVe	Adenomatous Polyp Prevention on Vioxx trial
Arg	Arginine
ASA	aspirin
CDCl_3	deuterated chloroform
$^{13}\text{C-NMR}$	^{13}C -Nuclear Magnetic Resonance Spectroscopy
COX	cyclooxygenase
COX-1	cyclooxygenase-1
COX-2	cyclooxygenase-2
<i>d</i>	doublet (for NMR signal)
<i>dd</i>	doublet of doublet (for NMR signal)
DMSO, <i>d</i> ₆	deuterated dimethylsulfoxide
EA	Elemental analyses
EIA	enzyme immunoassay
ESI	Electron Spray Ionization
FDA	Food and Drug Administration
FT-IR	Fourier-Transform Infrared Spectroscopy
GI	gastrointestine
$^1\text{H-NMR}$	^1H -Nuclear Magnetic Resonance Spectroscopy
HR-MS	High-Resolution Mass Spectrometry
Hz	hertz
Ile	isoleucine
Indo	inomehtacin
IR	Infrared Spectroscopy

<i>J</i>	coupling constant
Kb	kilobases
KDa	kilodaltons
5-LOX	5-lipoxygenase
LTs	leukotrienes
mp.	melting point
<i>m/z</i>	mass-over-charge ratio
NSAIDs	Nonsteroidal anti-inflammatory drugs
NSTDA	National Science and Technology Development Agency, Thailand
OTC	over-the-counter
PGD ₂	prostaglandin D ₂
PGE ₂	prostaglandin E ₂
PGF _{2α}	prostaglandin F _{2α}
PGG ₂	prostaglandin G ₂
PGH ₂	prostaglandin H ₂
PGI ₂	prostacyclin
PGs	prostaglandins
PGHS	prostaglandin synthase
POX	peroxidase
<i>s</i>	singlet (for NMR signal)
SAR	Structure Activity Relationships
<i>t</i>	triplet (for NMR signal)
TLC	Thin Layer Chromatography
TMPD	<i>N,N,N',N'</i> -tetramethyl- <i>p</i> -phenylenediamine
Try	tryptophan
TXA ₂	thromboxane A ₂
UV	Ultraviolet
Val	valine

CHAPTER 1

INTRODUCTION

1.1 Background and Rationale

Nonsteroidal anti-inflammatory drugs (NSAIDs) are among the most widely used therapeutics, primarily for the treatment of pain and inflammation, especially arthritis. From a historical viewpoint, the first NSAID with therapeutic benefits was aspirin, which has now been used for more than 100 years. In the 1970s, a scientific breakthrough occurred with the elucidation of the molecular mechanism of aspirin and other NSAIDs. Vane, Samuelson and Bergstrom succeeded in showing that these anti-inflammatory substances block the biosynthesis of prostaglandins (PGs) which contribute to a variety of physiological and pathophysiological functions (Vane and Botting, 1992). According to this discovery, at first, I would like to introduce the biosynthesis of PGs in brief as followed.

1.1.1 Biosynthesis of prostaglandins and prostanoid substances

Initial step in the biosynthesis of prostanoids is the liberation of arachidonic acid (AA) from the phospholipids of the cell membrane catalyzed by phospholipase A₂. The following step is the biotransformation of AA by cyclooxygenase (COX). In a bifunctional action, this first generates the unstable PG endoperoxide in the form of PGG₂ (a side-chain peroxide), the COX reaction itself, which is then immediately converted by reduction into PGH₂ (a side-chain hydroxyl) by the same enzyme in a peroxidase (POX) reaction (Vane and Botting, 1992). As shown in figure 1, PGG₂ and PGH₂ are unstable intermediates that react with other enzymes to form a chemically diverse family of prostanoids. It can be isomerized to the various ketol

derivatives; PGD_2 , PGE_2 , and $\text{PGF}_{2\alpha}$. The endoperoxide is also transformed into the extremely unstable and potent thromboxane A_2 (TXA_2). Another and equally important substance produced from the endoperoxide is prostacyclin (PGI_2), which is converted by prostacyclin synthase. The ultimate derivatives of PGH_2 metabolism are determined by the specific subsequent enzymes that are present in each cell. For example, in platelets nearly all PGH_2 is converted to the vasoconstricting TXA_2 by thromboxane synthase while endothelial cells primarily produce the vasodilatory PGI_2 . In the gastrointestinal tract, most PGs are converted to PGE_2 , $\text{PGF}_{2\alpha}$, and PGI_2 . (Cryer and Dubois, 1998) Moreover, the leukotrienes (LTs), bronchoconstrictors, are metabolites which synthesized through a shift in the metabolic pathway from the COX pathway to the 5-lipoxygenase (5-LOX) pathway (figure 1) (Nogrody and Weaver, 2005).

PGs , TXA_2 , and the LTs are lipids that are collectively called eicosanoids. Over the past twenty years, the eicosanoids have emerged as important molecules around which to target drug design and development. The pharmacological effects of the PGs , TXA_2 and LTs comprise many different activities. The lack of specificity of their activities implies a number of side effects, necessitating the development of selective synthetic compounds (Nogrody and Weaver, 2005). In table 1 summarized the effects of eicosanoids are known.

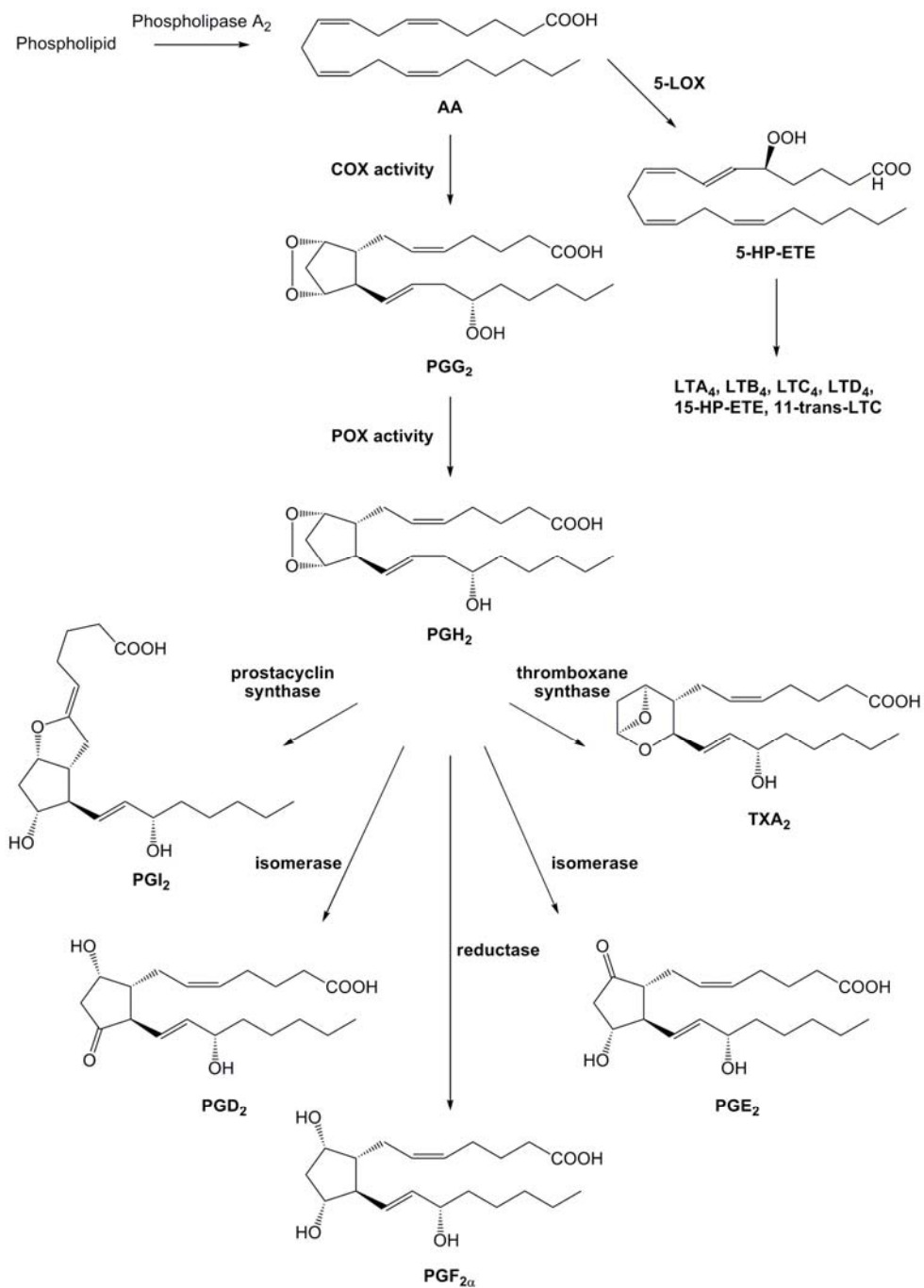


Figure 1. COX and 5-LOX pathway (Donge *et. al*, 2005; Nogrady and Weaver, 2005)

Substance	Observed biologic Activity
PGD ₂	Weak inhibitor of platelet aggregation
PGE ₁	Bronchodilatation Inhibitor of fat breakdown Inhibitor of platelet aggregation Stimulates contraction of gastrointestinal smooth muscle Vasodilation
PGE ₂	Elevates body temperature set-point in anterior hypothalamus Protects stomach lining acid degradation Reduces secretion of stomach acid Renal vasodilatation in kidneys Stimulates uterine smooth-muscle contraction
PGF _{2α}	Stimulates uterine smooth-muscle contraction
PGI ₂	Potent inhibitor of platelet aggregation Potent vasodilator
PGJ ₂	Inhibits cell proliferation Stimulates osteogenesis (bone formation)
TXA ₂	Potent inducer of platelet aggregation Potent vasoconstrictor Stimulates release of serotonin from platelets
LTB ₄	Increases leukocyte chemotaxis and aggregation
LTC/D ₄	Bronchoconstrictive
5- or 12-HPETE	Inhibits platelet aggregation Aggregates leukocytes Promotes leukocyte chemotaxis

Table 1 Biologic Activities Associated with the Eicosanoids (Nograpy and Weaver, 2005)

PGs are involved in numerous homeostatic biological functions. They are generated by COX and their biosynthesis and pharmacological actions are inhibited by clinically relevant NSAIDs. Next, I would like to review the target of NSAIDs, COX.

1.1.2 Cyclooxygenase (COX); target of NSAIDs

Cyclooxygenase (COX) is the key enzyme in the biosynthesis of prostaglandins (PGs) from arachidonic acid (Cryer and Dubois, 1998). There are two identified isoforms, namely cyclooxygenase-1 (COX-1) and cyclooxygenase-2 (COX-2). While both enzymes carry out essentially the same catalytic reaction, they differ in expression, function and structure (Charlier and Michaux, 2003).

With regard to potential therapeutic applications, the critical COX isoform distinctions are differences in their tissue distribution and differences in the regulation of their expression. COX-1 is constitutively expressed in most cells and tissues. Under normal homeostatic conditions it produces PGs that regulate essential physiologic (housekeeping) functions such as gastric mucosal protection, maintenance of normal kidney function, and platelet aggregation (figure 2). Inhibition of COX-1 function is therefore associated with the development of peptic ulcer and interference of renal and platelet functions. In most instances, COX-2 is usually barely detectable during normal physiologic conditions. However, in response to several pro-inflammatory stimuli such as mitogens, cytokines and other growth factors, COX-2 can be rapidly induced to increase PGs production ten-to eighty fold (Cryer and Dubois, 1998). The PGs produced by COX-2 play a major role in inflammatory reactions and are responsible for the characteristic inflammatory symptoms (redness, pain, edema, fever and loss of function) (figure 2). Thus, selective COX-2 inhibitors are clinically useful as anti-inflammatory drugs with less gastrointestinal and renal toxicity. The inducible isozyme has also been implicated in pathological processes such as various cancer types (colorectal, breast cancer) and Alzheimer and Parkinson's diseases. This opens a new spectrum for therapy with COX-2 inhibitors (Patrignani *et al.*, 2005).

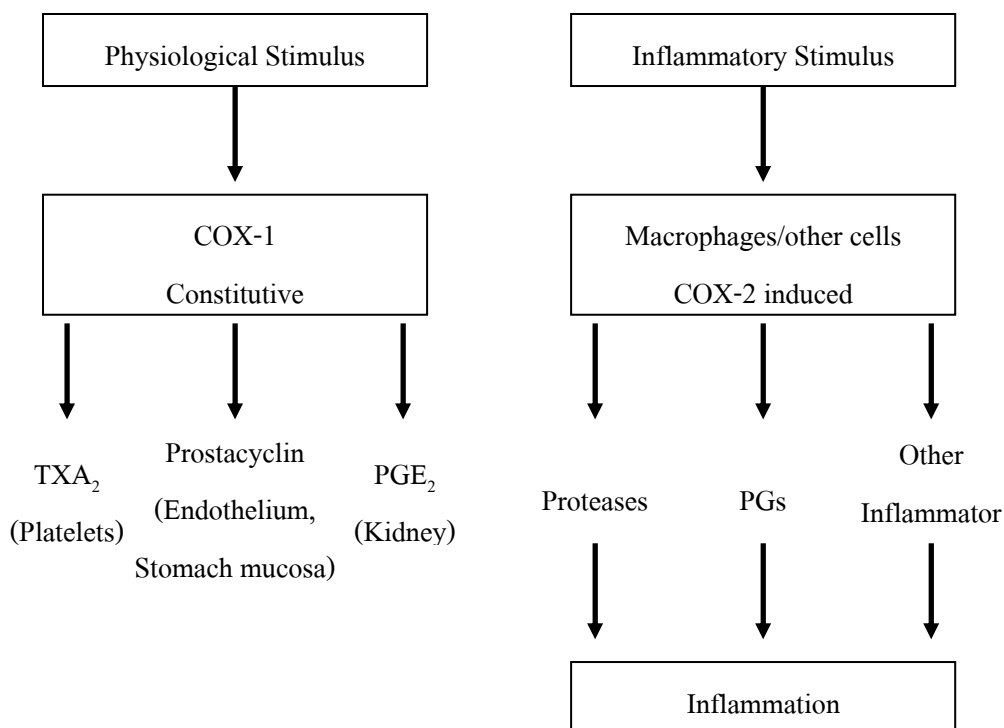


Figure 2. Role of COX-1 and COX-2 (Steinmeyer *et al.*, 2000)

COX-1 and COX-2 are bifunctional enzymes that carry out two sequential reactions in spatially distinct but mechanistically coupled active sites: AA oxygenation occurs in the COX active site, and PGG_2 reduction occurs in the POX active site. The first reaction is catalyzed by COX in the presence of O_2 and heme and the second reaction requires tryptophan (Try), probably as a source of electrons (figure 3). COX-1 and COX-2 are homodimers of 70 kDa subunits and dimerization is required for structural integrity and catalytic activity. There are now many COX crystal structures available, including several with bound inhibitors. These crystal structures prove that each subunit contained a COX and a POX active site, with inhibitor bound only in the COX active site. Each monomer of COX consists of three structural domains: a short *N*-terminal epidermal growth factor domain, a α -helical membrane binding domain, and a large globular C-terminal catalytic domain (figure 4). The COX and POX active sites are located on opposite sides of the catalytic domain with the heme prosthetic group positioned at the base of the POX site (Blobaum and Marnett, 2007).

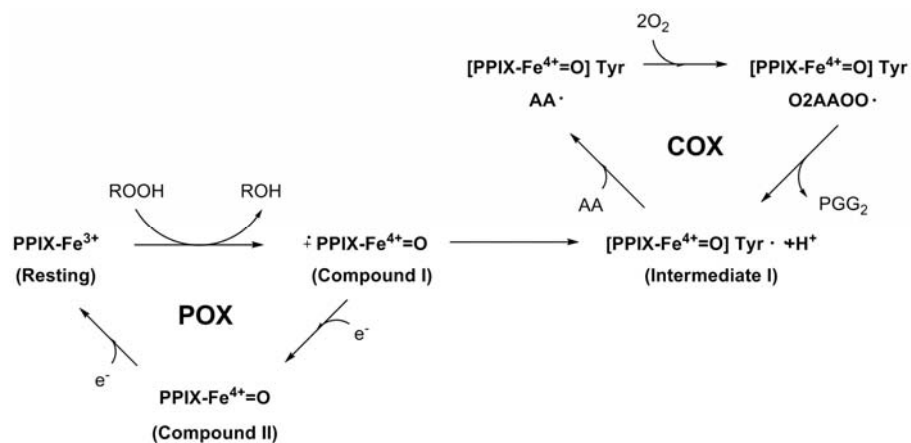


Figure 3 Reaction mechanism for COX enzymes. The COX reaction is peroxide-dependent and requires that the heme group at the peroxidase site undergo a two-electron oxidation. A tyrosyl (Tyr) radical is generated from the POX reaction and initiates the COX reaction, which then becomes autocatalytic in the presence of substrate, until radical induced inactivation occurs. (Blobaum and Marnett, 2007)

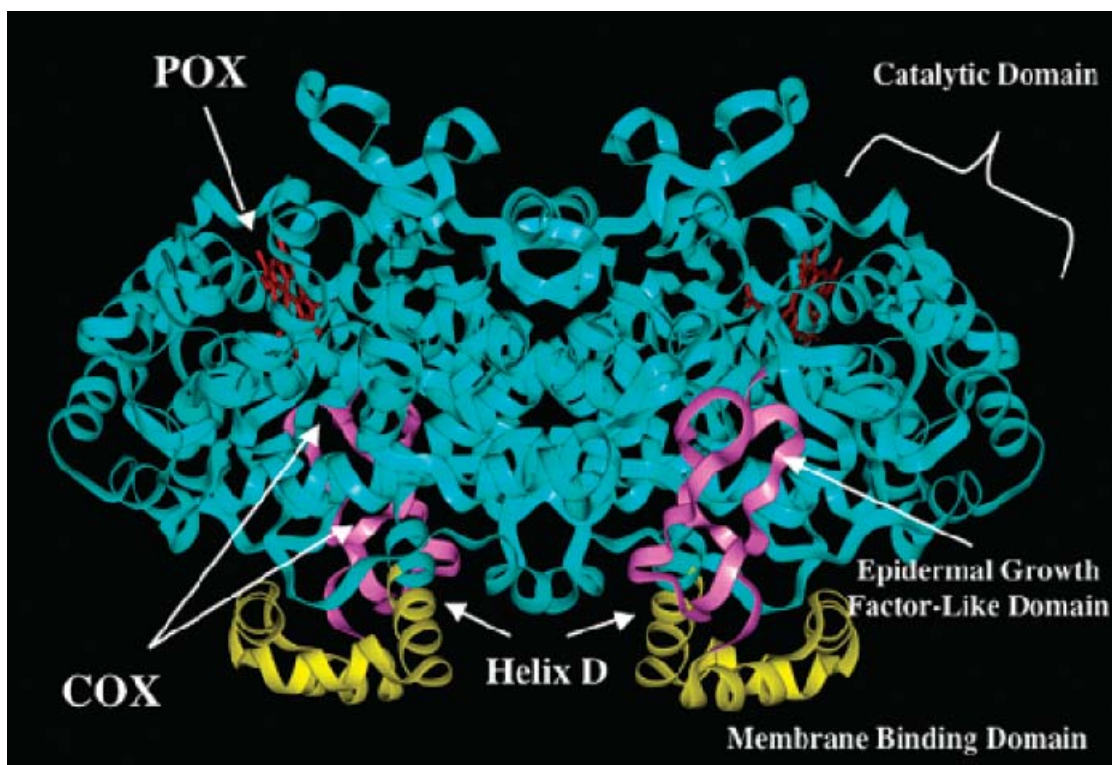


Figure 4 Structural representation of the murine COX-2 dimer. The *N*-terminal epidermal growth factor domain is designated in pink and leads into the four α -helices of the membrane binding domain (yellow). Helix D projects up into the COX active site, which is located at the base of the large, globular catalytic domain (cyan). The heme prosthetic group (red) lies in the POX active site. (Blobaum and Marnett, 2007).

Although COX-1 and COX-2 are closely related, they are unique in several ways, as shown in table 2.

	COX-1	COX-2
Chromosome	9	1
Homology mRNA	60%	60%
messenger RNA Size	2.7 kb	4.5 kb
Protein Size ^{a)}	65 kDa	70 kDa
Intracellular Location	Endoplasmic Reticulum Nuclear Envelope	Endoplasmic Reticulum (some) Nuclear Envelope (mostly)
Regulation	Constitutive	Inducible
Tissue Expression	Platelets, Endothelial cells Stomach, Kidney Smooth Muscle Most tissues	Most tissues, especially inflammatory cells Requires stimulation by: Growth Factors, Cytokines & Hormones
Proposed Role	Housekeeping	Inflammatory Response

a) The COX and POX enzyme regions are 90% conserved between the two isoforms.

Table 2 Comparisons of COX-1 and COX-2 (Cryer and Dubois, 1998)

Both isoenzymes are somewhat genetically similar, sharing 60% genetic homology in their coding regions. Despite the genetic differences, both enzymes have a molecular weight of approximately 70 kDa, have highly conserved active sites, and differ by less than 10% of amino acids within the AA binding domain (Cryer and Dubois, 1998).

The COX-2 active site is about 20% larger and has a slightly different form than that of COX-1. The solvent accessible surface in the COX-2 active site is larger than that of COX-1 (figure 5) (Blobsbaum and Marnett, 2007). These size and shape differences are caused

mainly by two changes in the amino acid sequence. Evidently the exchange of a valine (Val) at position 523 in COX-2 for a relatively bulky isoleucine (Ile) residue in COX-1 at the same position of the active site of the enzyme causes a structural modification. This modification in the COX-2 enzyme allows access to an additional side pocket, which is a pre-requisite for COX-2 drug selectivity. Access to this side pocket is restricted in the case of COX-1 (Dannhardt and Kiefer, 2001; Charlier and Michaux, 2003). These studies of the static 3D structure of the enzyme have been very helpful in the process of understanding the enzyme inhibition mechanisms and in the design of selective compounds.

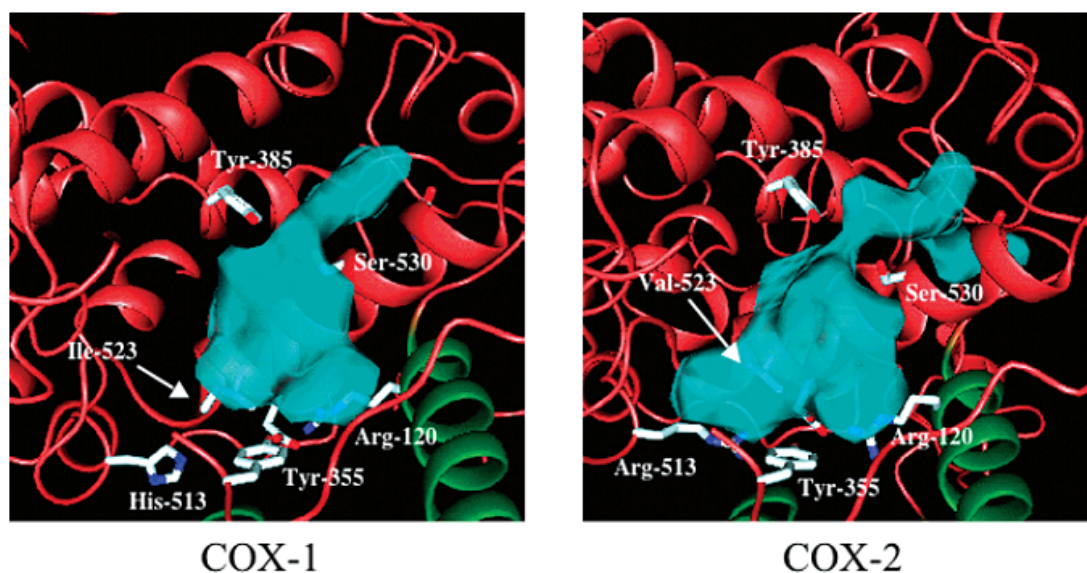


Figure 5 Solvent accessible surfaces in COX-1 and COX-2. The catalytic domains of the COX proteins are shown as red in a ribbon diagram with the membrane binding domains (predominantly helix D) shown in green. Residues lining the COX active site of both proteins are shown in white with the solvent accessible surfaces in the active site designated as translucent light-blue (Blobaum and Marnett, 2007).

1.1.3 Non-steroidal anti-inflammatory drugs (NSAIDs)

Anti-inflammatory agents are believed to act by disrupting the AA cascade. These drugs are widely used for the treatment of minor pain and arthritis. Some of them are antipyretics (drugs that reduce fever) in addition to having analgesic and anti-inflammatory actions. Some of these agents are widely available in over-the-counter (OTC) preparations. Collectively, these are referred to NSAIDs.

1.1.3.1 Mechanism of action

Vane, Samuelson and Bergstrom succeeded in showing that NSAIDs block the biosynthesis of PGs which contribute to a variety of physiological and pathophysiological functions (Vane and Botting, 1992). The NSAIDs block the COX enzyme that catalyzes the conversion of AA to the PGG₂ and PGH₂, as mentioned above. Since these two cyclic endoperoxides are the precursors of all other PGs, the implications of COX inhibition are significant. PGE₁ is known to be a potent pyrogen (fever-causing agent), and PGE₂ causes pain, edema, erythema (reddening of the skin), and fever. The PG endoperoxides (PGG₂ and PGH₂) can also produce pain, and inhibition of their synthesis can thus account for the action of the NSAIDs (Nogarty and Weaver, 2005).

1.1.3.2 Classification of NSAIDs

As the principal pharmacological effects of NSAIDs arise from their inhibition of COX enzymes, the available evidence suggests that the anti-inflammatory and analgesic properties are due to the inhibition of COX-2, whereas the side effects are associated with the inhibition of COX-1 (Blobaum and Marnett, 2007). Hence, these drugs can be subdivided into two classes: classical NSAIDs or non-selective COX inhibitors and selective COX-2 inhibitors.

1.1.3.2.1 Classical NSAIDs or Non-selective COX inhibitors

It may be classified on the basis of their basic chemical structures as listed in table 3. This list provides examples for each category. There are other analogs as well, reflecting the widespread use of these agents. (Nogrody and Weaver, 2005)

Basic chemical structures	Examples drugs
Arylanthranilic acids	mefenamic acid, meclofenamate
Arylbutyric acids	nabumetone
Arylpropionic acids	ibuprofen, ketoprofen, fenoprofen, naproxen
Indene derivatives	sulindac
Indole derivatives	indomethacin
Naphthylacetic acid derivatives	nabumetone
Oxicams	piroxicam, meloxicam, tenoxicam
Phenylacetic acid derivatives	diclofenac
Phenylalkanoic acid derivatives	flurbiprofen
Pyrazolone derivatives	phenylbutazone, azapropazone
Pyrrrolealkanoic acid derivatives	tolmetin
Salicylate derivatives	aspirin, diflunisal

Table 3 Non-selective COX inhibitors classify on the basis of their basic chemical structures and the examples for each category

Most of the NSAIDs are carboxylic acids. This presence of an acidic moiety structural feature accounts for the formation of a salt bridge between the carboxylic group of the inhibitors and Arg 120 at the bottom of the COX thus generating COX-1 inhibiting activity (Dannhardt and Kiefer, 2001).

Aspirin has been used since the turn of the last century to reduce pain and fever, but the parent compound, salicylic acid, has been known and used since antiquity, owing to its common occurrence as a glycoside in willow bark. Acetylation merely decreases its irritating effect. Among the numerous other salicylates known and used, flufenisal has a longer duration of activity and fewer side effects than aspirin. Mefenamic acid and flufenamic acid are derivatives of anthranilic acid, while ibuprofen and naproxen are derivatives of phenylacetic and naphthylacetic acids, respectively. Among indole derivatives, indomethacin is very widely used despite side effects. Its indene analog sulindac is a pro-drug, the active form being its —SH derivative. Piroxicam is a long-lasting anti-rheumatoid agent but can have serious gastrointestinal side effects. The once widely used phenylbutazone derivatives have too many side effects and have fallen into disrepute. The example of non-selective COX inhibitors was shown in figure 6.

Among the non-selective COX inhibitors, there is no clear-cut statistical evidence for the superiority of one or another of these useful drugs. Individual patients may do better with some than with others, and there are differences in side effects, primarily gastric bleeding and renal toxicity, which can be especially serious with the prolonged administration of high doses—necessary in chronic diseases such as rheumatoid arthritis.

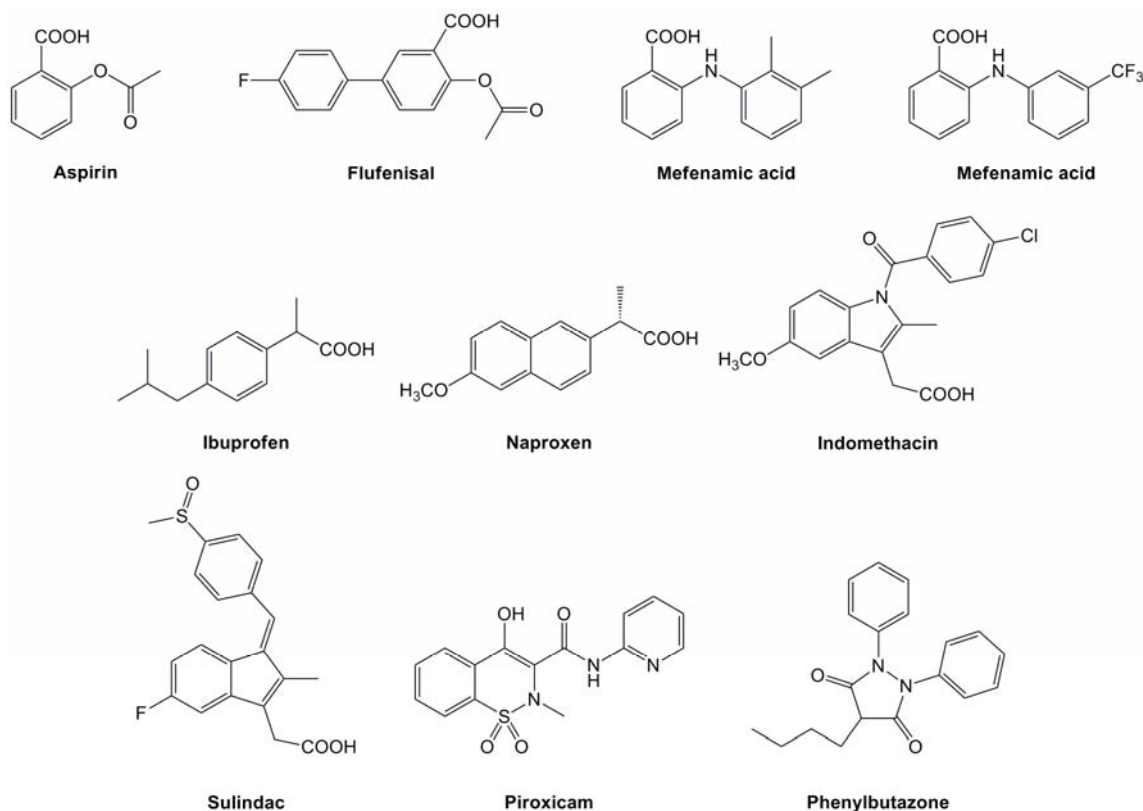


Figure 6 The example of non-selective COX inhibitors

1.1.3.2.2 Selective COX-2 inhibitors

The aspect of enzyme selectivity of NSAIDs becomes important particularly under the point of view of low risk NSAIDs with reduced side-effects. Therefore, the classic NSAIDs are being pushed increasingly into the background, whereas selective COX-2 inhibitors with an attractive pharmacological profile and reduced side-effects are being favored.

Contrary to the classic NSAIDs, this new class of enzyme inhibitors is lacking a carboxylic group, thus effecting COX-2 affinity by a different orientation within the enzyme without formation of a salt bridge. The selective COX-2 inhibitors belong to different structural classes as followed (Dannhardt and Kiefer, 2001).

1. *Modified known NSAIDs to improve COX-2 selectivity:*

Modifying well known NSAIDs into selective COX-2 inhibitors represents an interesting strategy. In principle, the strategy consisted of introducing larger substituents to fit into the active site volume of COX-2. Indomethacin, zomepirac, aspirin, flurbiprofen and diclofenac have been successfully elaborated into selective COX-2 inhibitors (figure 7).

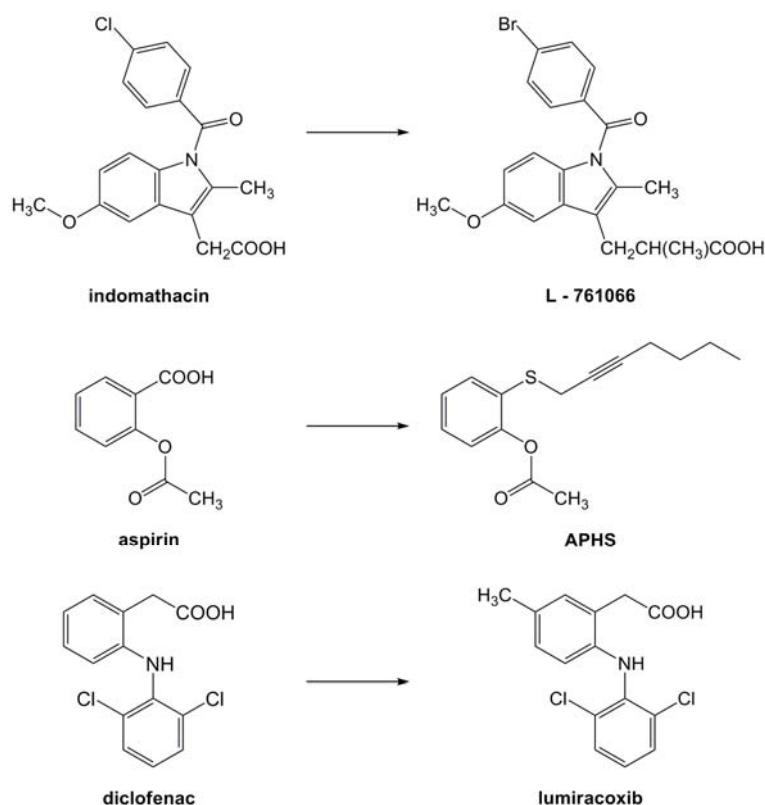


Figure 7 The example of modified known NSAIDs to improve COX-2 selectivity

2. *Diaryl- or aryl-heteroaryl-ethers (sulfonamide inhibitors):*

The examples of currently drugs used in this class are nimesulide and flosulide (figure 8). Structurally, nimesulide and flosulide (a diaryl ether and thioether structure, respectively), which bear a methansulfonamide moiety. The sulfonamide structure with its NH-acidity in all these compounds seems to be obligatory. It appears that nimesulide was the first

member of this class of drugs. Its mechanism of action, pharmacology and clinical results in rheumatic diseases, osteoarthritis and acute inflammation demonstrated that nimesulide possesses novel anti-inflammatory qualities. Flosulide is similar to nimesulide. The main difference between them is the incorporation of the electron-withdrawing substituent into the five-membered carbocyclic ring.

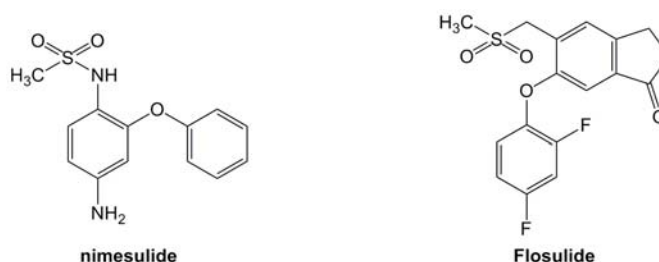


Figure 8 The example of diaryl- or aryl-heteroaryl-ethers (sulfonamide inhibitors)

3. Vicinal diaryl heterocycles:

The compounds are characterized by a central carbocyclic or heterocyclic ring system bearing two vicinal aryl moieties. These compounds represent the most important group of COX-2 inhibitors. It can be assumed that the heterocycle is responsible for the appropriate orientation to the aromatic rings in space and finally for the binding to the enzyme. A wide variety of heterocycles can serve as a template for COX-2 inhibitors, i.e. pyrrole, thiazole, oxazole, furane, imidazole, isoxazole, pyrimidine and thiophene, but at the moment pyrazole and cyclopentenone seem to be the most appropriate tools for COX-2 specificity. For optimal activity, one aromatic ring must be substituted with a methylsulfonyl or a sulfonamide substituent in *para* position. Substitution at *para* position of one of the aromatic systems with a sulfonamide or a methylsulfonyl group is essential for COX inhibition. Replacement of the methylsulfonyl group by a sulfonamide group reduces COX-2 selectivity but improves oral bioavailability.

Two heterocycles with the substitution pattern mentioned above were of special interest: the 1,5 diarylpyrazole derivative celecoxib (figure 9) and 3,4-diarylfuranone derivative

rofecoxib (figure 9). Celecoxib (Celebrex[®]) was approved by the FDA for the treatment of osteoarthritis and chronic polyarthritis in 1998. Rofecoxib (Vioxx[®]) has been launched in the USA for the treatment of osteoarthritis, acute pain and primary dysmenorrhea and is meanwhile also available in Germany, and approved within the EU for the treatment of osteoarthritis. Valdecoxib and parecoxib sodium (prodrug of valdecoxib) (figure 9) are the latest developments of COX-2 inhibitors and belong to the same chemical group.

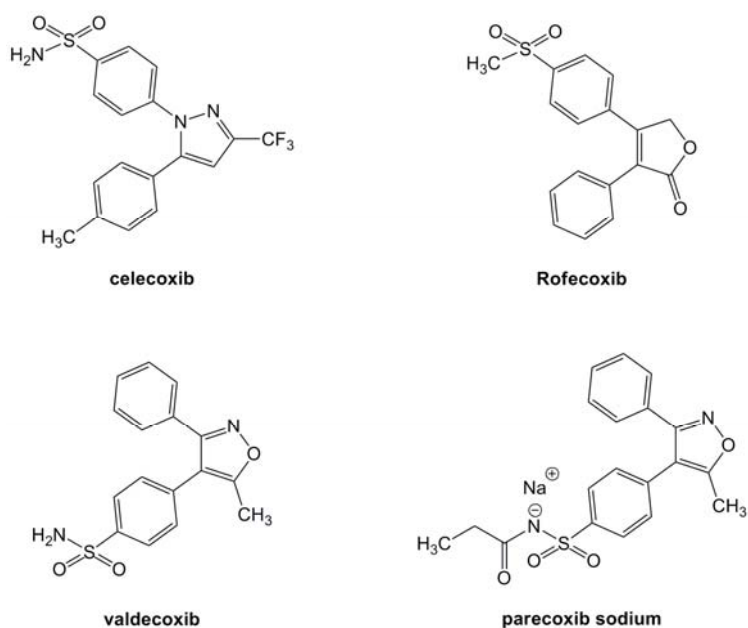


Figure 9 The example of vicinal diaryl heterocycles inhibitors

1.1.3.3 NSAIDs in therapeutics

As mentioned before, the classical NSAIDs reduce the production of pro-inflammatory PGs at sites of injury; via COX-2 inhibition, but also the formation of physiological PGs in the stomach and the kidney; via COX-1 inhibition for GI lesions and renal toxicity, leading at high doses to erosions, ulcerations, bleedings, and even to death (Dannhardt and Kiefer, 2001; Charlier and Michaux, 2003).

Six selective COX-2 inhibitors (coxibs) have reached the market, and other novel candidates are expected to be launched in the near future. Celecoxib and rofecoxib are the original entries from 1999 and are now widely prescribed for the treatment of the symptoms of osteoarthritis and rheumatoid arthritis. Valdecoxib and etoricoxib followed three years later, while parecoxib sodium, an injectable pro-drug of valdecoxib, was launched in 2003. Lumiracoxib is the newest entry to the field and has already been approved for market in the United Kingdom. Additionally, deracoxib is now available for the treatment of pain and inflammation associated with osteoarthritis in dogs. Multiple clinical trials have shown these drugs to have clinical efficacy comparable to that of NSAIDs (Doherty, 2004).

Recent pharmacological studies have raised questions about the two principal tenets underlying the design of specific COX-2 inhibitors, namely that PGs responsible for the gastric mucosal integrity and renal function are produced solely via COX-1 whereas PGs that mediate inflammatory responses are produced solely via COX-2.

Firstly, COX-2 is constitutively expressed in the kidney and the reproductive tract. In addition to its implication in the kidney development, this isoform plays an important part in the regulation of renal function (perfusion, water handling, renin release) in both normal and parapsyiological conditions (i.e., in patients with liver cirrhosis, renal insufficiency or congestive heart failure). Moreover, cyclic hormonal induction of COX-2 plays an important role in ovulation. This enzyme is also expressed in the uterine epithelium at different stages of pregnancy: in the beginning, it contributes to the ovum implementation and to angiogenesis essential for placenta establishment, while, at the end, it is important for the onset of the labor (parturition) (Dannhardt and Kiefer, 2001). As a result, like for classical NSAIDs, the use of selective COX-2 inhibitors should be avoided in the early stages of pregnancy whereas they should be useful in delaying premature delivery.

Secondly, COX-2 may be involved in the “adaptative cytoprotection” response in GI mucosa. When the latter is inflamed or ulcerated, COX-2 is rapidly induced at sites of

injury where it produces large amounts of PGs involved in the healing process. So, selective COX-2 inhibitors should be avoided in patients with gastric susceptibility (Blobaum and Marnett 2007). Finally, PGs produced by COX-1 have also been shown to contribute to inflammatory responses and hyperalgesia. In these cases, the anti-inflammatory efficacy of selective COX-2 inhibitors was only observed at doses that inhibited COX-1 (Charlier and Michaux, 2003).

In addition, several *in vitro*, *in vivo*, and clinical studies have demonstrated that COX-2 selective inhibitors may prevent colorectal cancer. Although the precise molecular mechanism involved in the chemopreventive action of these inhibitors is not entirely understood, the COX-2 isoenzyme has proven to play a central role in the development of colorectal cancer through the promotion of angiogenesis, increased invasiveness, and anti-apoptotic effects (Patrignani *et al.*, 2005). Additionally, COX-2 expression may be upregulated at certain site, in the microglia of cognitive centers within the hippocampus and cortex in Alzheimer's disease (AD). Enhanced COX-2 expression in the brain may be associated with beta-amyloid protein deposition in the neuritic plaques of AD. This protein and its peptide precursors are thought to be elaborated as part of an inflammatory cascade in which microglia, a rich source of prostanoids, probably participate. Since COX-2 expression in the brain and PGE₂ content in the cerebrospinal fluid have been reported to be elevated in AD together with the finding that COX-2 protein levels in the brain correlate with the severity of amyloidosis and clinical dementia, it has been suggested that COX-2 inhibition by NSAIDs might be involved in the apparent protection in this setting (Patrignani *et al.*, 2005).

Moreover, the incidence of the use of these compounds on cardiovascular diseases still requires vigilance. Indeed, COX-2 has been shown to generate PGI₂ in endothelial cells. Therefore, by decreasing vasodilatory and antiaggregatory PGI₂ production, selective COX-2 inhibitors may tip the natural balance PGI₂/TXA₂ in favor of prothrombotic TXA₂ and may lead to increase cardiovascular thrombotic events (Blobaum and Marnett 2007).

The long-term cardiovascular safety of COX-2 selective inhibitors was recently called into question with the results of two trials: the Adenomatous Polyp Prevention on Vioxx trial (APPROVe, rofecoxib) and the Adenoma Prevention with Celecoxib trial (APC, celecoxib). Both trials, which were conducted to evaluate the use of COX-2 selective inhibitors for the prevention of recurrence of colorectal polyps, revealed a higher incidence of cardiovascular events (death, myocardial infarction, and stroke) in patients taking the drugs for an extended period of time. Of particular note, the APPROVe trial enrolled only those patients who did not have a prior history of cardiovascular disease and was halted prematurely because of the 2- to 3-fold increased risk of cardiovascular events among patients in the group that was taking 25 mg of rofecoxib compared to placebo. This led to the withdrawal of rofecoxib from the worldwide market in 2004. It has since been reported that other COX-2 selective inhibitors (celecoxib, etoricoxib, parecoxib and valdecoxib) and some nonselective classical NSAIDs also might pose a risk for increased cardiovascular events. Nevertheless, COX-2 remains a very important pharmaceutical target for the treatment of debilitating diseases like rheumatoid arthritis and osteoarthritis and as a preventative agent for colon cancer. However, important questions remain concerning the benefit-risk profiles of traditional NSAIDs and both the diaryl heterocycle class of COX-2 selective inhibitors (Blobaum and Marnett 2007).

1.2 Review of Literatures

Although, many observations reported that the long-term use of some of selective COX-2 inhibitors, rofecoxib and valdecoxib, cause significant cardiovascular side effects (Patricia and Patrice, 2004). Nevertheless, the therapeutic treatment of inflammatory diseases with fewer side effects and additional efficacy in preventing and delaying the progression of colon cancer and perhaps also Alzheimer's disease of selective COX-2 inhibitors, could be a big step ahead to development of new selective COX-2 inhibitors.

According to structure of selective COX-2 inhibitors, most of them are belong to structure of sulfonyl-substituted diarylheterocycle (Dannhardt and Kiefer, 2001). The example of

currently drug used in this group is celecoxib or as known celeblex[®] in trade name. Celecoxib was approved by the FDA for the treatment of osteoarthritis and chronic polyarthritis in 1998. Celecoxib has an optimal *in vitro* and *in vivo* profile. The substance shows potent and selective *in vitro* activity (COX-1 IC₅₀ = 13 μmol, COX-2 IC₅₀ = 0.04 μmol) and marked anti-inflammatory activity in the rat adjuvant-induced arthritis assay (ED₅₀ = 0.4 mg/kg) (Penning *et al.*, 1997). Studies showed that the analgesic and antiphlogistic efficacy of 400 mg celecoxib daily is comparable to a daily dosage of 1,000 mg naproxen or 150 mg diclofenac. Celecoxib is contraindicated during pregnancy and interestingly in patients with GI ulcers. At this point the role of COX-2 for wound healing becomes evident, once an ulcerative injury is present, COX-2 expression is elevated in response to this disease and the COX-2 enzyme seems to be essential for wound healing in the stomach by enhancing gastric blood flow, reducing gastric acid secretion and allowing epithelial cell proliferation and granulation tissue contraction. Consequently, highly selective COX-2 inhibitors such as celecoxib lead to delayed wound healing and can aggravate the injury.

Consideration to structure of celecoxib found that including three main parts; lipophilic aryl ring or tolyl group, sulfonyl-substituted aryl ring or *p*-sulfamidophenyl ring and central ring that fuse two latter parts together (Garg *et al.*, 2003) (figure 10).

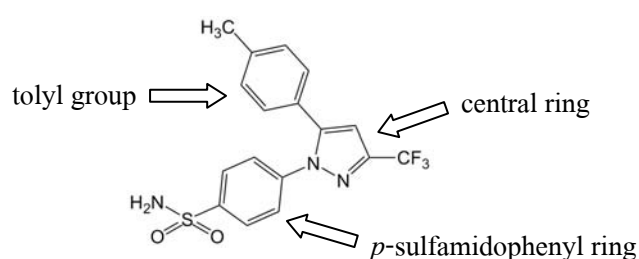


Figure 10 Three main structural features of celecoxib

Some studies have demonstrated a development of new selective COX-2 inhibitors by replacing the central ring with heterocyclic analogs, five membering (**I** and **II**) and six membering (**III**), (Biava *et al.*, 2005; Puig *et al.*, 2000; Rao *et al.*, 2003) or non-cyclic analogs (**IV-VIII**) (Chowdhury, 2008; Zarghi *et al.*, 2006; Zarghi *et al.*, 2008; Tsai *et al.*, 2006; Lin *et al.*, 2008) could provide efficiency COX-2 inhibitory activity and selectivity (figure 11).

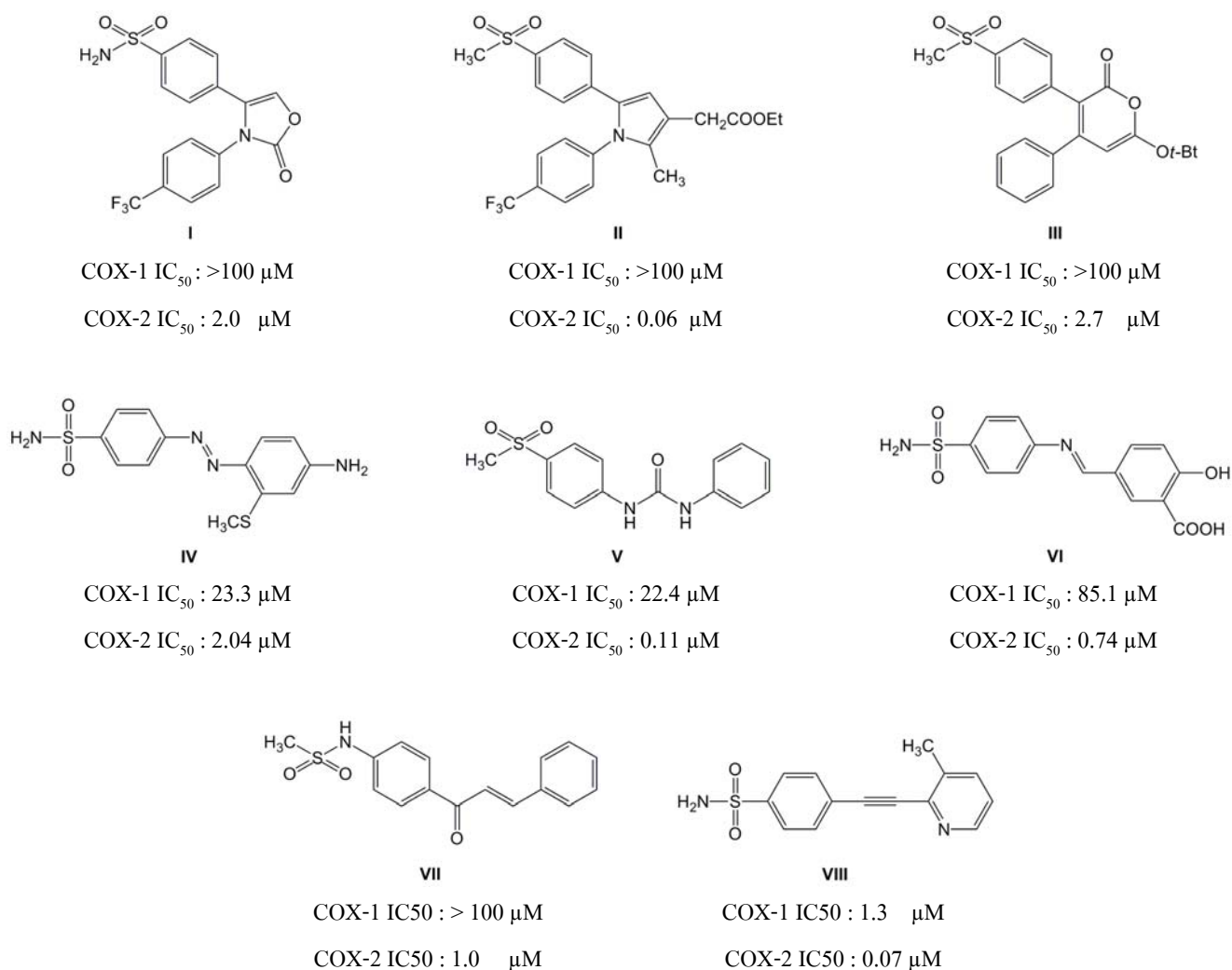


Figure 11 Compounds were reported as selective COX-2 inhibitors

According to a crystal structure of celecoxib analogue (SC-558) in active site of murine COX-2, showed the best appropriated conformation of celecoxib analogue which lipophilic aryl ring and sulfonyl-substituted aryl ring were existed in the same side (figure 12) (Kurumbail et al., 1996).

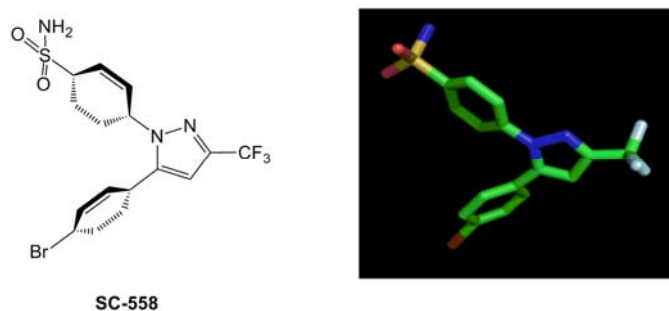


Figure 12 Conformation of celecoxib analogue, SC-558, in active site of murine COX-2

Assembly with several studies about conformation of aromatic amides, were proved that a *cis*-preference is general in *N*-methyl aromatic amides; that is, benzanilide (figure 13) exists exclusively in the *trans* conformation whereas *N*-methylbenzanilide (figure 13) exists predominantly in the *cis* structure both in solution state, crystal state (Itai *et al.*, 1989; Itai *et al.*, 1992) and *ab initio* molecular orbital calculation (Saito *et al.*, 1995).

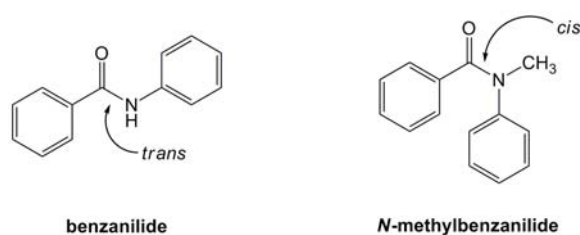
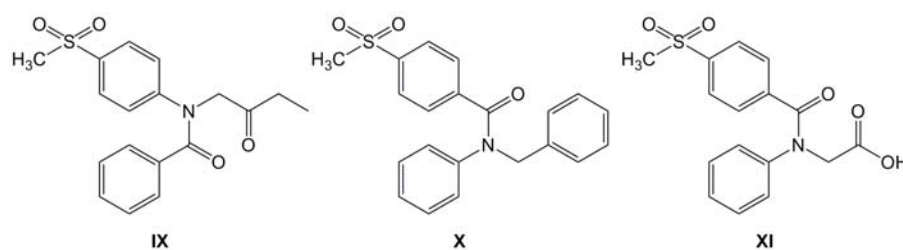


Figure 13 Conformation of benzanilide (*cis*) and *N*-methylbenzanilide (*trans*)

According to *cis*-preference in *N*-substituted aromatic amides and conformation of celecoxib analogue in active site of COX-2, lead to an idea; replacement of central ring of celecoxib by acyclic amide bond should allow the orientation of lipophilic aryl ring and sulfonyl-

substituted aryl ring similar to celecoxib. In prior studies (Songkram *et al.*, 2007), they designed and synthesized compounds which replaced central ring of celecoxib with acyclic amide linkage. Conformation of synthesized tertiary amides or *N*-substituted benzanilides is also existed in *cis*-preference in solution state. Moreover, some *N*-substituted benzanilides (**IX**, **X** and **XI**) exhibited some COX-2 inhibitory activity closely to aspirin which was positive control when compare quantitative of generated PGE₂ from knockout cell lines COX-1 and COX-2 using radioimmunoassay (table 4).



Cpd.	Conc. ($\mu\text{g/ml}$)	Anti COX-1		Anti COX-2		COX-2
		%PGE ₂	%inhibition	%PGE ₂	%inhibition	COX-1
XI	10	62 \pm 9	38	63 \pm 2	37	1.0
X	10	83 \pm 10	17	54 \pm 9	46	2.7
XI	10	140 \pm 34	-40	62 \pm 1	38	-
ASA	0.1	86 \pm 15	14	87 \pm 19	13	0.9
ASA	10	45 \pm 20	55	65 \pm 9	35	0.6

Table 4 COX inhibitory of *N*-substituted benzanilides (**IX**, **X** and **XI**) compare quantitative of generated PGE₂ from knockout cell lines COX-1 and COX-2 using radioimmunoassay

1.3 Objective of the thesis

In this investigation I described the design, synthesis and COX inhibitory activities for the *N*-phenylbenzohydrazides (figure 14) that possess a non-cyclic, amide bond, in place of the central ring of pharmacophore present in celecoxib. I do also make it more similar to celecoxib by replace nitrogen atom with carbon atom at nitrogen atom of amide and expect that this may be affect selectivity and potency of compounds. I vary substituent group (R_1 = non-substituent; H, electron withdrawing group; F and electron donating group; CH_3) at *para* position of the lipophilic aryl ring and vary at R_2 to alkyl (CH_3) and aryl (C_6H_5). Moreover, I also alternate structure in amide bond part; sulfonyl-substituted aryl ring attach at nitrogen of amide to attach at carbonyl of amide, for structure activity relationship (SAR) studies.

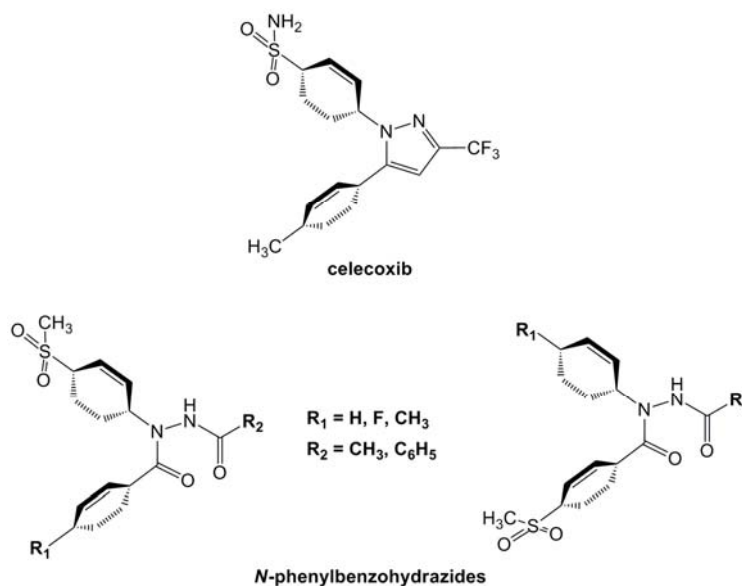


Figure 14 Compare structure of *N*-phenylbenzohydrazides and celecoxib

CHAPTER 2

EXPERIMENT

2.1 Materials and Equipments

2.1.1 Material and equipments in synthesis and characterization

All chemicals and solvents were purchased locally from Sigma-Aldrich (MO, U.S.A.), Riedel-de Haen (Germany), Labscan asia, Wako Pure Chemical Industries (Japan), TCI (Japan), Merck (NJ, U.S.A.) and Fisher Scientific (PA, U.S.A.). The chemicals and solvents used in the synthesis and characterization were listed in table 5. Column chromatography was performed using silica gel 60 for column chromatography (40-63 μm). TLC was performed on aluminum backed plates pre-coated with silica (0.1 mm, 60F₂₅₄) from Merck and developed using standard visualizing apparatus: UV fluorescence (254 nm). Melting points were determined with Melting point apparatus (Mel-Templl, Laboratory devices, USA). FT-IR spectra were recorded using FT-IR Model Spectrum One Perkin Elmer™. ¹H NMR and ¹³C NMR spectra were recorded in Acetone-*d*₆, CDCl₃ and DMSO-*d*₆ using FT-NMR 500 MHz; Model UNITY INOVA, Varin and JEOL GSX400 instrument operated at 400 MHz. High resolution mass spectrometry (HR-MS) were recorded on a micrOTOF, Bruker using ESI technique to generate ion. Elemental analyses (EA) were carried out in the Microanalytical Laboratory, Faculty of Pharmaceutical Sciences, University of Tokyo. X-ray crystallography experiment was performed using Bruker Smart1000 CCD diffractometer with graphite monocromated MoKa ($\lambda = 0.71073 \text{ \AA}$).

Chemical	Details
acetic anhydride	Sigma-Aldrich, (MO, U.S.A.)
aluminium chloride	Riedel-de Haen, Germany
benzoyl chloride	Wako, Japan
bromine	Fluka
calcium chloride	Unilab, Ajax Finechem
chloroform	Anhydrous, Lab scan asia
deuterated acetone (Acetone- d_6)	Cambridge Isotope Laboratories, Inc. (MA, USA)
deuterated chloroform (CDCl ₃)	Acrōs Organics, Belgium
deuterated dimethylsulfoxide (DMSO- d_6)	Cambridge Isotope Laboratories, Inc. (MA, USA)
dichloroethane	Anhydrous, Lab scan asia
dichloromethane	Anhydrous, Lab scan asia
diethyl ether	Lab scan asia
Ethanol (absolute)	Merck, Germany
ethyl acetate	commercial grade
4-fluorophenylhydrazine hydrochloride	Aldrich
4-fluorobenzoyl chloride	Aldrich
hexane	commercial grade
hydrazine monohydrate	Aldrich and Kanto, Japan
hydrochloric acid	Lab scan asia
methanol	analytical grade, Labscan asia
4-methylbenzoyl chloride	Fluka
4-(methylthio)benzoyl chloride	Aldrich
Oxone [®] peroxymonosulfate	Aldrich
phenylhydrazine	Fluka and Kanto, Japan
<i>p</i> -tolylhydrazine hydrochloride	Fluka
Pyridine	Merck (NJ, U.S.A.)

Table 5 The lists of chemicals and solvents used in synthesis and characterization

Chemical	Details
thioanisole	Aldrich
silica gel 60 for column chromatography	Merck (NJ, U.S.A.)
sodium hydroxide	Lab scan asia
sodium sulfate anhydrous	Fisher Scientific (PA, U.S.A.)

Table 5 (continue) The lists of chemicals and solvents used in synthesis and characterization

The synthesis works were performed in Department of Pharmaceutical Chemistry, Faculty of Pharmaceutical Sciences, Prince of Songkla University, Thailand and also in Department of Chemistry, Faculty of Science, Ochanomizu University, Japan. $^1\text{H-NMR}$ and $^{13}\text{C-NMR}$ determination were conducted by service of Scientific Equipment Center, Prince of Songkla University, Thailand and also conducted in Department of Chemistry, Faculty of Science, Ochanomizu University, Japan. Low resolution and HR-MS were determined at School of Biomedical Science, Institute of Biomaterials and Bioengineering, Tokyo Medical and Dental University, Tokyo, Japan. EA were carried out in the Microanalytical Laboratory, Faculty of Pharmaceutical Sciences, University of Tokyo. X-ray Crystallography experiment was performed by Dr. Isao Azumaya, Faculty of Pharmaceutical Sciences at Kagawa Campus, Tokushima Bunri University, Kagawa, Japan.

2.1.2 Materials and equipments in determination of biological activity

The *in vitro* COX inhibitory activity determination were conducted with the facility of laboratory of organic and medicinal chemistry, School of biomedical Science, Institute of Biomaterials and Bioengineering, Tokyo Medical and Dental University, Japan. Screening inhibitory activity both in COX-1 and COX-2 of the compounds was assessed with a colorimetric COX (ovine) inhibitory screening assay kit (Cayman Chemical; catalog No. 760111), purchased from Cayman Chemical Company. Additional items required in this assay kit were a plate reader capable of measuring absorbance at 560 nm (Beckman Coulter DTX 880 Multimode Detector,

CA, USA), adjustable pipettors and a repeat pipettors (Gilson Inc., France), micromixer (Taitec: micromixer E-36, Japan), and HPLC-grade water.

2.2 Method

2.2.1 Synthesis and characterization

Two sets of *N*-phenylbenzohydrazide derivatives which 4-methanesulfonylphenyl substituent is attached either to the carbonyl, *N'*-acyl-*N*-(4-substitutedphenyl)-4-(methylsulfonyl)benzohydrazides (**16-21**), or to the nitrogen, *N'*-acyl-4-substituted-*N*-[4-(methylsulfonyl)phenyl]benzohydrazides (**27-32**), of amide, were synthesized. The structures of designed compounds were showed in figure 15.

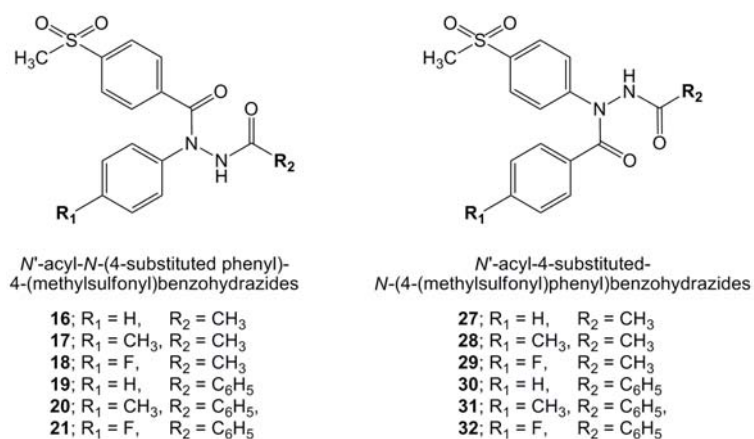


Figure 15 Structure of targeted *N*-phenylbenzohydrazide derivatives.

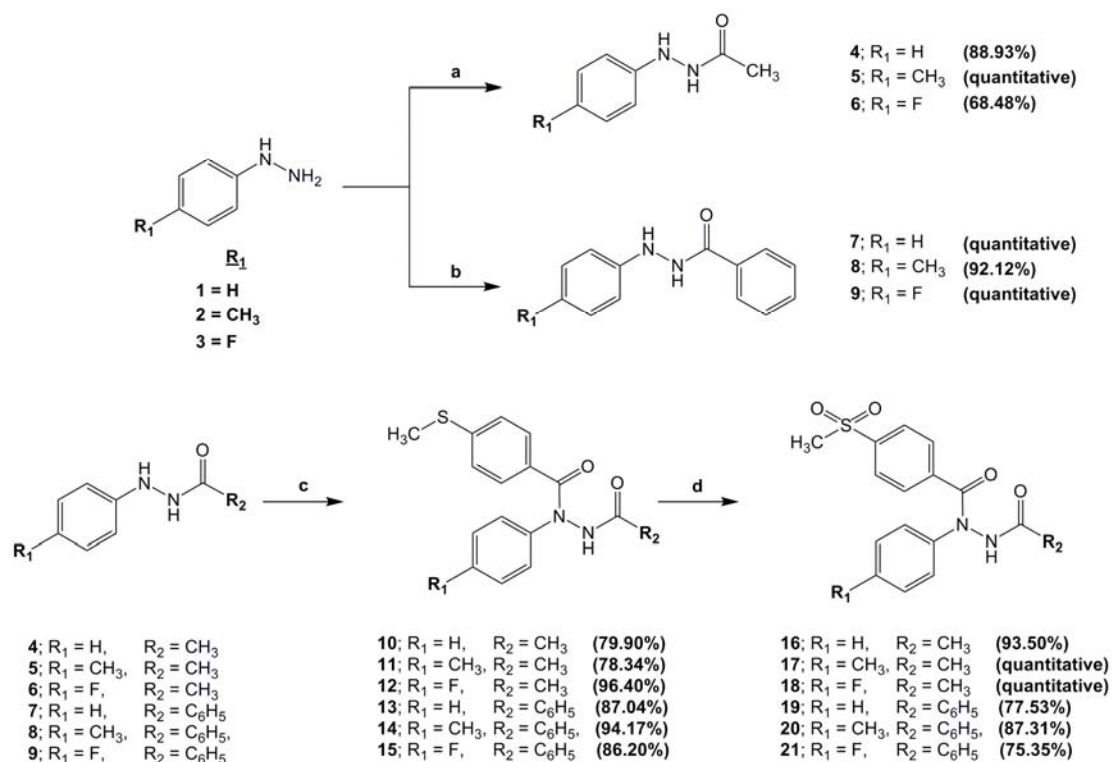
Physical and spectroscopy properties of synthesized compounds were examined. Melting points were measured using melting point apparatus. Infrared (IR) spectra were recorded using FT-IR model spectrum one Perkin Elmer™. ¹H- and ¹³C-NMR were recorded on the aforementioned instruments. The samples were dissolved in proper solvent, acetone-*d*₆, CDCl₃ or DMSO-*d*₆. Chemical shifts values (δ) were expressed in ppm and coupling constants (*J*) in

hertz (Hz). The elemental comparisons of all target compounds were confirmed either by HR-MS spectra or EA. The HR-MS experimental data were less than 3 ppm difference from theoretical data and the EA experimental values were within plus or minus 0.4 % of theoretical values.

2.2.1.1 Synthesis of *N'*-acyl-*N*-(4-substituted phenyl)-4-(methylsulfonyl)benzohydrazides (16-21)

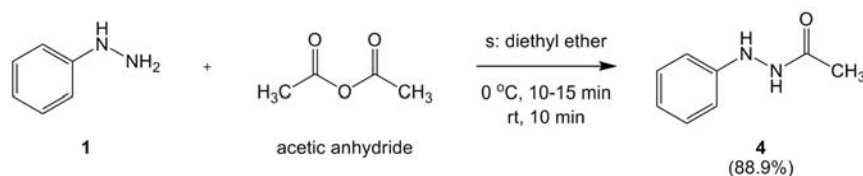
In this part of investigation composed of three-step synthetic pathway. Initially, *N'*-phenylacetohydrazides (**4**), *p*-substituted *N'*-phenylacetohydrazide (**5** and **6**), *N'*-phenylbenzohydrazide (**7**) and *N'*-(*p*-substituted) benzohydrazide (**8** and **9**) were synthesized through acetylation reaction and benzylation reaction of their corresponding phenylhydrazine, respectively. Secondly, the pyridine catalyzed cross-coupling reaction between *N'*-phenylacetohydrazides (**4-6**) or *N'*-phenylbenzohydrazides (**7-9**) and 4-(methylthio) benzoyl chloride under reflux in dry dichloroethane afforded the respective *N'*-acetyl-4-(methylthio)-*N'*-phenylbenzohydrazides (**10-12**) and *N'*-benzoyl-4-(methylthio)-*N'*-phenylbenzohydrazides (**13-15**). Finally, subsequent oxidation of **10-15** using Oxone[®] furnished the target *N'*-acetyl-4-(methylsulfonyl)-*N'*-phenylbenzohydrazides (**16-18**) and *N'*-benzoyl-4-(methylsulfonyl)-*N'*-phenylbenzohydrazides (**19-21**). All of synthesized compound were purified by suitable method such as solvent extraction, silica gel column chromatography and recrystallization.

Their syntheses were concluded in scheme 1, and the synthesis of each compounds in detail were described as follows.



Scheme 1 Synthesis of *N'*-acyl-*N*-(4-substituted phenyl)-4-(methylsulfonyl)benzohydrazides (**16-21**). Reagent: (a) acetic anhydride, diethyl ether; (b) benzoyl chloride, pyridine, diethyl ether; (c) 4-(methylthio)benzoyl chloride, pyridine, reflux; (d) Oxone[®], MeOH, H₂O.

N'-phenylacetohydrazide (**4**)



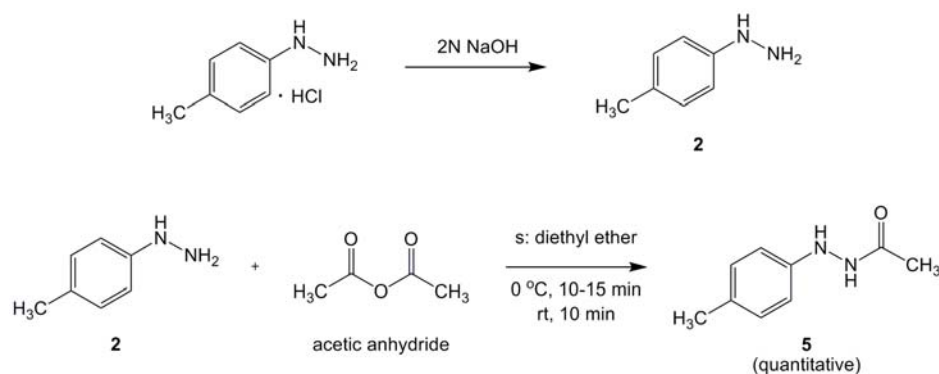
Diluted acetic anhydride (3.77 ml, 40 mmol, 4.00 equiv) in diethyl ether (20 ml) was slowly dropped into a solution of phenylhydrazine (**1**) (1,946 mg, 10 mmol) in diethyl ether (2.5 ml) with ice cooling. The mixture was stirred for 10-15 min. After that ice bath was removed and continually stirred for 10 min. The insoluble products were filtered and washed well

with cooled diethyl ether. The precipitated product was then redissolved in ethyl acetate and wash with 2N sodium hydroxide, water and brine. The obtained solution was dried over anhydrous sodium sulfate and then concentrated to give **4** as white solid (2.4039 g, 88.9%). Recrystallized with ethyl acetate/*n*-hexane gave white needles; mp. 126-129 °C.

IR (KBr), ν_{max} , cm^{-1} (Figure 16): 3286, 3235, ($\nu_{\text{N-H}}$, monohydrazide), 3030 ($\nu_{\text{C-H}}$, aromatic), 2939, 2857 ($\nu_{\text{C-H}}$, aliphatic), 1643 ($\nu_{\text{C=O}}$, amide), 1596, 1495 ($\nu_{\text{C=C}}$, aromatic)

$^1\text{H-NMR}$ (500MHz, $\text{DMSO-}d_6$), δ , ppm (Figure 17): 1.89 (*s*, 3H), 6.67 (*t*, $J = 5.9 \text{ Hz}$, 1H), 6.68 (*d*, $J = 8.5 \text{ Hz}$, 2H), 7.11 (*t*, $J = 7.9 \text{ Hz}$, 2H), 7.63 (*d*, $J = 2.7 \text{ Hz}$, 1H), 9.58 (*d*, $J = 2.7 \text{ Hz}$, 1H)

*N*¹-*p*-tolylacetohydrazide (**5**)



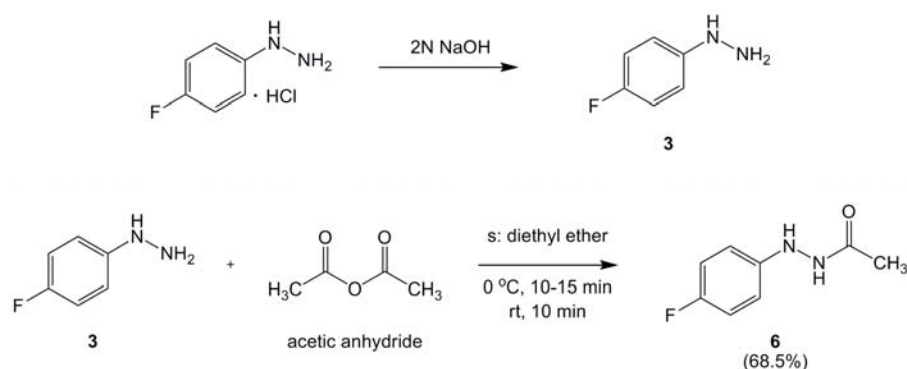
p-Tolylhydrazine hydrochloride (634 mg, 4.00 mmol) was neutralized into free base by stirred with 2N sodium hydroxide (2 ml). Then the free base (**2**) was extracted with diethyl ether (10 ml for 3 times), and dried over anhydrous sodium sulfate. The solution was then transfer into 50 ml reaction flask in ice bath. A diluted acetic anhydride (1.6 ml, 16 mmol, 4.00 equiv) in diethyl ether (15 ml) was added dropwise into a previous solution of *p*-tolylhydrazine. The mixture was stirred for 10-15 min. After that ice bath was removed and continually stirred for 10 min. The insoluble products were filtered and washed well with cooled diethyl ether. The precipitated product was then redissolved in ethyl acetate and wash with 2N sodium hydroxide, water and brine. The obtained solution was dried over anhydrous sodium sulfate and then

concentrated. Purification by silica gel column chromatography (eluent: ethyl acetate/*n*-hexane, 3:2) gave **5** (680 mg, quantitative). Recrystallized with ethyl acetate/*n*-hexane gave white solid; mp. 124-128 °C.

IR (KBr), ν_{max} , cm^{-1} (Figure 18): 3297 ($\nu_{\text{N-H}}$, monohydrazide), 3029 ($\nu_{\text{C-H}}$, aromatic), 2919, 2864 ($\nu_{\text{C-H}}$, aliphatic), 1675 ($\nu_{\text{C=O}}$, amide), 1595 ($\nu_{\text{C=C}}$, aromatic).

$^1\text{H-NMR}$ (500MHz, $\text{DMSO-}d_6$), δ , ppm (Figure 19): 1.86 (*s*, 3H), 2.16 (*s*, 3H), 6.59 (*d*, $J = 8.3$ Hz, 2H), 6.92 (*d*, $J = 8.3$ Hz, 2H), 7.45 (*d*, $J = 3.2$ Hz, 1H), 9.56 (*d*, $J = 3.1$ Hz, 1H).

***N*'-(4-fluorophenyl)acetohydrazide (6)**



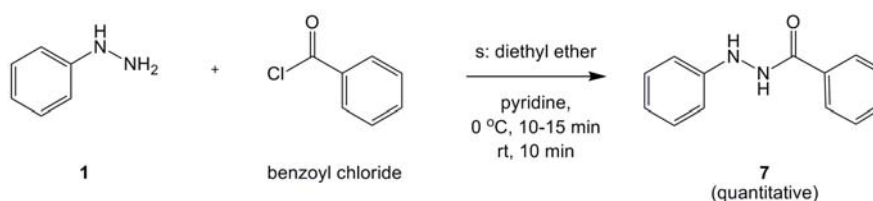
4-Fluorophenylhydrazine hydrochloride (1,626 mg, 10.00 mmol) was neutralized into free base by stirred with 2N sodium hydroxide (5.5 ml). Then free base (**3**) was extracted with diethyl ether (10 ml for 3 times), and dried over anhydrous sodium sulfate. The solution was then transfer into 50 ml reaction flask in ice bath. A diluted acetic anhydride (4 ml, 10 mmol, 4.00 equiv) in diethyl ether (15 ml) was added dropwise into a previous solution of 4-fluorophenylhydrazine. The mixture was stirred for 10-15 min. After that ice baht was removed and continually stirred for 10 min. The insoluble products were filtered and washed well with cooled diethyl ether. The precipitated product was then redissolved in ethyl acetate and wash with 2N sodium hydroxide, water and brine. The obtained solution was dried over anhydrous sodium sulfate and then concentrated. Purification by silica gel column chromatography (eluent:

ethyl acetate/*n*-hexane, 3:2) gave **6** (1,151 mg, 68.5%). Recrystallized with ethyl acetate/*n*-hexane gave light yellow solid; mp. 143-145 °C.

IR (KBr), ν_{max} , cm^{-1} (Figure 20): 3276 ($\nu_{\text{N-H}}$, monohydrazide), 3099 ($\nu_{\text{C-H}}$, aromatic), 2882, 2815 ($\nu_{\text{C-H}}$, aliphatic), 1664 ($\nu_{\text{C=O}}$, amide), 1576 ($\nu_{\text{C=C}}$, aromatic), 1224 ($\nu_{\text{C-F}}$, aromatic C-F).

$^1\text{H-NMR}$ (500MHz, $\text{DMSO-}d_6$), δ , ppm (Figure 21): 1.87 (*s*, 3H), 6.68 (*dd*, $J = 4.7, 9.0 \text{ Hz}$, 2H), 6.95 (*dd*, $J = 8.9, 8.9 \text{ Hz}$, 2H), 7.57 (*d*, $J = 3.0 \text{ Hz}$, 1H), 9.59 (*d*, $J = 3.0 \text{ Hz}$, 1H).

N'-phenylbenzohydrazide (**7**)

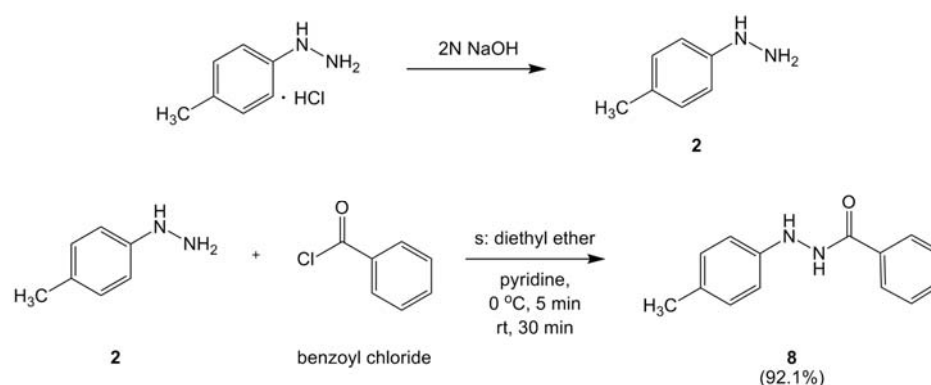


Diluted benzoyl chloride (1.52 g, 10.8 mmol, 1.08 equiv) in diethyl ether (2 ml) was slowly dropped into a mixture solution of phenylhydrazine (**1**) (1.08 mg, 10.00 mmol) and pyridine (800 mg, 10.11 mmol, 1.01 equiv) in diethyl ether (10 ml) with ice cooling. The mixture was stirred for 10-15 min. After that ice bath was removed and continually stirred for 10 min. The insoluble products were filtered and washed well with cooled diethyl ether. The precipitated product was then redissolved in ethyl acetate and wash with 2N sodium hydroxide, water and brine. The obtained solution was dried over anhydrous sodium sulfate and then concentrated to give **7** (2.29 g, quantitative). Recrystallized with dichloromethane/*n*-hexane gave white solid; mp. 165-167 °C.

IR (KBr), ν_{max} , cm^{-1} (Figure 22): 3246 ($\nu_{\text{N-H}}$, monohydrazide), 3054 ($\nu_{\text{C-H}}$, aromatic), 1647 ($\nu_{\text{C=O}}$, amide), 1578, 1496 ($\nu_{\text{C=C}}$, aromatic).

$^1\text{H-NMR}$ (500MHz, CDCl_3), δ , ppm (Figure 23): 4.34 (s, 1H), 6.71 (t, $J = 7.6$ Hz, 1H), 6.92 (d, $J = 7.3$ Hz, 2H), 7.22 (t, $J = 8.1$ Hz, 2H), 7.45 (t, $J = 7.6$ Hz, 2H), 7.54 (t, $J = 7.3$ Hz, 1H), 7.82 (d, $J = 6.8$ Hz, 2H), 8.04 (s, 1H).

***N*¹-*p*-tolylbenzohydrazide (**8**)**

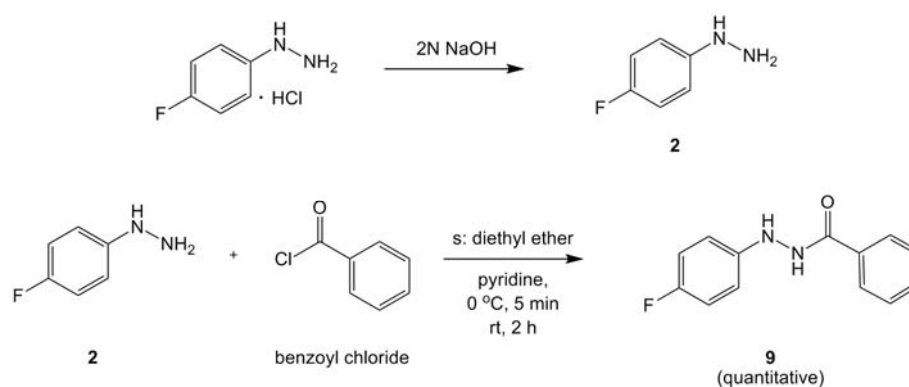


p-Tolylhydrazine hydrochloride (1.0 g, 6.30 mmol) was neutralized into free base by stirred with 2N sodium hydroxide (3.2 ml). Then free base (**2**) was extracted with diethyl ether (10 ml for 3 times), and dried over anhydrous sodium sulfate. The solution was then transfer into 100 ml reaction flask that contained pyridine (560 mg, 7.08 mmol, 1.12 equiv) in ice cooling. A diluted benzoyl chloride (905 mg, 6.44 mmol, 1.02 equiv) in diethyl ether (2 ml) was added dropwise into a previous mixture solution of *p*-tolylhydrazine and pyridine. The mixture was stirred for 5 min. After that ice bath was removed and continually stirred for 30 min. The mixture reaction was diluted in ethyl acetate and wash with, 2N hydrochloric acid, 2N sodium hydroxide, water and brine. The obtained solution was dried over anhydrous sodium sulfate and then concentrated. Purification by silica gel column chromatography (eluent: dichloromethane/*n*-hexane/ethyl acetate, 2:2:0.5) gave **8** (1.31 g, 92.1%). Recrystallized with ethyl acetate/*n*-hexane gave white solid; mp. 136-140 °C.

IR (KBr), ν_{max} , cm^{-1} (Figure 24): 3251 ($\nu_{\text{N-H}}$, monohydrazide), 3027 ($\nu_{\text{C-H}}$, aromatic), 2918, 2862 ($\nu_{\text{C-H}}$, aliphatic), 1647 ($\nu_{\text{C=O}}$, amide), 1597, 1512 ($\nu_{\text{C=C}}$, aromatic).

$^1\text{H-NMR}$ (500MHz, CDCl_3), δ , ppm (Figure 25): 2.24 (s, 3H), 4.28 (br, s, 1H), 6.83 (d, $J = 8.8$ Hz, 2H), 7.02 (d, $J = 8.3$ Hz, 2H), 7.44 (t, $J = 7.6$ Hz, 2H), 7.54 (t, $J = 7.3$ Hz, 1H), 7.81 (d, $J = 7.3$ Hz, 2H), 8.04 (br, s, 1H).

***N'*-(4-fluorophenyl)benzohydrazide (9)**

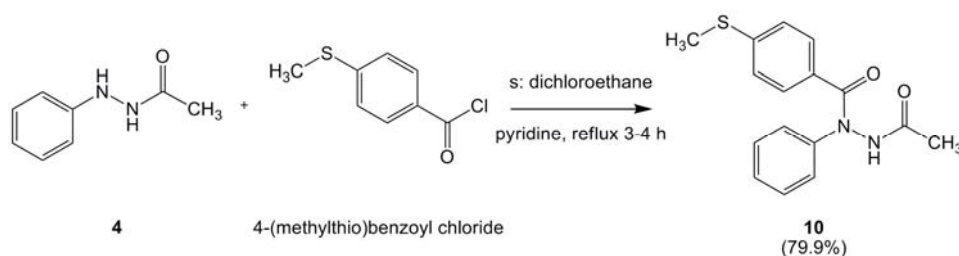


4-Fluorophenylhydrazine hydrochloride (1.0 g, 6.15 mmol) was neutralized into free base by stirred with 2N sodium hydroxide (3 ml). Then free base (3) was extracted with diethyl ether (10 ml, for 3 times), and dried over anhydrous sodium sulfate. The solution was transfer into 100 ml reaction flask that contained pyridine (1.03 g, 13.03 mmol, 2.12 equiv) in ice cooling. A diluted benzoyl chloride (970 mg, 6.90 mmol, 1.12 equiv) in diethyl ether (2 ml) was added dropwise into a previous mixture solution of *p*-tolylhydrazine and pyridine. The mixture was stirred for 5 min. After that ice baht was removed and continually stirred for 2 h. The mixture reaction was diluted in dichloromethane and wash with, 2N hydrochloric acid, 2N sodium hydroxide, water and brine. The obtained solution was dried over anhydrous sodium sulfate and then concentrated. Purification by silica gel column chromatography (eluent: dichloromethane/*n*-hexane/ethyl acetate, 2:2:0.5) gave **9** (1.50 g, quantitative). Recrystallized with ethyl acetate/*n*-hexane gave light yellow solid; mp. 140-144 °C.

IR (KBr), V_{max} , cm^{-1} (Figure 26): 3255 ($\text{V}_{\text{N-H}}$, monohydrazide), 3004 ($\text{V}_{\text{C-H}}$, aromatic), 1649 ($\text{V}_{\text{C=O}}$, amide), 1579, 1507($\text{V}_{\text{C=C}}$, aromatic).

$^1\text{H-NMR}$ (500MHz, CDCl_3), δ , ppm (Figure 27): 4.18 (br, s, 1H), 6.79 (dd, $J = 4.6, 9.0$ Hz, 2H), 6.98 (dd, $J = 8.5, 8.5$ Hz, 2H), 7.45 (t, $J = 7.6$ Hz, 2H), 7.55 (t, $J = 7.3$ Hz, 1H), 7.81 (d, $J = 7.8$ Hz, 2H), 8.04 (br, s, 1H).

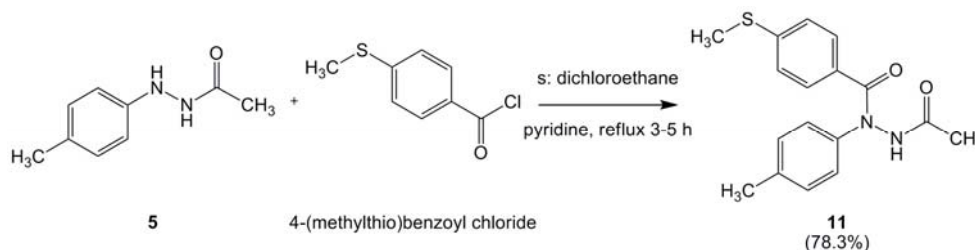
***N'*-acetyl-4-(methylthio)-*N*-phenylbenzohydrazide (10)**



To a solution of 4-(methylthio)benzoyl chloride (203 mg, 1.09 mmol, 1.08 equiv) in dichloroethane (5 ml) was added dropwise a mixture solution of *N'*-phenylacetohydrazide (**4**) (151 mg, 1.01 mmol) and pyridine (370 mg, 4.68 mmol, 4.29 equiv) in dichloroethane (5 ml). The mixture reaction was stirred and refluxed at 120 °C for 4 h. After cooling to room temperature, the excess solvent was removed using rotary evaporator. The crude mixture was extracted with dichloromethane (20 ml, twice times), washed well with 2N hydrochloric acid, 2N sodium hydroxide, water and brine, respectively. The collected organic phase was dried over anhydrous sodium sulfate and concentrated. Purification by silica gel column chromatography (eluent: dichloromethane/ethyl acetate, 3:1) gave **10** (240 mg, 79.9%). Recrystallized with ethyl acetate/diethyl ether gave white solid; mp. 126-129 °C.

IR (KBr), ν_{max} , cm^{-1} (Figure 28): 3258 ($\nu_{\text{N-H}}$, monohydrazide), 2993 ($\nu_{\text{C-H}}$, aliphatic), 1681 ($\nu_{\text{C=O}}$, 2° amide), 1660 ($\nu_{\text{C=O}}$, 3° amide), 1593, 1492 ($\nu_{\text{C=C}}$, aromatic).

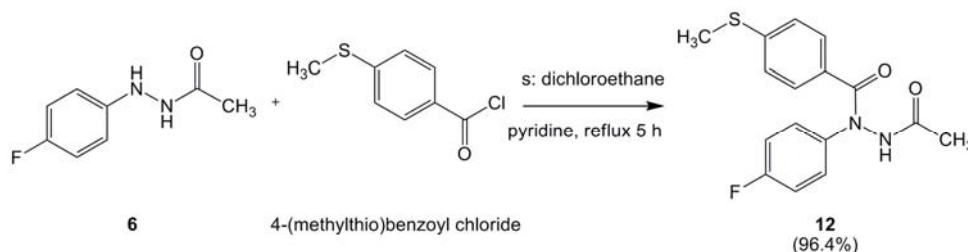
$^1\text{H-NMR}$ (500MHz, CDCl_3), δ , ppm (Figure 29): 2.20 (s, 3H), 2.40 (s, 3H), 7.02 (d, $J = 8.5$ Hz, 2H), 7.16 (t, $J = 6.8$ Hz, 2H), 7.17 (t, $J = 6.9$ Hz, 1H), 7.21 (d, $J = 7.5$ Hz, 2H), 7.35 (d, $J = 8.7$ Hz, 2H), 8.38 (s, 1H).

***N*¹-acetyl-4-(methylthio)-*N*-*p*-tolylbenzohydrazide (11)**

To a solution of 4-(methylthio)benzoyl chloride (273 mg, 1.46 mmol, 1.20 equiv) in dichloroethane (10 ml) was added dropwise a mixture solution of *N*¹-*p*-tolylacetohydrazide (**5**) (200 mg, 1.22 mmol) and pyridine (380 mg, 4.68 mmol, 4.80 equiv) in dichloroethane (10 ml). The mixture reaction was stirred and refluxed at 120 °C for 5 h. After cooling to room temperature, the excess solvent was removed using rotary evaporator. The crude mixture was extracted with dichloromethane (50 ml, three times), washed well with 2N hydrochloric acid, 2N sodium hydroxide, water and brine, respectively. The collected organic phase was dried over anhydrous sodium sulfate and concentrated. Purification by silica gel column chromatography (eluent: ethyl acetate/*n*-hexane, 1:1) gave **11** (300 mg, 78.3%). Recrystallized with ethyl acetate/*n*-hexane gave white solid; mp. 151-153 °C.

IR (KBr), ν_{max} , cm^{-1} (Figure 30): 3277 ($\nu_{\text{N-H}}$, monohydrazide), 3009 ($\nu_{\text{C-H}}$, aromatic), 2923 ($\nu_{\text{C-H}}$, aliphatic), 1683 ($\nu_{\text{C=O}}$, 2° amide), 1671 ($\nu_{\text{C=O}}$, 3° amide), 1593, 1508 ($\nu_{\text{C=C}}$, aromatic).

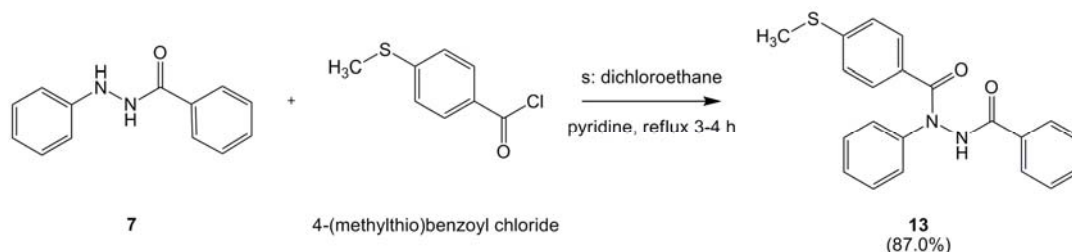
¹H-NMR (400MHz, Acetone-*d*₆), δ , ppm (Figure 31): 1.86 (*s*, 3H), 2.28 (*s*, 3H), 2.48 (*s*, 3H), 7.11 (*d*, *J* = 7.8 Hz, 2H), 7.19 (*d*, *J* = 8.8 Hz, 2H), 7.21 (*d*, *J* = 9.8 Hz, 2H), 7.45 (*d*, *J* = 8.3 Hz, 2H), 9.80 (*s*, 1H).

***N'*-acetyl-*N*-(4-fluorophenyl)-4-(methylthio)benzohydrazide (**12**)**

To a solution of 4-(methylthio)benzoyl chloride (494 mg, 2.64 mmol, 1.11 equiv) in dichloroethane (10 ml) was added dropwise a mixture solution of *N'*-(4-fluorophenyl)acetohydrazide (**6**) (400 mg, 2.38 mmol) and pyridine (752 mg, 9.51 mmol, 4.00 equiv) in dichloroethane (20 ml). The mixture reaction was stirred and refluxed at 120 °C for 5 h. After cooling to room temperature, the excess solvent was removed using rotary evaporator. The crude mixture was extracted with dichloromethane (50 ml, three times), washed well with 2N hydrochloric acid, 2N sodium hydroxide, water and brine, respectively. The collected organic phase was dried over anhydrous sodium sulfate and concentrated. Purification by silica gel column chromatography (eluent: ethyl acetate/*n*-hexane, 1:2) gave **12** (730 mg, 96.4%). Recrystallized with ethyl acetate/*n*-hexane gave white solid; mp. 139-140 °C.

IR (KBr), ν_{\max} , cm^{-1} (Figure 32): 3270 ($\nu_{\text{N-H}}$, monohydrazide), 3060 ($\nu_{\text{C-H}}$, aromatic), 3003 ($\nu_{\text{C-H}}$, aliphatic), 1672 ($\nu_{\text{C=O}}$, 2° and 3° amide), 1596, 1509 ($\nu_{\text{C=C}}$, aromatic).

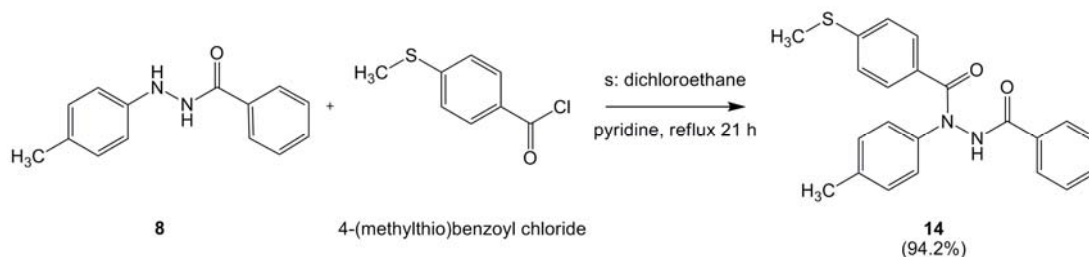
$^1\text{H-NMR}$ (400MHz, CDCl_3), δ , ppm (Figure 33): 2.03 (*s*, 3H), 2.42 (*s*, 3H), 6.91 (*dd*, $J = 8.5, 8.5$ Hz, 2H), 7.04 (*d*, $J = 8.3$ Hz, 2H), 7.19 (*dd*, $J = 4.9, 9.3$ Hz, 2H), 7.33 (*d*, $J = 8.8$ Hz, 2H), 8.19 (*s*, 1H).

***N'*-benzoyl-4-(methylthio)-*N*-phenylbenzohydrazide (13)**

To a solution of 4-(methylthio)benzoyl chloride (210 mg, 1.12 mmol, 1.08 equiv) in dichloroethane (5 ml) was added dropwise a mixture solution of *N'*-phenylbenzohydrazide (**7**) (220 mg, 1.04 mmol) and pyridine (345 mg, 4.36 mmol, 4.21 equiv) in dichloroethane (5 ml). The mixture reaction was stirred and refluxed at 120 °C for 4 h. After cooling to room temperature, the excess solvent was removed using rotary evaporator. The crude mixture was extracted with dichloromethane (20 ml, twice times), washed well with 2N hydrochloric acid, 2N sodium hydroxide, water and brine, respectively. The organic extract was dried over anhydrous sodium sulphate and concentrated. Purification by silica gel column chromatography (eluent: dichloromethane/*n*-hexane/ethyl acetate, 2:2:0.5) gave **13** (327 mg, 87.0%). Recrystallized with ethyl acetate/*n*-hexane/diethyl ether gave white solid; mp. 179-181 °C.

IR (KBr), ν_{\max} , cm^{-1} (Figure 34): 3276 ($\nu_{\text{N-H}}$, monohydrazide), 3062 ($\nu_{\text{C-H}}$, aromatic), 2921 ($\nu_{\text{C-H}}$, aliphatic), 1679 ($\nu_{\text{C=O}}$, 2° amide), 1655 ($\nu_{\text{C=O}}$, 3° amide), 1591, 1489 ($\nu_{\text{C=C}}$, aromatic).

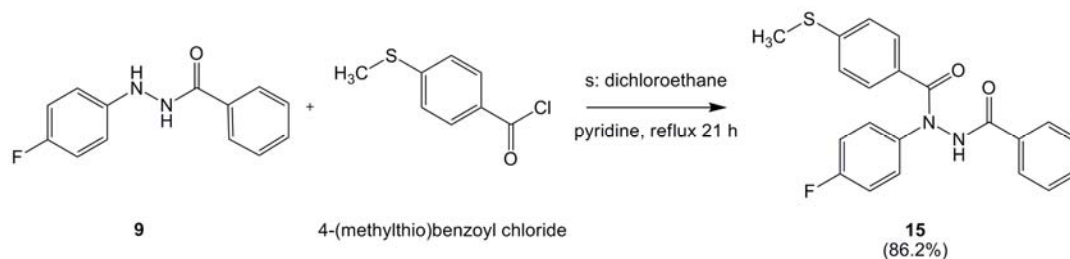
$^1\text{H-NMR}$ (400MHz, Acetone- d_6), δ , ppm (Figure 35): 2.46 (*s*, 3H), 7.19 (*d*, $J = 8.3$ Hz, 2H), 7.21 (*t*, $J = 7.3$ Hz, 1H), 7.35 (*t*, $J = 7.8$ Hz, 2H), 7.44 (*d*, $J = 10.2$ Hz, 2H), 7.46 (*t*, $J = 8.1$ Hz, 2H), 7.55 (*d*, $J = 8.3$ Hz, 2H), 7.56 (*t*, $J = 8.1$ Hz, 1H), 7.83 (*d*, $J = 7.3$ Hz, 2H), 10.57 (*s*, 1H).

***N'*-benzoyl-4-(methylthio)-*N-p*-tolylbenzohydrazide (14)**

To a solution of 4-(methylthio)benzoyl chloride (210 mg, 1.12 mmol, 1.11 equiv) in dichloroethane (5 ml) was added dropwise a mixture solution of *N'*-*p*-tolylbenzohydrazide (**8**) (230 mg, 1.02 mmol) and pyridine (340 mg, 4.30 mmol, 4.23 equiv) in dichloroethane (5 ml). The mixture reaction was stirred and refluxed at 120 °C for 5 h. After cooling to room temperature, the excess solvent was removed using rotary evaporator. The crude mixture was extracted with dichloromethane (30 ml, three times), washed well with 2N hydrochloric acid, 2N sodium hydroxide, water and brine, respectively. The organic extract was dried over anhydrous sodium sulphate and concentrated. Purification by silica gel column chromatography (eluent: dichloromethane) gave **14** (360 mg, 94.2%). Recrystallized with ethyl acetate/*n*-hexane/diethyl ether gave white solid; mp. 183-186 °C.

IR (KBr), ν_{max} , cm^{-1} (Figure 36): 3268 ($\nu_{\text{N-H}}$, monohydrazide), 3030 ($\nu_{\text{C-H}}$, aromatic), 2989, 2920 ($\nu_{\text{C-H}}$, aliphatic), 1686 ($\nu_{\text{C=O}}$, 2° amide), 1623 ($\nu_{\text{C=O}}$, 3° amide), 1594, 1508 ($\nu_{\text{C=C}}$, aromatic).

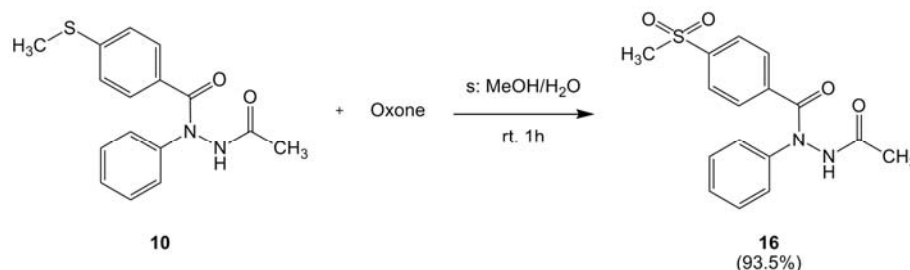
¹H-NMR (400MHz, CDCl₃), δ , ppm (Figure 37): 2.24 (s, 3H), 2.42 (s, 3H), 7.03 (d, $J = 7.8$ Hz, 2H), 7.04 (d, $J = 8.3$ Hz, 2H), 7.15 (d, $J = 8.3$ Hz, 2H), 7.37 (t, $J = 7.6$ Hz, 2H), 7.41 (d, $J = 8.3$ Hz, 2H), 7.47 (t, $J = 7.6$ Hz, 1H), 7.80 (d, $J = 7.3$ Hz, 2H), 8.94 (s, 1H).

***N'*-benzoyl-*N*-(4-fluorophenyl)-4-(methylthio)benzohydrazide (15)**

To a solution of 4-(methylthio)benzoyl chloride (210 mg, 1.12 mmol, 1.10 equiv) in dichloroethane (5 ml) was added dropwise a mixture solution of *N'*-(4-fluorophenyl)benzohydrazide (**9**) (235 mg, 1.02 mmol) and pyridine (345 mg, 4.36 mmol, 4.27 equiv) in dichloroethane (5 ml). The mixture reaction was stirred and refluxed at 120 °C for 5 h. After cooling to room temperature, the excess solvent was removed using rotary evaporator. The crude mixture was extracted with dichloromethane (30 ml, three times), washed with 2N hydrochloric acid, 2N sodium hydroxide, water and brine, respectively. The organic extract was dried over anhydrous sodium sulphate and concentrated. Purification by silica gel column chromatography (eluent: dichloromethane/*n*-hexane/ethyl acetate, 2:2:1) gave **15** (335 mg, 86.2%). Recrystallized with ethyl acetate/diethyl ether gave white solid; mp. 168-171 °C.

IR (KBr), ν_{max} , cm^{-1} (Figure 38): 3263 ($\nu_{\text{N-H}}$, monohydrazide), 3030 ($\nu_{\text{C-H}}$, aromatic), 2989, 2920 ($\nu_{\text{C-H}}$, aliphatic), 1687 ($\nu_{\text{C=O}}$, 2° amide), 1626 ($\nu_{\text{C=O}}$, 3° amide), 1599, 1506 ($\nu_{\text{C=C}}$, aromatic).

$^1\text{H-NMR}$ (400MHz, CDCl_3), δ , ppm (Figure 39): 2.42 (*s*, 3H), 6.92 (*dd*, $J = 8.5, 8.5$ Hz, 2H), 7.27 (*dd*, $J = 4.6, 9.0$ Hz, 2H), 7.05 (*d*, $J = 8.3$ Hz, 2H), 7.37 (*t*, $J = 7.8$ Hz, 2H), 7.38 (*d*, $J = 8.8$ Hz, 2H), 7.49 (*t*, $J = 7.6$ Hz, 1H), 7.78 (*d*, $J = 7.3$ Hz, 2H), 8.96 (*s*, 1H).

***N'*-acetyl-4-(methylsulfonyl)-*N*-phenylbenzohydrazide (**16**)**

To a solution of *N'*-acetyl-4-(methylthio)-*N*-phenylbenzohydrazide (**10**) (87 mg, 0.29 mmol) in methanol (3 ml) was added a solution of oxone[®] (390 mg, 0.63 mmol, 2.19 equiv) in water (3 ml). The mixture reaction was stirred at room temperature for 1 h. Then, the solvent was removed. The crude mixture was extracted with ethyl acetate (20 ml, three times), washed well with water and brine, respectively. The ethyl acetate extract was dried with anhydrous sodium sulfate and concentrated to give **16** (90 mg, 93.5%). Recrystallized with ethyl acetate gave white solid; mp. 209–210.5 °C.

IR (KBr), ν_{max} , cm^{-1} (Figure 40): 3235 ($\nu_{\text{N-H}}$, monohydrazide), 3017 ($\nu_{\text{C-H}}$, aromatic), 2920 ($\nu_{\text{C-H}}$, aliphatic), 1674 ($\nu_{\text{C=O}}$, 2° amide), 1664 ($\nu_{\text{C=O}}$, 3° amide), 1526, 1493 ($\nu_{\text{C=C}}$, aromatic), 1314, 1155 ($\nu_{\text{S=O}}$, sulfone).

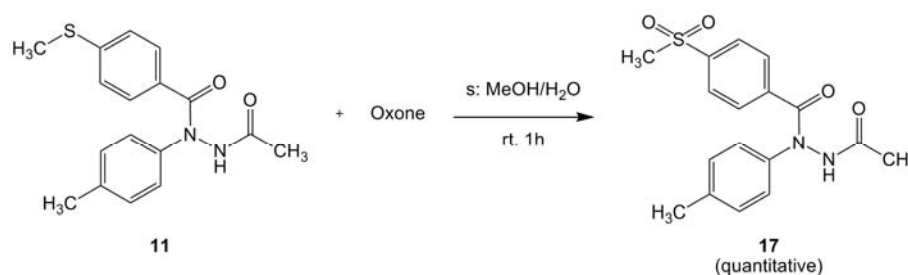
¹H-NMR (400MHz, DMSO-*d*₆, 90 °C), δ , ppm (Figure 41): 1.74 (s, 3H), 3.19 (s, 3H), 7.24 (t, $J = 6.6$ Hz, 1H), 7.35 (d, $J = 8.3$ Hz, 2H), 7.38 (t, $J = 7.3$ Hz, 2H), 7.72 (d, $J = 8.3$ Hz, 2H), 7.93 (d, $J = 8.3$ Hz, 2H), 10.7 (br, s, 1H).

¹³C-NMR (400MHz, DMSO-*d*₆, 90 °C), δ , ppm (Figure 42): 19.66, 43.06, 123.95, 126.00, 126.16, 127.68, 128.25, 140.07, 141.24, 141.80, 167.93, 168.23.

HR-MS (ESI) (Figure 43): Calcd. For C₁₆H₁₆N₂O₄S + Na: 355.072299. Found: 355.072618.

Anal. Calcd. for $C_{16}H_{16}N_2O_4S$: C 57.82; H 4.85; N 8.43. Found: C 57.64; H 4.88; N 8.37.

***N'*-acetyl-4-(methylsulfonyl)-*N-p*-tolylbenzohydrazide (**17**)**



To a solution of *N'*-acetyl-4-(methylthio)-*N-p*-tolylbenzohydrazide (**11**) (150 mg, 0.48 mmol) in methanol (2 ml) was added a solution of oxone[®] (650 mg, 1.06 mmol, 2.22 equiv) in water (5 ml). The mixture reaction was stirred at room temperature for 1 h. Then, the solvent was removed. The crude mixture was extracted with ethyl acetate (20 ml, three times), washed well with water and brine, respectively. The ethyl acetate extract was dried with anhydrous sodium sulfate and concentrated to give **17** (180 mg, quantitative). Recrystallized with ethyl acetate/*n*-hexane gave white solid; mp. 184 -185 °C.

IR (KBr), ν_{max} , cm^{-1} (Figure 44): 3259 (ν_{N-H} , monohydrazide), 3013 (ν_{C-H} , aromatic), 2927 (ν_{C-H} , aliphatic), 1681 ($\nu_{C=O}$, 2° and 3° amide), 1508 ($\nu_{C=C}$, aromatic), 1316, 1153 ($\nu_{S=O}$, sulfone).

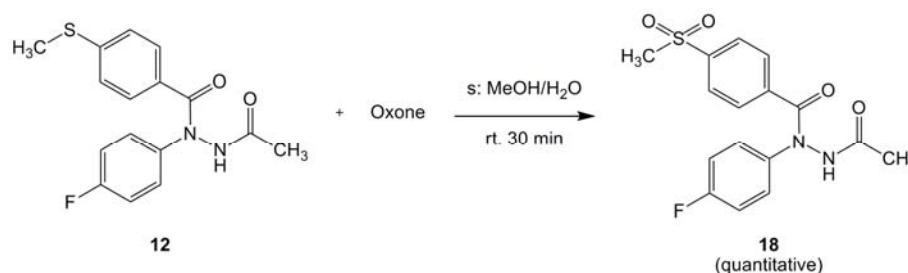
¹H-NMR (400MHz, CDCl₃, 52 °C), δ , ppm (Figure 45): 2.02 (s, 3H), 2.28 (s, 3H), 2.98 (s, 3H), 7.04 (d, $J = 7.8$ Hz, 2H), 7.09 (d, $J = 8.3$ Hz, 2H), 7.63 (d, $J = 7.8$ Hz, 2H), 7.80 (d, $J = 8.3$ Hz, 2H), 9.91 (br, s, 1H).

¹³C-NMR (400MHz, CDCl₃, 52 °C), δ , ppm (Figure 46): 20.79, 21.00, 44.31, 126.17, 127.13, 129.41, 129.97, 138.18, 139.39, 139.96, 142.20, 168.30, 169.42.

HR-MS (ESI) (Figure 47): Calcd. For $C_{17}H_{18}N_2O_4S + Na$: 369.087949. Found: 369.087992.

Anal. Calcd. for $C_{17}H_{18}N_2O_4S + 0.5H_2O$: C 57.45; H 5.39; N 7.88. Found: C 57.84; H 5.19; N 7.75.

***N'*-acetyl-*N*-(4-fluorophenyl)-4-(methylsulfonyl)benzohydrazide (**18**)**



To a solution of *N'*-acetyl-*N*-(4-fluorophenyl)-4-(methylthio)benzohydrazide (**12**) (318 mg, 1.00 mmol) in methanol (5 ml) was added a solution of oxone[®] (1,300 mg, 2.11 mmol, 2.11 equiv) in water (10 ml). The mixture reaction was stirred at room temperature for 1 h. Then, the solvent was removed. The crude mixture was extracted with ethyl acetate (40 ml, twice times), washed well with water and brine, respectively. The ethyl acetate extract was dried with anhydrous sodium sulfate and concentrated to give **18** (350 mg, quantitative). Recrystallized with ethyl acetate/*n*-hexane gave white solid; mp. 150 -153 °C.

IR (KBr), ν_{max} , cm^{-1} (Figure 48): 3231 ($\nu_{\text{N-H}}$, monohydrazide), 3017 ($\nu_{\text{C-H}}$, aromatic), 2920 ($\nu_{\text{C-H}}$, aliphatic), 1685 ($\nu_{\text{C=O}}$, 2° amide), 1664 ($\nu_{\text{C=O}}$, 3° amide), 1508 ($\nu_{\text{C=C}}$, aromatic), 1320, 1157 ($\nu_{\text{S=O}}$, sulfone).

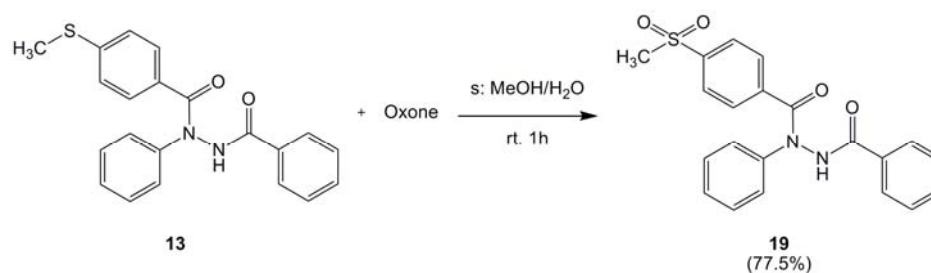
¹H-NMR (400MHz, DMSO-*d*₆, 90 °C), δ , ppm (Figure 49): 1.72 (*s*, 3H), 3.20 (*s*, 3H), 7.18 (*dd*, *J* = 8.8, 8.8 Hz, 2H), 7.43 (*dd*, *J* = 5.4, 7.8 Hz, 2H), 7.72 (*d*, *J* = 8.3 Hz, 2H), 7.94 (*d*, *J* = 7.8 Hz, 2H), 10.73 (*br, s*, 1H).

^{13}C -NMR (400MHz, DMSO- d_6 , 90 °C), δ , ppm (Figure 50): 19.70, 43.05, 114.82-115.05 (d , $J_{\text{F-C-C}} = 23.2$ Hz), 125.94, 126.24-126.33 (d , $J_{\text{F-C-C-C}} = 8.3$ Hz), 127.57, 137.44, 139.66, 141.74, 158.57-161.04 (d , $J_{\text{F-C}} = 247.9$ Hz), 167.89.

HR-MS (ESI) (Figure 51): Calcd. For $\text{C}_{16}\text{H}_{15}\text{FN}_2\text{O}_4\text{S} + \text{Na}$: 373.062877. Found: 373.062123.

Anal. Calcd. for $\text{C}_{16}\text{H}_{15}\text{FN}_2\text{O}_4\text{S}$: C 54.85; H 4.32; N 8.00. Found: C 54.84; H 4.37; N 7.75.

***N'*-benzoyl-4-(methylsulfonyl)-*N*-phenylbenzohydrazide (19)**



To a solution of *N'*-benzoyl-4-(methylthio)-*N*-phenylbenzohydrazide (**13**) (187 mg, 0.52 mmol) in methanol (15 ml) was added a solution of oxone[®] (700 mg, 1.14 mmol, 2.20 equiv) in water (3 ml). The mixture reaction was stirred at room temperature for 1 h. Then, solvent was removed. The crude mixture was extracted with ethyl acetate (20 ml, three times), washed well with water and brine, respectively. The ethyl acetate extract was dried with anhydrous sodium sulfate and concentrated. Purification by silica gel column chromatography (eluent: dichloromethane/ethyl acetate, 8:1) gave **19** (158 mg, 77.5%). Recrystallized with ethyl acetate/*n*-hexane gave white solid; mp. 133 –137 °C.

IR (KBr), ν_{max} , cm^{-1} (Figure 52): 3547, 3392 ($\nu_{\text{N-H}}$, monohydrazide), 2998, 2918 ($\nu_{\text{C-H}}$, aliphatic), 1683 ($\nu_{\text{C=O}}$, 2° amide), 1661 ($\nu_{\text{C=O}}$, 3° amide), 1595, 1491 ($\nu_{\text{C=C}}$, aromatic), 1307, 1149 ($\nu_{\text{S=O}}$, sulfone).

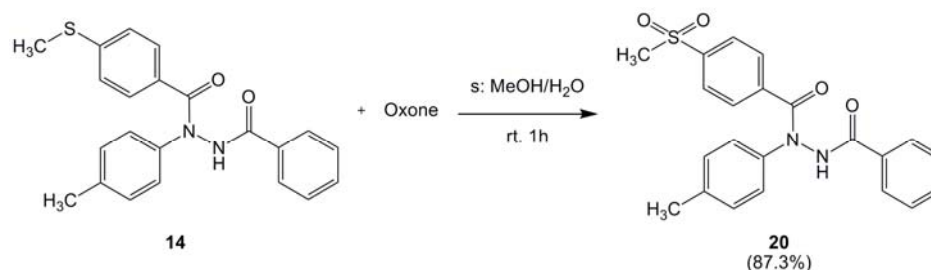
$^1\text{H-NMR}$ (400MHz, $\text{DMSO-}d_6$, 90°C), δ , ppm (Figure 53): 3.14 (s, 3H), 7.26 (t, $J = 7.3$ Hz, 1H), 7.40 (t, $J = 7.8$ Hz, 2H), 7.43 (t, $J = 7.8$ Hz, 2H), 7.49 (d, $J = 7.8$ Hz, 2H), 7.54 (t, $J = 7.3$ Hz, 1H), 7.65 (d, $J = 7.8$ Hz, 2H), 7.80 (d, $J = 8.3$ Hz, 2H), 7.92 (d, $J = 8.3$ Hz, 2H), 11.39 (br, s, 1H).

$^{13}\text{C-NMR}$ (400MHz, $\text{DMSO-}d_6$, 90°C), δ , ppm (Figure 54): 43.03, 125.96, 126.16, 126.69, 127.64, 127.98, 128.25, 131.38, 131.60, 139.97, 141.04, 141.71, 165.19.

HR-MS (ESI) (Figure 55): Calcd. For $\text{C}_{21}\text{H}_{18}\text{N}_2\text{O}_4\text{S} + \text{Na}$: 417.087949. Found: 417.087161.

Anal. Calcd. for $\text{C}_{21}\text{H}_{18}\text{N}_2\text{O}_4\text{S} + 1\text{H}_2\text{O}$: C 61.15; H 4.89; N 6.79. Found: C 61.26; H 4.93; N 6.85.

***N'*-benzoyl-4-(methylsulfonyl)-*N-p*-tolylbenzohydrazide (**20**)**



To a solution of *N'*-benzoyl-4-(methylthio)-*N-p*-tolylbenzohydrazide (**14**) (190 mg, 0.50 mmol) in methanol (15 ml) was added a solution of oxone[®] (680 mg, 1.11 mmol, 2.20 equiv) in water (3 ml). The mixture reaction was stirred at room temperature for 1 h. Then, solvent was removed. The crude mixture was extracted with ethyl acetate (20 ml, three times), washed well with water and brine, respectively. The ethyl acetate extract was dried with anhydrous sodium sulfate and concentrated. Purification by silica gel column chromatography (eluent: dichloromethane/ethyl acetate, 8:1) gave **20** (180 mg, 87.3%). Recrystallized with ethyl acetate/*n*-hexane gave white solid; mp. $202 - 204^\circ\text{C}$.

IR (KBr), ν_{max} , cm^{-1} (Figure 56): 3225 ($\nu_{\text{N-H}}$, monohydrazide), 3005 ($\nu_{\text{C-H}}$, aromatic), 2925 ($\nu_{\text{C-H}}$, aliphatic), 1686 ($\nu_{\text{C=O}}$, 2° amide), 1654 ($\nu_{\text{C=O}}$, 3° amide), 1509, 1489 ($\nu_{\text{C=C}}$, aromatic), 1314, 1153 ($\nu_{\text{S=O}}$, sulfone).

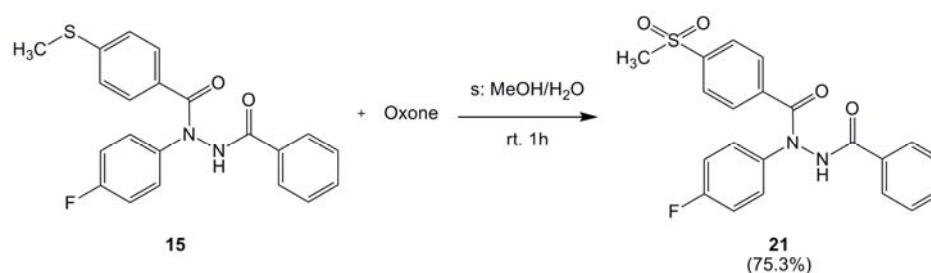
$^1\text{H-NMR}$ (400MHz, CDCl_3 , 50 °C), δ , ppm (Figure 57): 2.29 (s, 3H), 2.97 (s, 3H), 7.06 (d, $J = 8.3$ Hz, 2H), 7.19 (d, $J = 8.3$ Hz, 2H), 7.40 (t, $J = 7.8$ Hz, 2H), 7.52 (t, $J = 7.3$ Hz, 1H), 7.69 (d, $J = 8.3$ Hz, 2H), 7.76 (d, $J = 7.3$ Hz, 2H), 7.80 (d, $J = 8.8$ Hz, 2H), 8.62 (s, 1H).

$^{13}\text{C-NMR}$ (400MHz, CDCl_3 , 50 °C), δ , ppm (Figure 58): 20.99, 44.30, 126.12, 127.13, 127.43, 128.81, 129.42, 129.97, 131.80, 132.59, 138.13, 139.34, 140.04, 142.18, 167.00, 168.53.

HR-MS (ESI) (Figure 59): Calcd. For $\text{C}_{22}\text{H}_{20}\text{N}_2\text{O}_4\text{S} + \text{Na}$: 431.103599. Found: 431.102863.

Anal. Calcd. for $\text{C}_{22}\text{H}_{20}\text{N}_2\text{O}_4\text{S}$: C 64.69; H 4.94; N 6.86. Found: C 64.45; H 5.01; N 6.87.

***N'*-benzoyl-*N*-(4-fluorophenyl)-4-(methylsulfonyl)benzohydrazide (21)**



To a solution of *N'*-benzoyl-*N*-(4-fluorophenyl)-4-(methylthio)benzohydrazide (**15**) (190 mg, 0.50 mmol) in methanol (15 ml) was added a solution of oxone[®] (675 mg, 1.10 mmol, 2.19 equiv) in water (3 ml). The mixture reaction was stirred at room temperature for 1 h. Then, solvent was removed. The crude mixture was extracted with ethyl acetate (20 ml, three times), washed with water and brine, respectively. The ethyl acetate extract

was dried with anhydrous sodium sulfate and concentrated to give **21** (155 mg, 75.3%). Recrystallized with ethyl acetate/*n*-hexane gave white solid; mp. 171–174 °C.

IR (KBr), ν_{max} , cm^{-1} (Figure 60): 3344 ($\nu_{\text{N-H}}$, monohydrazide), 3036 ($\nu_{\text{C-H}}$, aromatic), 2936 ($\nu_{\text{C-H}}$, aliphatic), 1677 ($\nu_{\text{C=O}}$, 2° and 3° amide), 1507 ($\nu_{\text{C=C}}$, aromatic), 1308, 1153 ($\nu_{\text{S=O}}$, sulfone).

$^1\text{H-NMR}$ (400MHz, CDCl_3 , 50 °C), δ , ppm (Figure 61): 2.98 (s, 3H), 6.97 (dd, $J = 8.5, 8.5$ Hz, 2H), 7.34 (dd, $J = 4.6, 8.5$ Hz, 2H), 7.41 (t, $J = 7.8$ Hz, 2H), 7.53 (t, $J = 7.6$ Hz, 1H), 7.69 (d, $J = 8.3$ Hz, 2H), 7.73 (d, $J = 7.3$ Hz, 2H), 7.83 (d, $J = 8.8$ Hz, 2H), 8.63 (s, 1H).

$^{13}\text{C-NMR}$ (400MHz, CDCl_3 , 50 °C), δ , ppm (Figure 62): 44.31, 116.21-116.43 (d, $J_{\text{F-C}} = 22.3$ Hz), 127.28, 127.37, 128.23, 128.90, 129.25, 131.56, 132.83, 137.86, 139.76, 142.44, 160.52-163.00 (d, $J_{\text{F-C}} = 249.0$ Hz), 167.12.

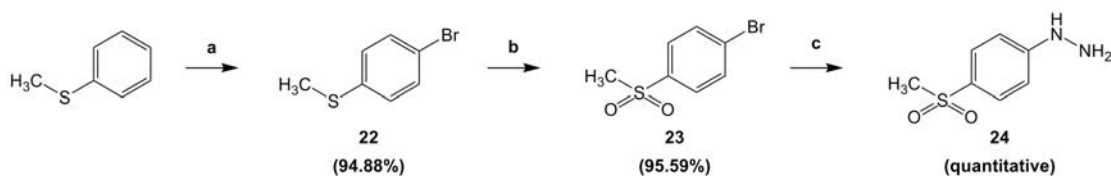
HR-MS (ESI) (Figure 63): Calcd. For $\text{C}_{21}\text{H}_{17}\text{FN}_2\text{O}_4\text{S} + \text{Na}$: 435.078527. Found: 435.078186.

Anal. Calcd. for $\text{C}_{21}\text{H}_{17}\text{FN}_2\text{O}_4\text{S} + \text{H}_2\text{O}$: C 58.60; H 4.45; N 6.51. Found: C 58.58; H 4.55; N 6.62.

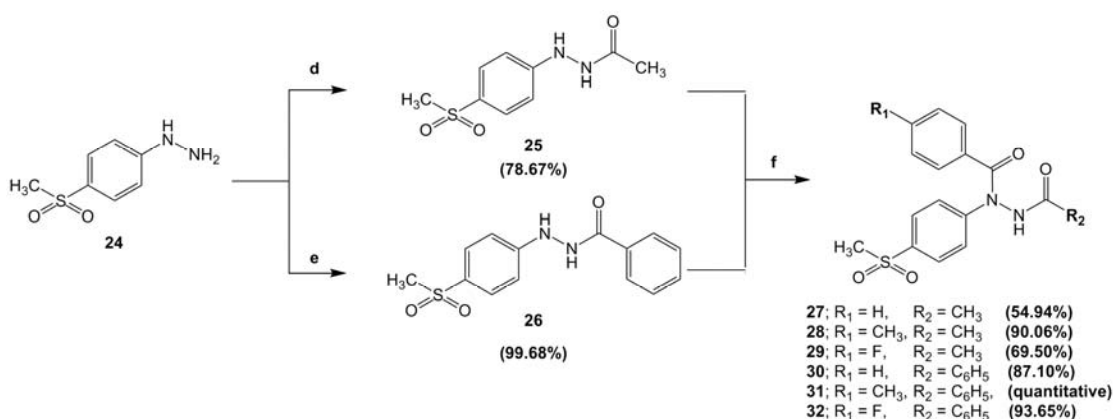
2.2.1.2 Synthesis of *N'*-Acyl-4-substituted-*N*-[4-(methylsulfonyl)phenyl]benzohydrazides (**27-32**)

In order to synthesize the designed *N'*-acyl-4-substituted-*N*-[4-(methylsulfonyl)phenyl]benzohydrazides (**27-32**), 4-(methylsulfonyl)phenylhydrazine (**24**) was first prepared from a three-step synthesis. Bromination of thioanisole, subsequent peroxymonosulfate oxidation of the obtained 4-bromothioanisole (**22**) and finally treating 4-bromomethylsulfone (**23**) with hydrazine under refluxed gave 4-(methylsulfonyl)phenylhydrazine (**24**) as starting material for next step in 90.7%. 4-(Methylsulfonyl)phenylhydrazine (**24**) was then allowed to react with acetic anhydride to prepare *N'*-(4-(methylsulfonyl)phenyl)acetohydrazide (**25**). Whereas *N'*-(4-

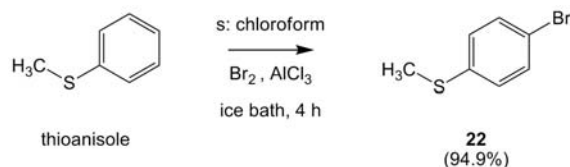
(methylsulfonyl) phenyl)benzohydrazide (**26**) was obtained by reacting 4-(methylsulfonyl)phenylhydrazine (**24**) benzoylation with benzoyl chloride. Finally, amidation of **25** or **26** with benzoyl chloride or *p*-substituted benzoyl chloride ($R_1 = \text{CH}_3$ and F), using same condition as previously described in the synthesis of *N*'-acetyl/benzoyl-4-(methylthio)-*N*-phenylbenzohydrazides (**10-15**), gave six target *N*'-acyl-4-substituted-*N*-[4-(methylsulfonyl)phenyl]benzohydrazides (**27-32**). All of synthesized compound were purified by suitable method such as solvent extraction, silica gel column chromatography and recrystallization. Their syntheses were concluded in scheme 2 and scheme 3. The synthesis of each compounds in detail were described as follows.



Scheme 2 Synthesis of 4-(methylsulfonyl)phenylhydrazine (**24**). Reagent: (a) Br_2 , AlCl_3 ; (b) Oxone[®], $\text{MeOH}/\text{H}_2\text{O}$; (c) 95% EtOH , $\text{NH}_2\text{NH}_2 \cdot \text{H}_2\text{O}$, reflux.



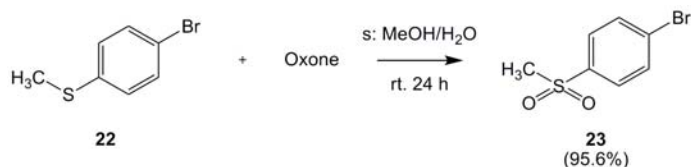
Scheme 3 Synthesis of *N*'-Acyl-4-substituted-*N*-[4-(methylsulfonyl)phenyl]benzohydrazides (**27-32**). Reagent: (a) acetic anhydride, $\text{CH}_2\text{Cl}_2/\text{MeOH}$; (b) benzoyl chloride, pyridine, CH_2Cl_2 ; (c) *p*-(substituted)benzoyl chloride ($R_1 = \text{H}$, CH_3 and F), pyridine, dichloroethane, reflux.

4-bromothioanisole (22)

Bromine (10 ml, 199.60 mmol, 1.17 equiv) was added dropwise into a mixture solution of thioanisole (20 ml, 170.20 mmol) and aluminium chloride (20mg, 0.15 mmol) in dry chloroform (20 ml) in ice bath. The mixture reaction was covered with guard tube that contained calcium chloride and stirred for 4 h. After the reaction was completed, saturated sodium metabisulfite ($\text{Na}_2\text{S}_2\text{O}_5$) was added to remove excess bromine until the mixture reaction became to light orange color. Then allowed the crude mixture to extract with chloroform (20 ml, twice times). Organic layer was washed well with 2N sodium hydroxide, water and brine, respectively. The collected organic extract was dried over anhydrous sodium sulfate and concentrated to give crude product as yellow semi-solid. 60% methanol was then added into crude product and the mixture was kept at $-20\text{ }^\circ\text{C}$ for 1 h. Filtered the precipitated products and subsequently washed the precipitate with cooled water gave 4-bromothioanisole, **22** as light yellow solid (32.8 g, 94.9%), mp. $38\text{ }^\circ\text{C}$.

IR (KBr), ν_{max} , cm^{-1} (Figure 64): 3036 ($\nu_{\text{C-H}}$, aromatic), 2917 ($\nu_{\text{C-H}}$, aliphatic), 1473, 1428, 1385 ($\nu_{\text{C-C}}$, aromatic), 750-570 (weak, $\nu_{\text{C-S}}$, methylthio), 480 ($\nu_{\text{C-Br}}$, aromatic bromine).

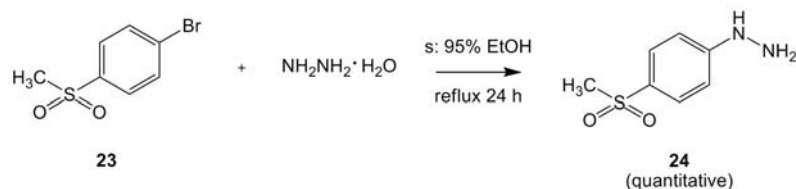
$^1\text{H-NMR}$ (500MHz, CDCl_3), δ , ppm (Figure 65): 2.43 (s, 3H), 7.09 (d, $J = 8.5\text{ Hz}$, 2H), 7.37 (d, $J = 8.5\text{ Hz}$, 2H).

4-bromomethylsulfone (23)

To a solution of 4-bromothioanisole (**22**) (5.2 g, 25.60 mmol) in methanol (35 ml) was added dropwise a solution of oxone[®] (60.95 g, 99.14 mmol, 3.87 equiv) in water (250 ml). The mixture reaction was stirred at room temperature for 24 h. When the reaction was completed, the solvent was removed using rotary evaporator. Filtered the precipitated product and washed well with water to remove unwanted inorganic salt gave **23** (5.81 g, 95.6%). Recrystallized with ethyl acetate/*n*-hexane gave white solid; mp. 101-103 °C.

IR (KBr), ν_{max} , cm⁻¹ (Figure 66): 3092, 3014 ($\nu_{\text{C-H}}$, aromatic), 2919 ($\nu_{\text{C-H}}$, aliphatic), 1573, 1465 ($\nu_{\text{C-C}}$, aromatic), 1308, 1147 ($\nu_{\text{S=O}}$, sulfone), 555 ($\nu_{\text{C-Br}}$, aromatic bromine).

¹H-NMR (500MHz, CDCl₃), δ , ppm (Figure 67): 3.02 (s, 3H), 7.69 (d, $J = 8.5$ Hz, 2H), 7.78 (d, $J = 8.6$ Hz, 2H).

(4-(methylsulfonyl)phenyl)hydrazine (24)

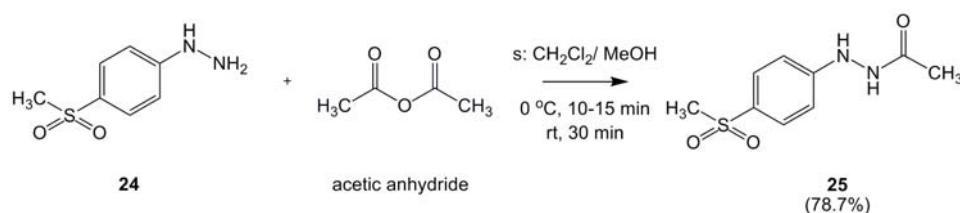
Hydrazine monohydrate (3.5 ml, 72.15 mmol, 17.0 equiv) was added dropwise into a solution of 4-bromomethylsulfone (**23**) (1.0 g, 4.25 mmol) in 95% ethanol (20 ml). The mixture reaction was stirred and reflux for 24 h. When the reaction was completed, allowed it to room temperature and then the solvent was removed using rotary evaporator. The crude mixture

was extracted with ethyl acetate (20 ml, twice times). Organic layer was washed well with water and brine, respectively. The collected organic extract was dried over anhydrous sodium sulfate and concentrated gave **24** (890 mg, quantitative). Recrystallized with ethyl acetate/*n*-hexane gave white solid; mp. 124-127 °C .

IR (KBr), ν_{max} , cm^{-1} (Figure 68): 3324 ($\nu_{\text{N-H}}$, monohydrazide), 3017, 3002 ($\nu_{\text{C-H}}$, aromatic), 2921 ($\nu_{\text{C-H}}$, aliphatic), 1596 ($\nu_{\text{C=C}}$, aromatic), 1322, 1137 ($\nu_{\text{S=O}}$, sulfone), 1269 ($\nu_{\text{C-N}}$, aromatic hydrazine).

$^1\text{H-NMR}$ (500MHz, $\text{DMSO-}d_6$), δ , ppm (Figure 69): 4.21 (*s*, 2*H*), 3.02 (*s*, 3*H*), 6.83 (*d*, $J = 8.7$ Hz, 2*H*), 7.55 (*d*, $J = 8.7$ Hz, 2*H*), 7.67 (*s*, 1*H*).

***N*'**-(4-(methylsulfonyl)phenyl)acetohydrazide (**25**)

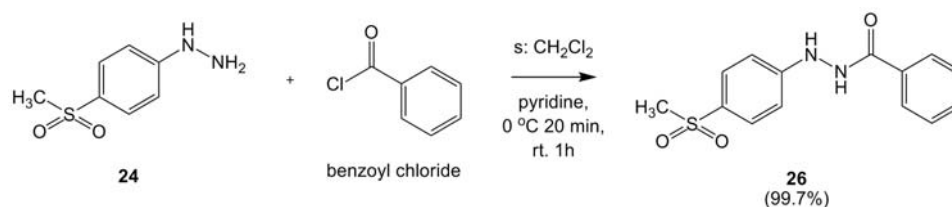


Acetic anhydride (2.00 ml, 21.14 mmol, 3.51 equiv) was slowly dropped into a solution of **24** (1,120 mg, 6.01 mmol) in dichloromethane (22 ml) and methanol (3 ml). The mixture was stirred for 10-15 min. After that ice bath was removed and continually stirred for 30 min. When the reaction was completed, added the water to dilute some acid. The insoluble products were filtered and washed well with cooled diethyl ether. The filtrate was extracted with dichloromethane (20 ml, twice times). The organic layer was allowed to wash well with water and brine. The dichloromethane extract was dried over anhydrous sodium sulfate and concentrated. Collected the obtained products together with previous precipitated products total gained **25** (1,080 mg, 78.7%). Recrystallized with ethyl acetate/methanol/*n*-hexane gave white solid; mp. 175-178 °C.

IR (KBr), ν_{\max} , cm^{-1} (Figure 70): 3327, 3216, ($\nu_{\text{N-H}}$, monohydrazide), 3019 ($\nu_{\text{C-H}}$, aromatic), 2929 ($\nu_{\text{C-H}}$, aliphatic), 1664 ($\nu_{\text{C=O}}$, amide), 1605, 1563, 1499 ($\nu_{\text{C-C}}$, aromatic), 1283, 1133 ($\nu_{\text{S=O}}$, sulfone).

$^1\text{H-NMR}$ (500MHz, $\text{DMSO-}d_6$), δ , ppm (Figure 71): 1.91 (*s*, 3H), 3.06 (*s*, 3H), 6.78 (*d*, $J = 8.8$ Hz, 2H), 7.63 (*d*, $J = 8.8$ Hz, 2H), 8.49 (*d*, $J = 1.5$ Hz, 1H), 9.77 (*d*, $J = 1.6$ Hz, 1H).

***N'*-(4-(methylsulfonyl)phenyl)benzohydrazide (26)**

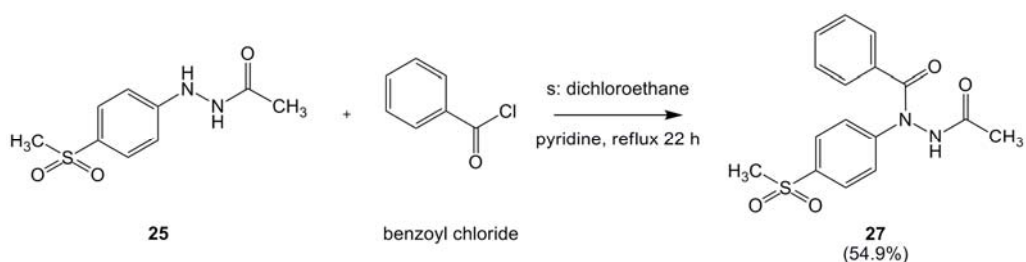


Diluted benzoyl chloride (595 mg, 4.23 mmol, 1.06 equiv) in dichloromethane (2 ml) was slowly dropped into a mixture solution of **24** (740 mg, 3.97 mmol) and pyridine (340 mg, 4.30 mmol, 1.08 equiv) in dichloromethane (5 ml). The mixture was stirred for 20 min. After that ice bath was removed and continually stirred for 1 h. Then, the insoluble products were filtered to collect and washed well with *n*-hexane. The filtrate was extracted with dichloromethane (20 ml, twice times). The organic layer was allowed to wash well with water and brine. The dichloromethane extract was dried over anhydrous sodium sulfate and concentrated. Collected the obtained products and previous precipitated products together gained total **26** (1,150 mg, 99.7%). Recrystallized with dichloromethane/methanol/*n*-hexane gave white solid; mp. 206-208.5 °C.

IR (KBr), ν_{\max} , cm^{-1} (Figure 72): 3302 ($\nu_{\text{N-H}}$, monohydrazide), 2996, 2917 ($\nu_{\text{C-H}}$, aliphatic), 1668 ($\nu_{\text{C=O}}$, amide), 1596 ($\nu_{\text{C-C}}$, aromatic), 1279, 1142 ($\nu_{\text{S=O}}$, sulfone).

$^1\text{H-NMR}$ (500MHz, $\text{DMSO-}d_6$), δ , ppm (Figure 73): 3.07 (s, 3H), 6.88 (d, $J = 8.8$ Hz, 2H), 7.52 (t, $J = 7.7$ Hz, 2H), 7.59 (t, $J = 7.4$ Hz, 1H), 7.67 (d, $J = 8.8$ Hz, 2H), 7.92 (d, $J = 7.2$ Hz, 2H), 8.75 (s, 1H), 10.51 (s, 1H).

***N'*-acetyl-*N*-(4-(methylsulfonyl)phenyl)benzohydrazide (27)**



To a solution of benzoyl chloride (205 mg, 1.46 mmol, 1.11 equiv) in dichloroethane (2 ml) was added dropwise a mixture solution of **25** (300 mg, 1.31 mmol) and pyridine (420 mg, 5.31 mmol, 4.04 equiv) in dichloroethane (20 ml). The mixture reaction was stirred and refluxed for 22 h. When the reaction was completed, allowed it to room temperature. Then solvent was removed using rotary evaporator. The crude mixture was extracted with dichloromethane (20 ml, twice times) and washed well with 2N hydrochloric acid, 2N sodium hydroxide, water and brine, respectively. The organic extract was dried over anhydrous sodium sulfate and concentrated. Purification by silica gel column chromatography (eluent: ethyl acetate/*n*-hexane, 2:1) gave **27** (240 mg, 54.9%). Recrystallized with ethyl acetate/*n*-hexane gave white solid; mp. 181-184 °C.

IR (KBr), ν_{max} , cm^{-1} (Figure 74): 3320 ($\nu_{\text{N-H}}$, monohydrazide), 3069, 3017, 3000 ($\nu_{\text{C-H}}$, aromatic), 2921 ($\nu_{\text{C-H}}$, aliphatic), 1707 ($\nu_{\text{C=O}}$, 2° amide), 1682 ($\nu_{\text{C=O}}$, 3° amide), 1588, 1491 ($\nu_{\text{C=C}}$, aromatic), 1298, 1147 ($\nu_{\text{S=O}}$, sulfone).

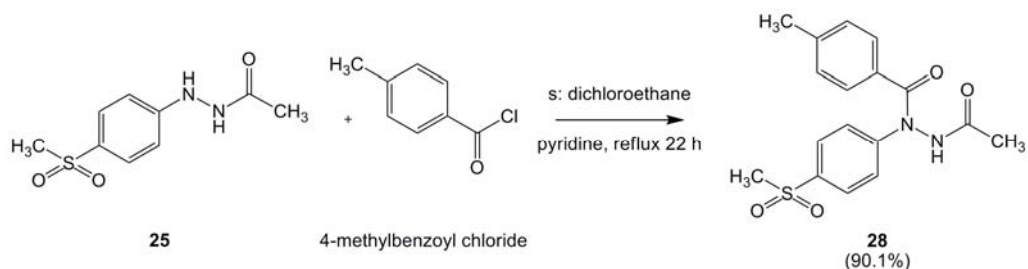
$^1\text{H-NMR}$ (400MHz, CDCl_3), δ , ppm (Figure75): 1.92 (s, 3H), 3.00 (s, 3H), 7.32 (t, $J = 7.6$ Hz, 2H), 7.36 (d, $J = 8.8$ Hz, 2H), 7.42 (t, $J = 7.6$ Hz, 1H), 7.51 (d, $J = 7.3$ Hz, 2H), 7.69 (d, $J = 8.8$ Hz, 2H), 8.59 (s, 1H).

^{13}C -NMR (400MHz, CDCl_3), δ , ppm (Figure 76): 20.67, 44.60, 124.11, 128.00, 128.06, 128.26, 131.23, 133.77, 136.98, 146.61, 169.43, 170.50.

HR-MS (ESI) (Figure 77): Calcd. For $\text{C}_{16}\text{H}_{16}\text{N}_2\text{O}_4\text{S} + \text{Na}$: 355.072299. Found: 355.072134.

Anal. Calcd. for $\text{C}_{16}\text{H}_{16}\text{N}_2\text{O}_4\text{S}$: C 57.82; H 4.85; N 8.43. Found: C 57.60; H 4.97; N 8.46.

***N'*-acetyl-4-methyl-*N*-(4-(methylsulfonyl)phenyl)benzohydrazide (**28**)**



To a solution of 4-methylbenzoyl chloride (230 mg, 1.49 mmol, 1.13 equiv) in dichloroethane (2 ml) was added dropwise a mixture solution of **25** (300 mg, 1.31 mmol) and pyridine (420 mg, 5.31 mmol, 4.04 equiv) in dichloroethane (20 ml). The mixture reaction was stirred and refluxed for 22 h. When the reaction was completed, allowed it to room temperature. Then solvent was removed using rotary evaporator. The crude mixture was extracted with dichloromethane (20 ml, twice times) and washed well with 2N hydrochloric acid, 2N sodium hydroxide, water and brine, respectively. The organic extract was dried over anhydrous sodium sulfate and concentrated. Purification by silica gel column chromatography (eluent: ethyl acetate/*n*-hexane, 2:1) gave **28** (410 mg, 90.1%). Recrystallized with ethyl acetate/*n*-hexane gave white solid, melting point 180-183 °C.

IR (KBr), ν_{max} , cm^{-1} (Figure 78): 3297 ($\nu_{\text{N-H}}$, monohydrazide), 3003 ($\nu_{\text{C-H}}$, aromatic), 2926 ($\nu_{\text{C-H}}$, aliphatic), 1701 ($\nu_{\text{C=O}}$, 2° amide), 1654 ($\nu_{\text{C=O}}$, 3° amide), 1589, 1490 ($\nu_{\text{C=C}}$, aromatic), 1307, 1149 ($\nu_{\text{S=O}}$, sulfone)

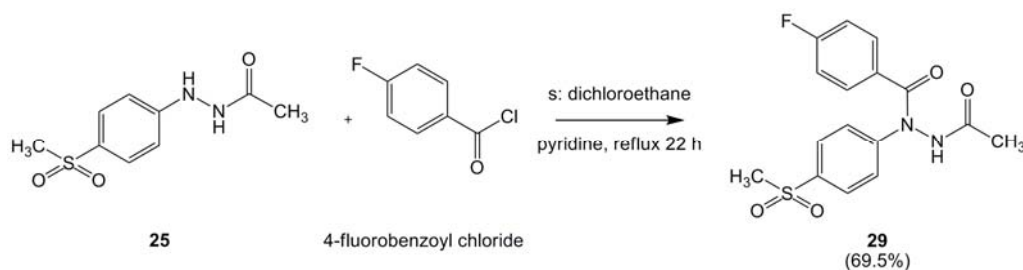
$^1\text{H-NMR}$ (400MHz, CDCl_3), δ , ppm (Figure 79): 1.61 (s, 3H), 2.33 (s, 3H), 3.00 (s, 3H), 7.10 (d, $J = 7.8$ Hz, 2H), 7.33 (d, $J = 8.8$ Hz, 2H), 7.39 (d, $J = 8.3$ Hz, 2H), 7.71 (d, $J = 8.8$ Hz, 2H), 8.44 (s, 1H).

$^{13}\text{C-NMR}$ (400MHz, CDCl_3), δ , ppm (Figure 80): 20.79, 21.61, 44.59, 124.48, 128.07, 128.45, 128.98, 130.52, 137.16, 141.98, 147.07, 169.63, 170.22.

HR-MS (ESI) (Figure 81): Calcd. For $\text{C}_{17}\text{H}_{18}\text{N}_2\text{O}_4\text{S} + \text{Na}$: 369.087949. Found: 369.088721.

Anal. Calcd. for $\text{C}_{17}\text{H}_{18}\text{N}_2\text{O}_4\text{S}$: C 58.94; H 5.24; N 8.09. Found: C 57.97; H 5.15; N 7.93.

***N'*-acetyl-4-fluoro-*N*-(4-(methylsulfonyl)phenyl)benzohydrazide (**29**)**



To a solution of 4-fluorobenzoyl chloride (230 mg, 1.45 mmol, 1.10 equiv) in dichloroethane (2 ml) was added dropwise a mixture solution of **25** (300 mg, 1.31 mmol) and pyridine (420 mg, 5.31 mmol, 4.04 equiv) in dichloroethane (20 ml). The mixture reaction was stirred and refluxed for 22 h. When the reaction was completed, allowed it to room temperature. Then solvent was removed using rotary evaporator. The crude mixture was extracted with dichloromethane (20 ml, twice times) and washed well with 2N hydrochloric acid, 2N sodium hydroxide, water and brine, respectively. The organic extract was dried over anhydrous sodium sulfate and concentrated. Purification by silica gel column chromatography (eluent: ethyl acetate/*n*-hexane, 2:1) gave **29** (320 mg, 69.5%). Recrystallized with ethyl acetate/*n*-hexane gave white solid, melting point 175-180 °C.

IR (KBr), ν_{max} , cm^{-1} (Figure 82): 3358 ($\nu_{\text{N-H}}$, monohydrazide), 3075, 3010 ($\nu_{\text{C-H}}$, aromatic), 2917 ($\nu_{\text{C-H}}$, aliphatic), 1698 ($\nu_{\text{C=O}}$, 2° amide), 1681 ($\nu_{\text{C=O}}$, 3° amide), 1510, 1489 ($\nu_{\text{C=C}}$, aromatic), 1300, 1148 ($\nu_{\text{S=O}}$, sulfone).

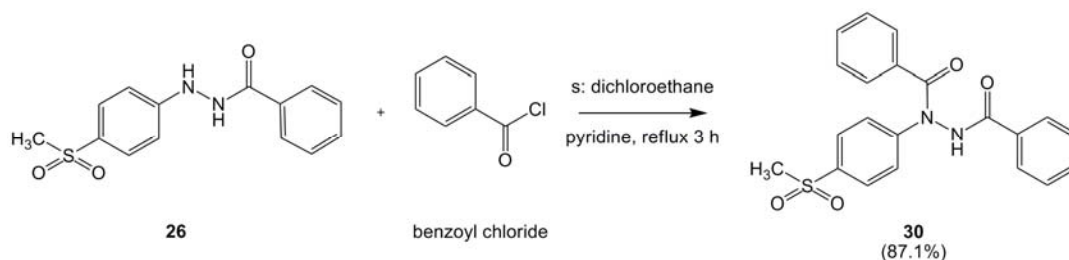
$^1\text{H-NMR}$ (400MHz, CDCl_3), δ , ppm (Figure 83): 1.98 (s, 3H), 3.01 (s, 3H), 7.02 (dd, $J = 8.5, 8.5$ Hz, 2H), 7.34 (d, $J = 8.8$ Hz, 2H), 7.56 (dd, $J = 5.4, 8.8$ Hz, 2H), 7.71 (d, $J = 9.3$ Hz, 2H), 8.41 (s, 1H).

$^{13}\text{C-NMR}$ (400MHz, CDCl_3), δ , ppm (Figure 84): 20.69, 44.61, 115.41-115.63 (d, $J_{\text{F-C-C}} = 22.0$ Hz), 124.04, 128.06, 130.63, 130.72, 137.04, 146.55, 162.92-165.46 (d, $J_{\text{F-C}} = 255.0$ Hz), 169.38, 169.48.

HR-MS (ESI) (Figure 85): Calcd. For $\text{C}_{16}\text{H}_{15}\text{FN}_2\text{O}_4\text{S} + \text{Na}$: 373.062877. Found: 373.062530.

Anal. Calcd. for $\text{C}_{16}\text{H}_{15}\text{FN}_2\text{O}_4\text{S}$: C 54.85; H 4.32; N 8.00. Found: C 54.66; H 4.39; N 8.01.

***N'*-benzoyl-*N*-(4-(methylsulfonyl)phenyl)benzohydrazide (30)**



To a solution of benzoyl chloride (160 mg, 1.34 mmol, 1.10 equiv) in dichloroethane (2 ml) was added dropwise a mixture solution of **26** (300 mg, 1.03 mmol) and pyridine (330 mg, 4.17 mmol, 4.04 equiv) in dichloroethane (12 ml). The mixture reaction was stirred and refluxed for 3 h. When the reaction was completed, allowed it to room temperature. Then solvent was removed using rotary evaporator. The crude mixture was extracted with dichloromethane (20 ml, twice times) and washed well with 2N hydrochloric acid, 2N sodium

hydroxide, water and brine, respectively. The organic extract was dried over anhydrous sodium sulfate and concentrated. Purification by silica gel column chromatography (eluent: dichloromethane/ethyl acetate, 6:1) gave **30** (355 mg, 87.1%). Recrystallized with ethyl acetate/*n*-hexane gave white solid; mp. 199-202 °C.

IR (KBr), ν_{max} , cm^{-1} (Figure 86): 3262 ($\nu_{\text{N-H}}$, monohydrazide), 3004 ($\nu_{\text{C-H}}$, aromatic), 2924 ($\nu_{\text{C-H}}$, aliphatic), 1690 ($\nu_{\text{C=O}}$, 2° amide), 1657 ($\nu_{\text{C=O}}$, 3° amide), 1592, 1488 ($\nu_{\text{C=C}}$, aromatic), 1291, 1147 ($\nu_{\text{S=O}}$, sulfone).

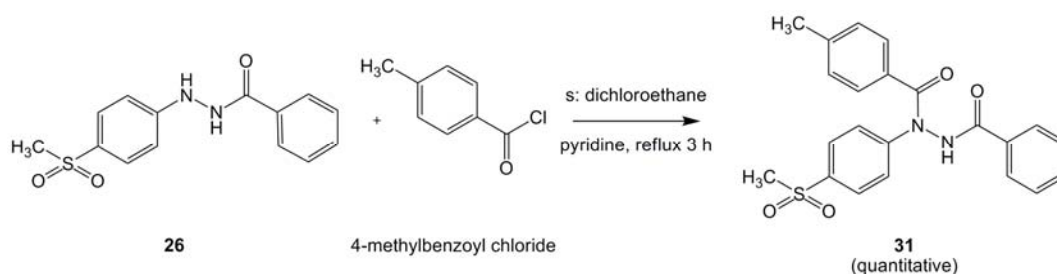
$^1\text{H-NMR}$ (400MHz, CDCl_3), δ , ppm (Figure 87): 3.00 (s, 3H), 7.30 (t, $J = 7.6$ Hz, 2H), 7.38 (m, 1H), 7.40 (t, $J = 7.8$ Hz, 2H), 7.43 (d, $J = 8.8$ Hz, 2H), 7.52 (t, $J = 7.3$ Hz, 1H), 7.57 (d, $J = 6.8$ Hz, 2H), 7.70 (d, $J = 8.3$ Hz, 2H), 7.71 (d, $J = 8.8$ Hz, 2H), 9.13 (s, 1H).

$^{13}\text{C-NMR}$ (400MHz, CDCl_3), δ , ppm (Figure 88): 44.62, 124.13, 127.29, 128.08, 128.13, 128.28, 128.79, 131.05, 131.25, 132.73, 133.81, 137.02, 146.63, 166.74, 170.66.

HR-MS (ESI) (Figure 89): Calcd. For $\text{C}_{21}\text{H}_{18}\text{N}_2\text{O}_4\text{S} + \text{Na}$: 417.087949. Found: 417.088171.

Anal. Calcd. for $\text{C}_{21}\text{H}_{18}\text{N}_2\text{O}_4\text{S}$: C 63.94; H 4.60; N 7.10. Found: C 63.75; H 4.72; N 7.09.

***N*'-benzoyl-4-methyl-*N*-(4-(methylsulfonyl)phenyl)benzohydrazide (31)**



To a solution of 4-methylbenzoyl chloride (175 mg, 1.13 mmol, 1.10 equiv) in dichloroethane (4 ml) was added dropwise a mixture solution of **26** (300 mg, 1.03 mmol) and pyridine (330 mg, 4.17 mmol, 4.04 equiv) in dichloroethane (12 ml). The mixture reaction was stirred and refluxed for 3 h. When the reaction was completed, allowed it to room temperature. Then solvent was removed using rotary evaporator. The crude mixture was extracted with dichloromethane (20 ml, twice times) and washed well with 2N hydrochloric acid, 2N sodium hydroxide, water and brine, respectively. The organic extract was dried over anhydrous sodium sulfate and concentrated. Purification by silica gel column chromatography (eluent: dichloromethane/ethyl acetate, 6:1) gave **31** (423 mg, quantitative). Recrystallized with ethyl acetate/*n*-hexane gave white solid, melting point 211-213 °C.

IR (KBr), ν_{\max} , cm^{-1} (Figure 90): 3380 ($\nu_{\text{N-H}}$, monohydrazide), 3082, 3017 ($\nu_{\text{C-H}}$, aromatic), 2925 ($\nu_{\text{C-H}}$, aliphatic), 1690 ($\nu_{\text{C=O}}$, 2° amide), 1674 ($\nu_{\text{C=O}}$, 3° amide), 1592, 1473 ($\nu_{\text{C=C}}$, aromatic), 1282, 1145 ($\nu_{\text{S=O}}$, sulfone).

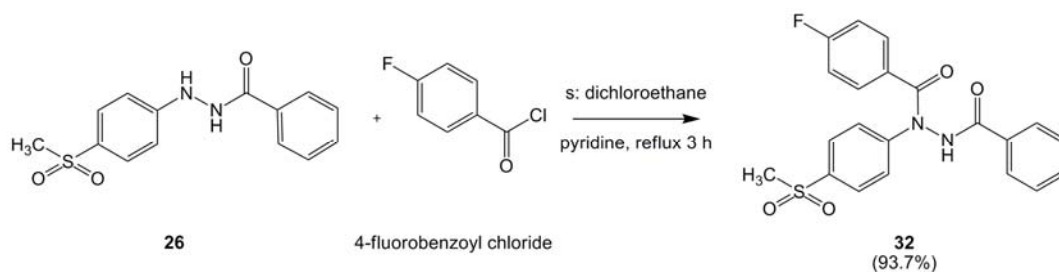
$^1\text{H-NMR}$ (400MHz, CDCl_3), δ , ppm (Figure 91): 2.31 (s, 3H), 3.00 (s, 3H), 7.09 (d, $J = 7.8$ Hz, 2H), 7.40 (d, $J = 6.8$ Hz, 2H), 7.41 (d, $J = 8.3$ Hz, 2H), 7.44 (d, $J = 7.8$ Hz, 2H), 7.52 (t, $J = 7.6$ Hz, 1H), 7.73 (t, $J = 8.3$ Hz, 2H), 7.72 (d, $J = 8.3$ Hz, 2H), 9.08 (s, 1H).

$^{13}\text{C-NMR}$ (400MHz, CDCl_3), δ , ppm (Figure 92): 21.60, 44.60, 124.45, 127.35, 128.12, 128.50, 128.78, 128.99, 130.57, 131.13, 132.71, 137.09, 141.99, 147.04, 166.86, 170.45.

HR-MS (ESI) (Figure 93): Calcd. For $\text{C}_{22}\text{H}_{20}\text{N}_2\text{O}_4\text{S} + \text{Na}$: 431.103599. Found: 431.103479.

Anal. Calcd. for $\text{C}_{22}\text{H}_{20}\text{N}_2\text{O}_4\text{S}$: C 64.69; H 4.94; N 6.86. Found: C 64.46; H 5.23; N 6.79.

***N*'-benzoyl-4-fluoro-*N*-(4-(methylsulfonyl)phenyl)benzohydrazide (**32**)**



To a solution of 4-fluorobenzoyl chloride (360 mg, 2.26 mmol, 2.20 equiv) in dichloroethane (4 ml) was added dropwise a mixture solution of **26** (300 mg, 1.03 mmol) and pyridine (330 mg, 4.17 mmol, 4.04 equiv) in dichloroethane (12 ml). The mixture reaction was stirred and refluxed for 3 h. When the reaction was completed, allowed it to room temperature. Then solvent was removed using rotary evaporator. The crude mixture was extracted with dichloromethane (20 ml, twice times) and washed well with 2N hydrochloric acid, 2N sodium hydroxide, water and brine, respectively. The organic extract was dried over anhydrous sodium sulfate and concentrated. Purification by silica gel column chromatography (eluent: dichloromethane/ethyl acetate, 6:1) gave **32** (399 mg, 93.7%). Recrystallized with ethyl acetate/*n*-hexane gave white solid; mp.141-143 °C.

IR (KBr), ν_{max} , cm^{-1} (Figure 94): 3244 ($\nu_{\text{N-H}}$, monohydrazide), 2988 ($\nu_{\text{C-H}}$, aliphatic), 1692 ($\nu_{\text{C=O}}$, 2° amide), 1654 ($\nu_{\text{C=O}}$, 3° amide), 1600, 1508 ($\nu_{\text{C=C}}$, aromatic), 1295, 1146 ($\nu_{\text{S=O}}$, sulfone).

$^1\text{H-NMR}$ (400MHz, CDCl_3), δ , ppm (Figure 95): 3.01 (*s*, 3H), 7.01 (*dd*, $J = 8.5, 8.5$ Hz, 2H), 7.43 (*d*, $J = 8.8$ Hz, 2H), 7.44 (*t*, $J = 8.1$ Hz, 2H), 7.56 (*t*, $J = 7.3$ Hz, 1H), 7.63 (*dd*, $J = 4.9, 8.8$ Hz, 2H), 7.74 (*d*, $J = 6.3$ Hz, 2H), 7.74 (*d*, $J = 8.8$ Hz, 2H), 8.97 (*s*, 1H).

$^{13}\text{C-NMR}$ (400MHz, CDCl_3), δ , ppm (Figure 96): 44.61, 115.44-115.65 (*d*, $J_{\text{F-C}} = 21.5$ Hz), 123.85, 127.37, 128.12, 128.95, 130.11, 130.75, 130.96, 132.96, 136.90, 146.57, 166.69, 169.98.

HR-MS (ESI) (Figure 97): Calcd. For $C_{21}H_{17}FN_2O_4S$ - H: 411.080932. Found: 411.081620.

Anal. Calcd. for $C_{21}H_{17}FN_2O_4S + 0.5H_2O$: C 59.85; H 4.30; N 6.65. Found: C 59.99; H 4.28; N 6.67.

2.2.2 Determination of molecular orientation

According to the molecular structure of *N*-phenylbenzohydrazide (**16-21** and **27-32**) in this investigation, they exhibit the probability to orientate in the one of geometric isomer, *cis* or *trans* isomer. The determination of their orientation was conducted using 1H -NMR and X-ray crystallographic technique to evaluate the conformational changes in solution and solid states, respectively.

2.2.2.1 1H -NMR

The determination of compound orientation in solution state was conducted using 1H NMR technique. 1H NMR spectra were recorded using FT-NMR 500 MHz; Model UNITY INOVA, Varin and JEOL GSX400 instrument operated at 400 MHz. A solvent used for the measurement was acetone- d_6 (25 °C – (-) 20 °C, acetone- d_6 as 2.05 ppm) and DMSO- d_6 (30 °C – 90 °C, DMSO- d_6 as 2.50 ppm). All measurements were started at room temperature (25 °C) and done by increasing or decreasing the temperature in steps of 10 °C. 1H -NMR determination was conducted by service of Scientific Equipment Center, Prince of Songkla University, Thailand and also conducted in Department of Chemistry, Faculty of Science, Ochanomizu University, Japan.

2.2.2.2 X-ray crystallography

The determination of compound orientation in solid state was conducted using X-ray crystallographic technique. All of *N*-phenylbenzohydrazide derivatives (**16-21** and **27-32**) were recrystallized in suitable solvent as described in the details of synthesis. Then the crystals

were determined their shape, clearness and surface by microscope. The X-ray crystal structure analyses were performed on crystals of compounds **16**, **19**, **27**, **29** and **31**. Intensity data were collected with a Bruker Smart1000 CCD diffractometer using graphite monocromated MoKa ($\lambda = 0.71073 \text{ \AA}$). This experiment was performed by Dr. Isao Azumaya, Faculty of Pharmaceutical Sciences at Kagawa Campus, Tokushima Bunri University, Kagawa, Japan. Structures were solved by using the freeware Mercury Program version 2.3 (crystal structure visualization program).

2.2.3 The evaluation of biological activities

All of synthesized *N*-phenylbenzohydrazide derivatives would be subject for the evaluation of their biological activities. For this investigation, *in vitro* model was selected. All of targeted compounds (**16-21** and **27-32**) were tested COX inhibitory activity *via* both on COX-1 and COX-2. A colorimetric COX (ovine) inhibitory screening assay kit (Cayman Chemical, catalog no. 760111) was selected for assay which measured the peroxidase activity of COX. The assay principle and protocol were described in brief below.

Colorimetric COX (ovine) inhibitory screening assay

The colorimetric COX (ovine) inhibitor screening assay measures the peroxidase component of COX. The peroxidase activity is assayed colorimetrically by monitoring the appearance of oxidized *N,N,N',N'*-tetramethyl-*p*-phenylenediamine (TMPD) at 560 nm using arachidonate as the substrate. (Ann, 2008) The oxidation of TMPD which generate a chromophore in colorimetric determination was shown in figure 98.

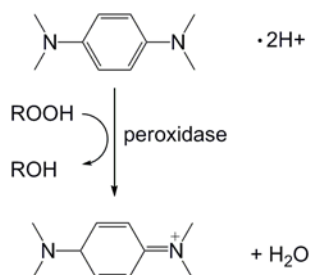


Figure 98 The oxidation of TMPD in colorimetric determination of peroxidase component in COXs.

Each experiment was initially performed at 100 μM of the test compounds as in the procedure of Kakuta and coworker (Kakuta, *et al*, 2008) and 10 μM of indomethacin which was positive control both in COX-1 and COX-2 inhibitory activity test. The assay was performed in triplicate. The assay protocol was followed with the supplier's protocol (Ann. 2008) which was described in brief below.

Reagent preparation

1. Assay Buffer: 3 ml of provided assay buffer concentrate was diluted with 27 ml of HPLC-grade water to obtain 0.1 M Tris-HCl, pH 8 then stored at 4 $^{\circ}\text{C}$. It should be use for dilution of heme and COX enzyme prior to assay.
2. Heme: 88 μl of provided heme solution in dimethyl sulfoxide was diluted with 1.912 ml of diluted assay buffer prior to be used.
3. COX-1 and COX-2: the vial contained a solution of COX-1 or COX-2 was kept on ice when thawed. Then, 350 μl of enzyme was diluted with 700 μl of diluted assay buffer and store on ice.
4. Arachidonic Acid: 110 μl of a solution of provided arachidonic acid in ethanol was tranfered into 5 ml eppendof and 110 μl of provided KOH was added, then vortex, and diluted with 1.98 ml of HPLC-grade water to achieve a final concentration of 1.1 mM. This prepared arachidonic acid solution should be used within 30 minutes.

5. Inhibitors or positive control solution: inhibitors and selected positive control were dissolved in dimethyl sulfoxide and were added to the assay in a final volume of 10 μ l.

Plate set up

The sample plate setting up 96-wells plate was shown in figure 99. Plate was separated into 2 sides, column 1 to column 6 were used for COX-1 screening and others columns were used for COX-2 screening. It had three wells designated as non-enzymatic or background wells (BW) and three wells designated as 100% initial activity wells (A) both in COX-1 and COX-2. Each experiment was performed as triplicate, and the mean value was calculated. The absorbance of BW must be subtracted from the absorbance measured in the COX well, inhibitors well (**16-21, 27-32**) or positive control well (indomethacin, IM).

	COX-1 screening						COX-2 screening					
	1	2	3	4	5	6	7	8	9	10	11	12
A	BW	BW	BW	21	21	21	BW	BW	BW	21	21	21
B	A	A	A	27	27	27	A	A	A	27	27	27
C	IM	IM	IM	28	28	28	IM	IM	IM	28	28	28
D	16	16	16	29	29	29	16	16	16	29	29	29
E	17	17	17	30	30	30	17	17	17	30	30	30
F	18	18	18	31	31	31	18	18	18	31	31	31
G	19	19	19	32	32	32	19	19	19	32	32	32
H	20	20	20				20	20	20			

Figure 99 The sample plate setting up 96-wells plate

Performing assays

1. Background Wells (BW): added 160 μ l of assay buffer and 10 μ l of heme to three wells.
2. 100% Initial Wells (A): added 150 μ l of assay buffer, 10 μ l of enzyme (either COX-1 or COX-2) to three wells.
3. Inhibitors Wells (16-21, 27-32, IM): added 150 μ l of assay buffer, 10 μ l of heme, and 10 μ l of enzyme (either COX-1 or COX-2) to three wells.
4. Added 10 μ l of inhibitor to the inhibitor wells and 10 μ l of solvent (DMSO) to the 100% initial activity wells and background wells.
5. Carefully shook the plate for a few seconds and incubated for five minutes at 25°C.
6. Added 20 μ l of colorimetric substrate solution to all the wells be using.
7. Added 20 μ l of arachidonic acid to all the wells be using.
8. Carefully shook the plate for a few seconds and incubated for five minutes at 25°C.
9. Read the absorbance at 560 nm using a microplate reader.

Calculations

1. Determined the average absorbance of all samples.
2. Subtracted the absorbance of the background well from absorbance of 100% initial activity and the inhibitor wells.
3. Subtracted each inhibitor sample from the 100% initial activity sample, then divided by the 100% initial activity sample and multiplied by 100 to give the %inhibition.

CHAPTER 3

RESULTS AND DISCUSSIONS

3.1 Synthesis and structure characterization

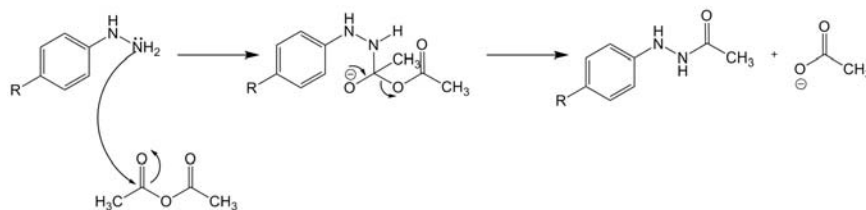
In this investigation, I designed and synthesized novel *N*-phenylbenzohydrazide derivatives for COX inhibitory evaluation. The synthesis works included the synthesis of two sets of *N*-phenylbenzohydrazide derivatives. First, I synthesized *N*-acyl-*N*-(4-substitutedphenyl)-4-(methylsulfonyl)benzohydrazides (**16-21**) which their 4-methanesulfonyl-phenyl substituents were attached to the carbonyl of amide. Second, I synthesized *N*-acyl-4-substituted-*N*-[4-(methylsulfonyl)phenyl]benzohydrazides (**27-32**) which their 4-methanesulfonyl phenyl substituents were attached to the nitrogen of amide. The results and discussions concerning the synthesis works is described in detail as follows.

3.1.1 Synthesis of *N*-acyl-*N*-(4-substitutedphenyl)-4-(methylsulfonyl)benzohydrazides (**16-21**)

N-phenylacetohydrazides (**4-6**)

As described in chapter 2, *N*-phenylacetohydrazide (**4**), *N*-*p*-tolylacetohydrazide (**5**) and *N*-(4-fluorophenyl) acetohydrazide (**6**) could be synthesized in satisfactory yields (Taylor and Hinkle, 1987). *N*-acetylation reactions were performed following a well known procedure using acetic anhydride as an acetylating agent (Brown *et al.*, 2005). The reaction mechanism could be demonstrated in scheme 4. Lone pair electron of NH₂ of the

corresponding *N*-phenylhydrazines attacked a carbonyl group of acetic anhydride to form N-C bond and follows by breaking of C-O bond to give the acetate anion and the *N*-acyl product.

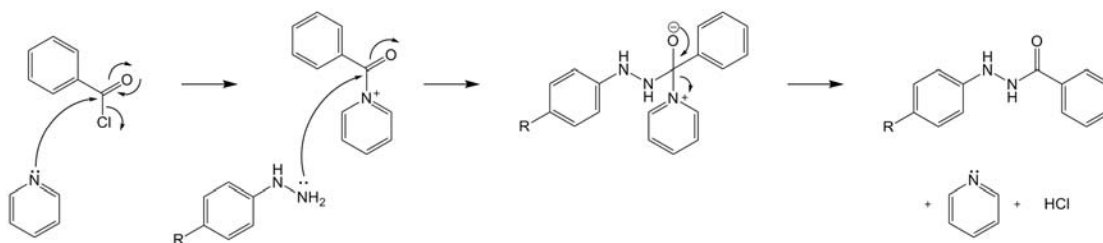


Scheme 4 The reaction mechanism of *N*-acetylation.

No catalyst was used in these reactions. The reactions were forced by increasing the stoichiometric ratio of the acetylating agent (approximate 4 equivalents by mole).

***N*'-phenylbenzohydrazide (7-9)**

In case of the *N*'-phenylbenzohydrazides (**7-9**), their synthesis were carried out by the benzylation of the corresponding *N*-phenylhydrazines (**1-3**) using benzoyl chloride as a benzylating agent in the presence of pyridine as a catalyst. The reactions were performed in diethyl ether to produce *N*'-phenylbenzohydrazide (**7**), *N*'-*p*-tolylbenzohydrazide (**8**) and *N*'-(4-fluorophenyl) benzohydrazide (**9**) in quantitative yields, 92.1% and quantitative yields, respectively. The mechanism of the reaction could be described in scheme 5. It is similar to the case of the previously described acetylation by acetic anhydride. The only difference is the participation of pyridine as a catalyst. Pyridine catalyzes benzylation involved initial formation of highly electrophilic benzoyl pyridinium ion (Denmark and Beutner, 2008). Once formed this highly electrophilic intermediate reacted with the corresponding *N*-phenylhydrazines (**1-3**) to produce *N*'-phenylbenzohydrazides (**7-9**), respectively. In this reaction pyridine also worked as a weak base to neutralize the byproduct HCl.



Scheme 5 The reaction mechanism of *N*-benzoylation.

Compounds **4-9** were finally purified by recrystallization in a suitable solvent that detailed in the experiment part. Their physical characteristic and spectroscopic properties were examined. The physical properties were obtained by measuring a melting point whereas the spectroscopic properties were obtained by IR and $^1\text{H-NMR}$. The results and discussions concerning the physical and spectroscopic data of each compound could be described in detail as follows.

Three *N'*-phenylacetohydrazides (**4-6**) and three *N'*-phenylbenzohydrazides (**7-9**) intermediates were synthesized and purified successfully resulting in white amorphous solid (**4**, **5**, **7** and **8**) and light yellow amorphous solid (**6** and **9**). Five of them, **4**, **5**, **7**, **8** and **9**, are known compounds. The melting point of each compound was compared to literature report and was summarized in table 6.

compound	R	R'	physical characteristic	melting point (°C)	
				(recrystallized solvent)	
				a*	b*
4	H	CH ₃	white solid	126-129 (ethyl acetate/ <i>n</i> -hexane)	130-131 ¹
5	CH ₃	CH ₃	white solid	124-128 (ethyl acetate/ <i>n</i> -hexane)	120 ²
6	F	CH ₃	light yellow solid	143-145 (ethyl acetate/ <i>n</i> -hexane)	N/A
7	H	C ₆ H ₅	white solid	165-167 (dichloromethane/ <i>n</i> -hexane)	165-167 ³
8	CH ₃	C ₆ H ₅	white solid	136-140 (ethyl acetate/ <i>n</i> -hexane)	145-146 ⁴
9	F	C ₆ H ₅	light yellow solid	140-144 (ethyl acetate/ <i>n</i> -hexane)	140-142 ⁵

a*: melting point from this investigation

b*: melting point from literature reported, 1; Taylor and Hinkle, 1987, 2; Stefan and Karl, 1922, 3; Hearn and Grimwade, 1980, 4; Ponzio and Charrier, 1911, 5; Bonini et al., 2009

Table 6 Physical characteristics and melting point of **4-9**

The spectroscopic data of *N*'-phenylacetohydrazides (**4-6**) and *N*'-phenyl benzohydrazides (**7-9**) were obtained by IR and ¹H-NMR spectroscopic experiments. Their IR spectra showed characteristic signals of important functional groups according to I would say proposed structure. To illustrate, *N*-H stretching of monohydrazide is assigned $\approx 3200\text{ cm}^{-1}$, C-H stretching of aromatic and aliphatic are assigned at upper wavenumbers (>3000) and lower wavenumbers (<3000), respectively. Strong sharp peaks of C=O stretching of secondary amide is

found at 1643-1675 cm^{-1} . ArC-C stretching of aromatic (1625-1575 cm^{-1}) is also found as a band with medium intensity. The comparison of IR spectra data of compounds **10-15** was shown in table 7.

compound	R	R'	V _{max} (cm ⁻¹)				
			V _{N-H}	V _{C-H}	V _{C-H}	V _{C=O}	V _{C-C}
			monohydrazide	aromatic	aliphatic	amide	aromatic
4	H	CH ₃	3286	3030	2939	1643	1596
5	CH ₃	CH ₃	3297	3029	2919	1675	1595
6	F	CH ₃	3276	3099	2882	1664	1576
7	H	C ₆ H ₅	3246	3054	-	1647	1578
8	CH ₃	C ₆ H ₅	3251	3027	2918	1647	1597
9	F	C ₆ H ₅	3255	3004	-	1649	1579

Table 7 The comparison of IR (KBr) data of **4-9**

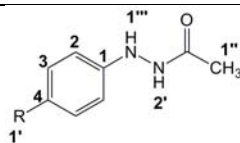
¹H-NMR spectra of *N*-phenylacetohydrazides (**4-6**) and *N*-phenylbenzohydrazides (**7-9**) were interpreted on the basis of the chemical shifts, multiplicity and integral intensity. The samples were dissolved and measured in DMSO-*d*₆ (**4-6**) and CDCl₃ (**7-9**) at 25 °C.

¹H-NMR spectra of **4-6** clearly corresponded to the relative abundance and connectivity of each hydrogen type found in their structure. Each spectrum was separated into two main sets of signals; aliphatic proton and aromatic proton. At aliphatic proton, the singlet signals of 3H at 1.89, 1.86 and 1.87 ppm were assignable to H signal of CH₃ in acetamide of compound **4-6**, respectively. Moreover, methyl substituted *N*-phenylacetohydrazide (**5**) and methyl substituted *N*-phenyl benzohydrazide (**8**) showed signals of methyl substituted at 2.16 and 2.24 ppm as singlet signals of 3H, respectively.

The aromatic proton signals of **4-9** are different, based on the substituent on aromatic (H, CH₃ and F) of each compound. According to these results, the aromatic proton signals were found at peak around 6.59-7.82 ppm in a good correlation of coupling constant (J -vaule, Hz). The J -vaules of vicinal coupling between H at position 2 and 3 of **4-9** and vicinal coupling between H at position 2' and 3' of **7-9** are 7.3-9.0 Hz and 6.8-7.8 Hz, respectively. From table 8, compound **4** exhibited aromatic H signals in three sets including: 6.68, 7.11, 6.67 ppm were assignable to H at position 2, 3 and 4, respectively. Compound **5** and **6** exhibited the aromatic H signals in two sets including: 6.59 (**5**), 6.68 (**6**) and 6.92 (**5**), 6.95 (**6**) ppm were assignable to H at position 2 and 3, respectively. From table 9, compound **7** showed aromatic H signals in six sets. Three of them, 6.92, 7.22 and 6.71 ppm, were assignable to H of aniline ring. The rest, 7.82, 7.45 and 7.54 ppm, were assignable to H of benzamide ring. Compound **8** and **9** exhibited the aromatic H signals in five sets. Two of them (6.83 (**8**), 6.79 (**9**) and 7.02 (**8**), 6.98 (**9**) ppm) were assignable to H of aniline ring. The rest (7.81 (**8**), 7.81 (**9**) and 7.44 (**8**), 7.45 (**9**) and 7.54 (**8**), 7.55 (**9**) ppm) were assignable to H of benzamide ring.

Moreover, the fluorine substituents, compound **6** and **9**, showed AA'XX' system for the aromatic protons (6.68-6.98 ppm) with additional $^3J_{\text{HF}}$ and $^4J_{\text{HF}}$ splitting. *N*-(4-fluorophenyl)acetohydrazide (**6**) exhibited the H_{XX'} and H_{AA'} signals as a pseudo-triplet at 6.95 ppm ($J = 8.9$ Hz) and as a doublet of doublets at 6.68 ppm ($J = 4.7$ Hz), while *N*-(4-fluorophenyl)benzohydrazide (**9**) showed the H_{XX'} and H_{AA'} signals as a pseudo-triplet at 6.98 ppm ($J = 8.5$ Hz) and as a doublet of doublets at 6.79 ppm ($J = 4.6$ Hz).

In addition, weak doublet signals of exchangeable proton (NH), 7.63, 7.45 and 7.57 ppm, were assignable to NH at position 1''' of compound **4-6**, respectively. While another exchangeable proton (NH position 2') appeared at lower field (9.58, 9.56 and 9.59 ppm) because of the electron withdrawing influence from carbonyl of amide. The doublet signals showed a good correlation of coupling constant, 2.7-3.2 Hz, vicinal coupling between two exchangeable protons. While compound **7-9** exhibited weak broadening singlet signals of two exchangeable protons at 4.18, 4.34 and 8.04 ppm, respectively (table 8 and table 9).



	4 (R = H)				5 (R = CH ₃)				6 (R = F)			
	δ , ppm	m ^{a)}	J, Hz	H ^{b)}	δ , ppm	m ^{a)}	J, Hz	H ^{b)}	δ , ppm	m ^{a)}	J, Hz	H ^{b)}
2	6.68	<i>d</i>	8.5	2 <i>H</i>	6.59	<i>d</i>	8.3	2 <i>H</i>	6.68	<i>dd</i>	4.7, 9.0	2 <i>H</i>
3	7.11	<i>t</i>	7.9	2 <i>H</i>	6.92	<i>d</i>	8.3	2 <i>H</i>	6.95	<i>dd</i>	8.9, 8.9	2 <i>H</i>
4	6.67	<i>t</i>	5.9	1 <i>H</i>	-	-	-	-	-	-	-	-
1'	-	-	-	-	2.16	<i>s</i>	-	3 <i>H</i>	-	-	-	-
1''	1.89	<i>s</i>	-	3 <i>H</i>	1.86	<i>s</i>	-	3 <i>H</i>	1.87	<i>s</i>	-	3 <i>H</i>
1'''	7.63	<i>d</i>	2.7	1 <i>H</i>	7.45	<i>d</i>	3.2	1 <i>H</i>	7.57	<i>d</i>	3.0	1 <i>H</i>
2'	9.58	<i>d</i>	2.7	1 <i>H</i>	9.56	<i>d</i>	3.1	1 <i>H</i>	9.59	<i>d</i>	3.0	1 <i>H</i>

a) Multiplicity

b) Number of proton

Table 8 The comparison of ¹H-NMR (500MHz, DMSO-*d*₆) data of **4-6**

	7 (R = H)				8 (R = CH ₃)				9 (R = F)			
	δ , ppm	m ^{a)}	J, Hz	H ^{b)}	δ , ppm	m ^{a)}	J, Hz	H ^{b)}	δ , ppm	m ^{a)}	J, Hz	H ^{b)}
2	6.92	<i>d</i>	7.3	2H	6.83	<i>d</i>	8.8	2H	6.79	<i>dd</i>	4.6, 9.0	2H
3	7.22	<i>t</i>	8.1	2H	7.02	<i>d</i>	8.3	2H	6.98	<i>dd</i>	8.5, 8.5	2H
4	6.71	<i>t</i>	7.6	1H	-	-	-	-	-	-	-	-
2'	7.82	<i>d</i>	6.8	2H	7.81	<i>d</i>	7.3	2H	7.81	<i>d</i>	7.8	2H
3'	7.45	<i>t</i>	7.6	2H	7.44	<i>t</i>	7.6	2H	7.45	<i>t</i>	7.6	2H
4'	7.54	<i>t</i>	7.3	1H	7.54	<i>t</i>	7.3	1H	7.55	<i>t</i>	7.3	1H
1''	-	-	-	-	2.24	<i>s</i>	-	3H	-	-	-	-
1'''	4.34	<i>s</i>	-	1H	4.28	<i>s (br)</i>	-	1H	4.18	<i>s (br)</i>	-	1H
2''	8.04	<i>s</i>	-	1H	8.04	<i>s (br)</i>	-	1H	8.04	<i>s (br)</i>	-	1H

a) Multiplicity

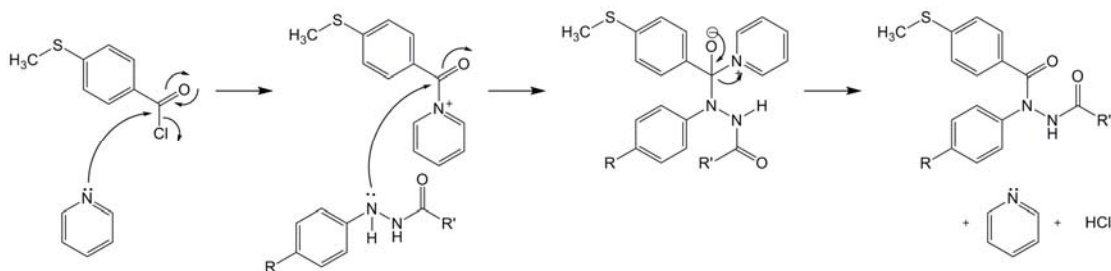
b) Number of proton

Table 9 The comparison of ¹H-NMR (500MHz, CDCl₃) data of **7-9**

N'-acyl-4-(methylthio)-N-phenylbenzohydrazides (10-15)

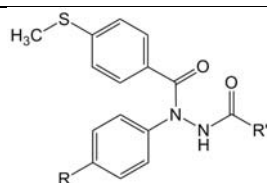
In this step, **10-15** could be synthesized by amidation of secondary amine (**4-9**), with 4-(methylthio)benzoyl chloride. The mechanism of the reaction was described in scheme 6. It was similar to the case of the previously described benzoylation by benzoyl chloride. The pyridine was also used to catalyze the reaction by formation of highly electrophilic acyl pyridinium ion (Denmark and Beutner, 2008). The only difference was heating to force the reaction. Because of in this case, the starting materials (**4-9**) contain two of secondary nitrogens; the weak nucleophilic amine and the very weak nucleophilic amide. The weak nucleophilic

amine could attack to the carbonyl of the electrophilic acyl pyridinium ion easier than that of the very weak nucleophilic amide. The reaction did not occur when it was performed at room temperature in dichloromethane. After increasing the temperature of reaction by refluxing in chloroform (bp. 61.2 °C), the reaction still did not occurred. The reaction occurred within 4-5 h when the reaction was refluxed in dichloroethane (bp. 83.5 °C).



Scheme 6 The reaction mechanism of amidation of **10-15**

The stoichiometric amount of all entities and % yield was concluded in table 10. The rate of reaction was not significantly different between acetamide substituted compounds (**10-12**) and benzamide substituted compounds (**13-15**).

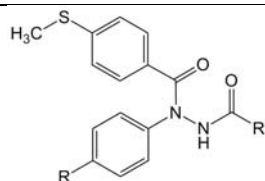


compound	R	R'	amount of entities (equivalent by mole)			time (hours)	% yield
			corresponding	4-(methylthio)	pyridine		
			2° amine	benzoyl chloride			
10	H	CH ₃	1.0	1.1	4.3	4	79.9
11	CH ₃	CH ₃	1.0	1.2	4.8	5	78.3
12	F	CH ₃	1.0	1.1	4.0	5	96.4
13	H	C ₆ H ₅	1.0	1.1	4.2	4	87.0
14	CH ₃	C ₆ H ₅	1.0	1.1	4.2	5	94.2
15	F	C ₆ H ₅	1.0	1.1	4.3	5	86.2

Table 10 The stoichiometric amount of all entities and % yield of **10-15**

After compounds **10-15** were finally purified by recrystallization, their physical characteristic and spectroscopic properties were examined by measuring a melting point, IR and ¹H-NMR.

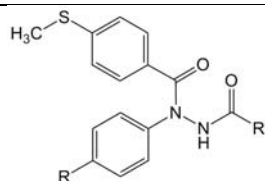
Compounds **10-15** were synthesized and purified successfully resulting in white amorphous solid. Their melting points were summarized in table 11.



compound	R	R'	physical characteristics	mp. (°C)	(recrystallized solvent)
10	H	CH ₃	white solid	126-129	(ethyl acetate/diethyl ether)
11	CH ₃	CH ₃	white solid	151-153	(ethyl acetate/ <i>n</i> -hexane)
12	F	CH ₃	white solid	139-140	(ethyl acetate/ <i>n</i> -hexane)
13	H	C ₆ H ₅	white solid	179-181	(ethyl acetate/ <i>n</i> -hexane/diethyl ether)
14	CH ₃	C ₆ H ₅	white solid	183-186	(ethyl acetate/ <i>n</i> -hexane/diethyl ether)
15	F	C ₆ H ₅	white solid	168-171	(ethyl acetate/diethyl ether)

Table 11 Physical characteristics and melting point of **10-15**

The spectroscopic data of *N'*-acetyl/benzoyl-4-(methylthio)-*N*-phenylbenzohydrazides (**10-15**) were obtained by IR and ¹H-NMR. IR spectra of compounds **10-15** have showed their characteristic signals of important functional groups according to the assumed structure. To illustrate, *N*-H stretching of monohydrazide was assigned $\approx 3200\text{ cm}^{-1}$, C-H stretching of aromatic and aliphatic were assigned at upper wavenumbers (>3000) and lower wavenumbers (<3000), respectively. Two strong sharp peaks of C=O stretching of 2° and 3° amide were found at $1680\text{-}1620\text{ cm}^{-1}$. ArC-C stretching of aromatic ($1625\text{-}1575\text{ cm}^{-1}$) was also found as band with medium intensity. The comparison of IR spectra data of compounds **10-15** was showed in table 12.



R	R'	Vmax (cm ⁻¹)						
		V _{N-H}	V _{C-H}	V _{C-H}	V _{C=O}	V _{C=O}	V _{arC-C}	
		monohydrazide	aromatic	aliphatic	2 ^o amide	3 ^o amide	aromatic	
10	H	CH ₃	3258	-	2993	1681	1660	1593
11	CH ₃	CH ₃	3277	3009	2923	1683	1671	1593
12	F	CH ₃	3270	3060	3003	1672	1672	1596
13	H	C ₆ H ₅	3276	3062	2921	1679	1655	1591
14	CH ₃	C ₆ H ₅	3268	3030	2989	1686	1623	1594
15	F	C ₆ H ₅	3263	3030	2989	1687	1626	1599

Table 12 The comparison of IR (KBr) data of **10-15**

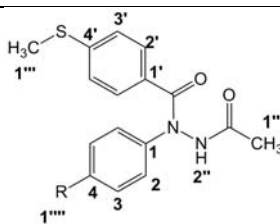
¹H-NMR spectra of *N'*-acetyl/benzoyl-4-(methylthio)-*N*-phenylbenzohydrazides (**10-15**) were interpreted on the basis of the chemical shifts, multiplicity and integrational intensity. The samples were dissolved and measured in CDCl₃ (**10**, **12**, **14** and **15**) and acetone-*d*₆ (**11** and **13**) at room temperature. For compound **11** and **13**, I initially used CDCl₃ as a solvent but its ¹H-NMR spectra exhibited unclear multiplicity whereas ¹H-NMR spectra showed distinct multiplicity when we using acetone-*d*₆ as solvent instead.

¹H-NMR spectra of **10-15** clearly corresponded to the relative abundance and connectivity of each hydrogen type founded in their structure. Each spectrum was separated into two main signals; aliphatic protons and aromatic protons. At aliphatic proton (table 13 and table 14), the singlet signal of 3H at 2.40, 2.48, 2.42, 2.46, 2.42 and 2.42 ppm were assignable to H signal of S-CH₃ of compound **10-15**, respectively. The singlet signal of 3H at 2.20, 1.86 and 2.03 ppm were assignable to H signal of CH₃ in acetamide of compound **10-12**, respectively.

Moreover, methyl substituted compounds (**11** and **14**) showed signal of methyl at 2.28 and 2.24 ppm as singlet signal of 3H, respectively.

The aromatic proton signals of **10-15** were different, based on the substituent on aromatic of each compound. From table 13, compound **10** exhibited aromatic H signals in five sets. Three of them (7.02, 7.16 and 7.17 ppm) were assignable to H of aniline ring. The rest (7.35 and 7.21 ppm) were assignable to H of 4-SCH₃ phenyl ring. Compound **11** and **12** exhibited aromatic H signals in four sets. Two of them (7.11 (**11**), 7.19 (**12**) and 7.19 (**11**), 6.91 (**12**) ppm) were assignable to H of aniline ring. The rest (7.45 (**11**), 7.33 (**12**) and 7.21 (**11**), 7.04 (**12**) ppm) were assignable to H of 4-SCH₃ phenyl ring. From table 14, compound **13** exhibited aromatic H signals in eight sets. Three of them (7.19, 7.35 and 7.21 ppm) were assignable to H of aniline ring. Three signals at 7.55, 7.44 and 7.83 ppm were assignable to H of 4-SCH₃ phenyl ring. The rest (7.46 and 7.56 ppm) were assignable to H of benzamide ring. Compound **14** and **15** exhibited aromatic H signals in seven sets. Two of them (7.03 (**14**), 7.27 (**15**) and 7.04 (**14**), 6.92 (**15**) ppm) were assignable to H of aniline ring. Two signals at 7.41 (**14**), 7.38 (**15**) and 7.15 (**14**) 7.05 (**15**) ppm were assignable to H of 4-SCH₃ phenyl ring. The rest (7.80 (**14**), 7.78 (**15**), 7.37 (**14**), 7.37 (**15**) and 7.47 (**14**), 7.49 (**15**) ppm) were assignable to H of benzamide ring.

Moreover, the fluorine substituent compounds (**12** and **15**) also showed AA'XX' system for the aromatic protons (6.91-7.27 ppm) with additional $^3J_{\text{HF}}$ and $^4J_{\text{HF}}$ splitting. *N'*-acetyl-*N*-(4-fluorophenyl)-4-(methylthio)benzohydrazide (**12**) exhibited the H_{XX'} and H_{AA'} signals as a pseudo-triplet at 6.91 ppm ($J = 8.5$ Hz) and as a doublet of doublets at 7.19 ppm ($J = 4.9$ Hz), while *N'*-benzoyl-*N*-(4-fluorophenyl)-4-(methylthio)benzohydrazide (**15**) showed the H_{XX'} and H_{AA'} signals as a pseudo-triplet at 6.92 ppm ($J = 8.5$ Hz) and as a doublet of doublets at 7.27 ppm ($J = 4.6$ Hz). In addition, the weak singlet signals of 1H appeared at 8.38, 9.80, 8.19, 10.57, 8.94 and 8.96 ppm were assignable to *NH* of compound **10-15**, respectively (table 13 and table 14).



	10^a (R = H)				11^b (R = CH ₃)				12^a (R = F)			
	δ , ppm	m ^c	J, Hz	H ^d	δ , ppm	m ^c	J, Hz	H ^d	δ , ppm	m ^c	J, Hz	H ^d
2	7.02	<i>d</i>	8.5	2 <i>H</i>	7.11	<i>d</i>	7.8	2 <i>H</i>	7.19	<i>dd</i>	4.9, 9.3	2 <i>H</i>
3	7.16	<i>t</i>	6.8	2 <i>H</i>	7.19	<i>d</i>	8.8	2 <i>H</i>	6.91	<i>dd</i>	8.5, 8.5	2 <i>H</i>
4	7.17	<i>t</i>	6.9	1 <i>H</i>	-	-	-	-	-	-	-	-
2'	7.35	<i>d</i>	8.7	2 <i>H</i>	7.45	<i>d</i>	8.3	2 <i>H</i>	7.33	<i>d</i>	8.8	2 <i>H</i>
3'	7.21	<i>d</i>	7.5	2 <i>H</i>	7.21	<i>d</i>	9.8	2 <i>H</i>	7.04	<i>d</i>	8.3	2 <i>H</i>
1''	2.20	<i>s</i>	-	3 <i>H</i>	1.86	<i>s</i>	-	3 <i>H</i>	2.03	<i>s</i>	-	3 <i>H</i>
1'''	2.40	<i>s</i>	-	3 <i>H</i>	2.48	<i>s</i>	-	3 <i>H</i>	2.42	<i>s</i>	-	3 <i>H</i>
1''''	-	-	-	-	2.28	<i>s</i>	-	3 <i>H</i>	-	-	-	-
2''	8.38	<i>s</i>	-	1 <i>H</i>	9.80	<i>s</i>	-	1 <i>H</i>	8.19	<i>s</i>	-	1 <i>H</i>

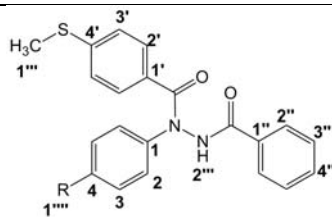
a: The samples were dissolved and measured in CDCl₃

b: The samples were dissolved and measured in acetone-*d*₆

c: multiplicity

d: number of proton

Table 13 The comparison of ¹H-NMR (500MHz) data of **10-12**



	13^a (R = H)				14^b (R = CH ₃)				15^b (R = F)			
	δ , ppm	m ^c	J, Hz	H ^d	δ , ppm	m ^c	J, Hz	H ^d	δ , ppm	m ^c	J, Hz	H ^d
2	7.19	<i>d</i>	8.3	2H	7.03	<i>d</i>	7.8	2H	7.27	<i>dd</i>	4.6, 9.0	2H
3	7.35	<i>t</i>	7.8	2H	7.04	<i>d</i>	8.3	2H	6.92	<i>dd</i>	8.5, 8.5	2H
4	7.21	<i>t</i>	7.3	1H	-	-	-	-	-	-	-	-
2'	7.55	<i>d</i>	8.3	2H	7.41	<i>d</i>	8.3	2H	7.38	<i>d</i>	8.8	2H
3'	7.44	<i>d</i>	10.2	2H	7.15	<i>d</i>	8.3	2H	7.05	<i>d</i>	8.3	2H
2''	7.83	<i>d</i>	7.3	2H	7.80	<i>d</i>	7.3	2H	7.78	<i>d</i>	7.3	2H
3''	7.46	<i>t</i>	8.1	2H	7.37	<i>t</i>	7.6	2H	7.37	<i>t</i>	7.8	2H
4''	7.56	<i>t</i>	8.1	1H	7.47	<i>t</i>	7.6	1H	7.49	<i>t</i>	7.6	1H
1'''	2.46	<i>s</i>	-	3H	2.42	<i>s</i>	-	3H	2.42	<i>s</i>	-	3H
1''''	-	-	-	-	2.24	<i>s</i>	-	3H	-	-	-	-
2'''	10.57	<i>s</i>	-	1H	8.94	<i>s</i>	-	1H	8.96	<i>s</i>	-	1H

a: The samples were dissolved and measured in acetone-*d*₆

b: The samples were dissolved and measured in CDCl₃

c: multiplicity

d: number of proton

Table 14 The comparison of ¹H-NMR (500MHz) data of **13-15**

***N*'-acyl-4-(methylsulfonyl)-*N*-phenylbenzohydrazides (16-21)**

This step is the final pathway to furnish the targeted *N*'-acyl-4-(methylsulfonyl)-*N*-phenylbenzohydrazides (**16-21**). The thioether intermediates (**10-15**) were oxidized using oxone[®] as oxidizing agent.

The composition of the oxidizing agent Oxone[®] is 2KHSO₅·KHSO₄·K₂SO₄. The active component potassium monopersulfate (KHSO₅, potassium peroxomonosulfate) is a salt from the Caro's acid H₂SO₅. Recently, Oxone[®] has attracted considerable interest because of its versatility as an oxidant: it oxidizes aldehydes to carboxylic acids; in the presence of alcoholic solvents, the esters may be obtained. Internal alkenes may be cleaved to two carboxylic acids, while terminal alkenes may be epoxidized. Moreover, thioethers could be oxidized to give sulfones and tertiary amines could be oxidized to give amine oxides (Travis *et al.*, 2003). The use of Oxone[®] has increased rapidly because following reasons: the stability, the simple handling, the non-toxic nature and the low costs.

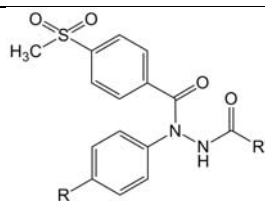
Two equivalent of Oxone[®] oxidizes a thioether to a sulfone. With one equivalent the reaction converts sulfide to sulfoxide, in much faster rate than that of sulfoxide to sulfone, so the reaction can conveniently be stopped at that stage if so desired (McCarthy *et al.*, 1998). In this investigation, the reaction was operated in methanol/water at room temperature. The reaction was completed in high yield within 1 h. The stoichiometric amount of all entities and % yield was concluded in table 15.

compound	R	R'	amount of entities (equivalent by mole)		time (hours)	% yield
			corresponding	oxone [®]		
			thioether			
16	H	CH ₃	1.0	2.2	1	93.5
17	CH ₃	CH ₃	1.0	2.2	1	quantitative
18	F	CH ₃	1.0	2.1	1	quantitative
19	H	C ₆ H ₅	1.0	2.2	1	77.5
20	CH ₃	C ₆ H ₅	1.0	2.2	1	87.3
21	F	C ₆ H ₅	1.0	2.2	1	75.3

Table 15 The stoichiometric amount of all entities and % yield of **16-21**

After compounds **16-21** were finally purified by recrystallization, their physical characteristic and spectroscopic properties were examined. The physical properties were obtained by measuring a melting points and analyzing for C, H and N elements in compound. The spectroscopic properties were obtained by IR, ¹H-NMR, ¹³C-NMR and HR-MS. The results and discussions concerning the physical and spectroscopic data of each compound are described in detail as follows.

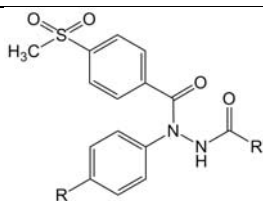
N'-acyl-4-(methylsulfonyl)-*N*-phenylbenzohydrazides (**16-21**) products were successfully synthesized and finally purified by recrystallization with ethyl acetate (**16**) and ethyl acetate/*n*-hexane (**17-21**) resulting in white solid. Their melting points were summarized in table 16.



compound	R	R'	physical characteristics	mp. (°C)	(recrystallized solvent)
16	H	CH ₃	white solid	209 – 210	(ethyl acetate)
17	CH ₃	CH ₃	white solid	184 - 185	(ethyl acetate/ <i>n</i> -hexane)
18	F	CH ₃	white solid	150 - 153	(ethyl acetate/ <i>n</i> -hexane)
19	H	C ₆ H ₅	white solid	133 – 137	(ethyl acetate/ <i>n</i> -hexane)
20	CH ₃	C ₆ H ₅	white solid	202 – 204	(ethyl acetate/ <i>n</i> -hexane)
21	F	C ₆ H ₅	white solid	171 – 174	(ethyl acetate/ <i>n</i> -hexane)

Table 16 Physical characteristics and melting point of **16-21**

IR spectra of compounds **16-21** have showed their characteristic signals of important functional groups according to the assumed structure. Structure of compounds **16-21** is differing from corresponding compounds, **10-15**, in additional sulfone functional group. Hence, the IR spectra of compounds **16-21** (table 17) showed similar peak to IR spectra of compounds **10-15** and had one more additional signal of sulfone in spectra. All spectra were showed *N*-H stretching of monohydrazide at $\approx 3200\text{ cm}^{-1}$ and C-H stretching of aromatic and aliphatic at upper wavenumbers (>3000) and lower wavenumbers (<3000), respectively. Two strong sharp peaks of C=O stretching (2° and 3° amides) were found at $1680\text{-}1620\text{ cm}^{-1}$. In addition, two strong sharp peaks of S=O stretching of sulfone were found in subrange $1370\text{-}1290\text{ cm}^{-1}$ and $1170\text{-}1110\text{ cm}^{-1}$.



R	R'	V _{max} (cm ⁻¹)					
		V _{N-H} , monohydrazide	V _{C-H} , aromatic	V _{C-H} , aliphatic	V _{C=O} , 2°, 3° amide	V _{S=O} , sulfone	
16	H	CH ₃	3235	3017	2920	1674, 1664	1314, 1155
17	CH ₃	CH ₃	3259	3013	2927	1681	1316, 1153
18	F	CH ₃	3231	3017	2920	1685, 1664	1320, 1157
19	H	C ₆ H ₅	3547	-	2998	1683, 1661	1307, 1149
20	CH ₃	C ₆ H ₅	3225	3005	2925	1686, 1654	1314, 1153
21	F	C ₆ H ₅	3344	3036	2936	1677	1308, 1153

Table 17 The comparison of IR (KBr) data of **16-21**

¹H-NMR spectra of **16-21** were also interpreted on the basis of the chemical shifts, multiplicity and integral intensity. The samples were dissolved and measured in CDCl₃ (**17**, **20** and **21**) and DMSO-*d*₆ (**16**, **18** and **19**). Because compounds **16**, **18** and **19** are hardly dissolved in CDCl₃, DMSO-*d*₆ was selected for used as solvent for them. Broadening of signal at aromatic proton region was found in the spectra of compound performed at room temperature. When temperature was increased from 30 °C to 90 °C in samples used DMSO-*d*₆ as solvent and from 30 °C to 50 °C in samples used CDCl₃ as solvent, resulting in sharpening of aromatic proton. This phenomenon was occurred accordance with Tony, M. B. and coworker's study in a dynamic NMR investigation of the conformational isomerism in novel 1, 3, 4, 5-tetrahydro-2, 1-benzoxazepines. The NMR found in spectra of these compounds an unusual degree of line broadening was attributable to a slow rotation of *N*-Ph and carbonyl-Ph processes. Because of these bonds rotation, relatively slow on the NMR timescale leading to the broadening signal. Elevation of the temperature resulted in time environments for all aromatic resonances as a result

of rapid rotation leading to sharpening signal. Figure 100 was showed the illustrative example of sharpening signal at aromatic region after increasing the temperature of **19**.

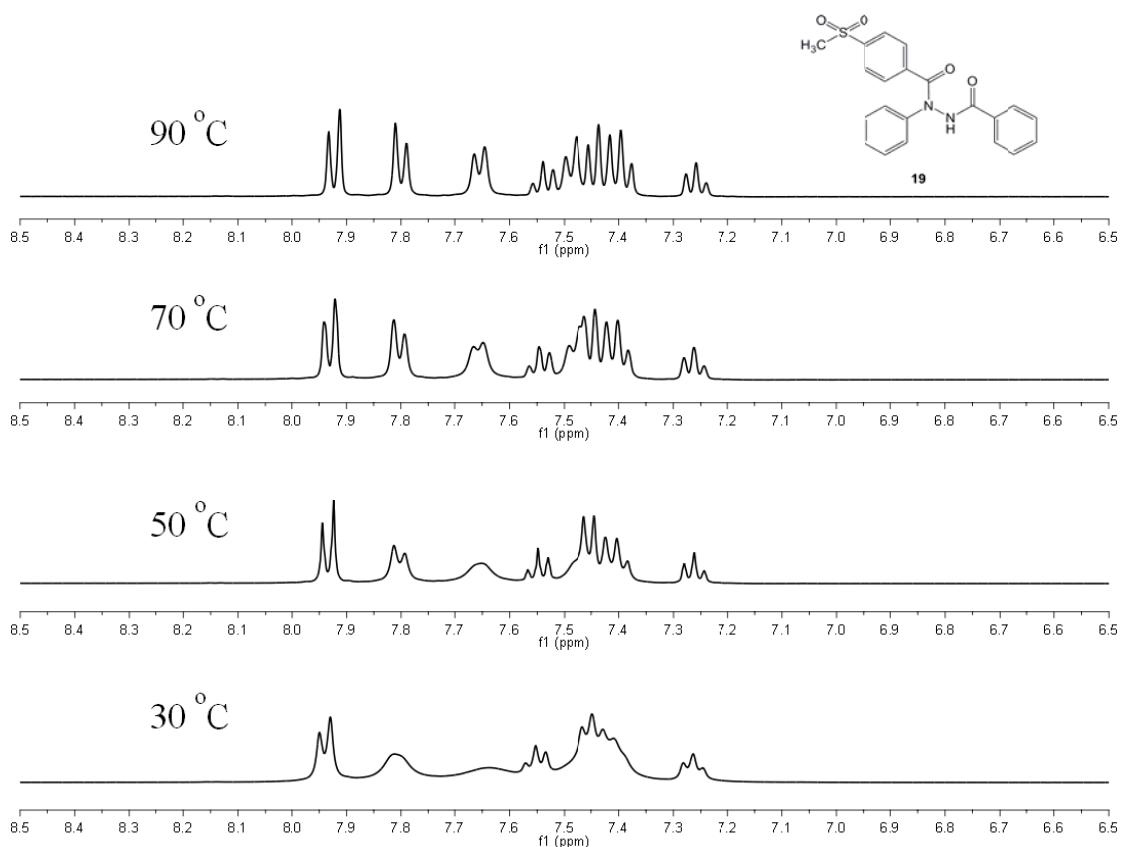


Figure 100 The comparison of $^1\text{H-NMR}$ (400MHz, $\text{DMSO-}d_6$) spectrum when operated at 30 °C, 50 °C, 70 °C and 90 °C (from below to top) of compound **19**.

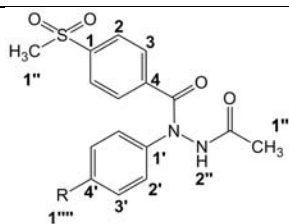
$^1\text{H-NMR}$ data of **16-21** (table 18 and table 19) clearly corresponded to the relative abundance and connectivity of each hydrogen type found in their structure. Each spectrum was separated into two main sets of signals; aliphatic proton and aromatic proton as in compound **10-15**. To concern at aliphatic proton, the singlet signals of 3H at 3.19, 2.98, 3.20, 3.14, 2.97 and 2.98 ppm were assignable to H signal of $\text{SO}_2\text{-CH}_3$ of **16-21**, respectively. The singlet signals of 3H at 1.74, 2.02 and 1.72 ppm were assignable to H signal of CH_3 in acetamide

of **16-18**, respectively. Moreover, methyl substituent compounds (**17** and **20**) showed signal of methyl at 2.28 and 2.29 ppm as singlet signal of 3H, respectively.

The aromatic proton signals of **16-21** were different, based on the substituent on aromatic of each compound. From table 18, compound **16** exhibited the aromatic H signals in five sets. Two of them (7.72 and 7.93 ppm) were assignable to H of 4-SO₂CH₃ phenyl ring. The rest (7.35, 7.38 and 7.24) were assignable to H of aniline ring.

From table 19, compound **19** exhibited the aromatic H signals in eight sets. Two of them (7.80 and 7.92 ppm) were assignable to H of 4-SO₂CH₃ phenyl ring. Three of them (7.49, 7.40 and 7.26 ppm) were assignable to H of aniline ring. The rest (7.65, 7.43 and 7.54 ppm) were assignable to H of benzamide ring. Compound **20** and **21** exhibited the aromatic H signals in seven sets. Two of them (7.76 (**20**), 7.73 (**21**) and 7.80 (**20**), 7.83 (**21**) ppm) were assignable to H of 4-SO₂CH₃ phenyl ring. Two of them (7.06 (**20**), 7.34 (**21**) and 7.19 (**20**), 6.97 (**21**) ppm) were assignable to H of aniline ring. The rest (7.69 (**20**), 7.69 (**21**), 7.40 (**20**), 7.41 (**21**) and 7.52 (**20**), 7.53 (**21**) ppm) were assignable to H of benzamide ring.

Likewise with compound **12** and **15**, the fluorine substituent compounds, **18** and **21**, also showed AA'XX' system for the aromatic protons (6.97-7.43 ppm) with additional ³J_{HF} and ⁴J_{HF} splitting. Compound **18** exhibited the H_{XX'} and H_{AA'} signals as a pseudo-triplet at 7.18 ppm (*J* = 8.8 Hz) and as a doublet of doublets at 7.43 ppm (*J* = 5.4 Hz), while compound **21** showed the H_{XX'} and H_{AA'} signals as a pseudo-triplet at 6.97 ppm (*J* = 8.5 Hz) and as a doublet of doublets at 7.34 ppm (*J* = 4.6 Hz). In addition, the weak broadening singlet signals of exchangeable proton (NH) of compound **16-21** were showed in the range of 8.62-11.39 ppm.



	16^a (R = H)				17^b (R = CH ₃)				18^a (R = F)			
	δ , ppm	m ^c	J, Hz	H ^d	δ , ppm	m ^c	J, Hz	H ^d	δ , ppm	m ^c	J, Hz	H ^d
2	7.72	<i>d</i>	8.3	2H	7.63	<i>d</i>	7.8	2H	7.72	<i>d</i>	8.3	2H
3	7.93	<i>d</i>	8.3	2H	7.80	<i>d</i>	8.3	2H	7.94	<i>d</i>	7.8	2H
2'	7.35	<i>d</i>	8.3	2H	7.04	<i>d</i>	7.8	2H	7.43	<i>dd</i>	5.4, 7.8	2H
3'	7.38	<i>t</i>	7.3	2H	7.09	<i>d</i>	8.3	2H	7.18	<i>dd</i>	8.8, 8.8	2H
4'	7.24	<i>t</i>	6.6	1H	-	-	-	-	-	-	-	-
1''	3.19	<i>s</i>	-	3H	2.98	<i>s</i>	-	3H	3.20	<i>s</i>	-	3H
1'''	1.74	<i>s</i>	-	3H	2.02	<i>s</i>	-	3H	1.72	<i>s</i>	-	3H
1''''	-	-	-	-	2.28	<i>s</i>	-	3H	-	-	-	-
2''	10.7	<i>s (br)</i>	-	1H	9.91	<i>s (br)</i>	-	1H	10.73	<i>s (br)</i>	-	1H

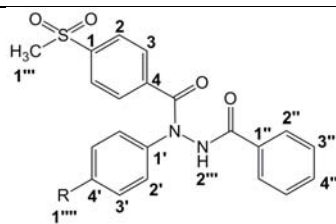
a: The samples were dissolved in DMSO-*d*₆ and measured at 90 °C

b: The samples were dissolved in CDCl₃ and measured at 52 °C

c: multiplicity

d: number of proton

Table 18 The comparison of ¹H-NMR (400MHz) data of **16-18**



	19^a (R = H)				20^b (R = CH ₃)				21^b (R = F)			
	δ , ppm	m ^c	J, Hz	H ^d	δ , ppm	m ^c	J, Hz	H ^d	δ , ppm	m ^c	J, Hz	H ^d
2	7.80	<i>d</i>	8.3	2H	7.76	<i>d</i>	7.3	2H	7.73	<i>d</i>	7.3	2H
3	7.92	<i>d</i>	8.3	2H	7.80	<i>d</i>	8.8	2H	7.83	<i>d</i>	8.8	2H
2'	7.49	<i>d</i>	7.8	2H	7.06	<i>d</i>	8.3	2H	7.34	<i>dd</i>	4.6, 8.5	2H
3'	7.40	<i>t</i>	7.8	2H	7.19	<i>d</i>	8.3	2H	6.97	<i>dd</i>	8.5, 8.5	2H
4'	7.26	<i>t</i>	7.3	1H	-	-	-	-	-	-	-	-
2''	7.65	<i>d</i>	7.8	2H	7.69	<i>d</i>	8.3	2H	7.69	<i>d</i>	8.3	2H
3''	7.43	<i>t</i>	7.8	2H	7.40	<i>t</i>	7.8	2H	7.41	<i>t</i>	7.8	2H
4''	7.54	<i>t</i>	7.3	1H	7.52	<i>t</i>	7.3	1H	7.53	<i>t</i>	7.6	1H
1'''	3.14	<i>s</i>	-	3H	2.97	<i>s</i>	-	3H	2.98	<i>s</i>	-	3H
1''''	-	-	-	-	2.29	<i>s</i>	-	3H	-	-	-	-
2'''	11.39	<i>s (br)</i>	-	1H	8.62	<i>s</i>	-	1H	8.63	<i>s</i>	-	1H

a: The samples were dissolved in DMSO and measured at 90 °C

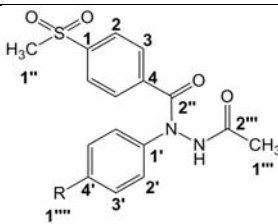
b: The samples were dissolved in CDCl₃ and measured at 50 °C

c: multiplicity

d: number of proton

Table 19 The comparison of ¹H-NMR (400MHz) data of **19-21**

The number of signals on ^{13}C -NMR spectra also confirmed the structure for the final products, **16-21**. ^{13}C -NMR observation for each compound was performed in the same condition as used in ^1H -NMR experiment. Their ^{13}C -NMR spectra (table 20 and table 21) were separated into 3 main parts: carbonyl carbon region, aromatic carbon region and aliphatic carbon region which show in accordance to the assumed structures. The aliphatic carbon signals of products **16-21** were assignable to that of methyl group of menthysulfone in range 43.03-44.31 ppm, methyl group of acetamide of products **16-18** (19.66, 20.79 and 19.70 ppm, respectively) and methyl group at position 1'''' of products **17** and **20** (21.00 and 20.99 ppm, respectively). Signals of aromatic carbons appeared in the region of 114.93-161.76 ppm while the carbonyl carbons were observed in the region of 165.19-169.42 ppm. However, compound **18**, **19** and **21** exhibited only one carbonyl carbon. This could be assumed that the signal of the two carbonyl carbons of these compounds might be appeared at the same chemical shift. In addition, the spectra of **18** and **21** showed signals of the fluorine-substituted carbon atoms which were found at 159.80 ppm ($J = 247.9$ Hz), and 161.76 ppm ($J = 249.0$ Hz), respectively. They were easily identified as a doublet. The fluorine substituent also led to the splitting of an *ortho* carbon signal into doublet with J values of 23.3 Hz (for **18**) at 114.93 ppm and 22.3 Hz (for **21**) at 116.32 ppm corresponding to a $^2J_{\text{CF}}$ coupling. A coupling constant of about 8.3 Hz was observed for **18**, which was characteristic for $^3J_{\text{CF}}$ coupling constant.

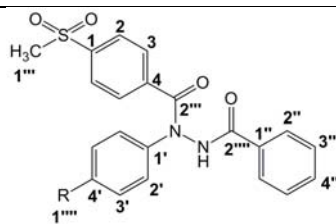


	16^a (R = H)	17^b (R = CH ₃)	18^a (R = F)
	δ , ppm	δ , ppm	δ , ppm
1	141.80	142.20	141.74
2	126.16	127.13	125.94
3	127.68	129.41	127.57
4	141.24	139.96	139.66
1'	140.07	139.39	137.44
2'	123.95	126.17	126.28 (<i>d</i> , $J_{\text{F-C-C}} = 8.3 \text{ Hz}$)
3'	128.25	129.97	114.93 (<i>d</i> , $J_{\text{F-C-C}} = 23.2 \text{ Hz}$)
4'	126.00	138.18	159.80 (<i>d</i> , $J_{\text{F-C}} = 247.9 \text{ Hz}$)
1''	43.06	44.31	43.05
1'''	19.66	20.79	19.70
2''	167.93	168.30	167.89
2'''	168.23	169.42	167.89
1''''	-	21.00	-

a: The samples were dissolved in DMSO-*d*₆ and measured at 90 °C

b: The samples were dissolved in CDCl₃ and measured at 52 °C

Table 20 The comparison of ¹³C-NMR (400MHz) data of **16-18**



	19^a (R = H)	20^b (R = CH ₃)	21^b (R = F)
	δ , ppm	δ , ppm	δ , ppm
1	141.71	142.18	142.44
2	126.69	127.13	127.37
3	127.98	128.81	128.90
4	141.04	140.04	139.76
1'	131.60	131.80	131.56
2'	125.96	126.12	127.28
3'	131.38	129.97	116.32 (<i>d</i> , $J_{F-C} = 22.3$ Hz)
4'	126.16	139.34	161.76 (<i>d</i> , $J_{F-C} = 249.0$ Hz)
1''	139.97	138.13	137.86
2''	127.64	127.43	128.23
3''	128.25	129.42	129.25
4''	131.60	132.59	132.83
1'''	43.03	44.30	44.31
2'''	165.19	167.00	167.12
2''''	165.19	168.53	167.12
1''''	-	20.99	-

a: The samples were dissolved in DMSO and measured at 90 °C

b: The samples were dissolved in CDCl₃ and measured at 50 °C

Table 21 The comparison of ¹³C-NMR (400MHz) data of **19-21**

Furthermore, HR-MS was used to confirm the element ratios of each molecule. HR-MS is one of method to determine a unique elemental composition by determination of exact mass of an ion m/z . The mass spectrometry instruments that have m/z discrimination of < 0.001 could provide important information that is not available at lower resolution. The elemental compositions of most organic compounds have calculated exact masses that differ from one another in the third or fourth decimal place or not more than 3 ppm even if the compounds have the same nominal mass (Smith, 2004). So, this technique can be applied for structural determination of synthesized compounds by the comparison of the calculated exact mass and the determined exact mass. The exact mass of compounds were determined and compared to the calculated theoretical data. The structure of all final products, **16-21**, could be confirmed for the accuracy of their assumed structure because the mass difference was not more than the acceptable limit of 3 ppm. The HR-MS results of **16-21** were demonstrated in table 22.

compound	Calcd. for	Theoretical data	Experimental data	ppm different
		(m/z)	(m/z)	
16	$C_{16}H_{16}N_2O_4S + Na$	355.0723	355.0726	0.23
17	$C_{17}H_{18}N_2O_4S + Na$	369.0879	369.0880	0.66
18	$C_{16}H_{15}FN_2O_4S + Na$	373.0629	373.0621	1.28
19	$C_{21}H_{18}N_2O_4S + Na$	417.0879	417.0872	1.77
20	$C_{22}H_{20}N_2O_4S + Na$	431.1036	431.1029	2.64
21	$C_{21}H_{17}FN_2O_4S + Na$	435.0785	435.0782	0.77

Table 22 The high resolution mass spectrometric results of **16-21**

In addition, the elemental analysis is one of method to determine a unique elemental composition by determination the percentage of each elemental composition in molecule. In this investigation, the percentage of carbon, hydrogen and nitrogen atom in molecule were determined and compared to the calculated theoretical data. The elemental analysis results of compound **16-21**, which were in all case within plus or minus 0.3% of the

calculated values, were consistent with the structure assigned of all compounds. However, it had some compounds, **17**, **19** and **21**, which there were molecule of water share in molecule in difference ratio. Two molecules of compound **17** were shared with one molecule of water. While compound **19** and **21**, there was one molecule of water share in molecule. The results of elemental analysis let to the conclusion that all of compounds should be the compounds that have the same of elemental component to the compound I intended to design and synthesize. The elemental analysis results of **16-21** were demonstrated and compared to their calculated values in table 23.

compound	Calcd. for		C	H	N
16	$C_{16}H_{16}N_2O_4S$	Calcd.	57.82	4.85	8.43
		Found	57.64	4.88	8.37
17	$C_{17}H_{18}N_2O_4S + 0.5H_2O$	Calcd.	57.45	5.39	7.88
		Found	57.84	5.19	7.75
18	$C_{16}H_{15}FN_2O_4S$	Calcd.	54.85	4.32	8.00
		Found	54.84	4.37	7.75
19	$C_{21}H_{18}N_2O_4S + 1H_2O$	Calcd.	61.15	4.89	6.79
		Found	61.26	4.93	6.85
20	$C_{22}H_{20}N_2O_4S$	Calcd.	64.69	4.94	6.86
		Found	64.45	5.01	6.87
21	$C_{21}H_{17}FN_2O_4S + 1H_2O$	Calcd.	58.60	4.45	6.51
		Found	58.58	4.55	6.62

Table 23 The elemental analysis data of **16-21**.

3.1.2 Synthesis of *N'*-Acyl-4-substituted-*N*-[4-(methylsulfonyl)phenyl]benzohydrazides (27-32)

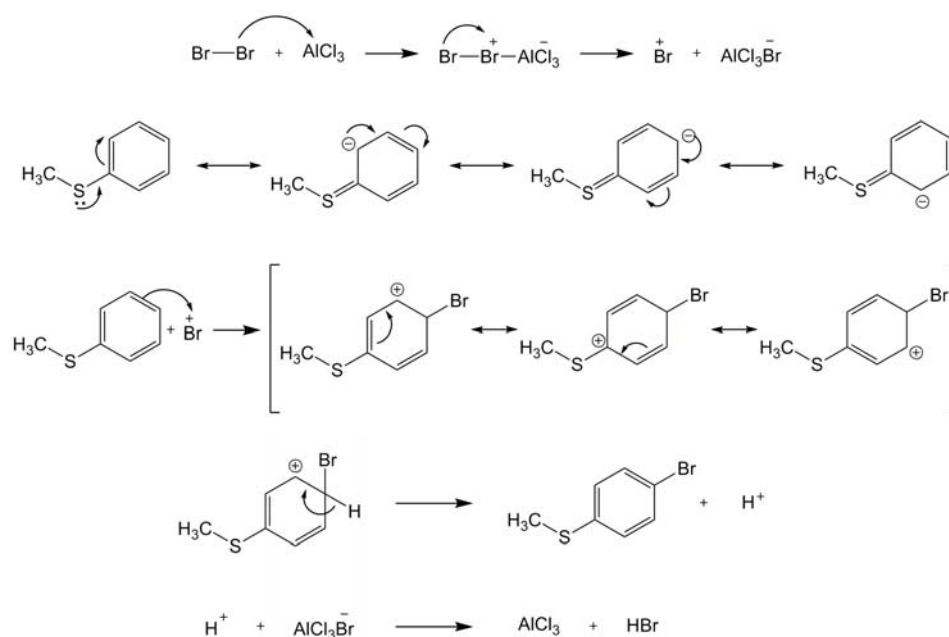
4-bromothioanisole (22)

Bromination of thioanisole was performed in order to produce 4-bromothioanisole (22). Bromination of thioanisole is a type of electrophilic aromatic substitution. Substituent, activator or deactivator, on aromatic ring is important factor which directly effect to electrophilic aromatic substitution. In this case of thioanisole, there was methylthio as activator which donates electron to the aromatic ring. These electrons could delocalize into ring system and increased reaction sensitivity to the aromatic ring. According to this fact, electrophilic substituent prefers to attack at *para* and *ortho* position than *meta* position.

Ratio of bromine to thioanisole is, moreover, also affect to the specificity of substitution on aromatic ring. If the amount of bromine is too much, more than one product will be performed: monosubstitution, disubstitution and trisubstitution product. Hence, the equivalence of bromine is necessary aspect to consider. In this investigation, 1.17 equivalent of bromine was added to the reaction afford to provide only one main product, *para*-bromothioanisole.

By the way, for typical benzene derivatives with less reactive substrates, a Lewis acid catalyst is required. Typical Lewis acid catalysts include AlCl_3 , FeCl_3 , FeBr_3 , and ZnCl_2 . These work by forming a highly electrophilic complex which attacks the benzene ring. In this investigation, AlCl_3 was selected to use as Lewis acid catalysts. The mechanism of thioanisole bromination using AlCl_3 as Lewis acid catalysts was described in this manner. Firstly, an electrophile was generated. In this reaction, the electrophile was the Br^+ ion generated by the reaction of bromine molecule with AlCl_3 , give brominium ion (Br^+) and AlCl_3Br^- . Secondly, the electrophile attacked the π electron system of the thioanisole at the most reactive position, *para* position and some *ortho* position, to form a nonaromatic carbocation. The positive charge on the

formed carbocation was delocalized throughout the molecule. The aromaticity was restored by the loss of a proton from the atom to which the bromine atom (the electrophile) had bonded. Finally, the proton reacted with the AlCl_3Br^- to regenerate the AlCl_3 catalyst and formed the product HBr (Brown *et al.*, 2005). The mechanism of this reaction could be concluded in scheme 7. The reaction was operated in dry chloroform in ice cooling to reduce excessive of reaction and was completed in high yield, 94.9% within 4 h.



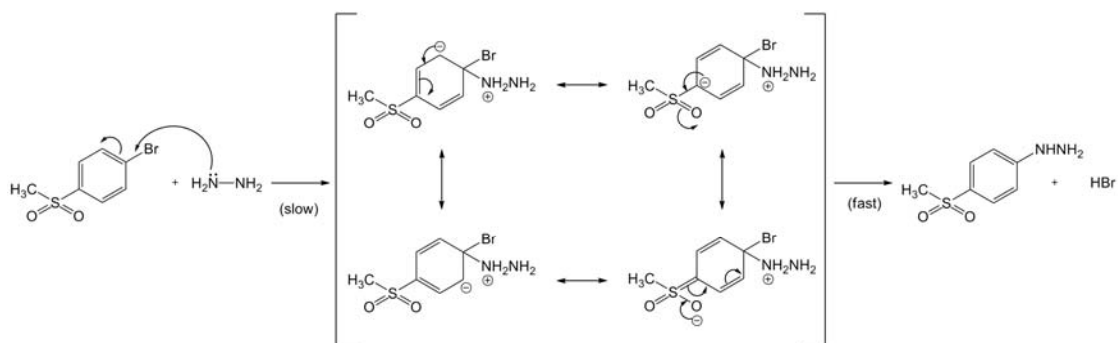
Scheme 7 The reaction mechanism of bromination of thioanisole.

4-bromomethylsulfone (**23**)

4-Bromomethylsulfone (**23**) was prepared by oxidation of 4-bromothioanisole (**22**) with oxone[®]. The reaction mechanism was the same as same as previous mechanism of *N*-acyl-4-(methylsulfonyl)-*N*-phenylbenzohydrazides (**16-21**) synthesis. The ratio of all entities used in this investigation was 1.0: 3.9 equivalents by mole of 4-bromothioanisole (**22**): oxone[®]. The reaction was performed in methanol/water for 24 hours in order to give high yield, 95.6%.

(4-(methylsulfonyl)phenyl)hydrazine (24)

(4-(methylsulfonyl)phenyl)hydrazine (**24**) was synthesized through S_N2 reaction or back side attack which is a type of nucleophilic aromatic substitution. In this investigation, **24** was generated from a reaction of hydrazine with 4-bromomethylsulfone (**23**). The reaction mechanism was considered following the well known addition-elimination mechanism of S_N2 nucleophilic aromatic substitution (Brown *et al.*, 2005). The reaction mechanism was shown in scheme 8. A lone pair from a nucleophile, hydrazine, attacked an electron deficient electrophilic center, formed bond to it and expelled a leaving group. The incoming group replaced the leaving group (Br) in one step. The formation of the addition intermediate was the rate determining step in this reaction. Finally, bromide ion was quickly expelled to complete substitution process because this addition intermediate was not stable.



Scheme 8 S_N2 mechanism nucleophilic aromatic substitution of 4-bromomethylsulfone (**23**).

In a similar manner, it was observed that the electron withdrawing groups facilitated the substitution reaction. There were several observations suggested that electron withdrawing groups lower the energy of activation by stabilizing the negative charge developed as the nucleophile adds to aromatic ring (Brown *et al.*, 2005). Herein, the methylsulfone group of 4-bromomethylsulfone (**23**) was electron withdrawing group clearly influences the rate of the reaction. A series of resonating structures for the cyclohexadienyl anion generated after the addition of the nucleophile to the aromatic system is also shown in scheme 8.

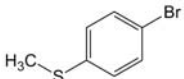
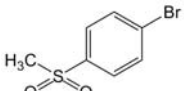
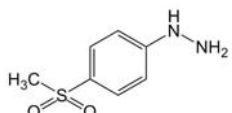
On the other hand, basicity of the leaving group is also important factors affecting reaction. Comparing the relative rates of S_N2 reaction of compounds with atoms among halides in periodic table, results show that the ability as a leaving group during an S_N2 reaction depends on its basicity. In general, the weaker basicity of a group, the greater it's leaving ability. Weak bases do not share their electrons well because their electrons are farther away from the nucleus, making it easier for their bonds to be broken. Looking at the periodic table, relative basicity decreases down a group, F⁻ > Cl⁻ > Br⁻ > I⁻, respectively. As the result, the iodide ion is a very weak base so it is the most reactive. In contrast, the fluoride ion is a stronger base than the other halides and, therefore, the least reactive. In fact, the fluoride ion is such a strong base that compounds involving them essentially do not undergo S_N2 reaction. From this fact, can be concluded that bromine atom at *para* position of 4-bromomethylsulfone (**23**) is good leaving group for the S_N2 reaction.

In this observation, the excess amount (17.0 equivalents by mole) of hydrazine monohydrate was used. The reaction was operated in polar protic solvent, 95% ethanol, and refluxed for 24 h to complete the reaction in quantitative yield.

After compounds **22-24** were finally purified by recrystallization, their physical characteristic and spectroscopic properties were examined. The physical properties were obtained by measuring a melting point while the spectroscopic properties were obtained by IR and ¹H-NMR. The results and discussions concerning their physical and spectroscopic data are described in detail as follows.

The 4-bromothioanisole (**22**) were successfully synthesized and finally purified by recrystallization with 60% methanol resulting in light yellow solid. Its melting point (38 °C) was correlated with literature reported, 38-39 °C (Weller and Hanzlik, 1991). For the 4-bromomethyl sulfone (**23**) and (4-(methylsulfonyl)phenyl)hydrazine (**24**) were successfully synthesized and finally purified by recrystallization with ethylacetate/*n*-hexane resulting in white solid. Their melting points were correlated with literature reported, 101-103 °C (Reddy *et al.*,

1989) and 132-133 °C (Takamizawa *et al.*, 1965), respectively. The physical characteristics and melting point of **22-24** could be summarized in table 24.

compound	structure	physical characteristics	melting point (°C)	
			(recrystallized solvent)	
			a*	b*
22		light yellow solid	38 (60% methanol)	38-39 ¹
23		white solid	101-103 (ethylacetate/ <i>n</i> -hexane)	101-103 ²
24		white solid	124-127 (ethylacetate/ <i>n</i> -hexane)	132-133 ³

a*: melting point from this investigation

b*: melting point from literature reported: 1; Weller and Hanzlik, 1991, 2; Reddy *et al.*, 1989, and 3; Takamizawa *et al.*, 1965

Table 24 Physical characteristics and melting point of **22-24**

The IR spectra of **22-24** also showed the similar spectrum to literature reported (Weller and Hanzlik, 1991; Reddy *et al.*, 1989; Takamizawa *et al.*, 1965). IR spectra of **22** showed characteristic signals of important functional groups according to the assumed structure. It showed peak at 3036 cm⁻¹ and 2917 cm⁻¹ assignable to C-H stretching of aromatic and aliphatic, respectively. ArC-C stretching of aromatic was also found at 1473, 1428 and 1385 cm⁻¹. In addition, C-S stretching of methylthio and C-Br stretching of aromatic bromine were found at 750-570 cm⁻¹ and 480 cm⁻¹, respectively. The IR spectra of **23** showed similar peak with IR spectra of **22**; C-H stretching of aromatic and aliphatic at 3092 cm⁻¹ and 2919 cm⁻¹, respectively, ArC-C stretching of aromatic at 1573 and 1465 cm⁻¹ and C-Br stretching at 555 cm⁻¹. In addition,

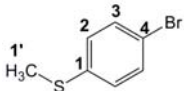
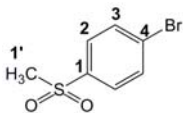
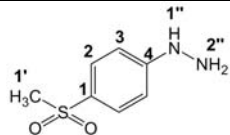
two strong sharp peaks of S=O stretching of sulfone was found at 1308 and 1147 cm^{-1} . IR spectra of **24** was similar to spectra of **23** such as, C-H stretching of aromatic and aliphatic was exhibited at 3017 cm^{-1} and 2921 cm^{-1} , respectively, ArC-C stretching of aromatic was found at 1596 cm^{-1} and two strong sharp peaks of S=O stretching of sulfone was found at 1322, 1137 cm^{-1} . Moreover, there were two peaks, N-H stretching of monohydrazide (3324 cm^{-1}) and C-N stretching of aromatic hydrazine (1269 cm^{-1}), added in spectra. The comparison of IR data of compound **22-24** could be summarized in table 25.

Cpd.	Vmax (cm^{-1})						
	V _{N-H}	V _{C-H}	V _{C-H}	V _{C-C}	V _{C-N}	V _{S=O}	V _{C-Br}
	mono hydrazide	aromatic	aliphatic	aromatic	aromatic hydrazine	sulfone	aromatic bromine
22	-	3036	2917	1428	-	-	480
23	-	3092	2919	1573	-	1308, 1147	555
24	3324	3017	2921	1596	1269	1322, 1137	-

Table 25 The comparison of IR (KBr) spectra data of **22-24**

For $^1\text{H-NMR}$ determination of **22-24**, samples was dissolved and measured in CDCl_3 (**22** and **23**) and $\text{DMSO-}d_6$ (**24**) at 25 $^\circ\text{C}$. Their spectrum also showed the similar spectrum to literature reported (Weller and Hanzlik, 1991; Reddy *et al.*, 1989; Takamizawa *et al.*, 1965). For compound **24**, it spectrum showed one of aliphatic proton at 2.43 ppm as singlet signal of 3H which was assignable to methyl proton of thiomethyl and two of aromatic proton as doublet signals with good correlatation of vicinal coupling constant, 8.5 Hz, at 7.09 and 7.37 ppm which were assignable to proton at position 2 and 3, respectively. For compound **23**, its spectrum showed one of aliphatic proton at 3.02 ppm as singlet signal of 3H which was assignable to methyl proton of methylthiosulfonyl and two of aromatic proton as doublet signals with a good correlatation of vicinal coupling constant, 8.5-8.6 Hz, at 7.69 and 7.78 ppm which were assignable to proton at position 2 and 3, respectively. For compound **24**, its spectrum also showed one of aliphatic

proton at 3.02 ppm as singlet signal of 3H which was assignable to methyl proton of methylthiosulfonyl and two of aromatic proton as doublet signals with good correlation of vicinal coupling constant, 8.7 Hz, at 6.83 and 7.55 ppm which were assignable to proton at position 2 and 3, respectively. In addition, deshield signal of primary amine, proton at position 2'', was found as singlet signal of 2H at 4.21 ppm and deshield signal of exchangeable proton (NH, proton at position 1'') was also found as singlet signal of 1H at 7.67 ppm. The comparison of ¹H-NMR data of compound **22-24** could be summarized in table 26.

												
	22^a				23^a				24^b			
	δ , ppm	m ^c	J, Hz	H ^d	δ , ppm	m ^c	J, Hz	H ^d	δ , ppm	m ^c	J, Hz	H ^d
2	7.09	<i>d</i>	8.5	2H	7.69	<i>d</i>	8.5	2H	6.83	<i>d</i>	8.7	2H
3	7.37	<i>d</i>	8.5	2H	7.78	<i>d</i>	8.6	2H	7.55	<i>d</i>	8.7	2H
1'	2.43	<i>s</i>	-	3H	3.02	<i>s</i>	-	3H	3.02	<i>s</i>	-	3H
1''	-	-	-	-	-	-	-	-	7.67	<i>s</i>	-	1H
2''	-	-	-	-	-	-	-	-	4.21	<i>s</i>	-	2H

a: The samples were dissolved and measured in CDCl₃.

b: The samples were dissolved and measured in DMSO.

c: multiplicity

d: number of proton

Table 26 The comparison of ¹H-NMR (500MHz) data of **22-24**

***N*'-(4-(methylsulfonyl)phenyl)acetohydrazide (25) and *N*'-(4-(methylsulfonyl)phenyl)benzohydrazide (26)**

N'-(4-(methylsulfonyl)phenyl)acetohydrazide (**25**) and *N*'-(4-(methylsulfonyl)phenyl)benzohydrazide (**26**) was prepared by *N*-acetylation and *N*-benzylation of (4-(methylsulfonyl)phenyl)hydrazine (**24**), respectively. The reaction mechanisms were followed as same as previous mechanism of *N*'-phenylacetohydrazides (**4-6**) and *N*'-phenylbenzohydrazides (**7-9**) synthesis.

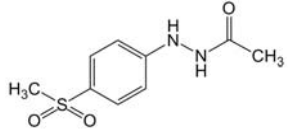
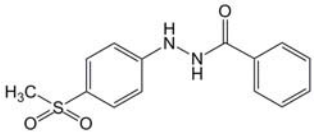
In the synthesis of *N*'-(4-(methylsulfonyl)phenyl)acetohydrazide (**25**), the molar ratio of (4-(methylsulfonyl)phenyl)hydrazine (**24**): acetic anhydride entities was 1.0: 3.5. The reaction was performed in dichloromethane/methanol for 30 min in order to give desired product in acceptable yield, 78.7%.

Furthermore, synthesis of *N*'-(4-(methylsulfonyl)phenyl)benzohydrazide (**26**), the ratio of (4-(methylsulfonyl)phenyl)hydrazine (**24**): benzoyl chloride: pyridine used was 1.0: 1.1: 1.1 by mole. The reaction was performed in dichloromethane for 1 h. The *N*'-(4-(methylsulfonyl)phenyl)benzohydrazide (**26**) could be synthesized in high yield, 99.7%.

After *N*'-(4-(methylsulfonyl)phenyl)acetohydrazide (**25**) and *N*'-(4-(methylsulfonyl)phenyl)benzohydrazide (**26**) were finally purified by recrystallization, their physical characteristic and spectroscopic properties were examined. The physical properties were obtained by measuring a melting point while the spectroscopic properties were obtained by IR and ¹H-NMR. The results and discussions concerning their physical and spectroscopic data are described in detail as follows.

Compound **25** and **26** were successfully synthesized and finally purified by recrystallization with ethylacetate/methanol/*n*-hexane and dichloromethane/methanol/*n*-hexane, respectively, resulting in white solid. The melting point of **25** was 175-178 °C. While the melting

point of **26** was 206-208.5 which correlated to literature reported 209-210 °C (Sui and Wachter, 2000). The physical characteristics and melting point of **25** and **26** could be summarized in table 27.

Cpd.	structure	physical characteristics	melting point (°C) (recrystallized solvent)	
			a*	b*
25		white solid	175-178 (ethylacetate/ methanol/ <i>n</i> -hexane)	N/A
26		white solid	206-208.5 (dichloromethane/ methanol/ <i>n</i> -hexane)	209-210 ¹

a*: melting point from this investigation

b*: melting point from literature reported: 1; Sui and Wachter, 2000

Table 27 Physical characteristics and melting point of **25-26**

The IR spectrum of **25** showed characteristic signals of important functional groups according to the assumed structure. It shows *N*-H stretching of monohydrazide at 3216 cm⁻¹ and C-H stretching of aromatic and aliphatic at 3019 cm⁻¹ and 2929 cm⁻¹, respectively. One strong sharp peak of C=O stretching of amide were also found at 1664 cm⁻¹. In addition, ArC-C stretching of aromatic was found at 1563 cm⁻¹ and two strong sharp peaks of S=O stretching of sulfone (R-SO₂-R) were found at 1283 cm⁻¹ and 1133 cm⁻¹. The IR spectra of **26** was similar to spectra of **25** such as, *N*-H stretching of monohydrazide was found at 3302 cm⁻¹ and C-H stretching aliphatic was found at 2917 cm⁻¹ and one strong sharp peak of C=O stretching of amide was also found at 1668 cm⁻¹. In addition, ArC-C stretching of aromatic was found at 1596 cm⁻¹ and two strong sharp peaks of S=O stretching of sulfone (R-SO₂-R) were found at 1279 cm⁻¹ and

1142 cm^{-1} as well. The comparison of IR data of compound **25-26** could be summarized in table 28.

Cpd.	Vmax (cm^{-1})					
	V _{N-H}	V _{C-H}	V _{C-H}	V _{C=O}	V _{C-C}	V _{S=O}
	monohydrazide	aromatic	aliphatic	amide	aromatic	sulfone
25	3216	3019	2929	1664	1563	1283, 1133
26	3302	-	2917	1668	1596	1279, 1142

Table 28 The comparison of IR (KBr) data of **25-26**

For $^1\text{H-NMR}$ spectra of **25** and **26**, samples were dissolved in $\text{DMSO-}d_6$ and measured at 25 °C. $^1\text{H-NMR}$ spectrum of **25**, the spectrum showed two of aliphatic proton at 1.91 and 3.06 ppm as singlet signals of 3H which were assignable to methyl proton of acetamide and methyl proton of methylthiosulfonyl, respectively. Moreover, two of aromatic protons that showed as doublet signals with a good correlation of vicinal coupling constant, 8.8 Hz, at 7.63 and 6.78 ppm, were assignable to proton at position 2 and 3, respectively. In addition, deshield signal of exchangeable proton, *NH* at position 1'' and 2'', were found as doublet signals of 1H with a good correlation of vicinal coupling constant, 1.5-1.6 Hz, at 8.49 ppm and 9.77 ppm, respectively. $^1\text{H-NMR}$ spectrum of **26**, the spectrum showed one of aliphatic proton at 3.07 ppm as singlet signals of 3H which was assignable to methyl proton of methylthiosulfonyl. Moreover, the aromatic proton signals were found at peak around 6.88 -7.92 ppm in good correlation of coupling constant (*J*-vaule, Hz). The *J*-vaules of vicinal coupling between H at position 2 and 3 and vicinal coupling between H at position 2' and 3' were 7.2-8.8 Hz and 7.7-8.8 Hz, respectively. The aromatic H signals were found in five sets. Two of them (7.92 and 6.88 ppm) were assignable to H of 4-SO₂CH₃ aniline ring. The rest (7.67, 7.52 and 7.59 ppm) were assignable to H of benzamide ring. In addition, deshield signal of exchangeable proton, *NH* at position 1''' and 2'', were found as singlet signals of 1H at 8.75 ppm and 10.51 ppm, respectively. The comparison of $^1\text{H-NMR}$ data of compound **25-26** could be summarized in table 29.

	25				26			
	δ , ppm	m ^a	J, Hz	H ^b	δ , ppm	m ^a	J, Hz	H ^b
2	7.63	<i>d</i>	8.8	2H	7.92	<i>d</i>	7.2	2H
3	6.78	<i>d</i>	8.8	2H	6.88	<i>d</i>	8.8	2H
2'	-	-	-	-	7.67	<i>d</i>	8.8	2H
3'	-	-	-	-	7.52	<i>t</i>	7.7	2H
4'	-	-	-	-	7.59	<i>t</i>	7.4	1H
1''	3.06	<i>s</i>	-	3H	3.07	<i>s</i>	-	3H
1'''	8.49	<i>d</i>	1.5	1H	8.75	<i>s</i>	-	1H
2''	9.77	<i>d</i>	1.6	1H	10.51	<i>s</i>	-	1H
1''''	1.91	<i>s</i>	-	3H	-	-	-	-

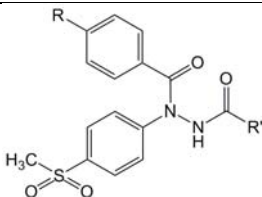
a: multiplicity

b: number of proton

Table 29 The comparison of ¹H-NMR (500MHz, DMSO-*d*₆) data of **25-26**

N'-acyl-*N*-(4-(methylsulfonyl)phenyl)benzohydrazides (**27-32**)

In this step, *N'*-acyl-*N*-(4-(methylsulfonyl)phenyl)benzohydrazides (**27-32**) could be synthesized by amidation of secondary amine (**25** and **26**) with their corresponding benzoyl chloride: benzoyl chloride, 4-methylbenzoyl chloride and 4-fluorobenzoyl chloride. The reaction mechanism and reaction's condition could be discussed as same as the previous described in synthesis of **10-15**. The stoichiometric amount of all entities and % yield was concluded in table 30.



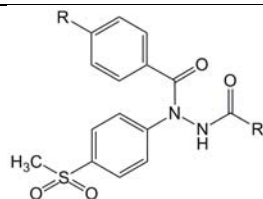
compound	R	R'	amount of entities (equivalent by mole)			time (hours)	% yield
			corresponding	corresponding	pyridine		
			2° amine	benzoyl chloride			
27	H	CH ₃	1.0	1.1	4.0	22	54.9
28	CH ₃	CH ₃	1.0	1.1	4.0	22	90.1
29	F	CH ₃	1.0	1.1	4.0	22	69.5
30	H	C ₆ H ₅	1.0	1.1	4.0	3	87.1
31	CH ₃	C ₆ H ₅	1.0	1.1	4.0	3	quant*
32	F	C ₆ H ₅	1.0	2.2	4.0	3	93.7

*quantitative

Table 30 The stoichiometric amount of all entities and % yield of **27-32**

After compound **27-32** were finally purified by recrystallization, their physical characteristic and spectroscopic properties were examined. The physical properties were obtained by measuring a melting points and analyzing for C, H and N elements in compound. The spectroscopic properties were obtained by IR, ¹H-NMR, ¹³C-NMR and HR-MS. The results and discussions concerning the physical and spectroscopic data of each compound are described in detail as follows.

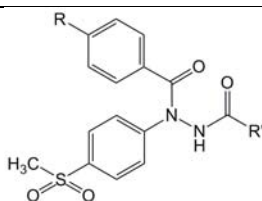
N'-acyl-*N*-(4-(methylsulfonyl)phenyl)benzohydrazides (**27-32**) products were successfully synthesized and finally purified by recrystallization with ethyl acetate/*n*-hexane resulting in white solid. Their melting points were summarized in table 31.



compound	R	R'	physical characteristics	mp. (°C)	(recrystallized solvent)
27	H	CH ₃	white solid	181-184	(ethyl acetate/ <i>n</i> -hexane)
28	CH ₃	CH ₃	white solid	180-183	(ethyl acetate/ <i>n</i> -hexane)
29	F	CH ₃	white solid	175-180	(ethyl acetate/ <i>n</i> -hexane)
30	H	C ₆ H ₅	white solid	199-202	(ethyl acetate/ <i>n</i> -hexane)
31	CH ₃	C ₆ H ₅	white solid	211-213	(ethyl acetate/ <i>n</i> -hexane)
32	F	C ₆ H ₅	white solid	141-143	(ethyl acetate/ <i>n</i> -hexane)

Table 31 Physical characteristics and melting point of **27-32**

IR spectra of compounds **27-32** showed their characteristic signals of important functional groups according to the assumed structure. Eventhough, structure of compounds **27-32** was different to compounds **16-32** at position of their 4-methanesulfonyl phenyl substituent. Compounds **27-32**, 4-methanesulfonyl phenyl was attached to nitrogen of amide while 4-methanesulfonyl phenyl was attached to carbonyl of amide in compounds **16-21**. But their functional groups were alike. Hence, compounds **27-32** should give the IR spectra similar to IR spectra of compounds **16-21**. All spectra (table 32) were showed *N*-H stretching of monohydrazide at $\approx 3200\text{ cm}^{-1}$ and C-H stretching of aromatic and aliphatic at upper wavenumbers (>3000) and lower wavenumbers (<3000), respectively. Two strong sharp peaks of C=O stretching of 2° and 3° amide were also found at $1680\text{-}1620\text{ cm}^{-1}$. In addition, two strong sharp peaks of S=O stretching of sulfone (R-SO₂-R) were found in subrange $1370\text{-}1290\text{ cm}^{-1}$ and $1170\text{-}1110\text{ cm}^{-1}$ as well.



	R	R'	V _{max} (cm ⁻¹)				
			V _{N-H} , monohydrazide	V _{C-H} , aromatic	V _{C-H} , aliphatic	V _{C=O} , 2°, 3° amide	V _{S=O} , sulfone
27	H	CH ₃	3320	3069	2921	1707, 1682	1298, 1147
28	CH ₃	CH ₃	3297	3003	2926	1701, 1654	1307, 1149
29	F	CH ₃	3358	3075	2917	1698, 1681	1300, 1148
30	H	C ₆ H ₅	3262	3004	2924	1690, 1657	1291, 1147
31	CH ₃	C ₆ H ₅	3380	3082	2925	1690, 1674	1282, 1145
32	F	C ₆ H ₅	3244	-	2988	1692, 1654	1295, 1146

Table 32 The comparison of IR (KBr) data of **27-32**

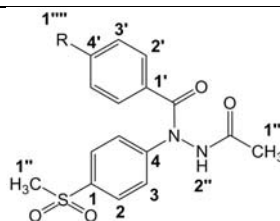
¹H-NMR spectra of **27-32** were also interpreted on the basis of the chemical shifts, multiplicity and intergral intensity. All samples were dissolved and measured in CDCl₃ at 25 °C. Compound in these series did not show the broadening signal at aromatic proton region when measured at room temperature. As the resulted, it might be indicated that the rotation of amide bond were not affected to compound in this group.

The ¹H-NMR data of **27-32** (table 33 and table 34) clearly corresponded to the relative abundance and connectivity of each hydrogen type founded in their structure. Likewise compound **16-21**, each spectrum was separated into two main set of signals; aliphatic proton and aromatic proton. At aliphatic proton region, the singlet signals of 3H at 3.00-3.01 ppm were assignable to H signal of SO₂-CH₃. The singlet signals of 3H at 1.92, 1.61 and 1.98 ppm were assignable to H signal of CH₃ in acetamide of compound **27-29**, respectively. Moreover, methyl

substituent compounds (**28** and **31**) showed signal of methyl at 2.33 and 2.31 ppm as singlet signal of 3H, respectively.

The aromatic proton signals of **27-32** were different, based on the substituent on aromatic of each compound. From table 33, compound **27** exhibited aromatic H signals in five sets. Two of them (7.69 and 7.36 ppm) were assignable to H of 4-SO₂CH₃ aniline ring. The rest (7.51, 7.32 and 7.42 ppm) were assignable to H of carbonyl-phenyl ring. Compound **28** and **29** exhibited aromatic H signals in four sets. Two of them (7.71 (**28**), 7.71 (**29**) and 7.33 (**28**), 7.34 (**29**) ppm) were assignable to H of 4-SO₂CH₃ aniline ring. The rest (7.39 (**28**), 7.56 (**29**) and 7.10 (**28**), 7.02 (**29**) ppm) were assignable to H of carbonyl-phenyl ring. From table 34, compound **30** exhibited aromatic H signals in eight sets. Two of them (7.71 and 7.43 ppm) were assignable to H of 4-SO₂CH₃ aniline ring. Three of them (7.70, 7.40 and 7.52 ppm) were assignable to H of carbonyl-phenyl ring. The rest (7.57, 7.30 and 7.38 ppm) were assignable to H of benzamide ring. Compound **31** and **32** exhibited aromatic H signals in seven sets. Two of them (7.72 (**31**), 7.74 (**32**) and 7.40 (**31**), 7.43 (**32**) ppm) were assignable to H of 4-SO₂CH₃ aniline ring. Two of them (7.41 (**31**), 7.63 (**32**) and 7.09 (**31**), 7.01 (**32**) ppm) were assignable to H of carbonyl-phenyl ring. The rest (7.44 (**31**), 7.74 (**32**), 7.73 (**31**), 7.44 (**32**) and 7.52 (**31**), 7.56 (**32**) ppm) were assignable to H of benzamide ring.

Moreover, the fluorine substituent compounds (**29** and **32**) also showed AA'XX' system for the aromatic protons (7.01-7.63 ppm) with additional ³J_{HF} and ⁴J_{HF} splitting. **29** exhibited the H_{XX'} and H_{AA'} signals as a pseudo-triplet at 7.02 ppm (*J* = 8.5 Hz) and as a doublet of doublets at 7.56 ppm (*J* = 5.4 Hz), while **32** showed the H_{XX'} and H_{AA'} signals as a pseudo-triplet at 7.01 ppm (*J* = 8.5 Hz) and as a doublet of doublets at 7.63 ppm (*J* = 4.9 Hz). In addition, the weak broadening singlet signals of exchangeable proton (NH) of compound **16-21** were shown in range 8.41-9.13 ppm.



	27 (R = H)				28 (R = CH ₃)				29 (R = F)			
	δ , ppm	m ^a	J, Hz	H ^b	δ , ppm	m ^a	J, Hz	H ^b	δ , ppm	m ^a	J, Hz	H ^b
2	7.69	<i>d</i>	8.8	2H	7.71	<i>d</i>	8.8	2H	7.71	<i>d</i>	9.3	2H
3	7.36	<i>d</i>	8.8	2H	7.33	<i>d</i>	8.8	2H	7.34	<i>d</i>	8.8	2H
2'	7.51	<i>d</i>	7.3	2H	7.39	<i>d</i>	8.3	2H	7.56	<i>dd</i>	5.4, 8.8	2H
3'	7.32	<i>t</i>	7.6	2H	7.10	<i>d</i>	7.8	2H	7.02	<i>dd</i>	8.5, 8.5	2H
4'	7.42	<i>t</i>	7.6	1H	-	-	-	-	-	-	-	-
1''	3.00	<i>s</i>	-	3H	3.00	<i>s</i>	-	3H	3.01	<i>s</i>	-	3H
1'''	1.92	<i>s</i>	-	3H	1.61	<i>s</i>	-	3H	1.98	<i>s</i>	-	3H
1''''	-	-	-	-	2.33	<i>s</i>	-	3H	-	-	-	-
2''	8.59	<i>s</i>	-	1H	8.44	<i>s</i>	-	1H	8.41	<i>s</i>	-	1H

a: multiplicity

b: number of proton

Table 33 The comparison of ¹H-NMR (400MHz, CDCl₃) data of **27-29**

	30 (R = H)				31 (R = CH ₃)				32 (R = F)			
	δ , ppm	m ^a	J, Hz	H ^b	δ , ppm	m ^a	J, Hz	H ^b	δ , ppm	m ^a	J, Hz	H ^b
2	7.71	<i>d</i>	8.8	2H	7.72	<i>d</i>	8.3	2H	7.74	<i>d</i>	6.3	2H
3	7.43	<i>d</i>	8.8	2H	7.40	<i>d</i>	6.8	2H	7.43	<i>d</i>	8.8	2H
2'	7.70	<i>d</i>	8.3	2H	7.41	<i>d</i>	8.3	2H	7.63	<i>dd</i>	4.9, 8.8	2H
3'	7.40	<i>t</i>	7.8	2H	7.09	<i>d</i>	7.8	2H	7.01	<i>dd</i>	8.5, 8.5	2H
4'	7.52	<i>t</i>	7.3	1H	-	-	-	-	-	-	-	-
2''	7.57	<i>d</i>	6.8	2H	7.44	<i>d</i>	7.8	2H	7.74	<i>d</i>	8.8	2H
3''	7.30	<i>t</i>	7.6	2H	7.73	<i>t</i>	8.3	2H	7.44	<i>t</i>	8.1	2H
4''	7.38	<i>m</i>	-	1H	7.52	<i>t</i>	7.6	1H	7.56	<i>t</i>	7.3	1H
1''''	3.00	<i>s</i>	-	3H	3.00	<i>s</i>	-	3H	3.01	<i>s</i>	-	3H
1''''	-	-	-	-	2.31	<i>s</i>	-	3H	-	-	-	-
2'''	9.13	<i>s</i>	-	1H	9.08	<i>s</i>	-	1H	8.97	<i>s</i>	-	1H

a: multiplicity

b: number of proton

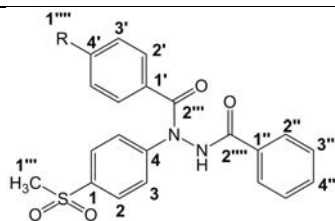
Table 34 The comparison of ¹H-NMR (400MHz, CDCl₃) data of **30-32**

The number of signals on ¹³C-NMR spectra also confirmed the structure of products, **27-32** (table 35 and table 36). Likewise compounds **16-21**, their ¹³C-NMR spectra were separated into 3 main parts: carbonyl carbon region, aromatic carbon region and aliphatic carbon region. The aliphatic carbon signals were assignable to that of methyl group of menthysulfone in range 44.59-44.62 ppm, methyl group of acetamide of products **27-29** (20.67, 20.79 and 20.69 ppm, respectively) and methyl group at position 1'''' of products **28** and **31** (21.61 and 21.60 ppm, respectively). Signals of aromatic carbons appeared in the region of 115.52-166.69 ppm while

the carbonyl carbons were observed in the region of 166.74-170.66 ppm. However, compound **32** exhibited only one carbonyl carbon. This indicated that two carbonyl carbons of this compound might be appeared at the same chemical shift. In addition, the spectra of **29** showed signals of the fluorine-substituted carbon atoms which were found at 164.19 ppm as a doublet ($J = 255.0$ Hz). The fluorine substituent also leads to the splitting of an *ortho* carbon signal into doublet with J values of 22.0 Hz (for **29**) at 115.52 ppm and 21.5 Hz (for **32**) at 115.54 ppm corresponding to a $^2J_{CF}$ coupling. A coupling constant of $^3J_{CF}$ was not appeared both in **29** and **32**.

	27 (R = H)	28 (R = CH ₃)	29 (R = F)
	δ , ppm	δ , ppm	δ , ppm
1	136.98	137.16	137.04
2	128.26	128.45	128.06
3	124.11	124.48	124.04
4	146.61	141.98	146.55
1'	133.77	130.52	130.72
2'	128.00	128.07	130.63
3'	131.23	128.98	115.52 (<i>d</i> , $J_{F-C-C} = 22.0$ Hz)
4'	128.06	147.07	164.19 (<i>d</i> , $J_{F-C} = 255.0$ Hz)
1''	44.60	44.59	44.61
1'''	20.67	20.79	20.69
2''	169.43	169.63	169.38
2'''	170.50	170.22	169.48
1''''	-	21.61	-

Table 35 The comparison of $^{13}\text{C-NMR}$ (400MHz, CDCl_3) data of **27-29**



	30 (R = H)	31 (R = CH ₃)	32 (R = F)
	δ , ppm	δ , ppm	δ , ppm
1	131.05	130.57	130.75
2	128.13	128.50	128.12
3	124.13	124.45	123.85
4	146.63	141.99	146.57
1'	137.02	131.13	130.96
2'	128.08	127.35	128.95
3'	128.28	128.99	115.54 (<i>d</i> , $J_{\text{F-C-C}} = 21.5 \text{ Hz}$)
4'	132.73	147.04	166.69
1''	131.25	137.09	136.90
2''	127.29	128.12	127.37
3''	128.79	128.78	130.11
4''	133.81	132.71	132.96
1'''	44.62	44.60	44.61
2'''	166.74	166.86	169.98
2''''	170.66	170.45	169.98
1''''	-	21.60	-

Table 36 The comparison of ¹³C-NMR (400MHz, CDCl₃) data of **30-32**

HR-MS was also used to confirm the element ratios of each molecule. The exact mass of compounds were determined and compared to the calculated theoretical data. The structure of all final products, **27-32**, could be confirmed for the accuracy of their assumed

structure because the mass difference was not more than the acceptable limit of 3 ppm. The HR-MS results of **27-32** were demonstrated and compared to their calculated exacted mass in table 37.

compound	Calcd. for	Theoretical data	Experimental data	ppm different
		(m/z)	(m/z)	
27	C ₁₆ H ₁₆ N ₂ O ₄ S + Na	355.0723	355.0721	1.65
28	C ₁₇ H ₁₈ N ₂ O ₄ S + Na	369.0879	369.0887	0.77
29	C ₁₆ H ₁₅ FN ₂ O ₄ S + Na	373.0629	373.0625	1.12
30	C ₂₁ H ₁₈ N ₂ O ₄ S + Na	417.0879	417.0882	0.06
31	C ₂₂ H ₂₀ N ₂ O ₄ S + Na	431.1036	431.1035	0.81
32	C ₂₁ H ₁₇ FN ₂ O ₄ S - H	411.0809	411.0816	1.23

Table 37 The high resolution mass spectrometric results of **27-32**

In addition, the elemental analysis was also performed in order to confirm the characteristic of synthesized compounds. In this investigation, the percentage of carbon, hydrogen and nitrogen atom in molecule were determined and compared to the calculated theoretical data. The elemental analysis results of compound **27-32**, which were in all case within plus or minus 0.3% of the calculated values, were consistent with the structure assigned of all compounds. However, there was molecule of water share in molecule of compounds **32** in ratio 0.5:1. The results of elemental analysis let to the conclusion that all of compounds should be the compounds that have the same of elemental component to the compound we intended to design and synthesize. The elemental analysis results of **27-32** were demonstrated and compared to their calculated values in table 38.

compound	Calcd. for		C	H	N
27	$C_{16}H_{16}N_2O_4S$	Calcd.	57.82	4.85	8.43
		Found	57.60	4.97	8.46
28	$C_{17}H_{18}N_2O_4S$	Calcd.	58.94	5.24	8.09
		Found	57.97	5.15	7.93
29	$C_{16}H_{15}FN_2O_4S$	Calcd.	54.85	4.32	8.00
		Found	54.66	4.39	8.01
30	$C_{21}H_{18}N_2O_4S$	Calcd.	63.94	4.60	7.10
		Found	63.75	4.72	7.09
31	$C_{22}H_{20}N_2O_4S$	Calcd.	64.69	4.94	6.86
		Found	64.46	5.23	6.79
32	$C_{21}H_{17}FN_2O_4S + 0.5H_2O$	Calcd.	59.85	4.30	6.65
		Found	59.99	4.28	6.67

Table 38 The elemental analysis data of 27-32

The total yields of **16-21** and **27-32** through two-step or three-step synthesis pathway started from their corresponding phenylhydrazines were summarized in table 39.

Compound	R	R'	R''	Synthesis Pathway	Total Yield (%)
16	-SO ₂ CH ₃	-CH ₃	-H	Three-step Synthesis*	66.4
17	-SO ₂ CH ₃	-CH ₃	-CH ₃	Three-step Synthesis*	78.3
18	-SO ₂ CH ₃	-CH ₃	-F	Three-step Synthesis*	66.0
19	-SO ₂ CH ₃	-C ₆ H ₅	-H	Three-step Synthesis*	67.5
20	-SO ₂ CH ₃	-C ₆ H ₅	-CH ₃	Three-step Synthesis*	75.7
21	-SO ₂ CH ₃	-C ₆ H ₅	-F	Three-step Synthesis*	65.0
27	-H	-CH ₃	-SO ₂ CH ₃	Two-step Synthesis**	43.2
28	-CH ₃	-CH ₃	-SO ₂ CH ₃	Two-step Synthesis**	70.9
29	-F	-CH ₃	-SO ₂ CH ₃	Two-step Synthesis**	54.7
30	-H	-C ₆ H ₅	-SO ₂ CH ₃	Two-step Synthesis**	86.8
31	-CH ₃	-C ₆ H ₅	-SO ₂ CH ₃	Two-step Synthesis**	93.4
32	-F	-C ₆ H ₅	-SO ₂ CH ₃	Two-step Synthesis**	99.7

* through three-step synthesis pathway started from their corresponding phenylhydrazines

** through two-step synthesis pathway started from (4-(methylsulfonyl)phenyl)hydrazine (**24**)

Table 39 Total yield of twelve desired *N*-phenylbenzohydrazides (**16-21** and **27-32**).

As conclusion of synthetic investigation provided twenty eight synthesized compounds, nineteen of them were novel chemical entities; **6**, **10-21**, **25** and **27-32** and the rest were known compounds; **4-5**, **7-9**, **22-24** and **26**. According to the total yield **16-21** and **27-32**

(table 39), could be concluded that these synthetic procedure could provide the good and acceptable amounts (43-99 %) of product.

According to all of spectroscopic data, IR, $^1\text{H-NMR}$, $^{13}\text{C-NMR}$, HRMS and elemental analysis data, I can conclude that I could successfully synthesize twelve novel chemical entities; **16-21** and **27-32**.

3.2 Determination in molecular orientation

Stereoisomers are separated into two main types including optical isomer and geometric isomer. Optical isomer is commonly described for complementary chirality compounds which can rotate the plane of polarized light. Whereas the geometric isomer is normally explained for restricted rotation compounds such as alkene and cyclic compounds, exhibit as *cis* or *trans* isomer (Brown *et al.*, 2005).

Moreover, in fact of amide chemistry, the lone pair of electrons on the nitrogen is delocalized onto the carbonyl, thus forming a partial double bond between nitrogen and carbonyl carbon. Consequently the nitrogen in amides is not pyramidal but is planar (Zabicky, 1970). The planar conformation of amide based on C-N bond resonance is demonstrated in figure 101 (Zabicky, 1970). From this fact indicates that compounds containing amide bond are strong enough to prevent fast bond rotations, which are similar to that of alkene, probable to orientate in *cis* or *trans* isomer. Based on the Cahn-Ingold-Prelog system, each substituent group at adjacent atoms of double bond is ranked by the sequene rules. Then that conformer with the two higher ranking groups on the same side of the double bond is called *cis*. In contrary, conformer is called *trans* if two higher ranking groups are on the opposit side of the double bond (March, 1992).

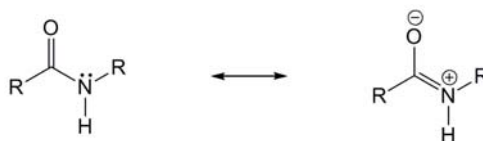


Figure 101 Planar conformation of acetamide based on C-N bond resonance

Although the partial double bond of amide is strong enough to prevent fast bond rotation but weak enough to permit both possible geometrical isomers to be present (Zabicky, 1970). Hence, the molecular orientation of synthesized *N*-phenylbenzohydrazides (**16-21** and **27-32**) containing two of amide bonds moiety should be determined whether they are probably to orientate in *cis* or *trans* conformer. Here, the conformation will be denoted as “c” (for *cis*) or “t” (for *trans*). Due to the containing two amide bonds moiety in structure of designed compounds (**16-21** and **27-32**), therefore, the possibility conformers of them can be expressed as four types: (c, c), (c, t), (t, c) and (t, t) which are illustrated in figure 102.

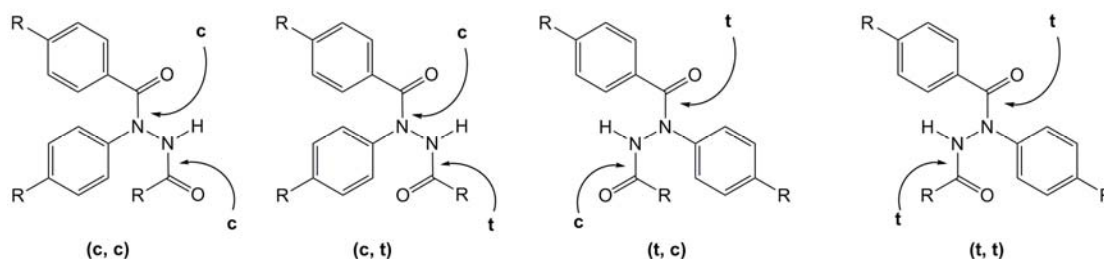


Figure 102 The possibility conformers of synthesized *N*-phenyl benzohydrazide derivatives (**16-21** and **27-32**): (c, c), (c, t), (t, c) and (t, t)

A *cis*-preference was general in *N*-methyl aromatic amides; that was, benzanilide (figure 103) existed exclusively in the *trans* conformation both in the crystal and in solution, whereas *N*-methylbenzanilide (figure 103) existed predominantly in the *cis* structure (Kashino *et al.*, 1979; Itai *et al.*, 1989; Azumaya *et al.*, 1991).

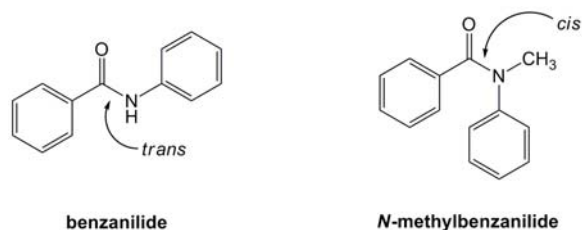


Figure 103 Conformation of benzanilide (*cis*) and *N*-methylbenzanilide (*trans*)

Moreover investigation by the use of *ab initio* molecular orbital (MO) calculation indicated that *trans* structure was more stable by 2.15 kcal/mol than the *cis* one in acetanilide (figure 104), whereas *cis* structure was more stable by 3.5 kcal/mol than the *trans* one in *N*-methylacetanilide (figure 104) (Saito *et al.*, 1995). The *cis*-preference in *N*-methylacetanilides seems to be ascribed to destabilization of the *trans* structure due to steric hindrance between two methyl groups and to electronic repulsion between carbonyl lone-pair electrons and phenyl π -electrons in the twisted orientation (Saito *et al.*, 1995). The energy relationships of conformers of acetanilide and *N*-methylacetanilide are illustrated in figure 104. Where ΔE_1 as reflecting the loss of π -conjugation, ΔE_2 as reflecting the electronic repulsion between π and oxygen lone pair, $\Delta E_1 + \Delta E_3$, as reflecting the sum of the loss of π -conjugation and the steric repulsion (*N*-methyl group and phenyl ring), and $\Delta E_2 + \Delta E_4$, as reflecting the sum of the electronic repulsion and the steric repulsion (*N*-methyl and *C*-methyl groups).

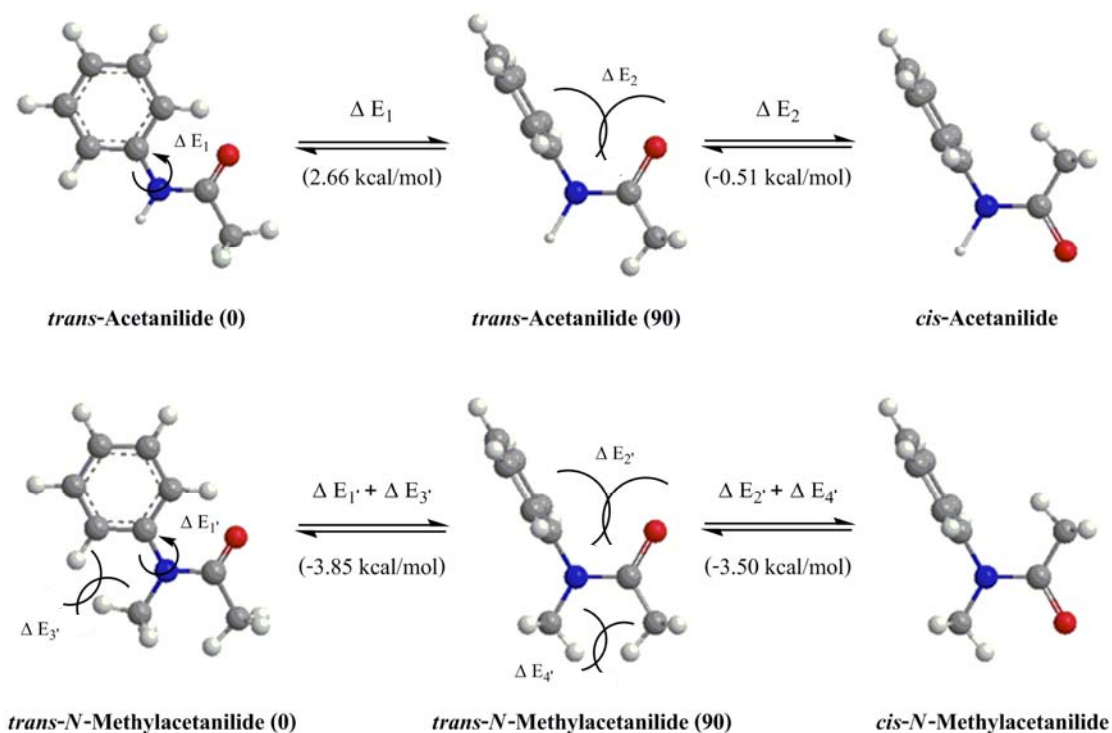


Figure 104 The energy relationships of conformers of acetanilide and *N*-methylacetanilide.

Based on the *trans*-preference of secondary aromatic amides (benzanilide or acetanilide) and *cis*-preference of tertiary aromatic amides (*N*-methylbenzanilide or *N*-methylacetanilide) that described before, I would like to confirm whether this conformation preference still exists in our designed compounds (**16-21** and **27-32**) or not. The determination of their orientation was conducted using $^1\text{H-NMR}$ and X-Ray crystallographic technique to evaluate the conformational changes in solution and solid states, respectively.

3.2.1 $^1\text{H-NMR}$ spectra studies

In several reports, $^1\text{H-NMR}$ technique was selected as tool for studying about conformation preference of aromatic amides in solution state (Azuyama *et al.*, 1995; Azuyama *et al.*, 1996). According to $^1\text{H-NMR}$ spectral data of all targeted compounds (**16-21** and **27-32**) found that $^1\text{H-NMR}$ spectrum of **16-21** exhibited broaden peaks at aromatic region when measured in $\text{DMSO-}d_6$ at room temperature (25°C) whereas compounds **27-32** did not exhibit.

This phenomenon indicated that **16-21** were existed more than one conformers which arise from bond rotation. Elevation of the temperature resulted in time environments for all aromatic resonances as a result of rapid rotation leading to sharpening signal of one average conformer, for example, in compound **19** as shown in figure 105.

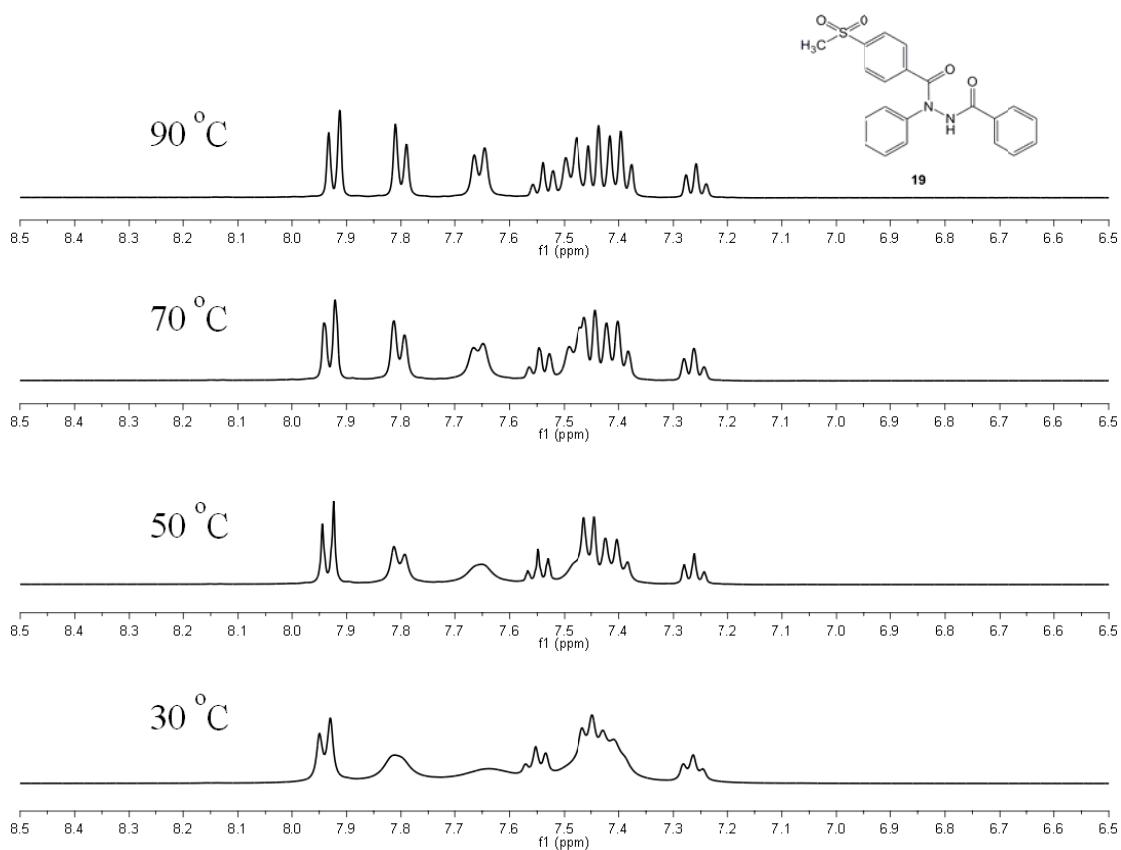


Figure 105 ¹H-NMR signals of **19** in aromatic region at 30 °C, 50 °C, 70 °C and 90 °C

In our previous work, we synthesized 4-(methylsulfonyl)-*N*-phenylbenzamide (PCB02) and *N*-methyl-4-(methylsulfonyl)-*N*-phenyl benzamide (PCB04) and studied their conformation by ¹H-NMR (Songkram *et al.*, 2007). As the ¹H-NMR spectral data of PCB02 and PCB04 in table 40, the remarkable high-field shifts of aromatic proton signals of PCB04 compared with their secondary analogues (from 8.17-7.13 ppm to 7.77-7.18 ppm), implied that they should exist in a different conformation in solution. These significant high-field shifts of

aromatic protons (0.09-0.58 ppm) presumably arise from the ring current effect of the benzene ring when benzamide exists as face to face in *cis*-conformation. From this result can conclude that PCB02 is preferred to exist in *trans*-conformer whereas PCB04 exists in *cis*-conformer, which consistent with previous investigation on benzamide and *N*-methylbenzanilide, respectively (Azuyama *et al.*, 1995; Azuyama *et al.*, 1996).

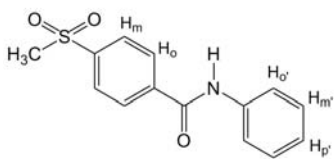
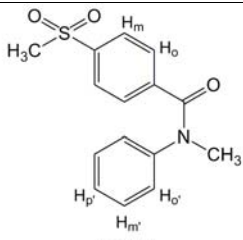
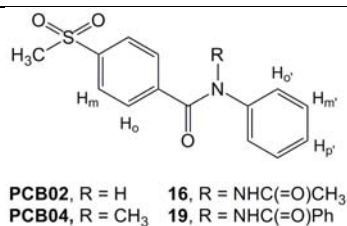
	 PCB02					 PCB04				
	Chemical shift of aromatic proton (ppm)					$\Delta\delta$ (ppm)				
	H _o	H _m	H _{o'}	H _{m'}	H _{p'}	H _o	H _m	H _{o'}	H _{m'}	H _{p'}
PCB02	8.17	8.08	7.78	7.37	7.13					
PCB04	7.77	7.50	7.21	7.28	7.18	0.4	0.58	0.57	0.09	-0.05

Table 40 ¹H-NMR spectral data of PCB02 and PCB04

Compound **16** and **19** were selected as representative to study conformation preference of compound in this group (**16-21**). In order to define which conformer is preferred (*cis* or *trans*) in solution state, ¹H-NMR spectral of **16** and **19** were compared to structurally related compounds (PCB02 and PCB04). The ¹H-NMR spectral comparison of compound **16** and **19** with PCB02 and PCB04 are summarized in table 41.



	Chemical shift of aromatic proton (ppm)				
	H _o	H _m	H _{o'}	H _{m'}	H _{p'}
PCB02 (<i>trans</i>)	8.17	8.08	7.78	7.37	7.13
PCB04 (<i>cis</i>)	7.77	7.50	7.21	7.28	7.18
16	7.93	7.72	7.35	7.38	7.24
19	7.92	7.80	7.49	7.40	7.26

Table 41 ¹H-NMR spectral data of PCB02, PCB04, **16** and **19**

As the spectral data from table 41, the chemical shift of aromatic proton of **16** and **19** when compared with PCB02 (*trans*-preference) and PCB04 (*cis*-preference) showed middle values between *trans* and *cis* conformation. That is, I cannot clearly define the conformation of **16** and **19** by this method. Since flexibility structure, two of amide bonds rotation (Zabicky, 1970) and also N-N bond rotation (Verma and Prasad, 1973), of compounds might be affected to considered chemical shift of aromatic proton.

To further investigation I also observed the conformational equilibrium of **16** in solution by temperature dependence NMR technique (measure in acetone-*d*₆ from 25 °C to -20 °C) and found a minor conformer at -10 °C and -20 °C, as judged from a signal N-H proton. As decreased the temperature from 25 °C to -20 °C, chemical shift of aromatic proton did not change but gave more broaden peak (figure 106) because of slowly rotated of N-Ph and carbonyl-Ph. Whereas N-H signal was split one more peak at higher field, of which the minor peak (10.35 ppm at -10 °C and 10.41 ppm at -20 °C, figure 106) was assigned to the N-H of minor conformer. This minor conformer might be occurred by rotation of N-N bond and allowed N-H to locate in

anisotropic area of carbonyl of tertiary amide. This situation is occurred only as *cis*-conformation, two of aromatic rings are orientated in the same side of amide bond (figure 107).

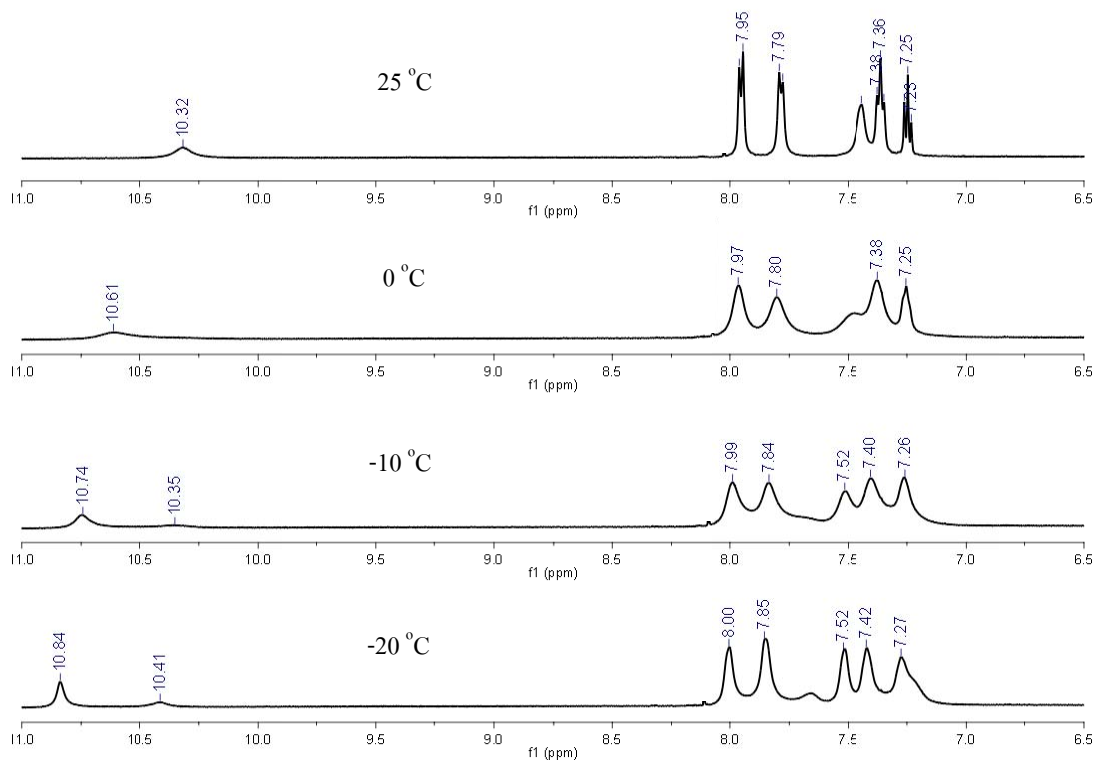


Figure 106 The temperature dependence of $^1\text{H-NMR}$ (from 25 °C to -20 °C) signals of **16** in aromatic region and *N-H* proton region

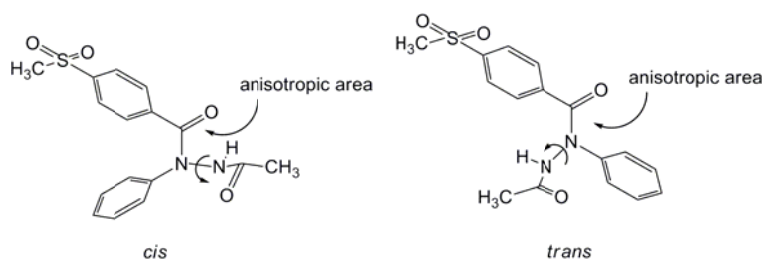


Figure 107 Possible minor conformation of **16** when *N-N* bond rotated and allowed *N-H* to locate in anisotropic area of carbonyl of tertiary amide.

According to spectra in figure 106 and possible minor conformer of **16** in figure 107, it indicated that two phenyl rings are orientated as face to face, *cis*-conformer, at each temperature. At 25 °C, N-N bond rotated and locked N-H to locate at anisotropic area of carbonyl of tertiary amide. While at 0 °C, proton of N-H was located out of anisotropic area of carbonyl of tertiary amide. At -10 °C and -20 °C, two conformers which different in N-H position were equilibrated. Major conformer is a conformer which N-H was located out of anisotropic area and minor conformer is a conformer which N-H was located at anisotropic area of carbonyl of tertiary amide. Figure 108 showed the preference conformer, major and minor conformers at each temperature (25 °C, 0 °C, -10 °C and -20 °C).

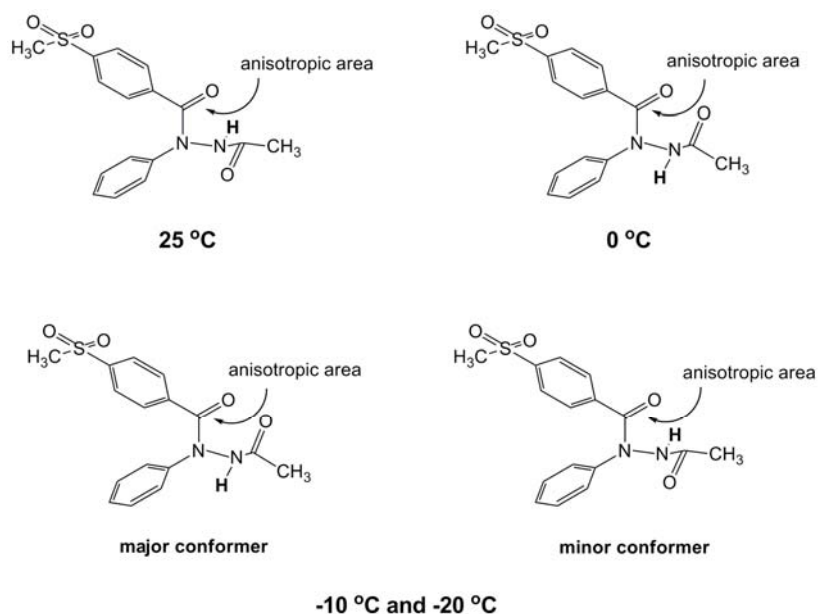


Figure 108 The preference conformer, major and minor conformers of compound **16** at each temperature (25 °C, 0 °C, -10 °C and -20 °C)

Although the detail conformational behaviors could not be elucidated in comparison to the chemical shifts of aromatic proton, their conformation equilibrium indicated that tertiary amide of **16** is possibly existed predominantly in *cis*-conformation (two of aromatic

rings are orientated in the same side of amide bond) in solution state and here, we could not evaluate the conformation of another amide bond of **16**.

For compound **27-32**, their $^1\text{H-NMR}$ spectral did not show broaden peak at aromatic region when measured in $\text{DMSO-}d_6$ at room temperature. I conclude that **27-32** exhibited only one conformation at room temperature in solution state. In order to define their conformation, the chemical shifts of aromatic proton of **27** and **30** were compared with structurally related compounds, *N*-(4-(methylsulfonyl)phenyl)benzamide (PCA02) and *N*-methyl-*N*-(4-(methylsulfonyl)phenyl)benzamide (PCA04) (Songkram *et al.*, 2007). As the $^1\text{H-NMR}$ spectral data of PCA02 and PCA04 in table 42, the remarkable high-field shifts of aromatic proton signals of PCA04 compared with their secondary analogues (from 8.05-7.56 ppm to 7.80-7.27 ppm), implied that they should exist in a different conformation in solution. These significant high-field shifts of aromatic protons (0.18-0.76 ppm) presumably arise from the ring current effect of the benzene ring when benzamide exists as face to face in *cis*-conformation. Form this result, we concluded that PCA02 is preferred to exist in *trans*-conformer whereas PCA04 exists in *cis*-conformer, which also consistent with previous investigation on benzamide and *N*-methylbenzanilide, respectively (Azuyama *et al.*, 1995; Azuyama *et al.*, 1996).

Compound **27** and **30** were selected as representative to study conformation preference of compound in this group (**27-32**). In order to define which conformer they preferred (*cis* or *trans*) in a solution state, $^1\text{H-NMR}$ spectral of **27** and **30** were compared to structurally related compounds (PCA02 and PCA04). The $^1\text{H-NMR}$ spectral comparison of compound **27** and **30** with PCA02 and PCA04 are summarized in table 43.

	PCA02					PCA04				
	Chemical shift of aromatic proton (ppm)					$\Delta\delta$ (ppm)				
	H _o	H _m	H _p	H _{o'}	H _{m'}	H _o	H _m	H _p	H _{o'}	H _{m'}
PCA02	8.05	7.56	7.63	7.98	7.91					
PCA04	7.29	7.32	7.27	7.80	7.43	0.76	0.24	0.36	0.18	0.48

Table 42 ¹H-NMR spectral data of PCA02 and PCA04

	Chemical shift of aromatic proton (ppm)				
	H _o	H _m	H _p	H _{o'}	H _{m'}
PCA02 (<i>trans</i>)	8.05	7.56	7.63	7.98	7.91
PCA04 (<i>cis</i>)	7.29	7.32	7.27	7.80	7.43
27	7.54	7.42	7.50	7.59	7.91
30	7.61	7.46	7.56	7.68	7.94

Table 43 ¹H-NMR spectral data of PCA02, PCA04, **27** and **30**

Although, the chemical shift of aromatic proton of **27** and **30** when compared to PCA02 (*trans*-preference) and PCA04 (*cis*-preference) showed middle values between *trans* and *cis* conformation. But, chemical shift of H_o which is the most influenced from anisotropic effect of the benzene ring when benzamide exists as face to face in *cis*-conformation, shifted to higher

field (8.05 ppm to 7.54 ppm in **27** and 8.05 ppm to 7.61 ppm in **30**) when compared to PCA02 (*trans*-preference). This high-field shift (0.44-0.51 ppm) is more effect than low-field shift (0.25-0.32 ppm) from PCA04 (*cis*-preference). This result indicated that tertiary amide of **27** and **30** are possibly existed predominantly in *cis*-conformation (two aromatic rings are orientated in the same side of amide bond) in solution state. Here, I cannot evaluate the conformation of another amide bond of **27** and **30**.

3.2.2 X-ray crystallography studies

The conformations of targeted compounds in solid state were studied by X-ray crystallographic technique. Among all of recrystallized targeted compounds (**16-21** and **27-32**), compounds **16**, **19**, **27**, **29** and **31** were recrystallized from a mixed solution of ethyl acetate and methanol except for compound **29** was recrystallized from only ethyl acetate, provided the best crystal properties in clearness, shape, size and planar surface. These compounds were selected as the representative of *N*-phenylbenzohydrazides to determine the orientation of molecules whether they prefer to exist in *cis*- or *trans*-isomer.

All crystals showing two amide bonds were almost planar with torsion angles (R-N-C(=O)-R) of 2.7° and 3.1° (**16**), 4.8° and 8.7° (**19**), 3.6° and 3.7° (**27**), 0.3° and 1.7° (**29**), 7.1° and 0.3° (**31**), respectively, as well as observing in ordinary amide compound (Zabicky, 1970). Moreover, there were no significant differences in bond lengths and bond angles related to the amide bond among the five compounds **16**, **19**, **27**, **29** and **31**. The mean value of the amide C-N bond length was 1.37 Å which is an intermediate between the single-bond C-N length of 1.47 Å and the double-bond C-N length of 1.24 Å (Zabicky, 1970). The summations of the three valence angles around the nitrogen were almost 360°, indicating the sp² character of the nitrogen atom. These facts suggest that the *N*-acetamide or *N*-benzamide amide bond in *trans* conformation retains partial double bond character similar to that of a free amide bond in *trans* conformation (1.34 Å in proteins and peptides and 1.376 Å in gaseous formamide (Zabicky, 1970), and the hybridization nature of the amide nitrogen atom is not affected by acetamide or benzamide

substitution. The torsion angle of R-N-C(=O)-R ($^{\circ}$), N-C bond length (\AA) and sum of three valence angles around N ($^{\circ}$) of compound **16**, **19**, **27**, **29** and **31** are demonstrated in table 44.

	Torsion angle (R-N-C(=O)-R), $^{\circ}$		N-C bond length (\AA)		Sum of three valence angles around N, $^{\circ}$	
	16	2.7	3.1	1.393	1.343	359.2
19	4.8	8.7	1.373	1.351	358.0	360
27	3.6	3.7	1.360	1.373	358.2	360
29	0.3	1.7	1.392	1.363	358.8	360
31	7.1	0.3	1.391	1.363	358.7	360

Table 44 Torsion angle of R-N-C(=O)-R ($^{\circ}$), N-C bond length (\AA) and sum of three valence angles around N ($^{\circ}$) of compound **16**, **19**, **27**, **29** and **31**

Crystal structure data and details of structure refinement for compounds **16**, **19**, **27**, **29** and **31** are shown in table 45.

	16	19	27	29	31
Formular	C ₁₆ H ₁₆ N ₂ O ₄ S	C ₂₁ H ₂₀ N ₂ O ₅ S	C ₁₆ H ₁₆ N ₂ O ₄ S	C ₁₆ H ₁₅ FN ₂ O ₄ S	C ₂₂ H ₂₀ N ₂ O ₄ S
Mr	332.37	412.45	332.37	350.36	408.46
Recryst. solvent	EtOAc/MeOH	EtOAc/MeOH	EtOAc/MeOH	EtOAc	EtOAc/MeOH
Crystal system	Orthorhombic	Monoclinic	Triclinic	Monoclinic	Monoclinic
Lattice parameter					
a, (Å)	9.5859(11)	19.0547(19)	8.350(3)	8.4469(10)	14.6876(15)
b, (Å)	15.8192(18)	8.3620(8)	9.236(3)	12.8289(16)	14.7621(15)
c, (Å)	21.061(2)	12.5870(12)	11.340(4)	14.9747(18)	9.4880(9)
α, (°)	90	90	85.390(5)	90	90
β, (°)	90	99.8120(10)	89.134(5)	101.165(2)	107.720(2)
γ, (°)	90	90	67.792(4)	90	90
V, (Å ³)	3193.7(6)	1976.2(3)	807.0(4)	1592.0(3)	1959.6(3)
Space group	Pbca	P2 _{(1)/c}	P-1	P2 _{(1)/n}	P2 _{(1)/c}
D _{calc} , (Mg/m ³)	1.383	1.386	1.368	1.462	1.385
Z value	8	4	2	4	4
R	0.0439	0.0662	0.0742	0.0519	0.0566

Table 45 Crystal structure data and details of structure refinement for compounds **16**, **19**, **27**, **29** and **31**

It was proved that the molecules of all these compounds adopt the (t, t)-amides structure (figure 109) when recrystallized in solvent system as shown in table 45.

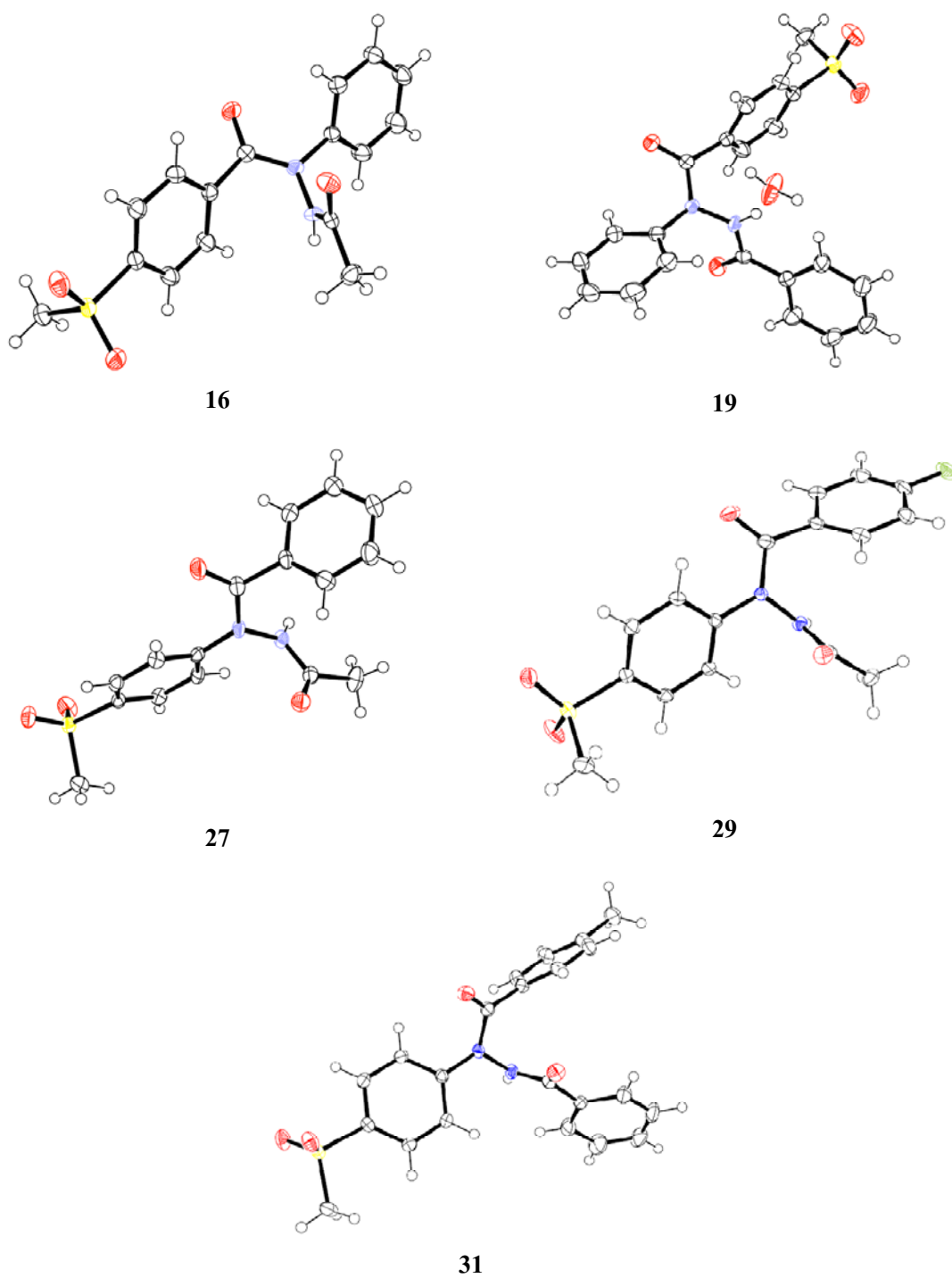


Figure 109 The ORTEP drawings of compounds 16, 19, 27, 29 and 31

These (t, t)-amides preference of **16**, **19**, **27**, **29** and **31** in solid state are controlled by intermolecular bonding in crystal packing. The related intermolecular bonds and its distance (Å) of crystal packing of compounds **16**, **19**, **27**, **29** and **31** can conclude and demonstrate in table 46. Figure 110 and Figure 111 are illustrated a unit cell (left column) and the crystal packing with related intermolecular bonds (right column) of each compound.

compound	Distance of intermolecular bond (Å)				
	H-bond	H-C...O interaction	C-H... π interaction ^{a)}	π - π stacking (Ar interaction)	O...H short contact ^{a)}
16	1.904 ^{b)} (red)	3.201 (blue)	-	-	2.361-2.482 (green)
19	1.835-1.936 ^{c)} (red)	-	2.793-2.881 (blue)	-	2.423-2.640 (green)
27	2.037 ^{b)} (red)	3.210 (magenta)	2.865-2.894 (blue)	3.346 (orange)	2.381-2.707 (green)
29	2.315 ^{b)} (red)	3.103, 3.122 (magenta)	2.881 (blue)	3.381, 3.276 (orange)	2.381-2.707 (green)
31	2.141 ^{b)} (red)	-	2.719-2.750 (blue)	3.814 (orange)	2.333-2.718 (green).

a) < sum of their vdW radii

b) H-bond between N-H...O=S=O

c) H-bond between atom of molecule and H₂O

Table 46 The related intermolecular bonds and its distance (Å) of crystal packing of compounds **16**, **19**, **27**, **29** and **31**

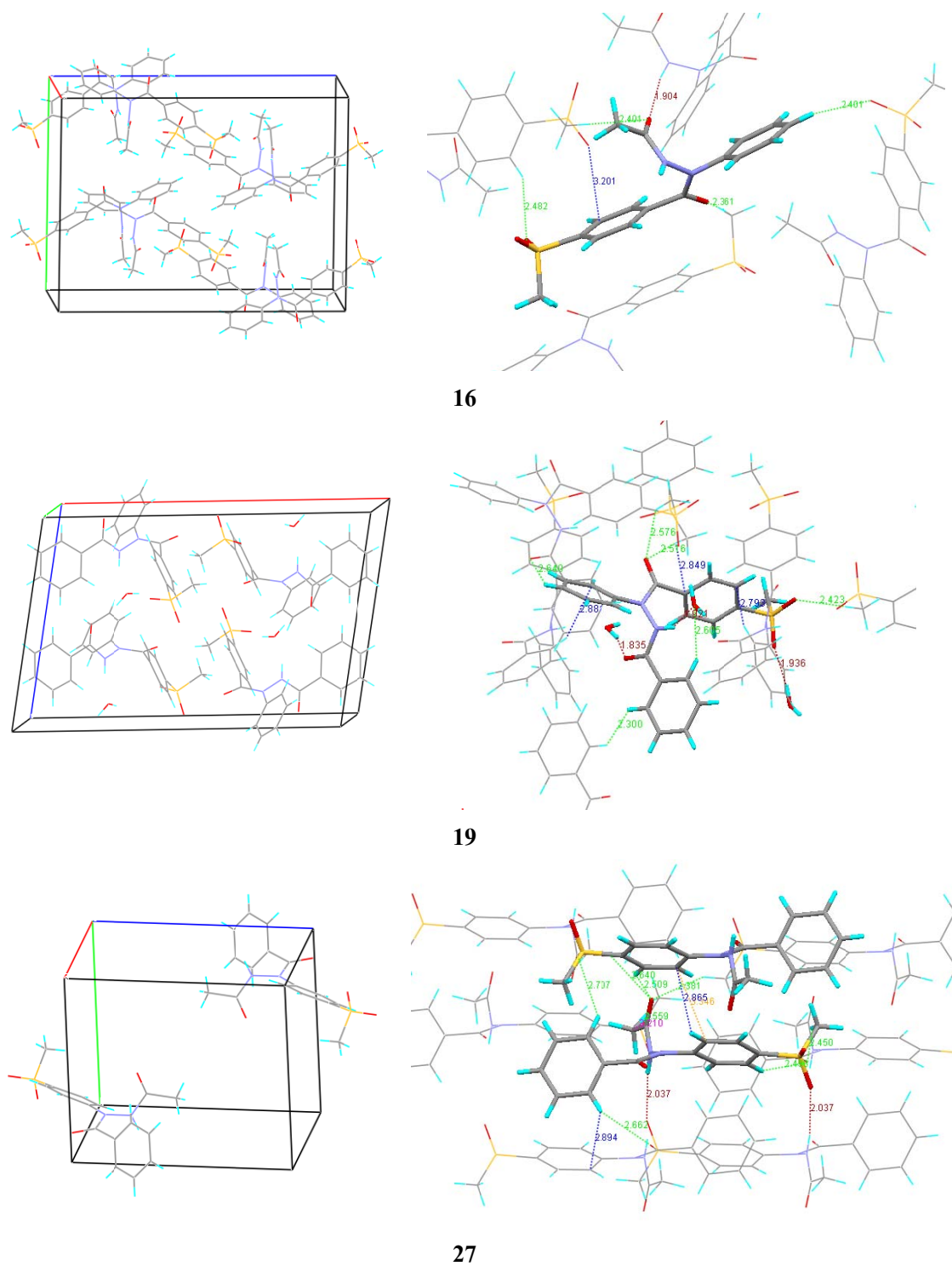


Figure 110 A unit cell (left column) and the crystal packings with related intermolecular bonds (right column) of compound 16, 19 and 27

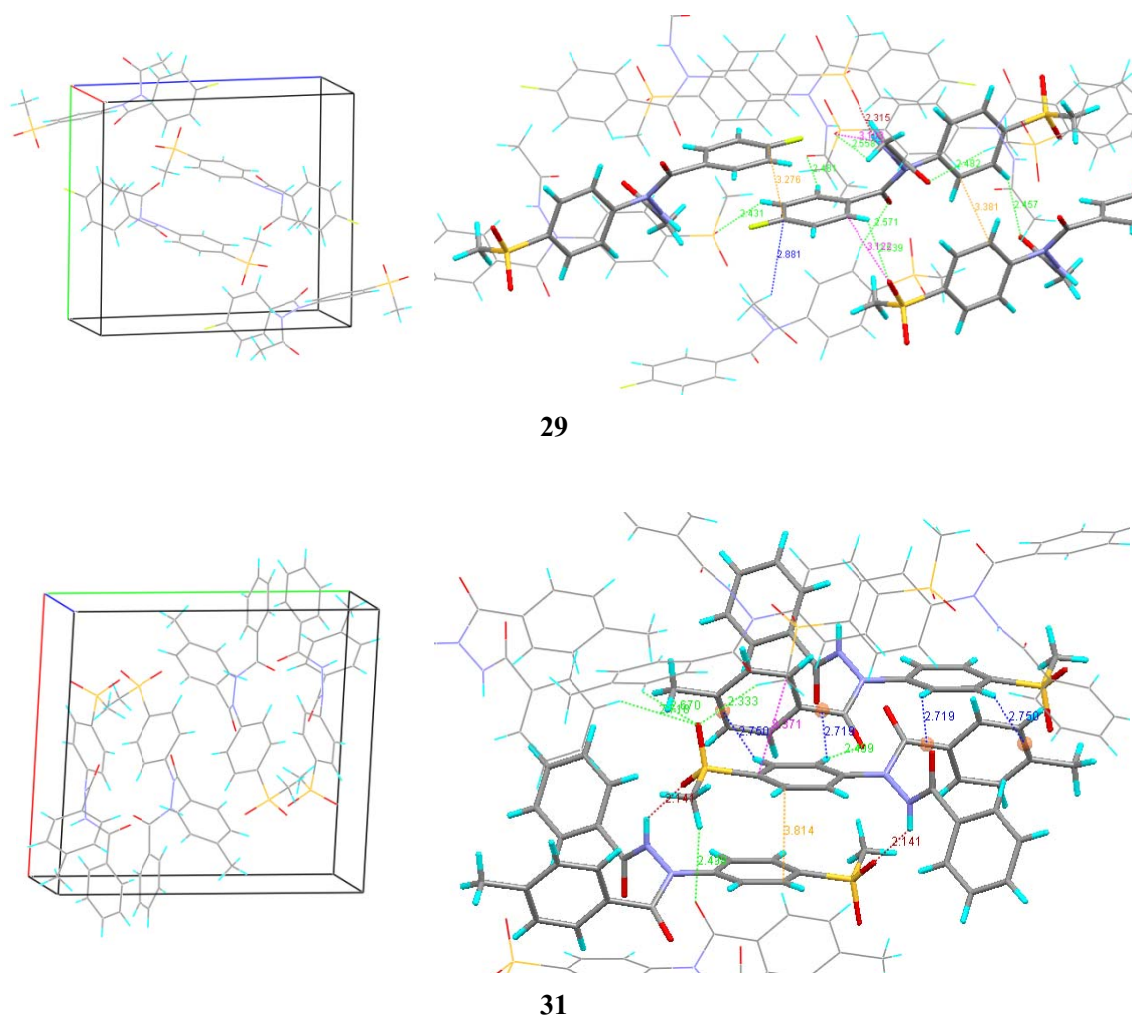


Figure 111 A unit cell (left column) and the crystal packings with related intermolecular bonds (right column) of compound **29** and **31**

Interestingly, all of X-Ray structures of compounds **16**, **19**, **27**, **29** and **31** exhibited higher ranking groups orientated in the different side of both of amide bonds demonstrate that they prefer to exist in (t, t)-amides which is differ from *cis*-preference of *N*-substituent aromatic amides of previous studies (Azuyama *et al.*, 1995). However, there was an observation reported that conformation could be interconverted between two or more stable states when exposed to an external stimulus, such as light, electricity or a chemical reaction (Yamazaki Ryu *et al.*, 2003). For instance, Yamazaki Ryu and coworker reported that the substituent effects

observed in acetamides can be applied to achieve amide conformational switching induced by acid (Yamazaki Ryu *et al.*, 2003). That is, the conformation of acetamides having a basic amino group on the aromatic ring is expected to be altered by protonation on the amino group. To illustrate, in the case of *N*-(3,5-bis(dimethylamino)phenyl)-*N*-methylacetamide with two dimethylamino groups, the major conformation (>99.9% *cis* in CD₂Cl₂) dramatically changed to *trans* (76.1%) upon the addition of TFA-*d* (figure 112).

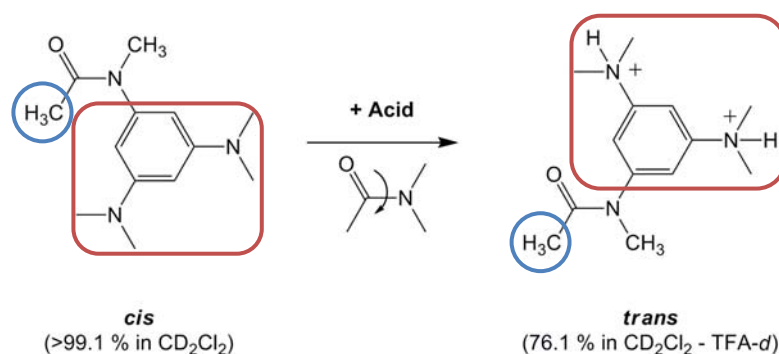


Figure 112 Amide conformational switching by acid of *N*-(3,5-bis(dimethylamino)phenyl)-*N*-methylacetamide.

As the amide conformational switching by external stimulus, remote protonation at *N*-aromatic ring (Yamazaki Ryu *et al.*, 2003), could be say that the conformational preference between *cis* and *trans* of *N*-substituent aromatic amides usually prefer to exist in *cis*-conformer unless affected from external stimulus. These review implied that other external stimulus, the intermolecular interactions (hydrogen bond (N-H...O=S=O), π - π stacking, C-H... π interaction, C-H...O interaction and O...H short contact) which were found in crystal packing of synthesized *N*-phenylbenzohydrazides (**16**, **19**, **27**, **29** and **31**), cause (t, t)-amides preference of **16**, **19**, **27**, **29** and **31** in solid state.

To conclusion in the topic of determination in molecular orientation, although I cannot completely define total conformation of targeted compounds (**16-21** and **27-32**) but I can conclude that the tertiary amides are possibly existed predominantly in *cis*-conformation (two of aromatic ring are orientated in the same side of amide bond) in solution state by ¹H-NMR studied.

In contrary, their conformation in solid state studied by X-ray crystallographic technique indicated that **16**, **19**, **27**, **29** and **31** are preference existed in (t, t)-amides because of the intermolecular interactions in crystal packing.

3.3 Determination of biological activities

Finding a COX-2 specific inhibitor that exhibits anti-inflammatory and analgesic effects without the adverse effects characterize the currently available NSAIDs accounts for the majority of COX research. At the biochemical level, COX inhibitors are usually characterized by comparing their *in vitro* inhibitory effects on COX activity. Several methods have been described for the determination of COX activity.

COX oxidises arachidonic acid to PGG₂, using two molecules of dioxygen, through cyclooxygenase activity of COX. PGG₂ is further metabolised by the same enzyme to PGH₂, in the presence of a reducing substrate such as phenol or epinephrine, through peroxydase activity of COX. The conversion of arachidonic acid to PGH₂ as illustrated in figure 113.

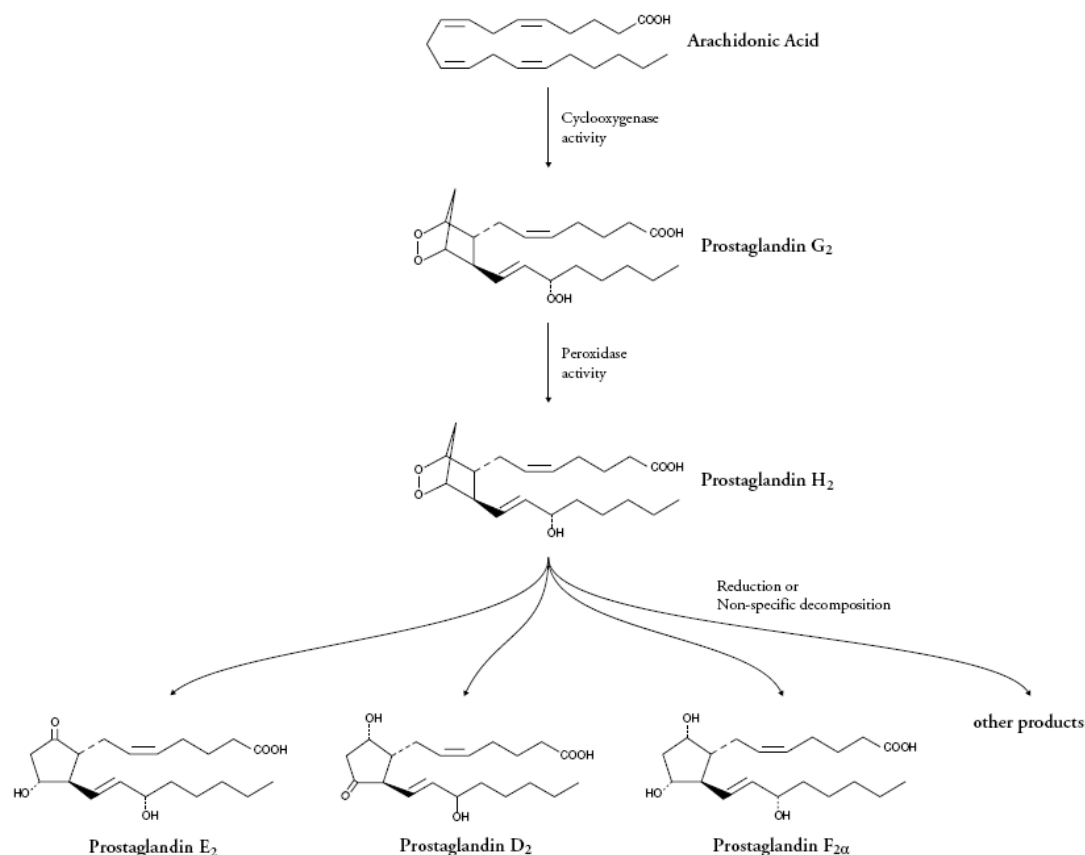


Figure 113 The conversion of arachidonic acid to PGH₂

There are three methods can be used for measuring the activity of COX (Maxey and Johnson, 2001). The first assay relies on the measurement of the rate of oxygen consumption using a Clark oxygen electrode (did not mention in this investigation). The second assay relies on the measurement prostaglandins (PGF_{2α} and PGE₂) derived from PGH₂ using enzyme immunoassay (EIA). The third assay is measurement the peroxidase activity of COX using a spectrophotometer. In this investigation, the latter assay was selected to evaluate COX inhibitory activity of the targeted compounds (**16-21** and **27-32**). Reaction in this method requires a second reducing substrate which is oxidized while the hydroperoxide is reduced. Phenol is the usual reducing substrate for COX activity assay but it may be replaced by the others oxidizable aromatics. Selected reducing substrate generates a chromophore when oxidized, detectable by UV/Vis detection.

A colorimetric COX (ovine) inhibitory screening assay is one of general methods for determining the peroxidase activity of COX. Determination of peroxidase in this assay could be determined by following the oxidation of *N,N,N',N'*-tetramethyl-*p*-phenylene diamine (TMPD) using arachidonic acid as the substrate. The reaction mixture included heme, TMPD and COX. The reaction is initiated with substrate; arachidonic acid, and an increasing in absorbance at 560 nm is detected and recorded on a spectrophotometer. The oxidation of TMPD which generate a chromophore in colorimetric determination could be demonstrated as in figure 114.

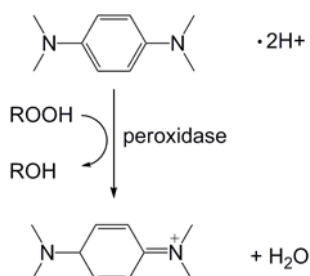
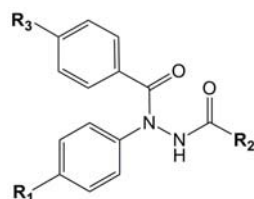


Figure 114 The oxidation of TMPD in colorimetric determination of peroxidase component in COX (Ann, 2008)

In this investigation, 100 μM is the concentration of tested compounds for screening and 10 μM indomethacin was selected as the positive control as in the procedure of Kakuta and coworker (Kakuta *et al.*, 2008). The colorimetric COX inhibitory screening assay results of compound **16-21** and **27-32** were summarized in table 47 and could be illustrated in bar chart as shown in figure 115.



Cpd.	R ₁	R ₂	R ₃	% inhibition		COX-2 selectivity
				COX-1	COX-2	
16	-H	-CH ₃	-SO ₂ CH ₃	-3.06	9.92	COX-2 preference ^{a)}
17	-CH ₃	-CH ₃	-SO ₂ CH ₃	4.85	16.46	3.39
18	-F	-CH ₃	-SO ₂ CH ₃	-3.76	9.46	COX-2 preference ^{a)}
19	-H	-C ₆ H ₅	-SO ₂ CH ₃	-0.60	17.81	COX-2 preference ^{a)}
20	-CH ₃	-C ₆ H ₅	-SO ₂ CH ₃	0.91	19.49	21.42
21	-F	-C ₆ H ₅	-SO ₂ CH ₃	-0.85	14.91	COX-2 preference ^{a)}
27	-SO ₂ CH ₃	-CH ₃	-H	-1.75	15.87	COX-2 preference ^{a)}
28	-SO ₂ CH ₃	-CH ₃	-CH ₃	0.24	18.70	77.92
29	-SO ₂ CH ₃	-CH ₃	-F	0.72	18.17	25.24
30	-SO ₂ CH ₃	-C ₆ H ₅	-H	5.58	18.14	3.25
31	-SO ₂ CH ₃	-C ₆ H ₅	-CH ₃	13.53	21.25	1.57
32	-SO ₂ CH ₃	-C ₆ H ₅	-F	9.37	26.26	2.80
Indo^{b)}				47.51	48.55	1.02

a) Compound exhibited only COX-2 inhibitory

b) Indomethacin

Table 47 COX inhibitory activity of compounds 16-21 and 27-32 using colorimetric COX (ovine) inhibitory screening assay

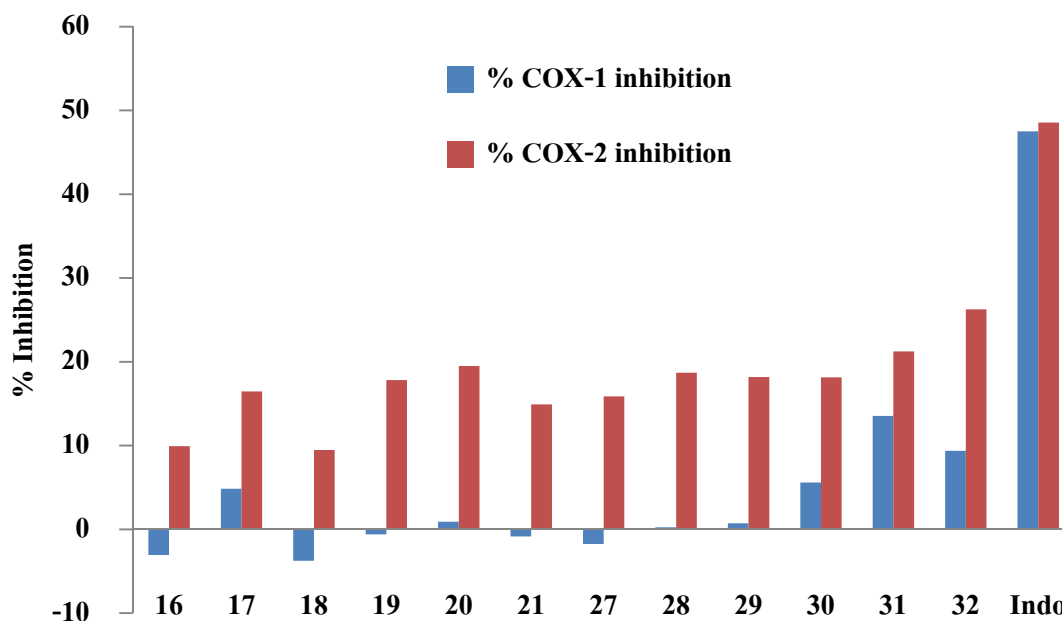


Figure 115 % inhibition to COX-1 and COX-2 of 100 μ M **16-21** and **27-32** compare with 10 μ M indomethacin (Indo)

As can be seen from table 47, the non-selective COX inhibitor, indomethacin, exhibited potent inhibitory activity towards both COX-1 (47.5% inhibition) and COX-2 (48.5% inhibition) at the concentration of 10 μ M with a selectivity index of 1.0. This result is accordance to previous reported (Kakuta *et al.*, 2008) indicate the appropriate reliability of assay kit. In this assay, compounds **16-21** and **27-32** produced a weak to moderate inhibition of COX-2 isoform (9.5-26.3 % inhibition), with selectivity index values superior than that of indomethacin. A comparison among twelve synthesized *N*-phenylbenzohydrazides demonstrated an observably higher COX-2 inhibitory of *N*-acetyl/benzyl-*N*-(4-(methylsulfonyl)phenyl)benzohydrazide derivatives (**27-32**) than those of *N*-acetyl/benzyl-4-(methylsulfonyl)-*N*-phenylbenzohydrazide derivatives (**16-21**). For instance, *N*-acetyl-*N*-(4-fluorophenyl)-4-(methylsulfonyl)benzohydrazide (**18**) was shown to be nearly two times less active (9.5% inhibition) than *N*-acetyl-4-fluoro-*N*-(4-(methylsulfonyl)phenyl)benzohydrazide (**29**) (18.2% inhibition). Moreover, secondary benzamides substituent at nitrogen atom of diaryl amide (**19-21** and **30-32**) exhibited higher COX-2 inhibitory potency than those of their secondary acetamides analogue (**16-18** and

27-29). These implied that the presence of methylsulfonyl substituent at the *para*-position of the *N*-phenyl ring and secondary benzamide substituent at nitrogen atom of diarylamide appear to be more useful for COX-2 inhibition.

The insertion of an electron-withdrawing fluorine substituent at the *para*-position of the remaining aromatic ring afforded compound **18** and **29**, which showed no difference potency comparable to that of the parent analogues. In particular, the replacement of the *p*-fluoro substituent with an electron donating, methyl, afforded compound **17** and **28**, which displayed irrelevant differences in inhibitory potency (16.5 % and 18.7 %, respectively). Among twelve *N*-phenylbenzohydrazides, *N*'-benzoyl-4-fluoro-*N*-(4-(methylsulfonyl)phenyl) benzohydrazide (**32**) containing methylsulfonyl substituent at the *para*-position of the *N*-phenyl ring, secondary benzamide substituent at nitrogen atom of diarylamide and *p*-fluoro substituent at *C*-phenyl ring, proved to be the most inhibitory activity (26.3%). However, according to a low percent inhibition, a COX IC₅₀ is not further determined.

Although extensive structure–activity relationships (SARs) of *N*-phenylbenzohydrazides on COX inhibitory activity are not yet available, this *in vitro* result indicated that the presence of *p*-methylsulfonylaryl moiety in structure is obligatory for COX-2 selectivity. This could be seen from the selectivity index values of all targeted compounds were superior to that of indomethacin. This COX-2 selectivity might result from the insertion of *p*-SO₂CH₃ substituent into the secondary pocket presence in only COX-2 isozyme (Kurumbail *et al.*, 1996). As the result of *cis*-preference conformation in solution state of designed compound (mentioned in conformation studies part), is as expected accordance with the conformation of celecoxib analogue (SC-558) in active site of murine COX-2 (Kurumbail *et al.*, 1996). This might be one more reason for COX-2 selectivity. In addition, the presence of a hydrogen acceptor group such as fluorine substituent at the *para*-position of *C*-phenyl moiety might improve potency for COX-2 inhibition. However, the inferior potency of compounds to indomethacin might be caused by flexibility of molecular structure which mentioned in conformation studies part. This flexibility of molecular orientation might induce inappropriated affinity between ligand and enzyme.

However, in order to prove this hypothesis, molecular modeling such as docking is considered as further investigation to find mode of inhibitors alignment in the binding pocket.

Furthermore, COX inhibitory activities and enzyme selectivity depend on a test system, cell types, stimulating agents and culture condition used (Dannhardt and Kiefer, 2001). Hence, the COX inhibitory activities of *N*-phenylbenzohydrazides are still required the further studies in the other methods such as *in vitro* whole cell assay system in murine COX-1 null fibroblast cell line or in other *in vitro* anti inflammatory studies, etc to finally conclude their inhibitory action and the SARs in further.

CHAPTER 4

CONCLUSION

Although the Coxibs, selective COX-2 inhibitors, possess anti-inflammatory therapeutic profile as the NSAIDs with fewer GI toxicity profiles. Unfortunately, many observations reported that the long-term use of some Coxib drugs significantly increased cardiovascular side effects to patients. The recent withdrawal of rofecoxib and valdecoxib due to their adverse cardiovascular events clearly delineates the need to develop selective COX-2 inhibitors with improved safety profiles. In the development of novel selective COX-2 inhibitors accumulated evidences indicated that the inhibitory activities of COX could present in the absence of traditional central heterocyclic or carbocyclic ring template. Accordingly, in this investigation, I reported on the design, synthesis and cyclooxygenase inhibitory activities of *N*-phenylbenzohydrazide derivatives containing a COX-2 methylsulfonyl pharmacophore at the *para*-position of phenyl ring and possess acyclic amide bond, in place of the central ring template present in celecoxib.

The new twelve *N*-phenylbenzohydrazides (**16-21** and **27-32**) and their intermediates were synthesized. All of them could be prepared in acceptable yields (43-99%). Their physical and spectroscopic properties were examined. All spectral data were in accordance with assumed structures. ¹H- NMR spectrum of compound **16-21** gave broadening signal at aromatic proton region when operated at room temperature while, this phenomenon did not affect to compound **27-32**. Because of *N*-Ph and carbonyl-Ph bond rotation, relatively slow on the NMR timescale leading to the broadening signal. Elevation of the temperature results in time environments for all aromatic resonances as a result of rapid rotation leading to sharpening signal.

The determination of their orientation was conducted using $^1\text{H-NMR}$ and X-Ray crystallographic techniques to evaluate the conformational changes in solution and solid states, respectively. In solution state, the detail conformational behaviors of compound **16** (representative of compound **16-21**) would not be elucidated due to comparison of the chemical shifts of aromatic proton, but their conformational equilibrium suggested that **16** is possibly existed predominantly in *cis*-conformation at tertiary amide. While, the conformational behaviors of compound **27** and **30** (representative of compound **27-32**) could be elucidated due to comparison of the chemical shifts of aromatic proton. This result showed that **27** and **30** are also possibly existed predominantly in *cis*-conformation at tertiary amide as compound **16**. In solid state, compounds **16**, **19**, **27**, **29** and **31** provided the best crystal properties in clearness, shape, size and planar surface. The X-Ray structures of these compounds exhibited the higher ranking groups orientated in the different side of both amide bonds demonstrate that it prefer to exist in (*trans, trans*)-conformers. These (*trans, trans*)-preferences were controlled by external stimulus, intermolecular bonding (hydrogen bond (N-H...O=S=O), π - π stacking, C-H... π interaction, C-H...O interaction and O...H short contact) in crystal packing.

The inhibitory activities at 100 μM of targeted compounds were evaluated in comparison to 10 μM indomethacin. Compounds **16-21** and **27-32** produced a weak to moderate inhibition of COX-2 (9.5-26.3 % inhibition) with selectivity index values superior to indomethacin. *N*-benzoyl-4-fluoro-*N*-(4-(methylsulfonyl)phenyl)benzohydrazide (**32**) which have methylsulfonyl substituent at the *para*-position of the *N*-phenyl ring, secondary benzamide substituent at nitrogen atom of diaryl amide and *p*-fluoro substituent at *C*-phenyl ring, proved to be the most potency compound (26.3%). Due to the low percent inhibition of them, their COX IC_{50} were not further determined. Their SARs could be briefly concluded as follows. The presence of methylsulfonyl substituent at the *para*-position of the *N*-phenyl ring and secondary benzamide substituent at nitrogen atom of diarylamide appeared to be more useful for COX-2 inhibitory effect. In addition, the presence of a hydrogen acceptor group such as fluorine substituent at the *para*-position of *C*-phenyl moiety may improve potency for COX-2 inhibition.

The selectivity index values of all targeted compounds were superior to that of indomethacin. This might result from the insertion of *p*-SO₂CH₃ substituent into the secondary pocket present in only COX-2 isozyme. Moreover, as the results of *cis*-preference conformation in solution state of our designed compound are as expected accordance with the conformation of celecoxib analogue (SC-558) in active site of murine COX-2. This might be one more reason for COX-2 selectivity of our compounds.

On the other hand, the inferior potency of our compounds to indomethacin might be caused by flexibility of molecular structure. This flexibility might induce inappropriate affinity between ligand and enzyme. In order to prove this hypothesis, molecular modeling such as docking is considered as further investigation to find mode of inhibitors alignment in the binding pocket. However, the COX inhibitory activities of *N*-phenylbenzohydrazides are still required the further investigation by other methods to finally conclude their inhibitory action and SARs.

Even though, *in vitro* COX-2 inhibitory potency of *N*-phenylbenzohydrazides is lower than the reference compound, indomethacin, all of them demonstrated several folds higher in COX-2 selectivity. This finding suggested the novel structural motif of *N*-phenylbenzohydrazides might be further developed to be novel selective COX-2 inhibitors even if their SARs are still not explicit and require the further study.

REFERENCES

- Ann, A. (2008), "Colorimetric COX (ovine) Inhibitor Screening Assay: Catalog No. 760111", *Cayman Chemical Company.*, pp.1-16.
- Azumaya, I., Kagechika, H., Fujiwara, Y., Itoh, M., Yamaguchi, K., and Shudo, K. (1991) "The structure of N-methylbenzanilide in the crystal or in solution", *J. Am. Chem. Soc.*, vol. 113, pp.2833-2838.
- Azumaya, I., Kagechika, H., Yamaguchi, K., and Shudo, K. (1995) "Stereochemistries of Aromatic N-Methylamides in Crystal and Solution. Temperature-dependent Conformational Conversion and Attracting Aromatic-Aromatic Interactions", *Tetrahedron.*, vol. 51, pp. 5277-5290.
- Azumaya, I., Kagechika, H., Yamaguchi, K., and Shudo, K. (1996) "Facile Formation of Aromatic Cyclic N-Methylamides Based on *cis* Conformational Preference", *Tetrahedron Letters*, vol. 37, pp.5003-5006.
- Banks, T. M., Cowin, G. J., Glover, S. A., Tarrant, G. J., Rowbottom, C. A., Tucker, D. J., and Zengjia, Y. A dynamic NMR investigation of the conformational isomerism in novel 1,3,4,5-tetrahydro-2,1-benzoxazepines. (online) Available <http://www.ch.ic.ac.uk/ectoc/echet96/papers/107/index.htm#introduction> (5 May 2009)
- Biava, M., Poretta, G. C., Cappelli, A., Vomero, S., Manetti, F., Botta, M., and *et al.* (2005), "1, 5-Diarylpyrrole-3-Acetic Acids and Ester as Novel Classes of Potent and Highly Selective Cyclooxygenase-2 Inhibitors", *J. Med. Chem.*, vol. 48, no. 9, pp.3428-32.
- Blobaum, A. L. and Marnett, L. J. (2007) "Structural and Funtional Basis of Cyclooxygenase Inhibition", *J. Med. Chem.*, vol. 50, pp.1425-1441.
- Bonini, B. F., Franchini, M. C., Gentili, D., Locatelli, E., Ricci, A. (2009) "1,3-Dipolar cycloaddition of nitrile imines with functionalized acetylenes: regiocontrolled Sc(OTf)₃-catalyzed synthesis of 4- and 5-substituted pyrazoles", *Syn.lett.*, vol.14, pp.2328-2332.

- Brown, W. H., Foote, C. S., and Iverson, B. L. (2005) *Organic Chemistry*. 4th Ed. Thomson Brooks. USA.
- Charlier, C. and Michaux C. (2003) "Dual inhibition of cyclooxygenase-2 (COX-2) and 5-lipoxygenase (5-LOX) as a new strategy to provide safer non-steroidal anti-inflammatory drugs", *Eur. J. Med. Chem.*, vol. 38, pp.645-659.
- Chowdhury, M. A., Dong, Y., Chen Q.H., Khaled, R., Abdellatif, A., and Knaus, E.E. (2008), "Synthesis and Cyclooxygenase Inhibitory Activities of Linear 1-(Methanesulfonylphenyl or Benzenesulfonamido)-2-(pyridyl)acetylene Regioisomers", *Bioorg. Med. Chem.*, vol. 16, no. 4, pp.1948-56.
- Cryer, B., and Dubois, A. (1998) "The Advent of Highly Selective Inhibitors of Cyclooxygenase—A Review", *Prosta. & oth. Lip. Media.*, vol. 56, no. 5-6, pp.341-61.
- Dannhardt, G., and Kiefer, W. (2001), "Cyclooxygenase Inhibitors: Current Status and Future Prospects", *Eur. J. Med. Chem.*, vol. 36, no. 2, pp.109-26.
- Denmark, S. E., and Beutner, G. L. (2008) "Lewis Base Catalysis" *Angew. Chem. Int. Ed.*, Vol. 47, pp.1560 – 1638.
- Dogne, J.M., Supuran, C. T., and Pratico, D. (2005) "Adverse Cardiovascular Effects of the Coxibs", *J. Med. Chem.*, vol. 48, no. 7, pp.2251-2257.
- Doherty, A. M. (2004) "Selective Cyclooxygenase-2 Inhibitors. *In Annual Reports in Medicinal Chemistry*", vol. 39, pp. 125-138.
- Garg, R., Kurup, A., Mekapati, S. B., and Hansch, C. (2003), "Cyclooxygenase (COX) Inhibitors: A Comparative QSAR study", *Chem. Rev.*, vol. 103, no. 3, pp.703-31.
- Hearn, M. J., and Grimwade, J. E. (1980) "A convenient method for the preparation of 1-acyl-2-phenylhydrazines", *Organic Preparations and Procedures International.*, vol 12, pp.249-251.
- Itai, A, Toriumi, Y., Saito, S., Kagechika, H., and Shudo, K. (1992), "Preference for *cis*-Amide Structure in *N*-acyl-*N*-methylanilines", *J. Am. Chem. Soc.*, vol. 114, no. 26, pp.10649-50.

- Itai, A., Toriumi, Y., Tomioka, N., Kagechika, H., Azumaya, I., and Shudo, K. (1989),
“Stereochemistry of *N*-methylbenzanilide and Benzanilide”, *Tetrahedron lett.*,
vol. 30, no. 45, pp.6177-80.
- Kakuta, H., Zheng, X., Oda, H., Haruda, S., Sugimoto, Y., Sasaki, K., *et al.* (2008)
“Cyclooxygenase-1-Selective Inhibitors Are Attractive Candidates for
Analgesics That Do Not Cause Gastric Damage. Design and in Vitro/in Vivo
Evaluation of a Benzamide-Type Cyclooxygenase Inhibitor”, *J. Med. Chem.*,
vol. 51, pp.2400-2411.
- Kashino, S., Ito, K., and Haisa, M. (1979) “The crystal structure of benzanilide”,
Bull. Chem. Soc. Jpn., vol. 52, pp.365-369.
- Kurumbail, R. G., Stevens, A. M., Gierse, J. K., McDonald, J. J., Stegeman, R. A., Pak, J. Y. *et al.*, (1996) “Structural basis for selective inhibition of cyclooxygenase-2 by anti-inflammatory agents”, *Nature.*, vol. 384, pp.644-648.
- Lin, S.J., Tsai, W.J., Chiou, W.F., Yang, T.H., and Yang, L.M. (2008), “Selective COX-2
Inhibitors. Part 2: Synthesis and Biological Evaluation of 4-Benzylideneamino-
and 4-Phenylimino methylbenzenesulfonamides”, *Bioorg. Med. Chem.*, vol. 16,
no. 5, pp.2697-706.
- March, J. (1992) *Advanced Organic Chemistry: Reactions, Mechanisms, and Structure*. 4th Ed.
Wiley-Interscience. New York.
- Maxey, K. M. D., and Johnson, J. (2001) “Detecting and Measuring Cyclooxygenases”, *Cayman
Chemical Company: Currents*. Iss. 10.
- McCarthy, J. R., Matthews, D. P., and Paolini, J. P. (1998) “Reaction of Sulfoxides with
Diethylaminosulfur Trifluoride”, *Org. Synth.*, vol. 9, pp.446.
- Nogady, T. and Weaver, D.F. (2005) “Medicinal Chemistry: A Molecular and Biochemical
Approach”, 3rd Ed. Oxford University Press. New York.
- Patricia, A.H., and Patrice, D. (2004), “Non Steroidal Anti-inflammatory Drugs and Cardiovascular
Risk”, *J. Am. Coll. Cardio.*, vol. 43, no. 4, pp.519-25.
- Patrignani, P., Tacconelli, S., Sciulli, M. G., Capone, M. L. (2005) “New insights into COX-2
biology and inhibition”, *Brain Research Reviews.*, vol. 48. pp.352– 359.

- Penning, T.D., Talley, J.J., Bertenshaw, S.R., Carter, J.S., Collins, P.W., Docter, S. *et al.*, (1997)
 “Synthesis and Biological Evaluation of the 1,5-Diarylpyrazole Class of Cyclooxygenase-2 Inhibitors: Identification of 4-[5-(4-Methylphenyl)-3-(trifluoromethyl)-1*H*-pyrazol-1-yl]benzenesulfonamide (SC-58635, Celecoxib)”, *J. Med. Chem.*, vol. 40, pp.1347– 1365.
- Ponzio, G., and Charrier, G (1911) “Behavior of Some Diazonium Salts toward Ether”, *Gazzetta Chimica Italiana.*, vol. 39, pp.625-634.
- Puig, C., Crespo, M. I., Godessart, N., Feixas, J., Ibarzo, J., Jimenez J. M., and *et al.* (2000),
 “Synthesis and Biological Evaluation of 3,4-Diaryloxazolones: A New Class of Orally Active Cyclooxygenase-2 Inhibitors”, *J. Med. Chem.*, vol. 43, no. 2, pp.214-23.
- Rao, P. N. P., Amini, M., Li, H., Habeeb, A. G., and Knaus, E. E. (2003), “Design, Synthesis, and Biological Evaluation of 6-Substituted-3-(4-methanesulfonylphenyl)-4-phenylpyran-2-ones: A Novel Class of Diarylheterocyclic Selective Cyclooxygenase-2 Inhibitors”, *J. Med. Chem.*, vol. 46, no. 23, pp.4872-82.
- Reddy, M. V. R., Reddy, S., Reddy, D. B., and Biradavolu, S. (1989) “A new route for the preparation of methyl aryl sulfones”, *Acta Chimica Hungarica.*, vol. 126, pp.825-827.
- Saito, S., Toriumi, Y., Tomioka, N., and Itai, A. (1995), “Theoretical Studies on *cis*-Amide Preference in *N*-Methylanilides”, *J. Org. Chem.*, vol. 60, no. 15, pp.4715-20.
- Smith, R. M. (2004) *Understanding mass spectra: a basic approach*, 2nd Ed. Wiley-Interscience. New Jersey.
- Songkram, C., Diloknawarit, W., Wongmayura, A., Puripattavong, J., Canyuk, B., and Kagechika, H. (2007), “Synthesis and Cyclooxygenase Inhibitory Activity of *N*-substituted benzanilides”, *การประชุมนักวิจัยรุ่นใหม่ พบ เมธีวิจัยอาวุโส สกว. ครั้งที่ 7, ชลบุรี, ประเทศไทย.*
- Stefan, G., and Karl, E. (1992) “Amine oxidation. III. Bivalent nitrogen: diarylacylhydrazyls”, *Berichte der Deutschen Chemischen Gesellschaft*, vol. 55b, pp.616-628.

- Steinmeyer, J. (2000), "Review: Pharmacological Basis for the Therapy of Pain and Inflammation with Nonsteroidal Anti-inflammatory Drugs", *Arthritis Res*, vol. 2, no. 5, pp.379-85.
- Sui, Z., and Wachter, M. (2000) "Aryl phenylhydrazides as selective COX-2 inhibitors for the treatment of inflammation", US6077869 A20000620.
- Takamizawa, A., Hayashi, S., Sato, H. (1965) "Synthesis of pyrazole derivatives. VIII. Supplement of the reaction of propionitriles and related compounds with arylhydrazines", *Yakugaku Zasshi.*, vol. 85, pp.158-165.
- Taylor, E. C., and Hinkle, J. S. (1987) "New Routes to 1,2-Diazetid-3-ones", *J. Org. Chem.*, vol. 52, no. 18. pp. 4107-4110
- Travis, B. R., Sivakumar, M.G., Hollist, O. and Borhan, B. (2003) "Facile Oxidation of Aldehydes to Acids and Esters with Oxone", *Org. Lett.*, vol. 5. pp.1031-1034.
- Tsai, W.J., Shiao, Y.J., Lin, S.J., Chiou, W.F., Lin, L.C., Yang, T.H., and *et al.* (2006). "Selective COX-2 Inhibitors. Part 1: Synthesis and Biological Evaluation of Phenylazobenzene Sulfonamides", *Bioorg. Med. Chem. Lett.*, vol. 16, no. 17, pp.4440-43.
- Vane, J.R. and Botting, R.M. (1992) "Aspirin and Other Salicylates", Chapman & Hall Medical. London.
- Verma, S. M., and Prasad, R. (1973) "Conformational Analysis about the Nitrogen-Nitrogen' Bond by Nuclear Magnetic Resonance Spectroscopy. *N'*- Sulfonyl Derivatives of N-Aminocamphorimide", *J. Org. Chem.*, vol. 58, pp.3745-3749.
- Weller, P. E., and Hanzlik, R. P. (1991) "Isolation of S-(Bromopheny)cysteine Isomers from Liver Proteins of Bromobenzene-Treated Rats" *Chem. Res. Toxicol.*, vol. 4, pp.17-20.
- Yamasaki, R., Tanatani, A., Azumaya, I., Saito, S., Yamaguchi, K., and Kagechika, H. (2003) "Amide Conformational Switching Induced by Protonation of Aromatic Substituent" *Org. Lett.*, vol. 5, pp.1265-1267.
- Zabicky, J. (1970) *The Chemistry of Amides*. Interscience Publishers: London.

- Zarghi, A., Arfaee, S., Rao, P.P.N., and Knauw, E.E. (2006). "Synthesis and Biological Evaluation of 1,3-Diphenylprop-2-en-1-ones: A Novel Class of Cyclooxygenase-2 Inhibitors", *Bioorg. Med. Chem.*, vol. 14, no. 8, pp.2600-05.
- Zarghi, A., Kakhgi, S., Hadipoor, A., Daraee, B., Dadrass, O.G., and Hedayati, M. (2008). "Design and Synthesis of 1,3-Diaryurea Derivatives as Selective Cyclooxygenase (COX-2) Inhibitors", *Bioorg. Med. Chem. Lett.*, vol. 18, no. 4, pp.1336-39.

APPENDIX

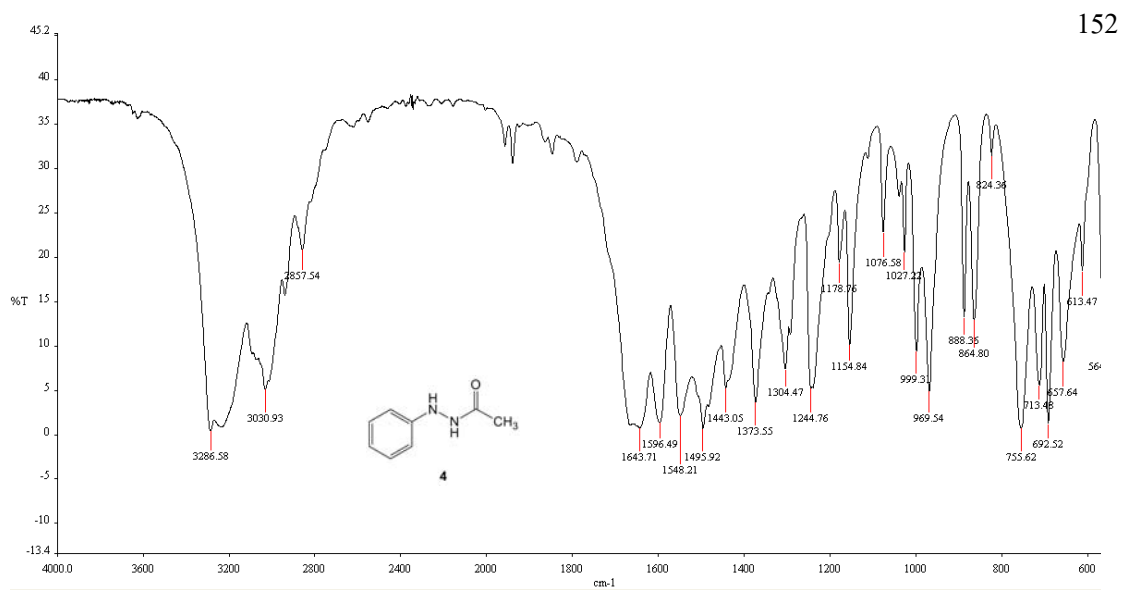


Figure 16 IR spectrum (KBr) of *N*-phenylacetohydrazide (**4**)

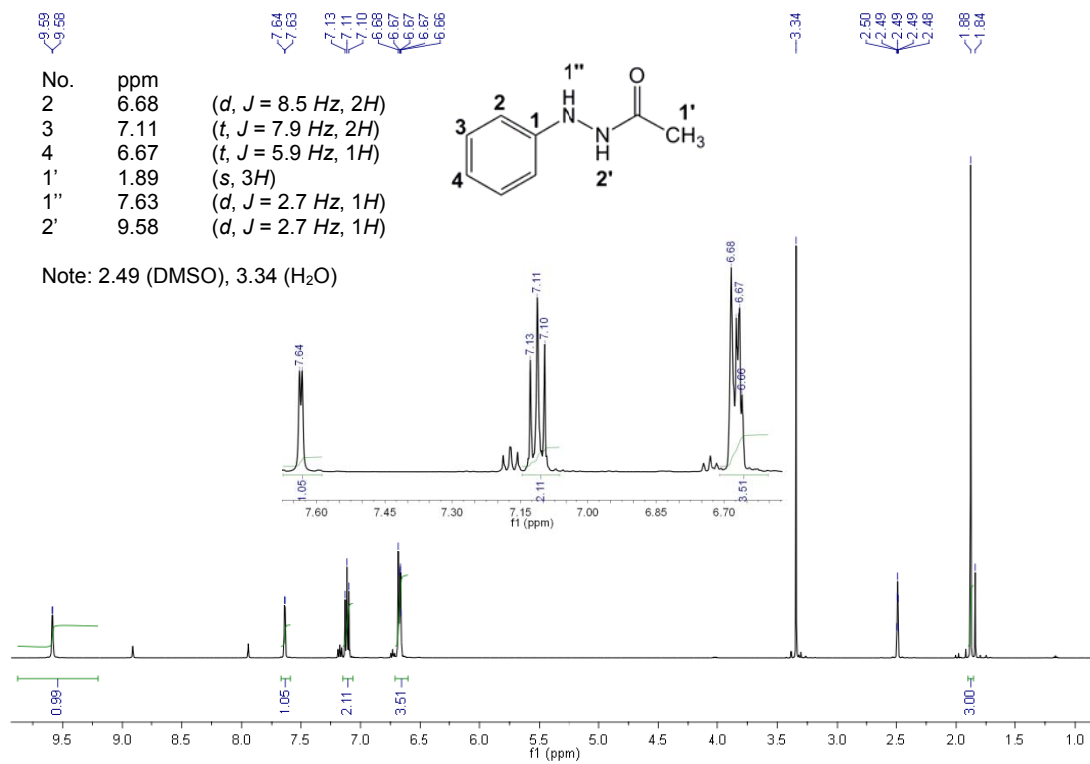


Figure 17 $^1\text{H-NMR}$ (500MHz, DMSO- d_6) spectrum of N' -phenylacetohydrazide (**4**)

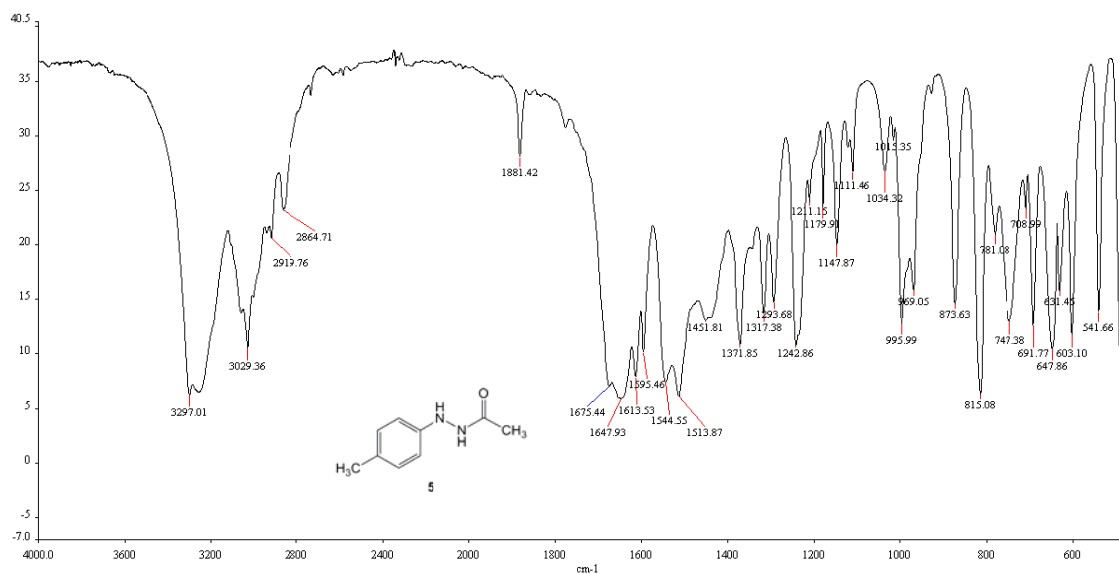


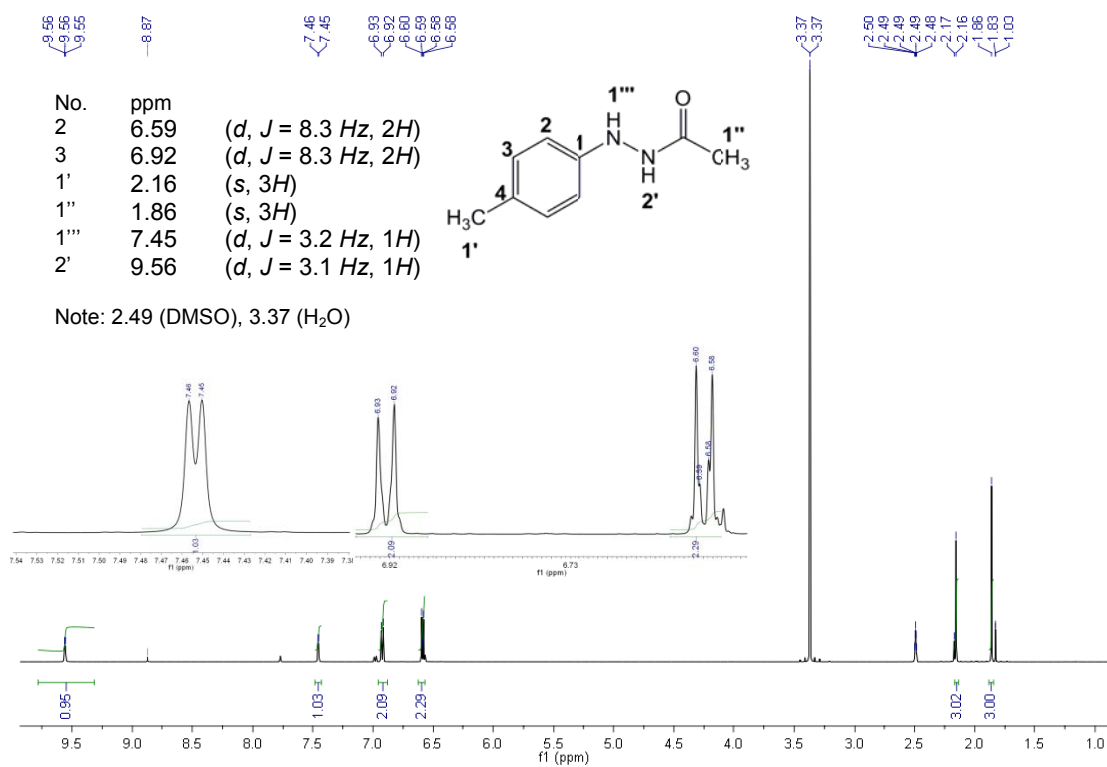
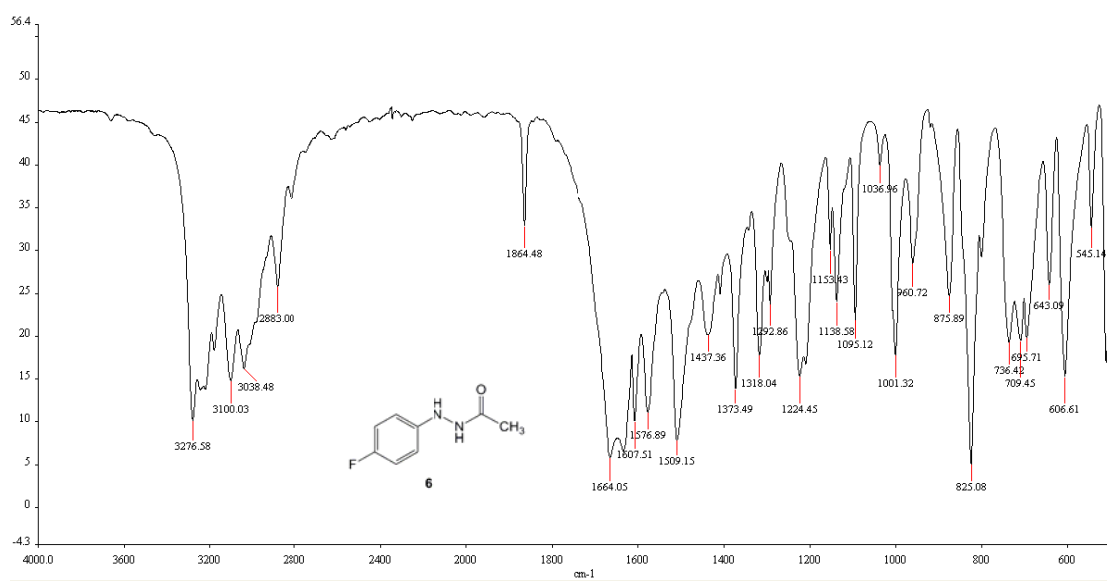
Figure 18 IR spectrum (KBr) of *N'*-*p*-tolylacetohydrazide (**5**)**Figure 19** ¹H-NMR (500MHz, DMSO-*d*₆) spectrum of *N'*-*p*-tolylacetohydrazide (**5**)

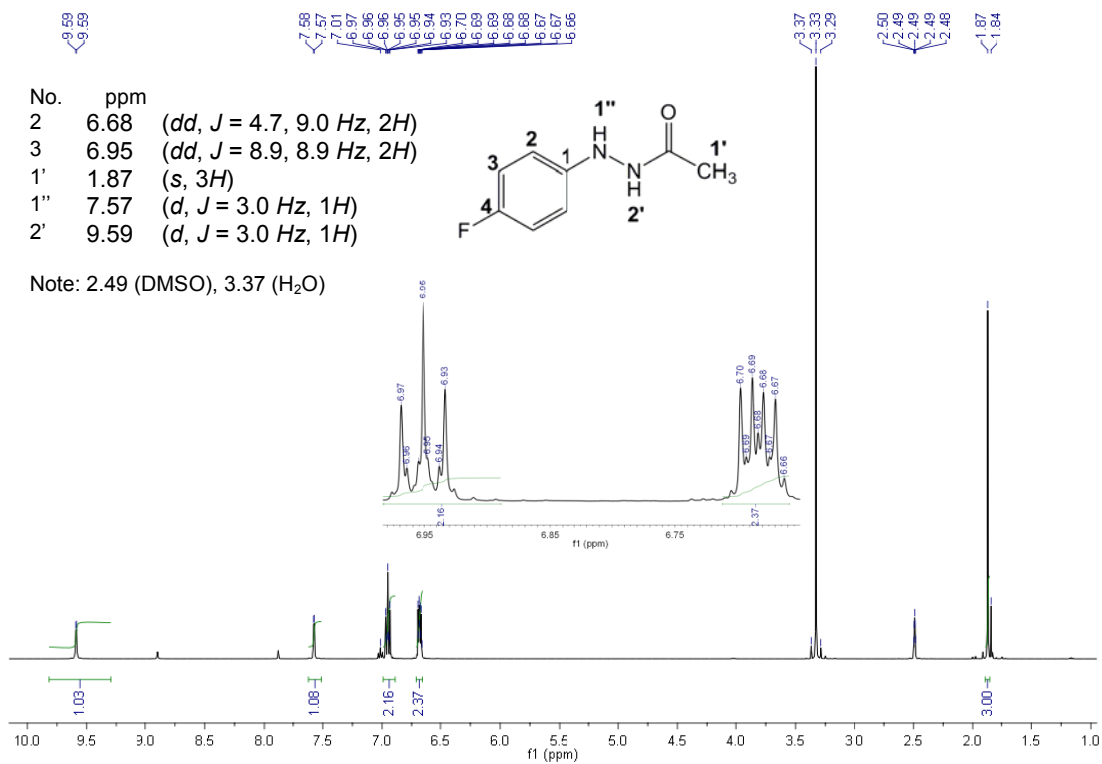
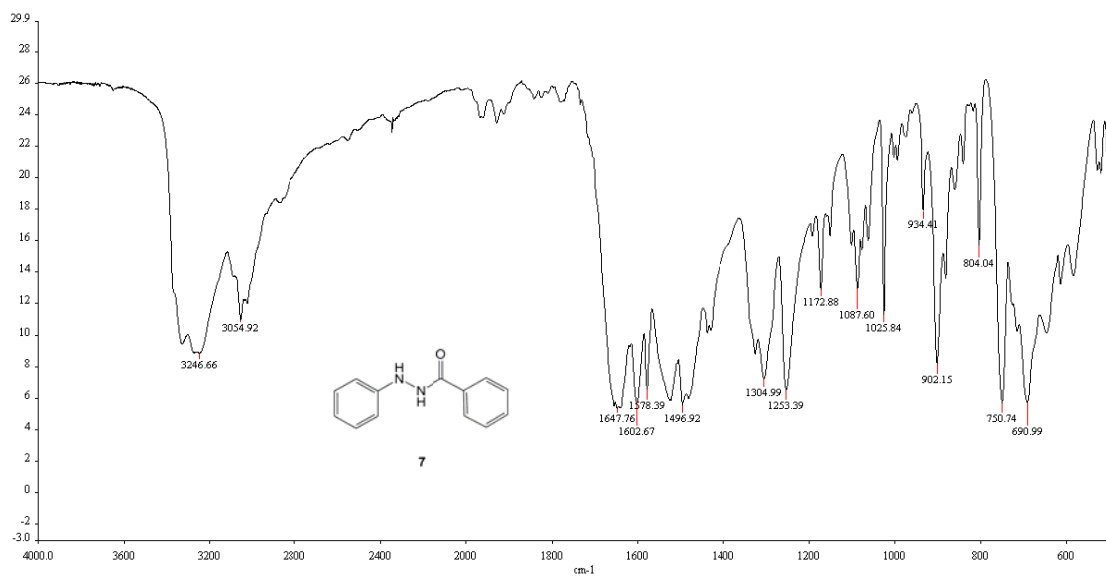
Figure 20 IR spectrum (KBr) of *N'*-(4-fluorophenyl)acetohydrazide (**6**)**Figure 21** ¹H-NMR (500MHz, DMSO-*d*₆) spectrum of *N'*-(4-fluorophenyl)acetohydrazide (**6**)

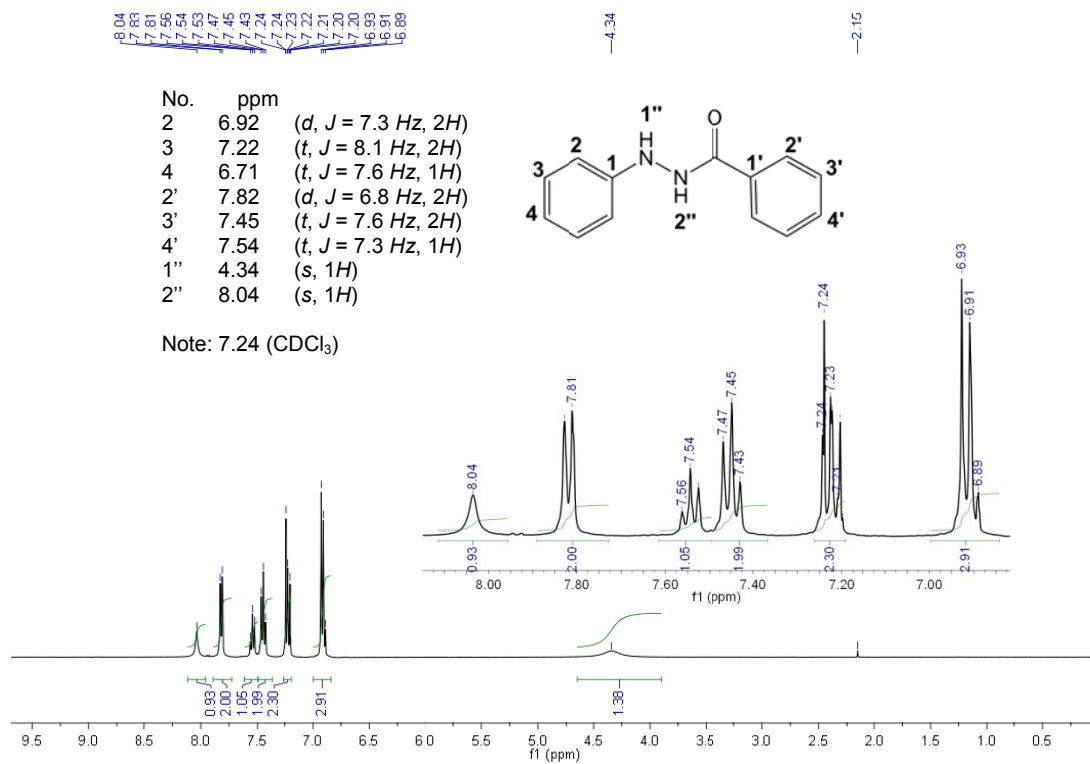
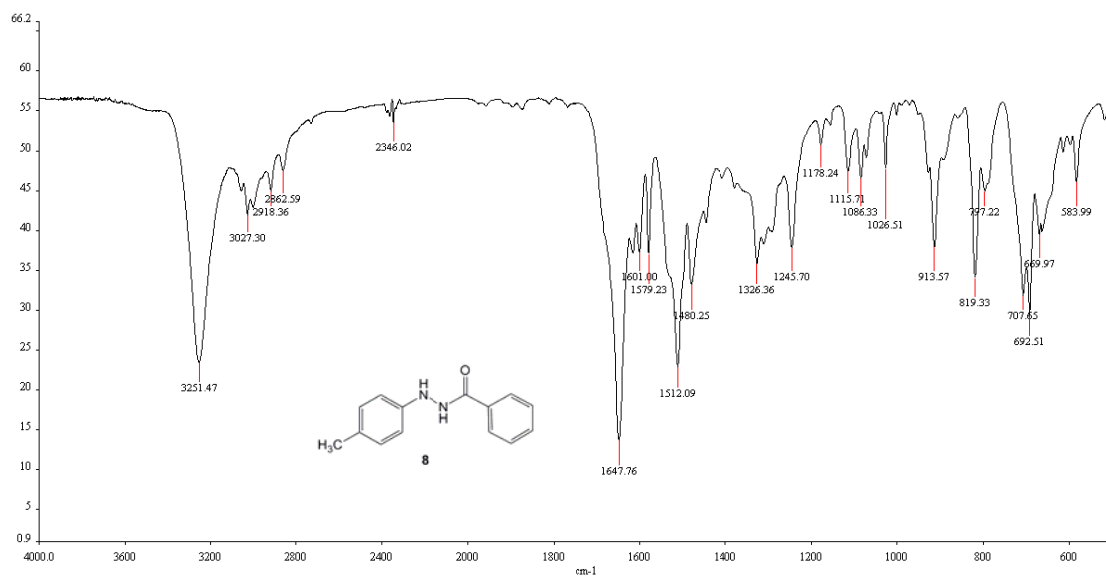
Figure 22 IR spectrum (KBr) of *N'*-phenylbenzohydrazide (7)**Figure 23** ¹H-NMR (500MHz, CDCl₃) spectrum of *N'*-phenylbenzohydrazide (7)

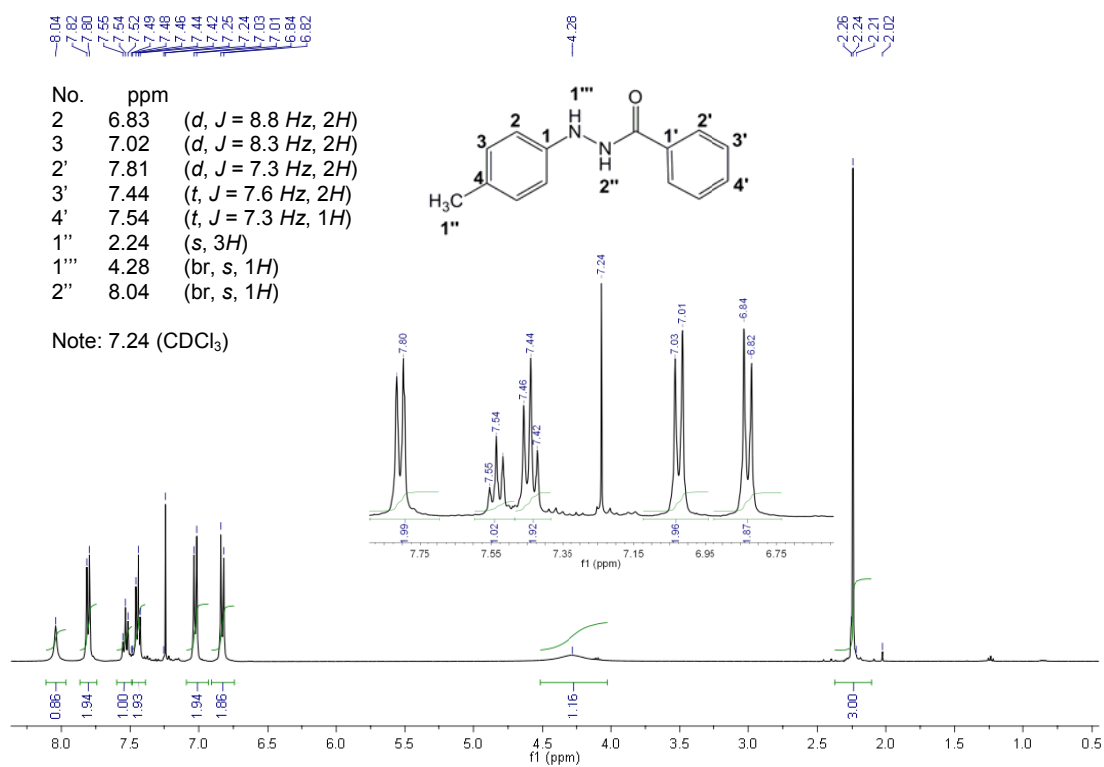
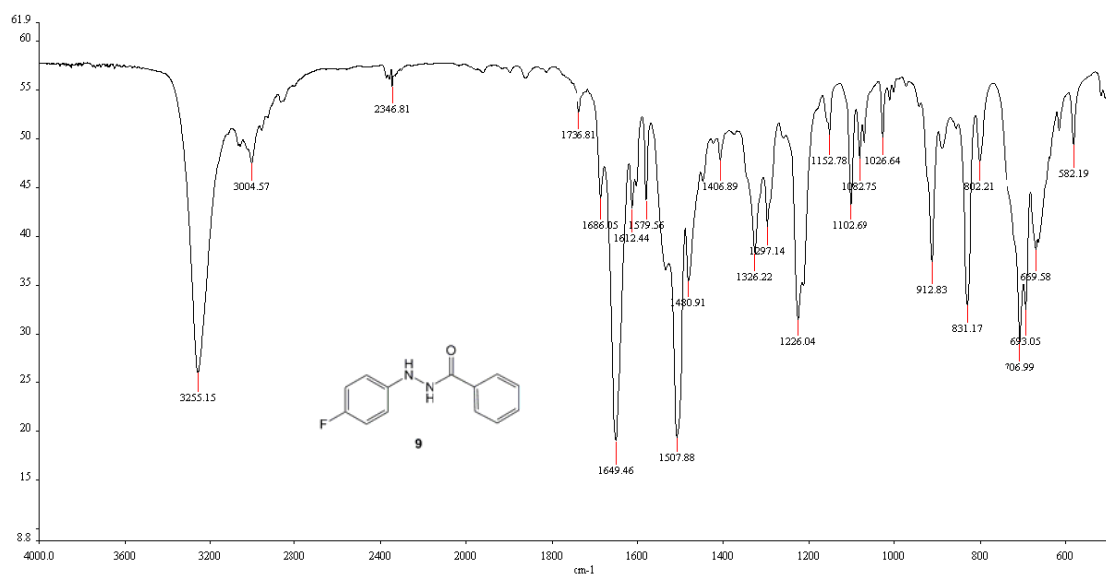
Figure 24 IR spectrum (KBr) of *N'*-*p*-tolylbenzohydrazide (**8**)**Figure 25** ¹H-NMR (500MHz, CDCl₃) spectrum of *N'*-*p*-tolylbenzohydrazide (**8**)

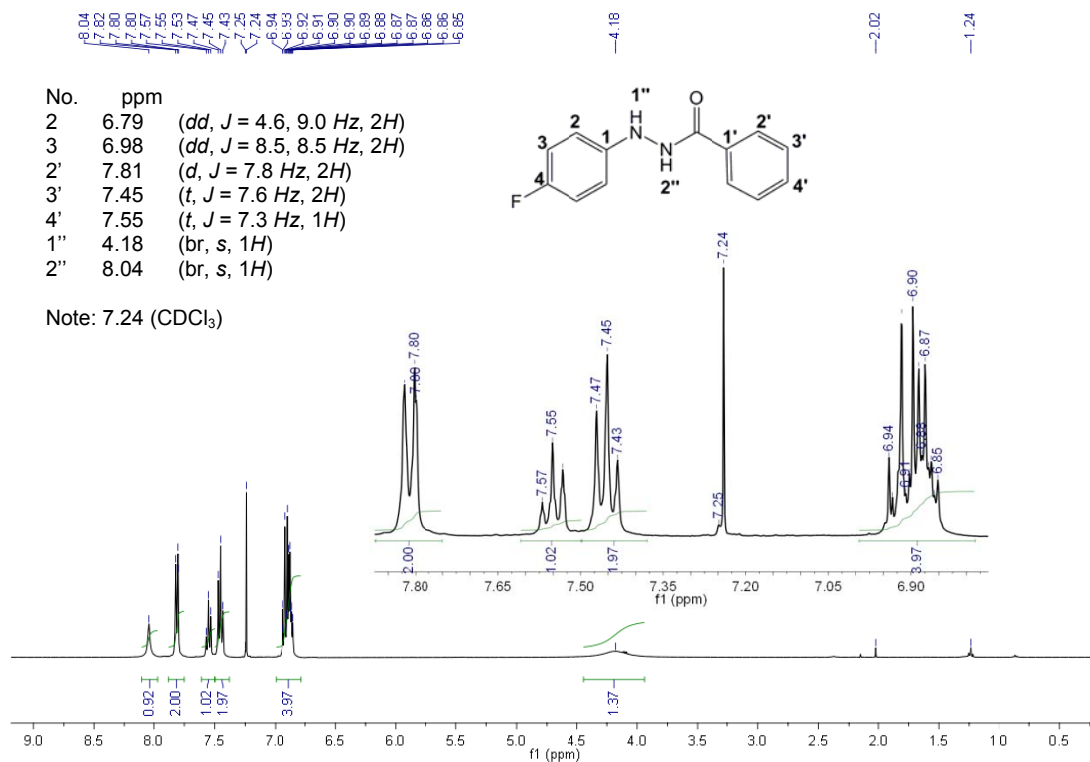
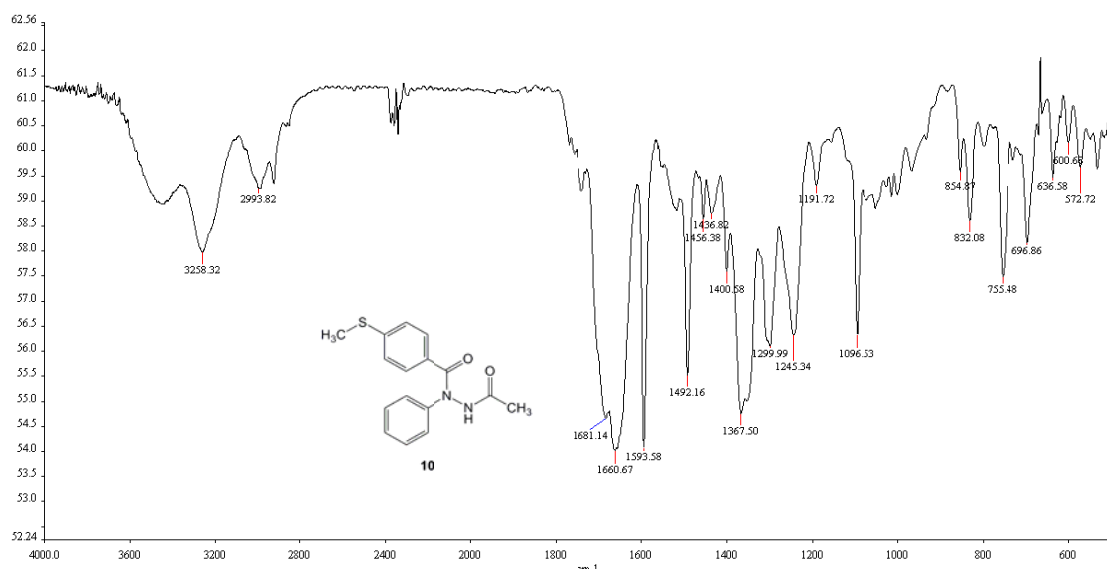
Figure 26 IR spectrum (KBr) of *N'*-(4-fluorophenyl)benzohydrazide (**9**)**Figure 27** ¹H-NMR (500MHz, CDCl₃) spectrum of *N'*-(4-fluorophenyl)benzohydrazide (**9**)

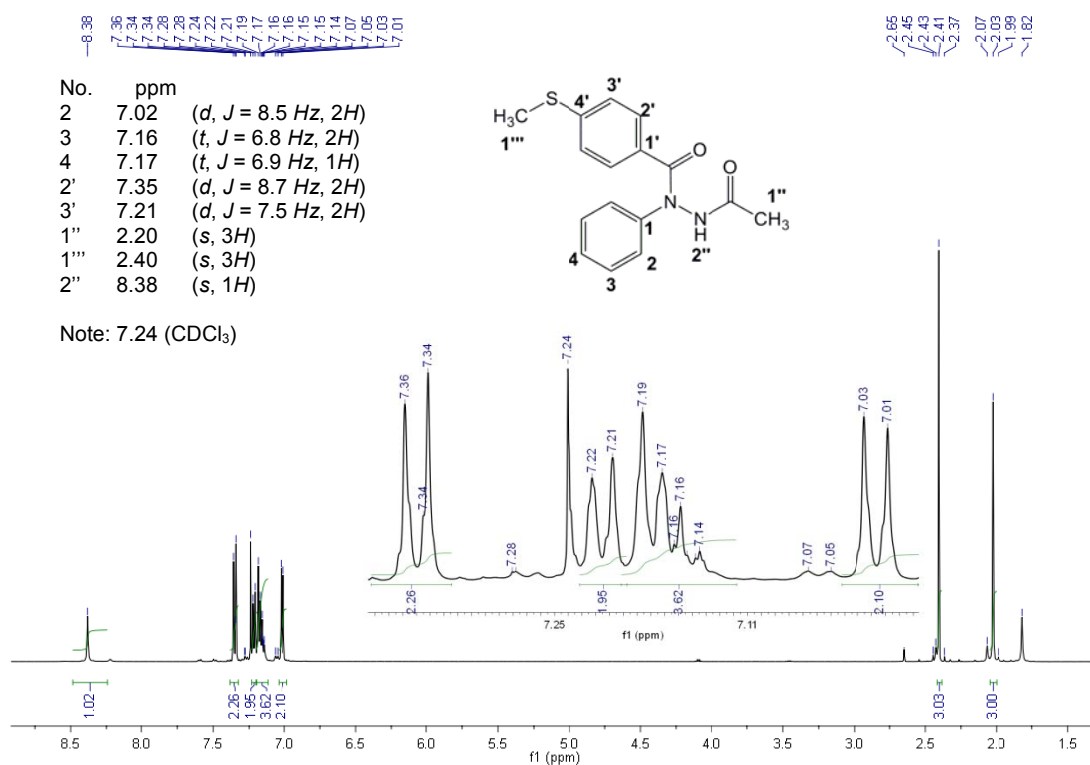
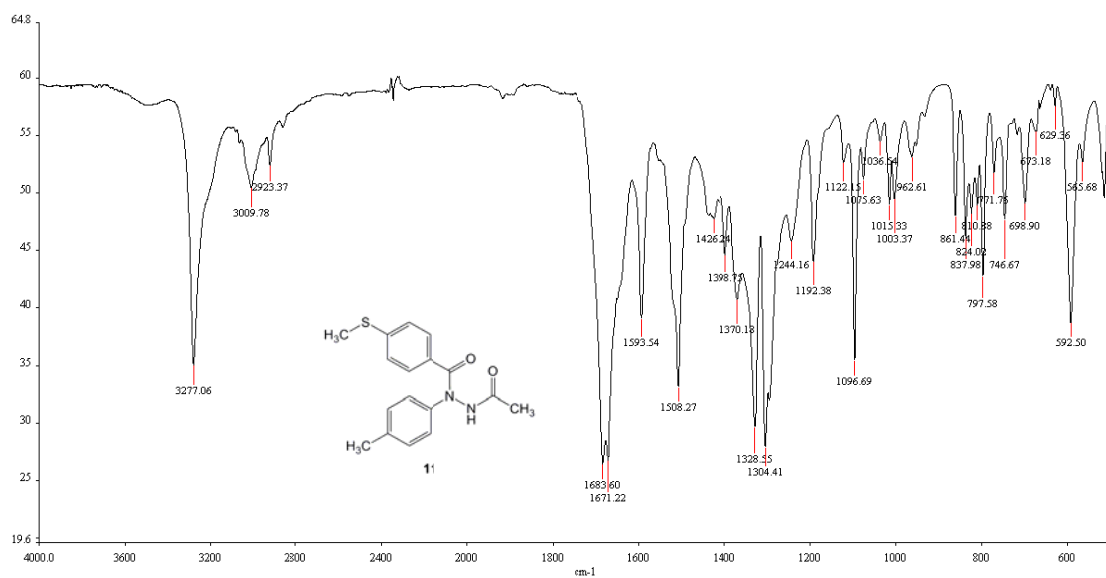
Figure 28 IR spectrum (KBr) of *N*'-acetyl-4-(methylthio)-*N*-phenylbenzohydrazide (**10**)**Figure 29** ¹H-NMR (500MHz, CDCl₃) spectrum of *N*'-acetyl-4-(methylthio)-*N*-phenylbenzohydrazide (**10**)

Figure 30 IR spectrum (KBr) of *N*'-acetyl-4-(methylthio)-*N*-*p*-tolylbenzohydrazide (**11**)

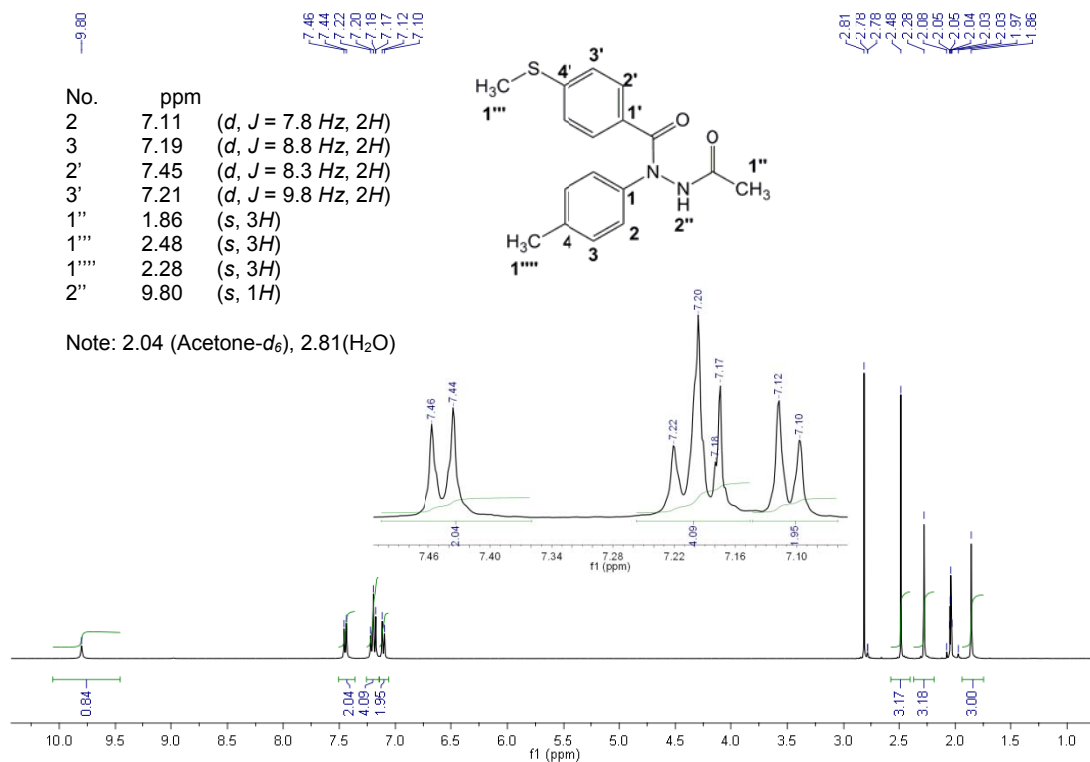


Figure 31 $^1\text{H-NMR}$ (400MHz, Acetone- d_6) spectrum of *N*'-acetyl-4-(methylthio)-*N*-*p*-tolyl benzohydrazide (**11**)

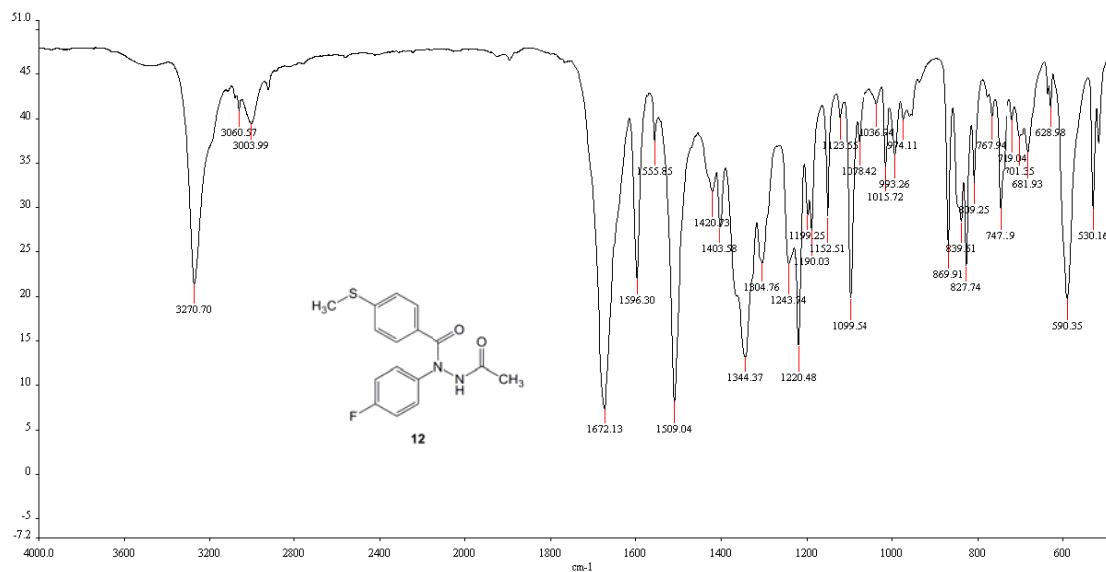


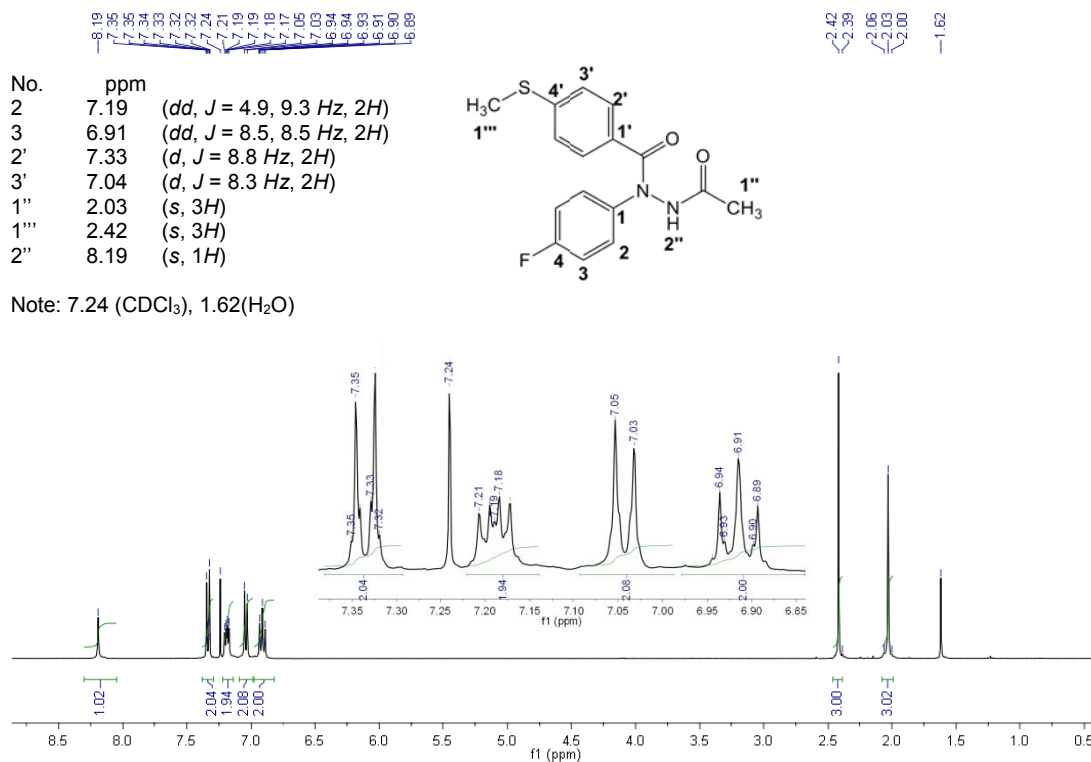
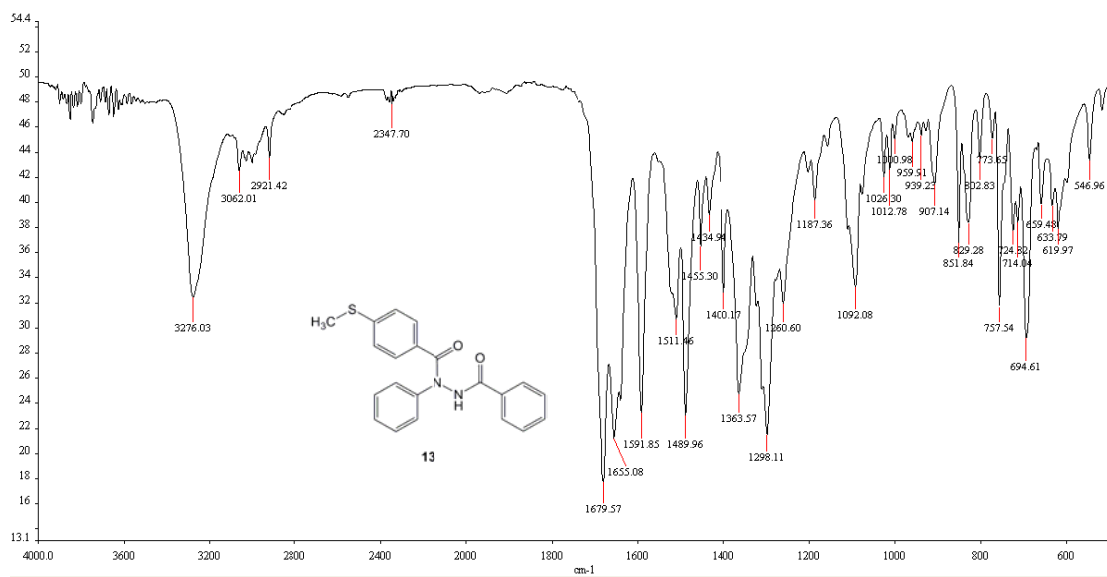
Figure 32 IR spectrum (KBr) of *N*'-acetyl-*N*-(4-fluorophenyl)-4-(methylthio)benzohydrazide (**12**)**Figure 33** ¹H-NMR (400MHz, CDCl₃) spectrum of *N*'-acetyl-*N*-(4-fluorophenyl)-4-(methylthio) benzohydrazide (**12**)

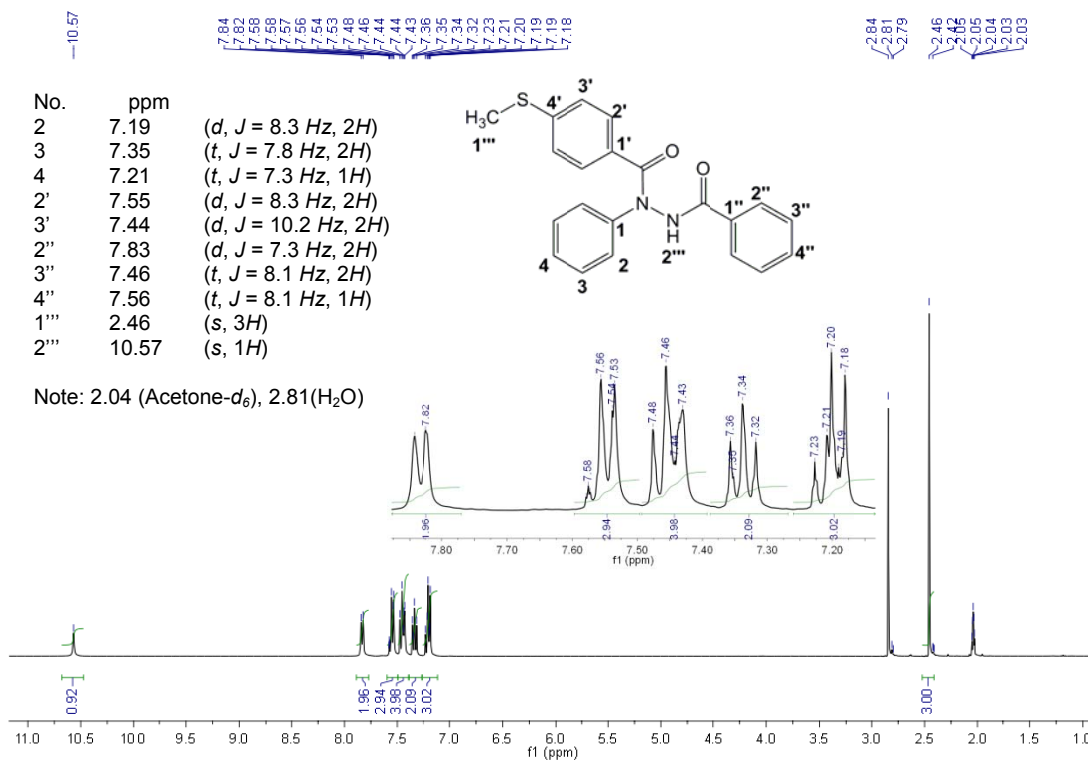
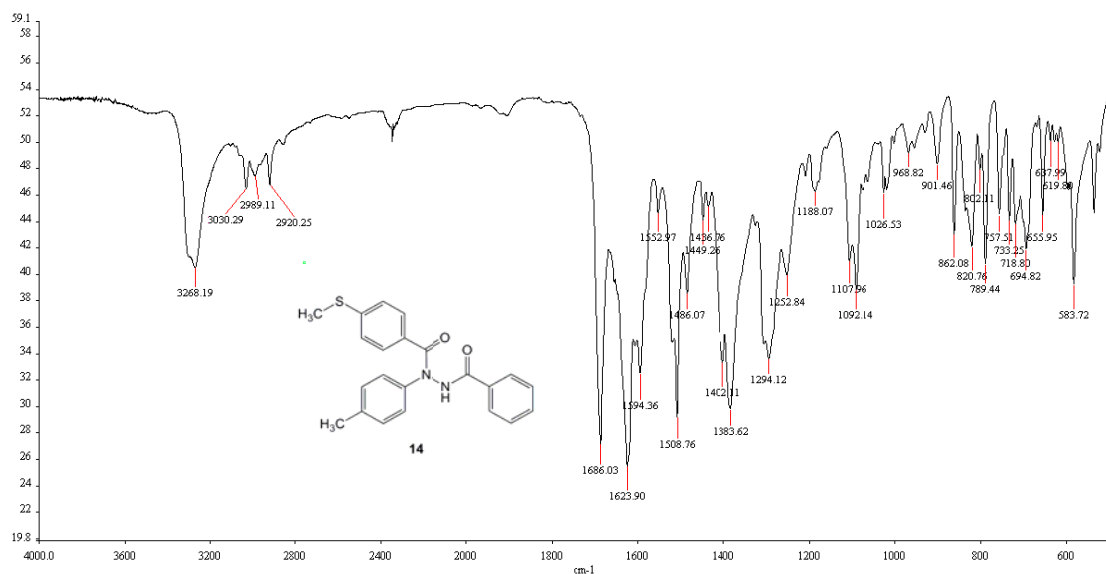
Figure 34 IR spectrum (KBr) of *N'*-benzoyl-4-(methylthio)-*N*-phenylbenzohydrazide (**13**)**Figure 35** $^1\text{H-NMR}$ (400MHz, Acetone- d_6) spectrum of *N'*-benzoyl-4-(methylthio)-*N*-phenylbenzohydrazide (**13**)

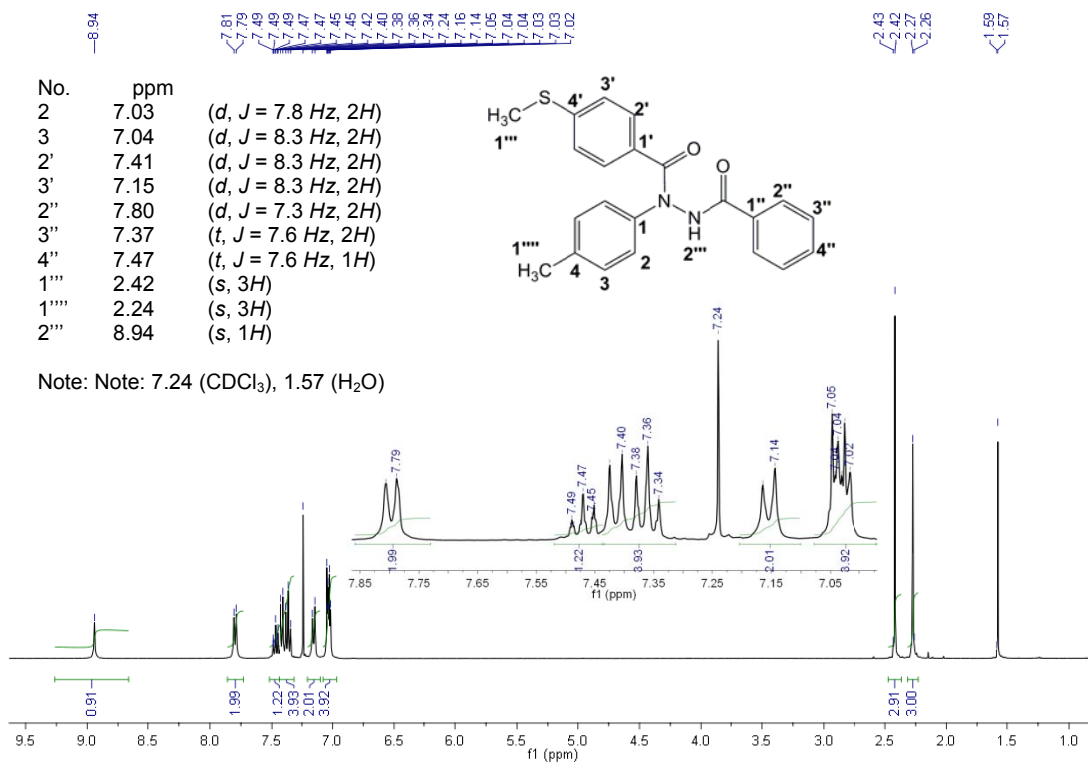
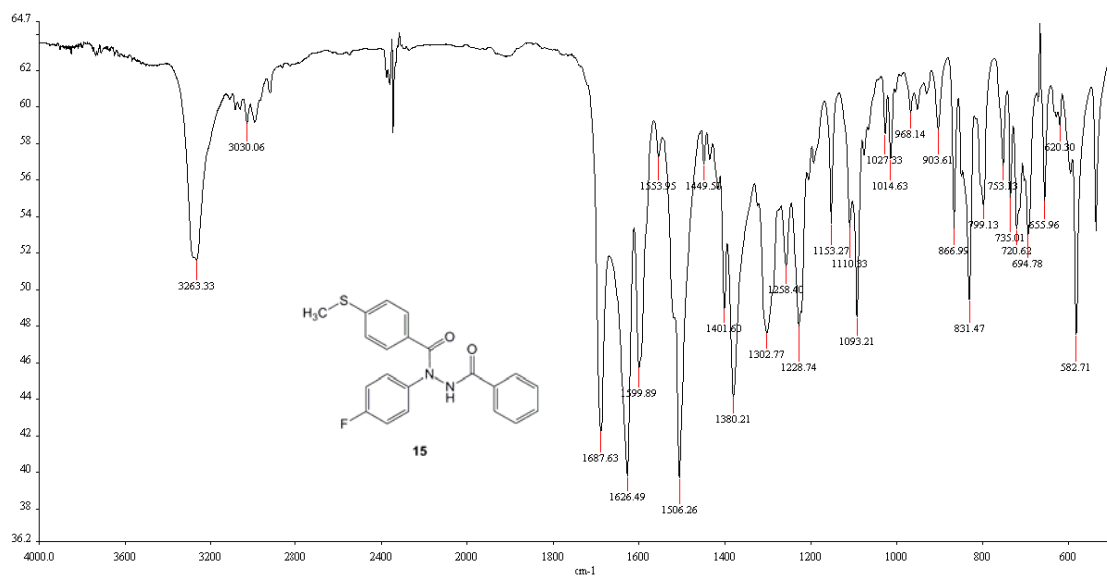
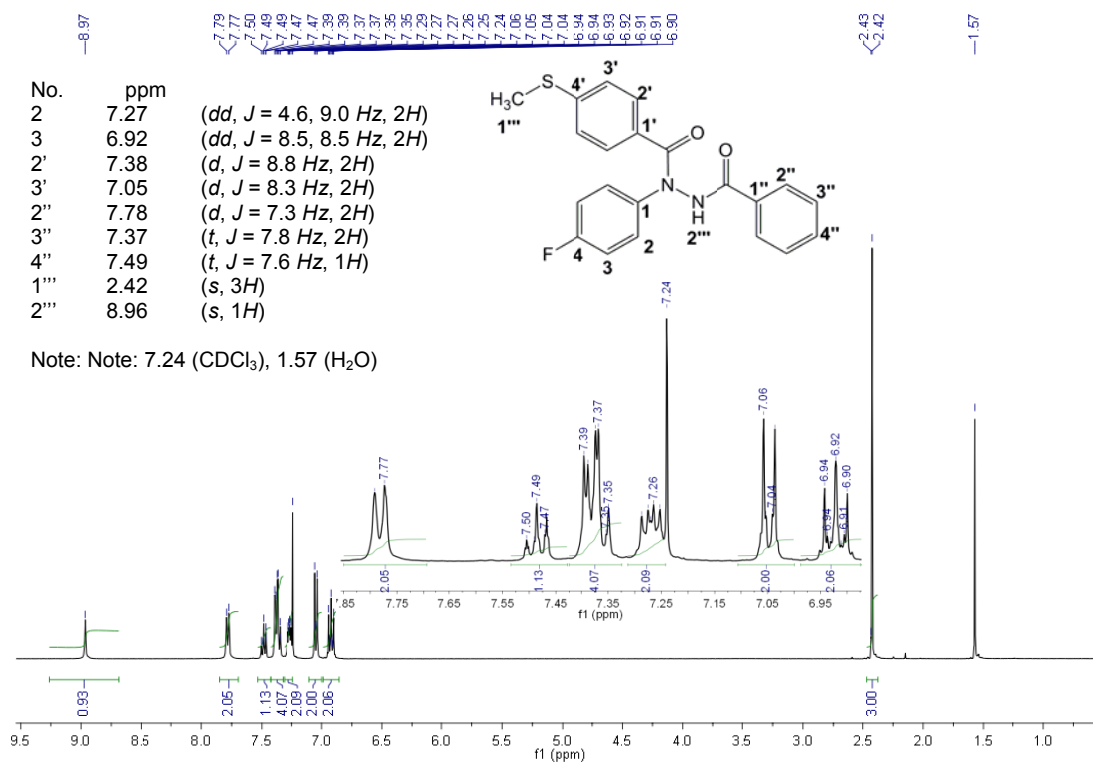
Figure 36 IR spectrum (KBr) of *N'*-benzoyl-4-(methylthio)-*N-p*-tolylbenzohydrazide (**14**)**Figure 37** ¹H-NMR (400MHz, CDCl₃) spectrum of *N'*-benzoyl-4-(methylthio)-*N-p*-tolylbenzohydrazide (**14**)

Figure 38 IR spectrum (KBr) of *N*-benzoyl-*N*-(4-fluorophenyl)-4-(methylthio)benzohydrazide

(15)

**Figure 39** ¹H-NMR (400MHz, CDCl₃) spectrum of *N*-benzoyl-*N*-(4-fluorophenyl)-4-(methylthio)benzohydrazide (15)

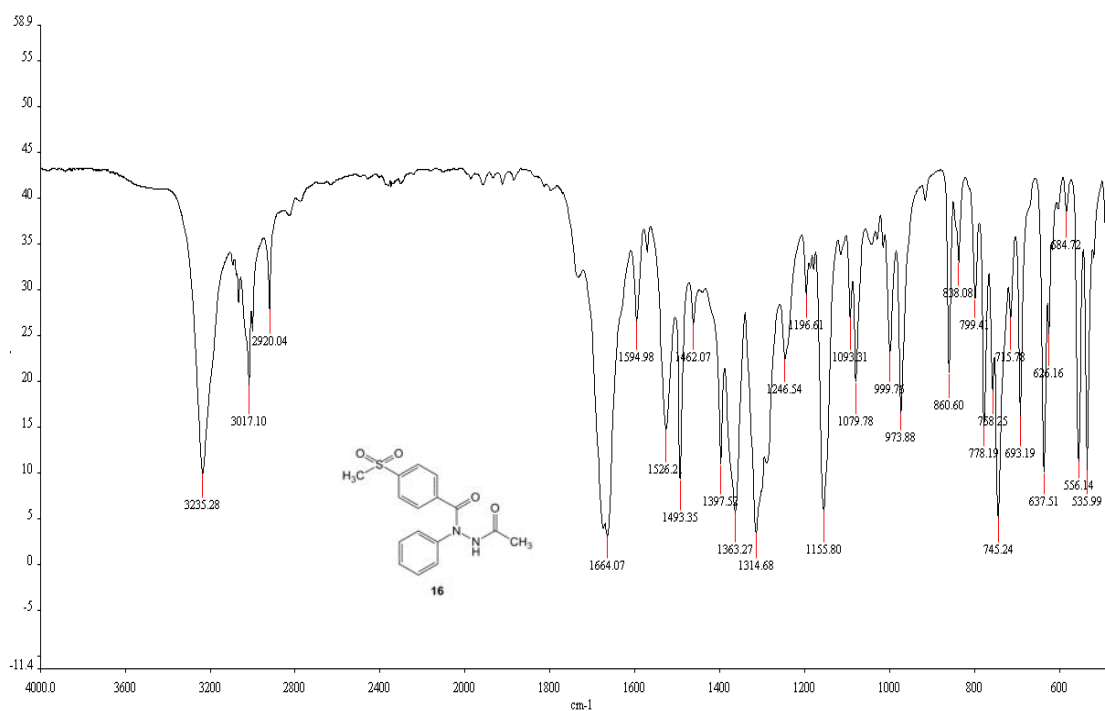


Figure 40 IR spectrum (KBr) of *N'*-acetyl-4-(methylsulfonyl)-*N*-phenylbenzohydrazide (**16**)

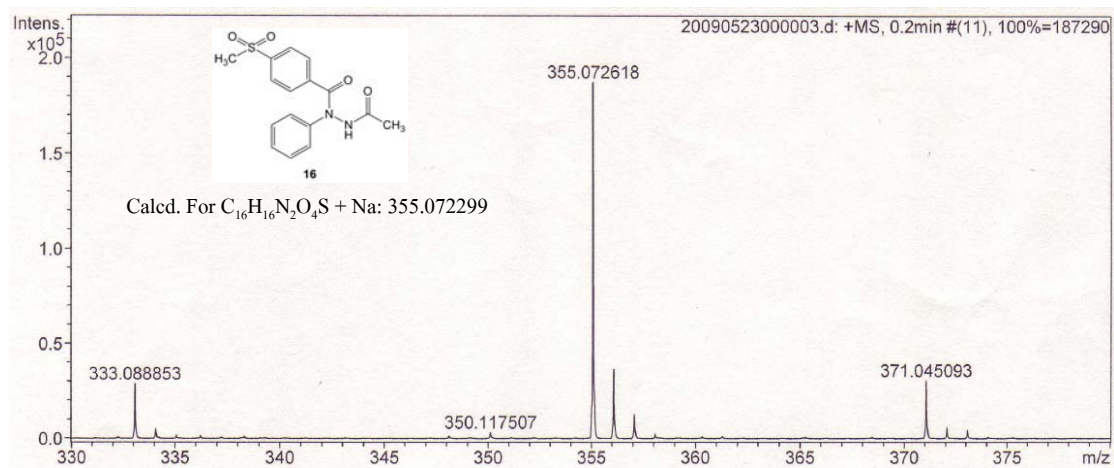


Figure 43 The mass (HR-MS; ESI) spectrum of *N'*-acetyl-4-(methylsulfonyl)-*N*-phenylbenzohydrazide (**16**)

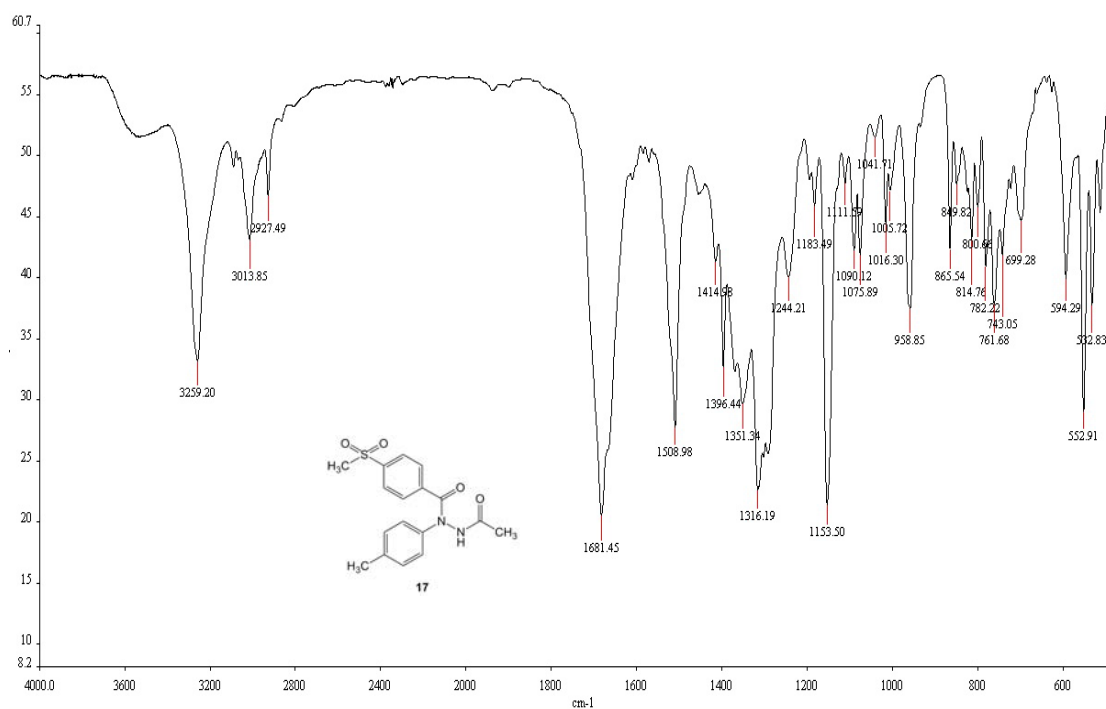


Figure 44 IR spectrum (KBr) of *N*-acetyl-4-(methylsulfonyl)-*N*-*p*-tolylbenzohydrazide (**17**)

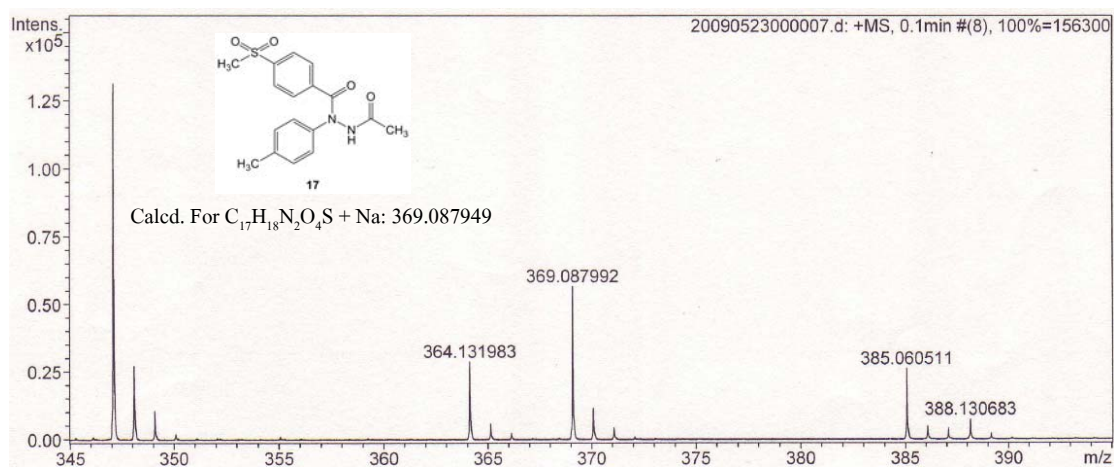


Figure 47 The mass (HR-MS; ESI) spectrum of *N*-acetyl-4-(methylsulfonyl)-*N*-*p*-tolylbenzohydrazide (**17**)

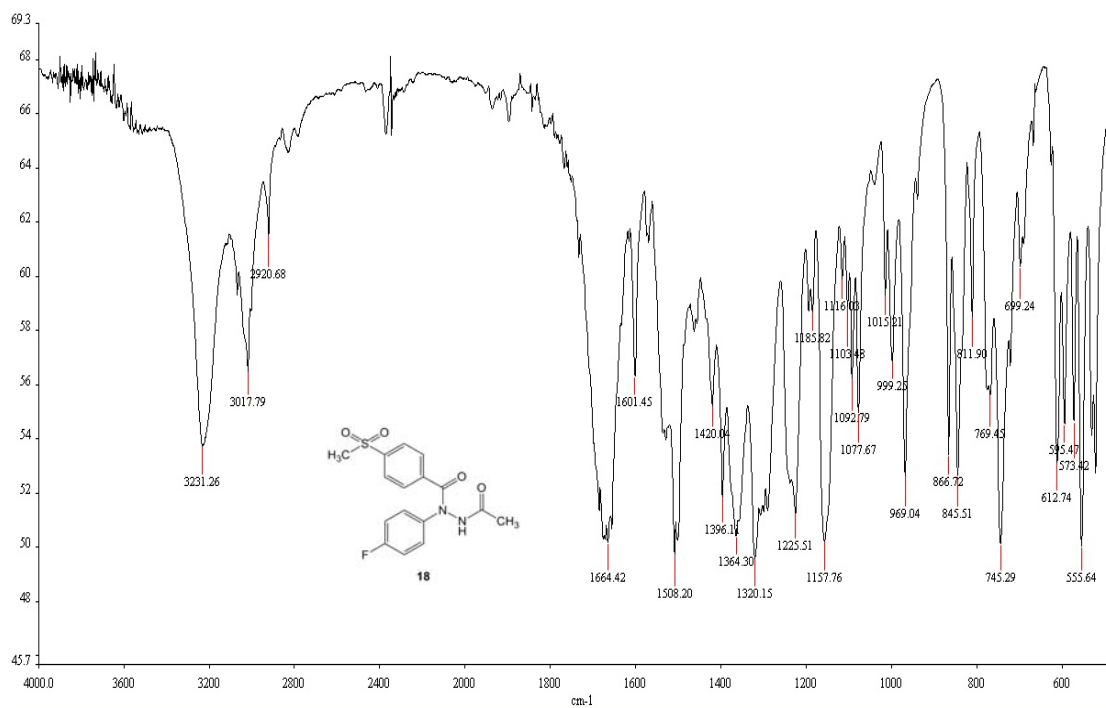


Figure 48 IR spectrum (KBr) of *N'*-acetyl-*N*-(4-fluorophenyl)-4-(methylsulfonyl)benzohydrazide (**18**)

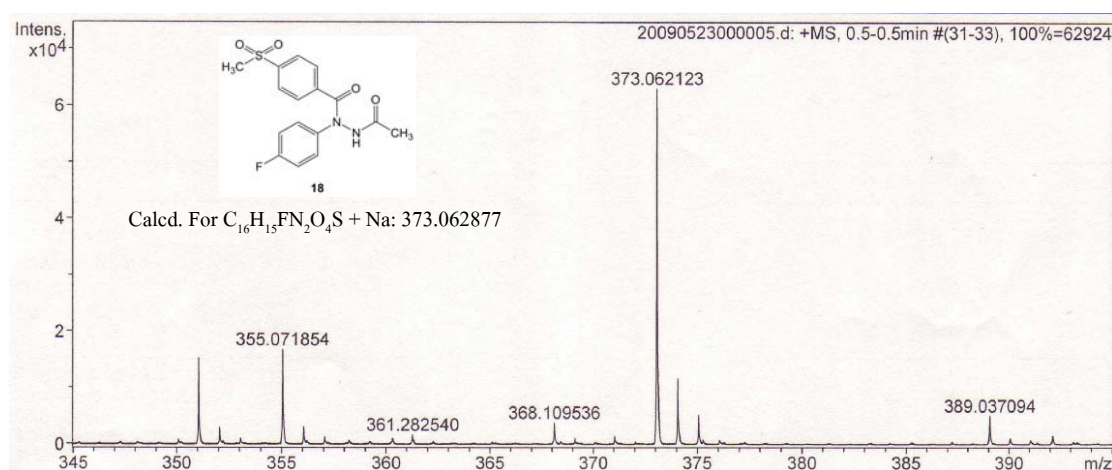


Figure 51 The mass (HR-MS; ESI) spectrum of *N'*-acetyl-*N*-(4-fluorophenyl)-4-(methylsulfonyl)benzohydrazide (**18**)

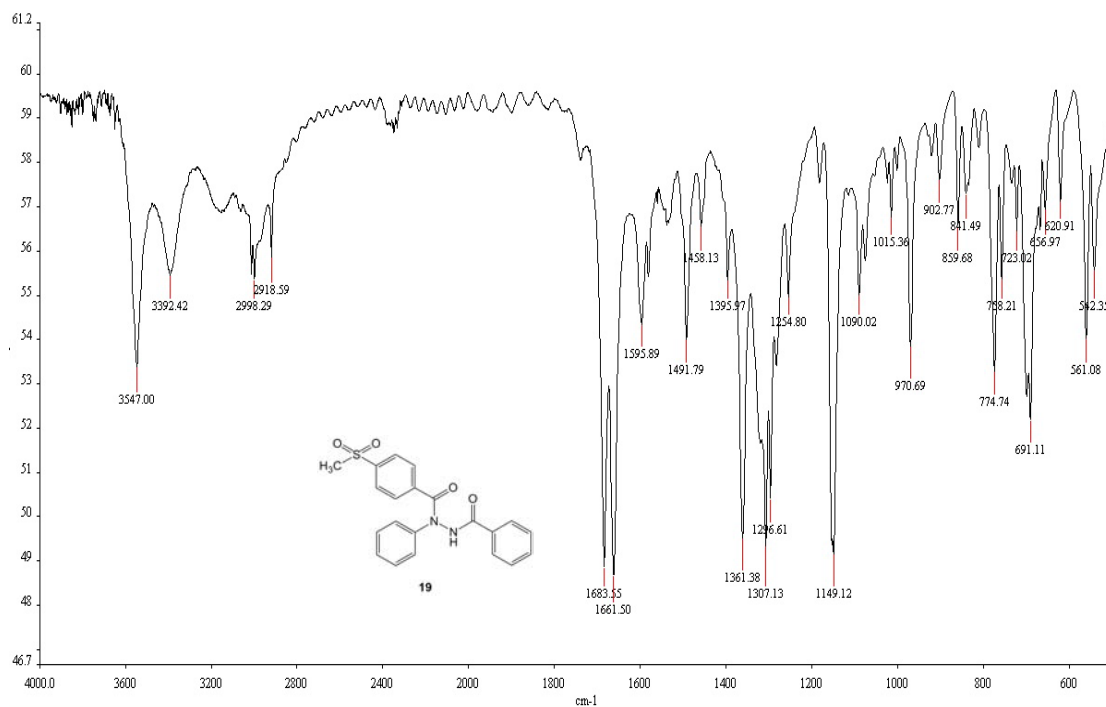


Figure 52 IR spectrum (KBr) of *N'*-benzoyl-4-(methylsulfonyl)-*N*-phenylbenzohydrazide (**19**)

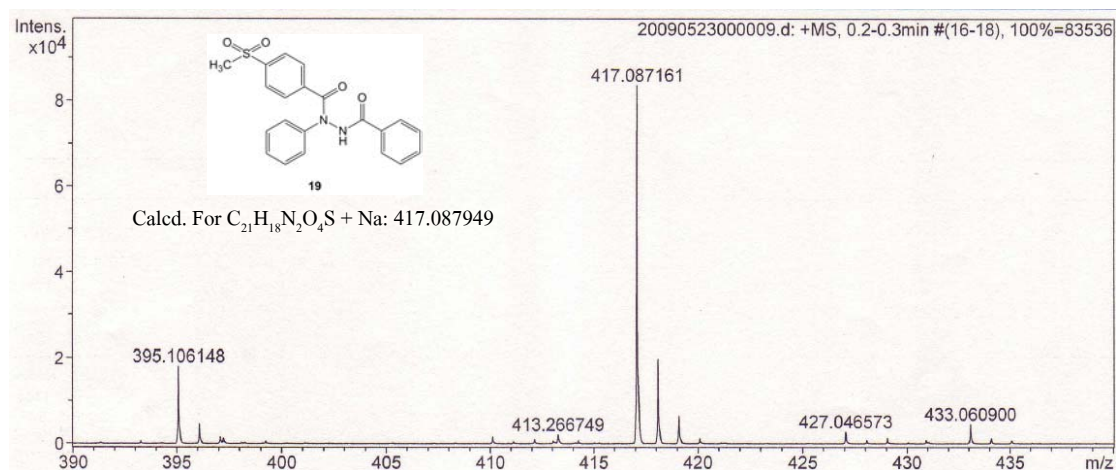


Figure 55 The mass (HR-MS; ESI) spectrum of *N'*-benzoyl-4-(methylsulfonyl)-*N*-phenylbenzohydrazide (**19**)

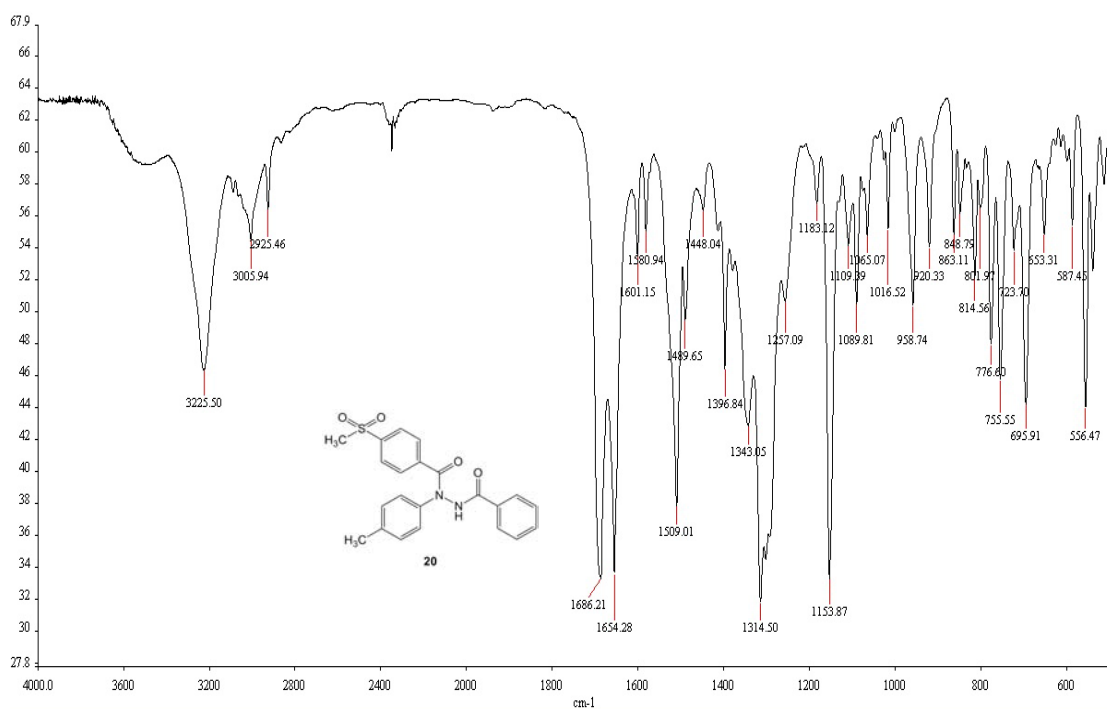


Figure 56 IR spectrum (KBr) of *N'*-benzoyl-4-(methylsulfonyl)-*N-p*-tolylbenzohydrazide (**20**)

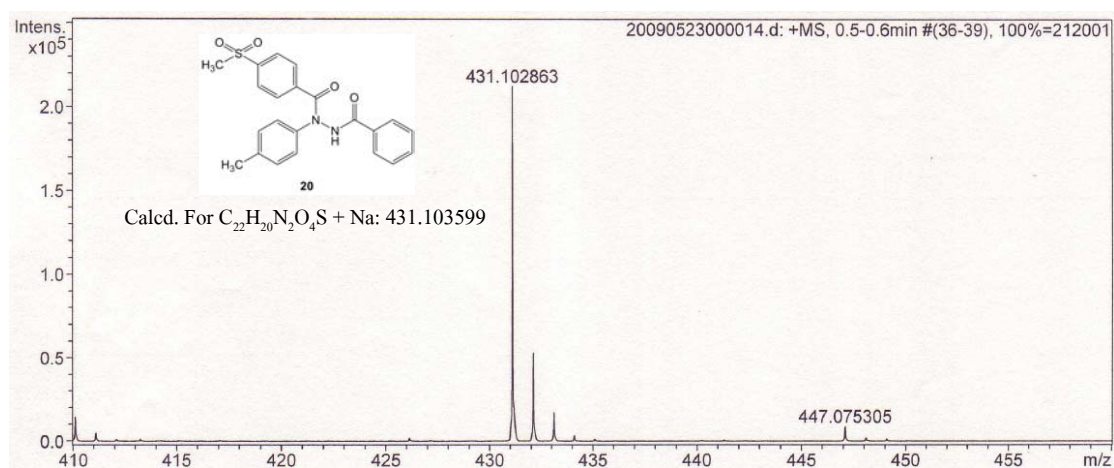


Figure 59 The mass (HR-MS; ESI) spectrum of *N'*-benzoyl-4-(methylsulfonyl)-*N-p*-tolylbenzohydrazide (**20**)

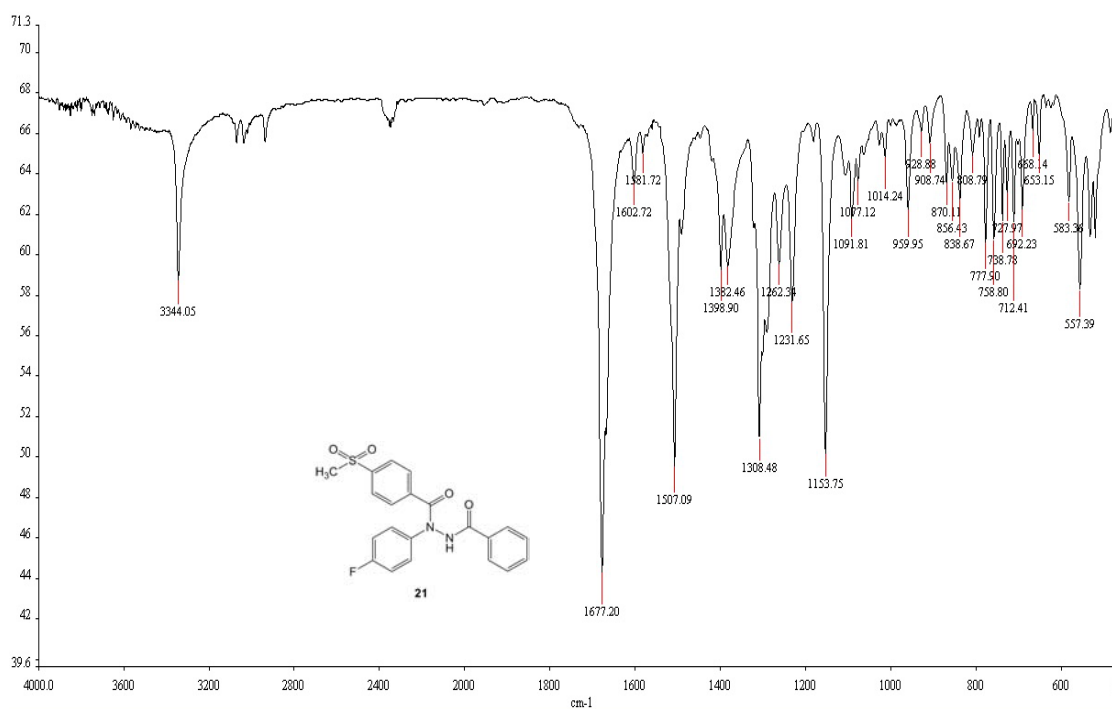


Figure 60 IR spectrum (KBr) of *N'*-benzoyl-*N*-(4-fluorophenyl)-4-(methylsulfonyl)benzohydrazide (**21**)

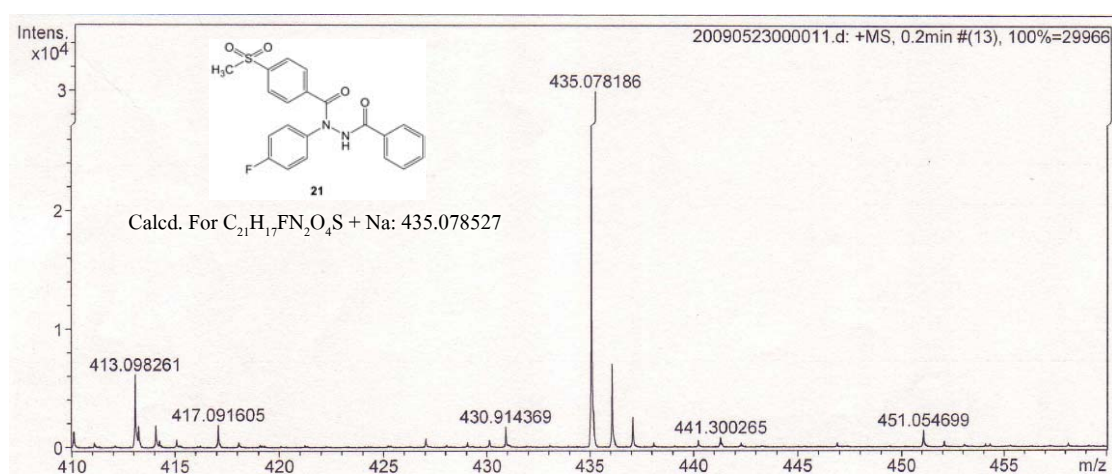


Figure 63 The mass (HR-MS; ESI) spectrum of *N'*-benzoyl-*N*-(4-fluorophenyl)-4-(methylsulfonyl)benzohydrazide (**21**)

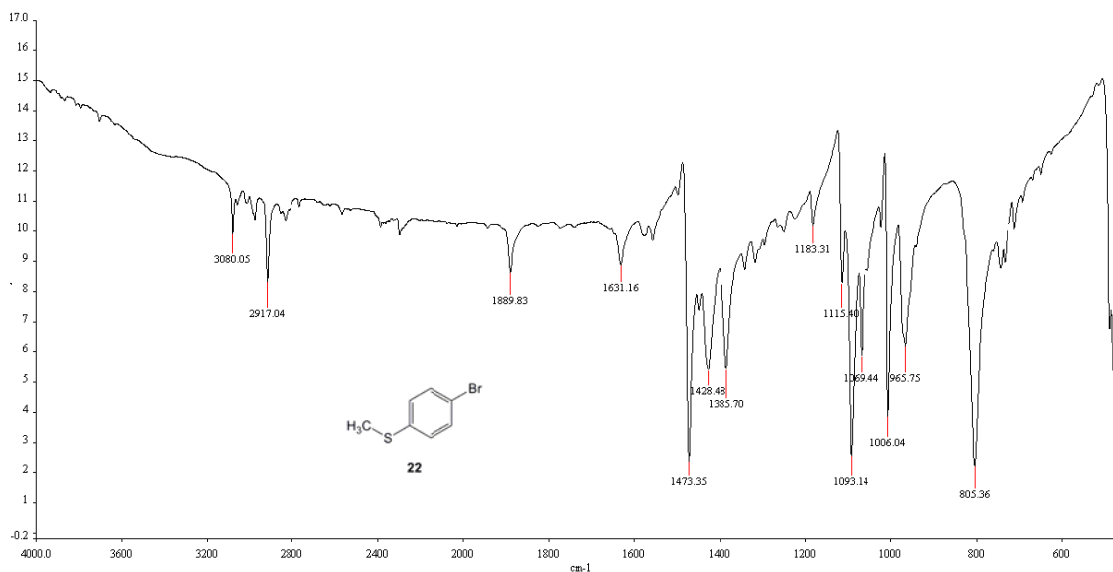


Figure 64 IR spectrum (KBr) of 4-bromothioanisole (**22**)

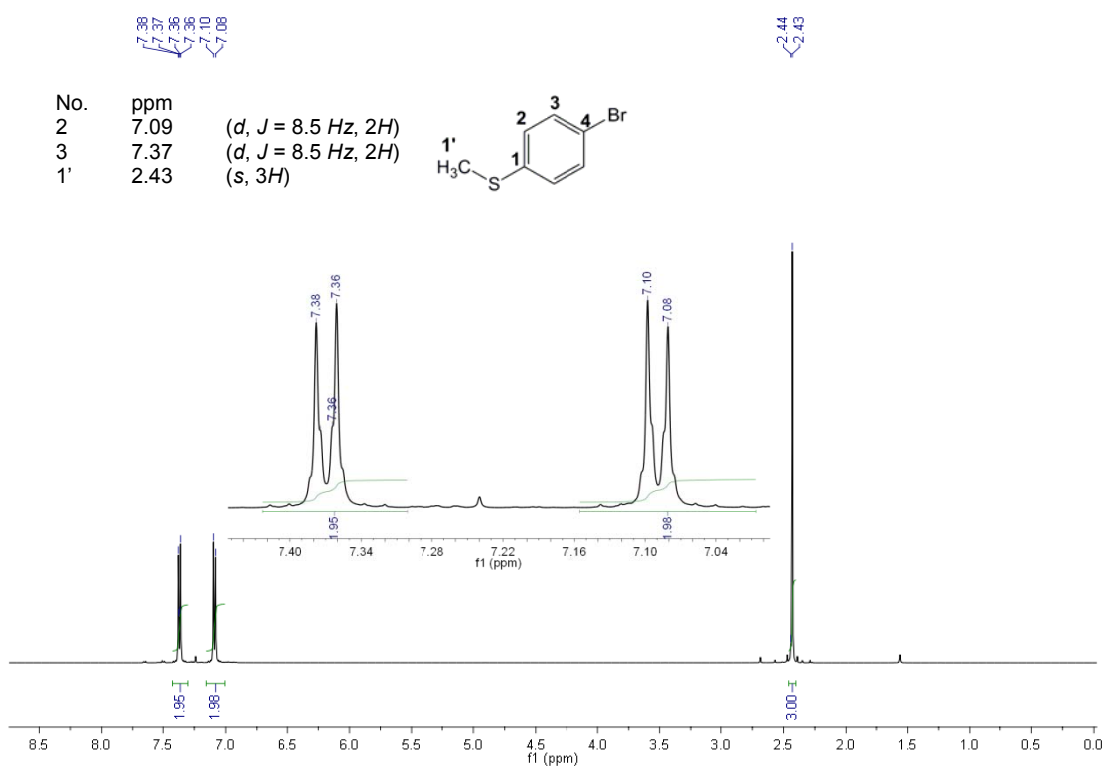


Figure 65 $^1\text{H-NMR}$ (500MHz, CDCl_3) spectrum of 4-bromothioanisole (**22**)

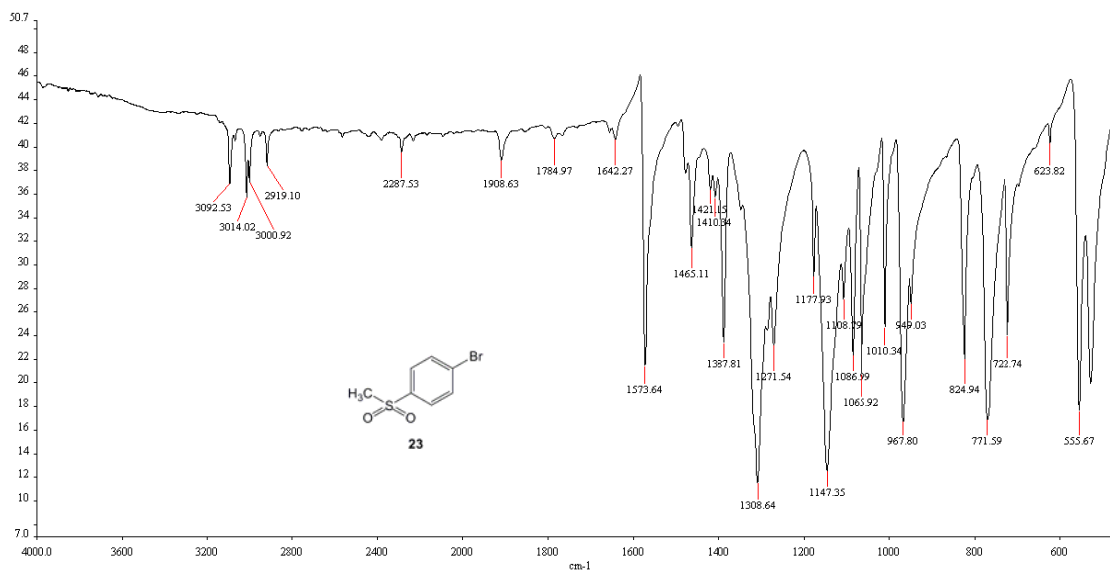


Figure 66 IR spectrum (KBr) of 4-bromomethylsulfone (**23**)

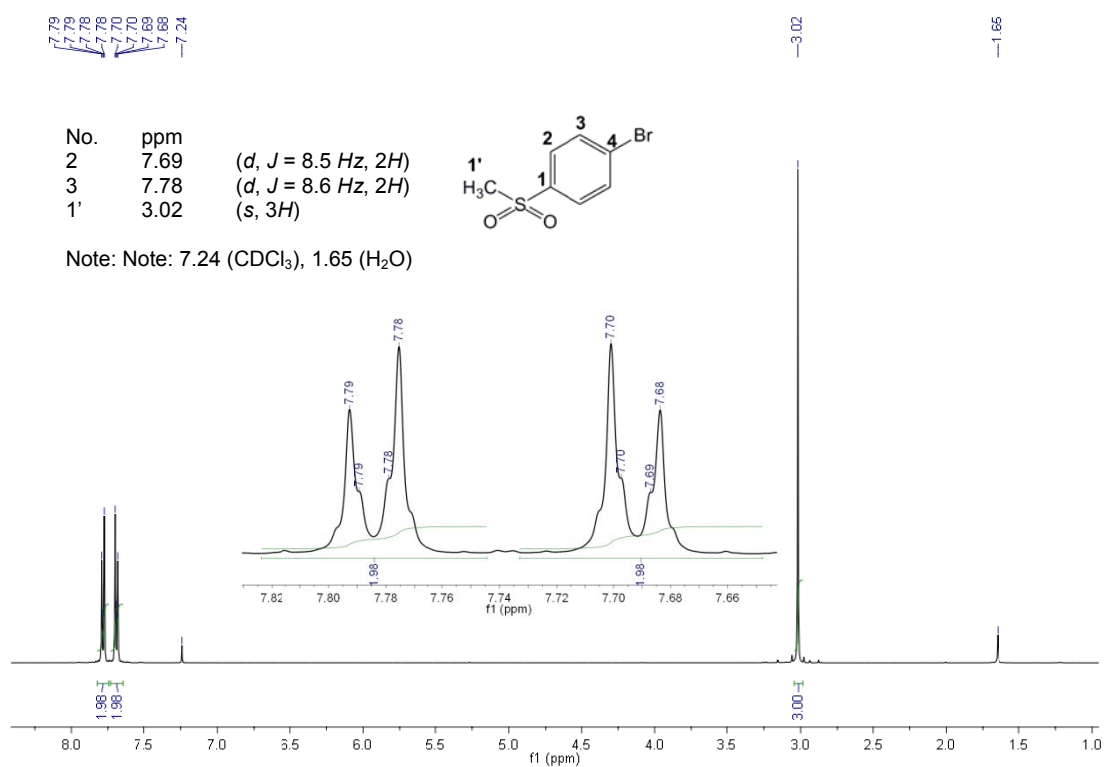


Figure 67 ¹H-NMR (500MHz, CDCl₃) spectrum of 4-bromomethylsulfone (**23**)

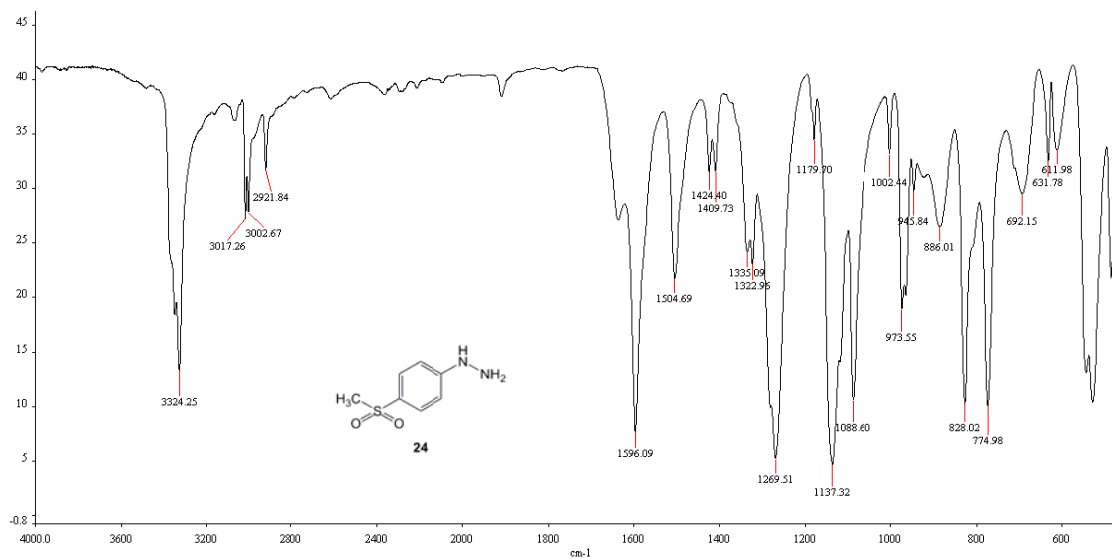


Figure 68 IR spectrum (KBr) of (4-(methylsulfonyl)phenyl)hydrazine (**24**)

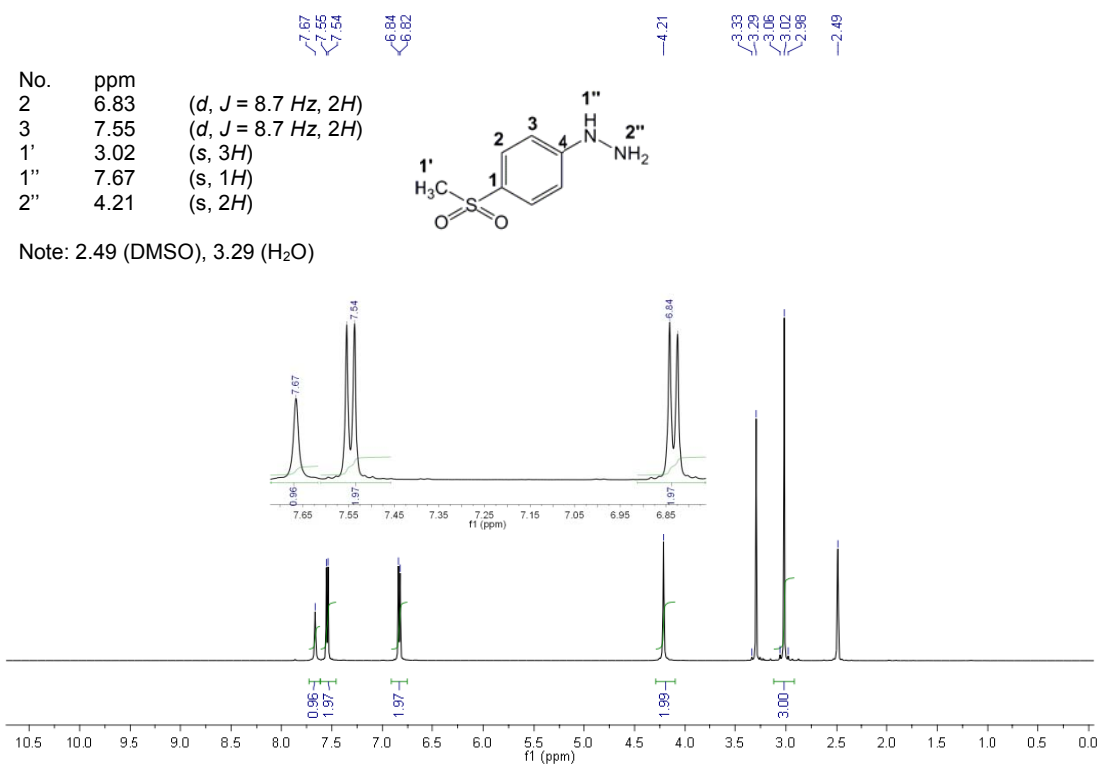


Figure 69 ¹H-NMR(500MHz, DMSO-*d*₆) spectrum of (4-(methylsulfonyl)phenyl)hydrazine (**24**)

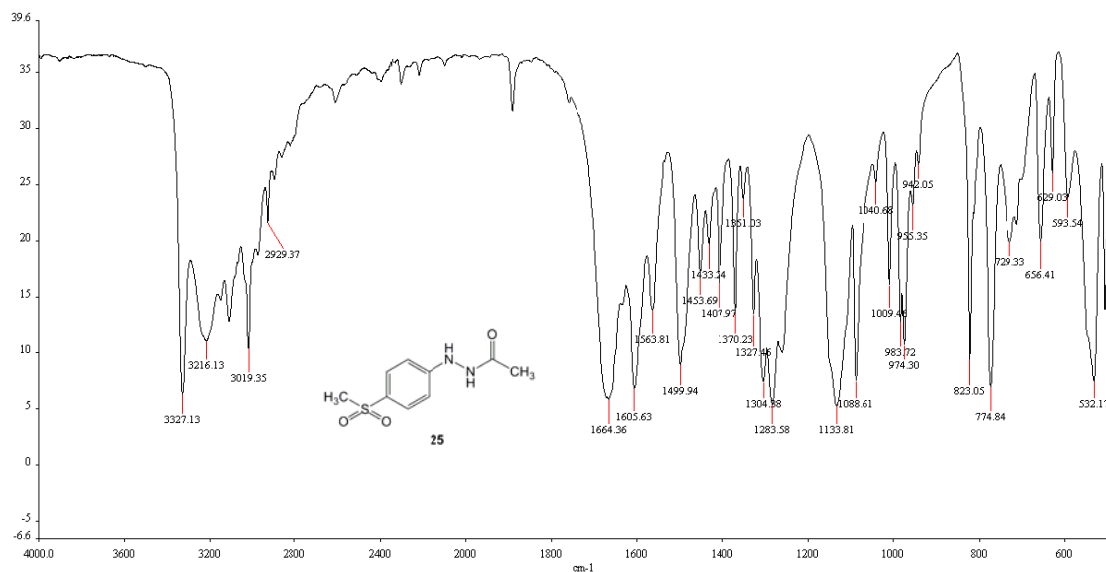


Figure 70 IR spectrum (KBr) of *N*-(4-(methylsulfonyl)phenyl)acetohydrazide (**25**)

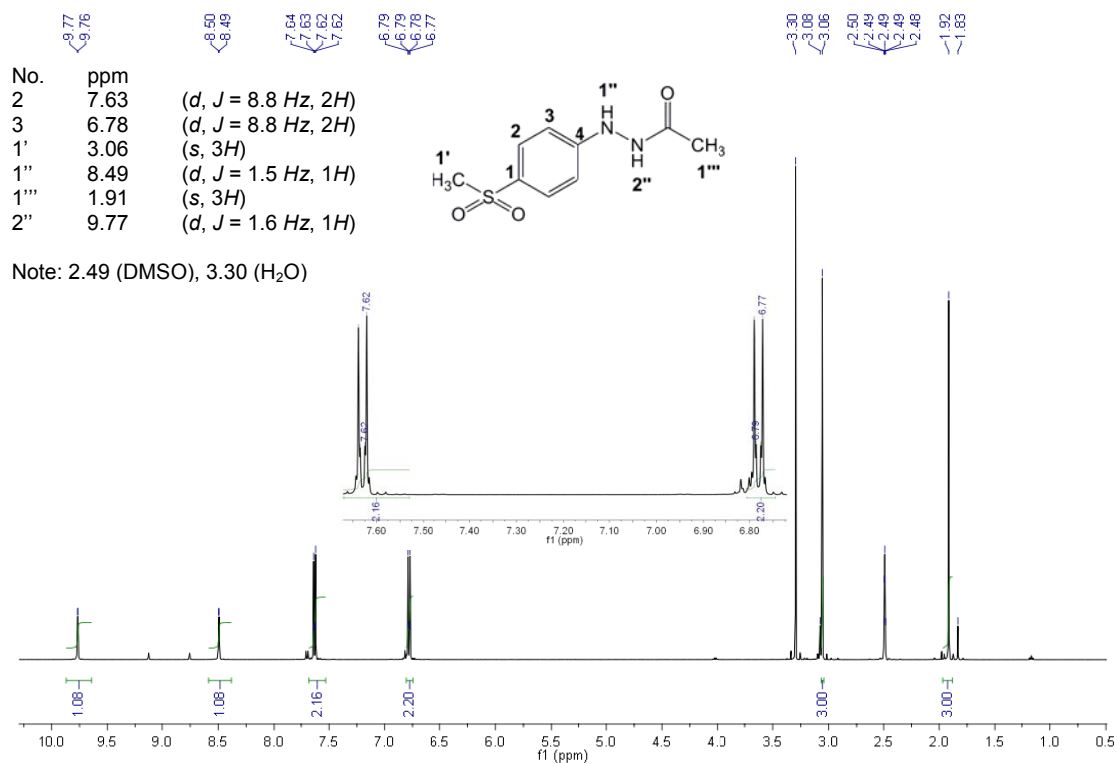


Figure 71 $^1\text{H-NMR}$ (500MHz, $\text{DMSO-}d_6$) spectrum of *N*-(4-(methylsulfonyl)phenyl)acetohydrazide (**25**)

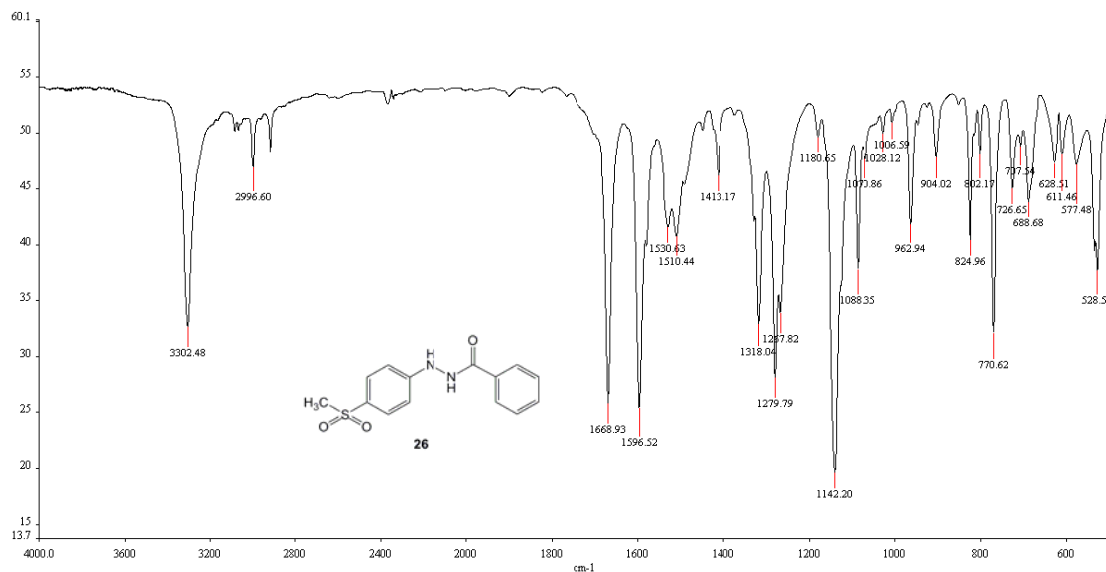


Figure 72 IR spectrum (KBr) of *N'*-(4-(methylsulfonyl)phenyl)benzohydrazide (**26**)

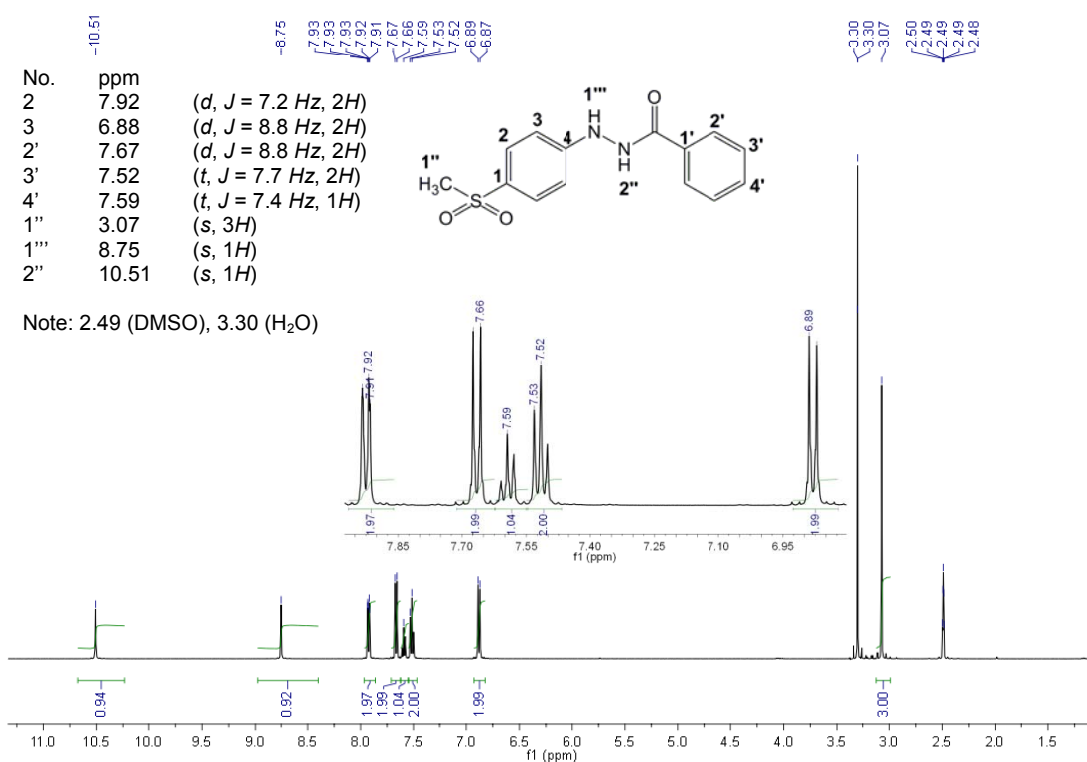


Figure 73 ¹H-NMR (500MHz, DMSO-*d*₆) spectrum of *N'*-(4-(methylsulfonyl)phenyl)benzohydrazide (**26**)

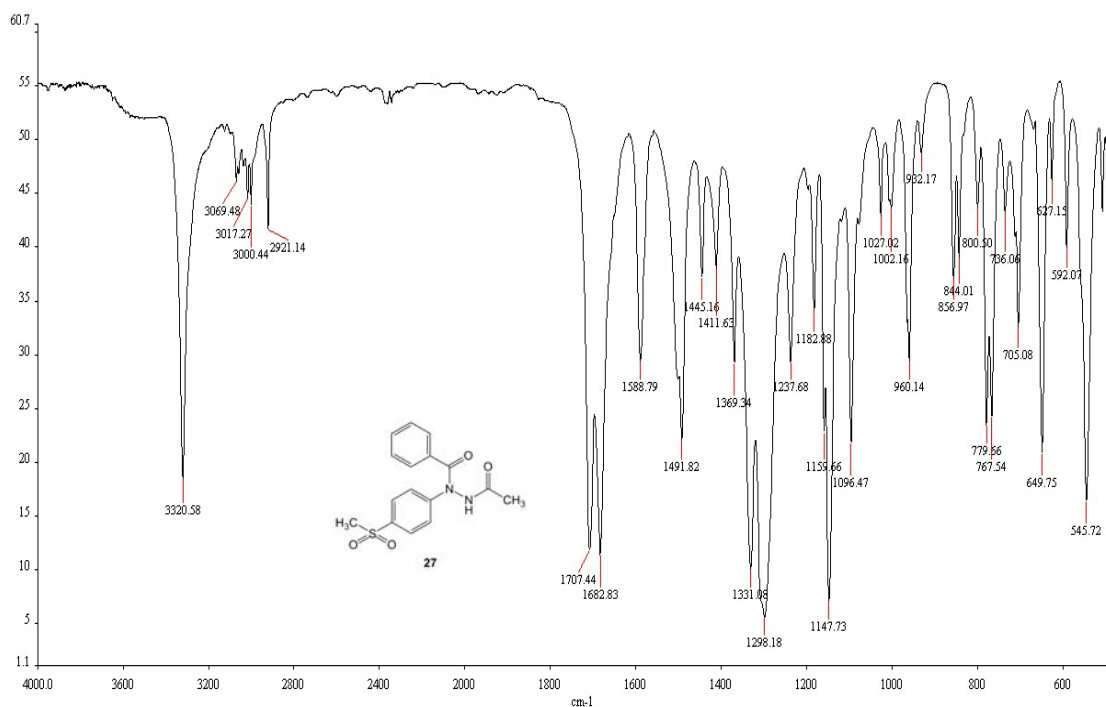


Figure 74 IR spectrum (KBr) of *N'*-acetyl-*N*-(4-(methylsulfonyl)phenyl)benzohydrazide (**27**)

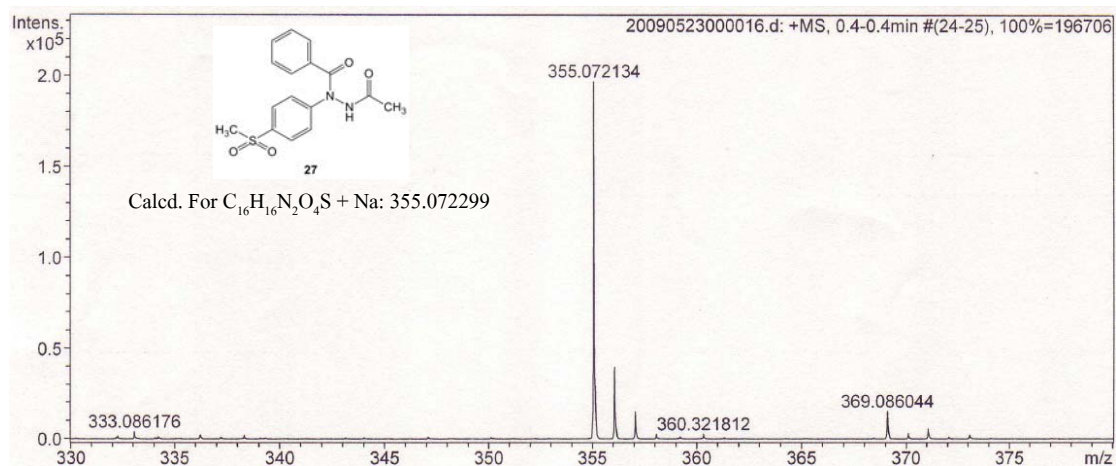


Figure 77 The mass (HR-MS; ESI) spectrum of *N'*-acetyl-*N*-(4-(methylsulfonyl)phenyl)benzohydrazide (**27**)

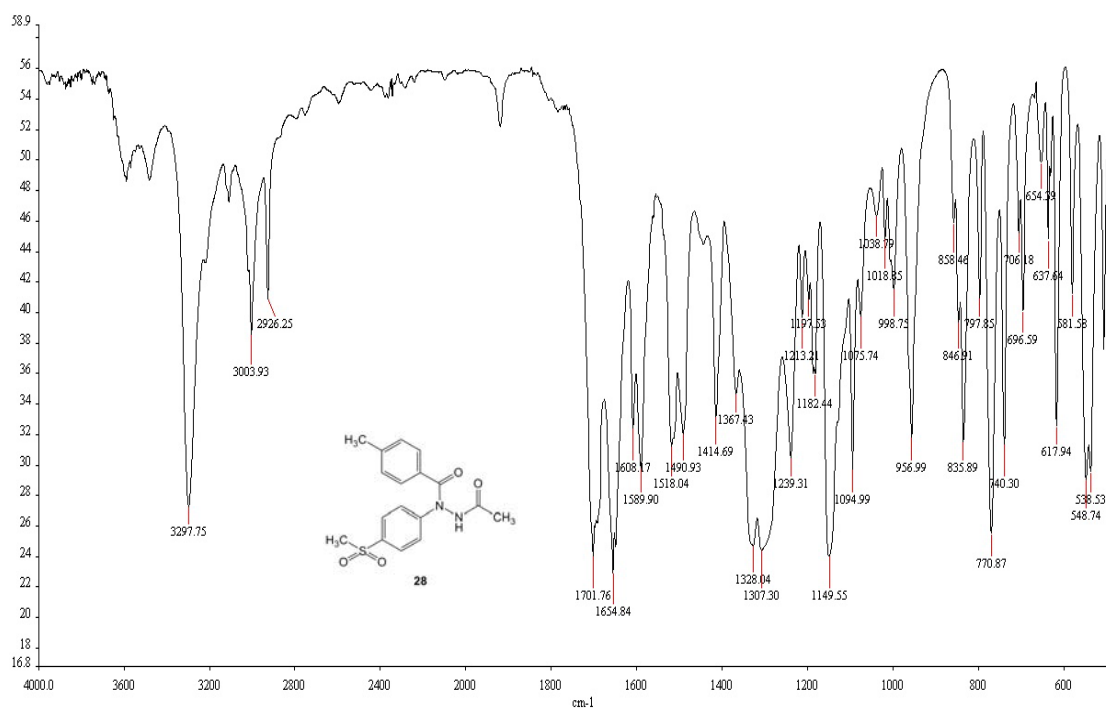


Figure 78 IR spectrum (KBr) of *N'*-acetyl-4-methyl-*N*-(4-(methylsulfonyl)phenyl)benzohydrazide (**28**)

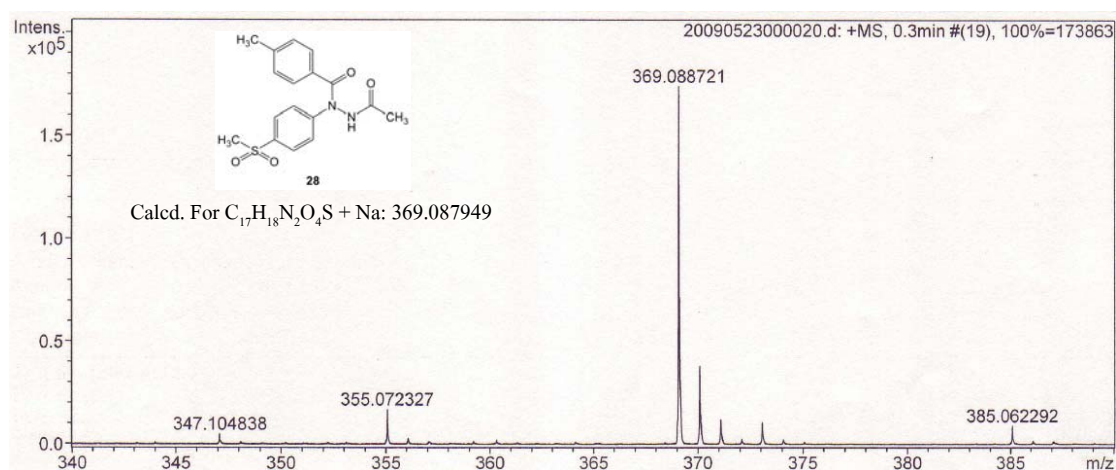


Figure 81 The mass (HR-MS; ESI) spectrum of *N'*-acetyl-4-methyl-*N*-(4-(methylsulfonyl)phenyl)benzohydrazide (**28**)

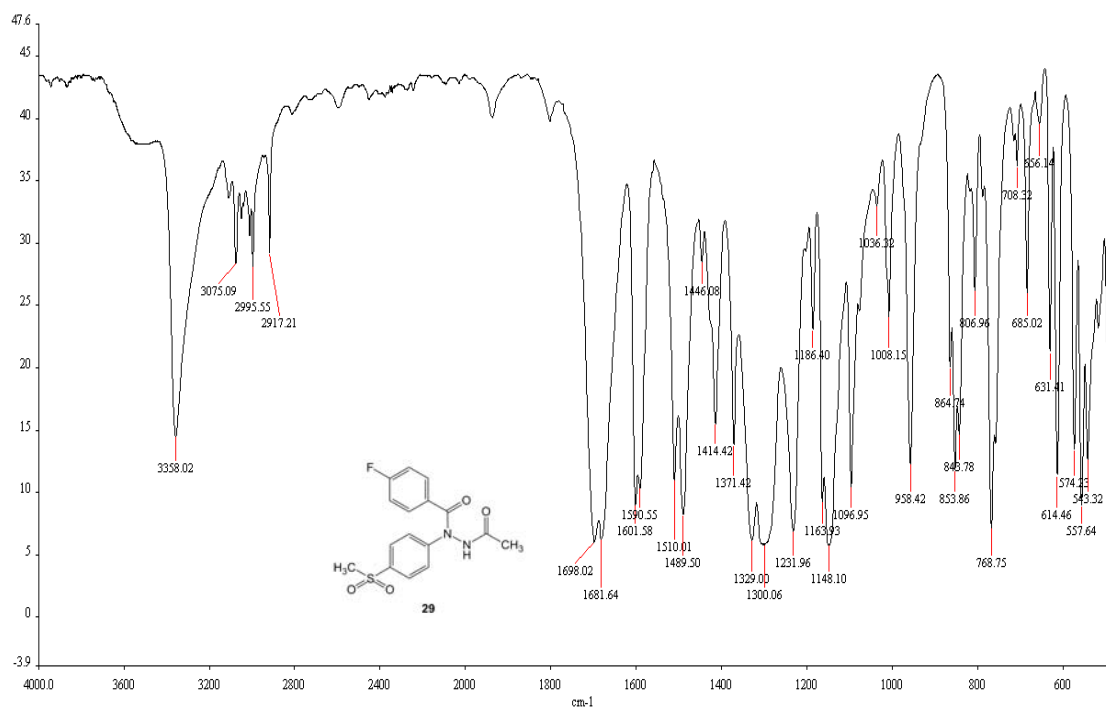


Figure 82 IR spectrum (KBr) of *N'*-acetyl-4-fluoro-*N*-(4-(methylsulfonyl)phenyl)benzohydrazide (**29**)

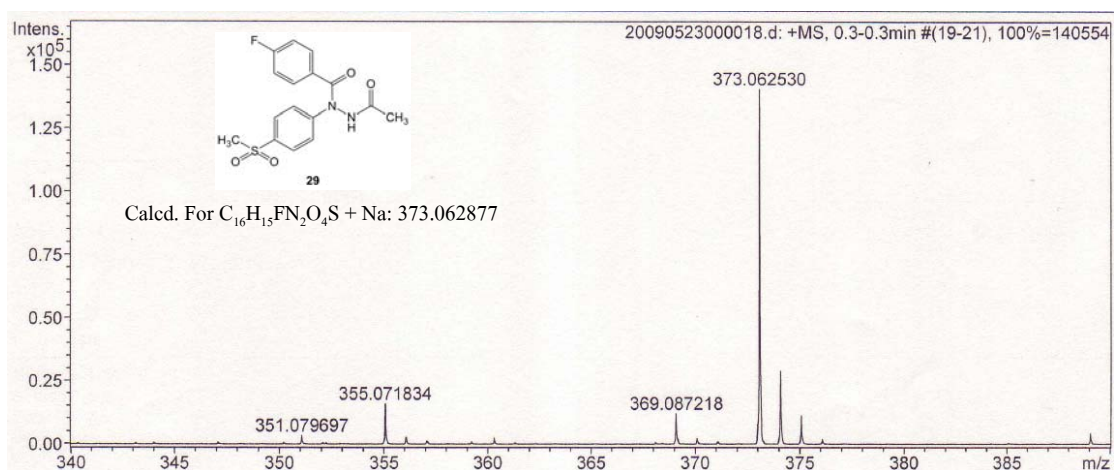


Figure 85 The mass (HR-MS; ESI) spectrum of *N'*-acetyl-4-fluoro-*N*-(4-(methylsulfonyl)phenyl)benzohydrazide (**29**)

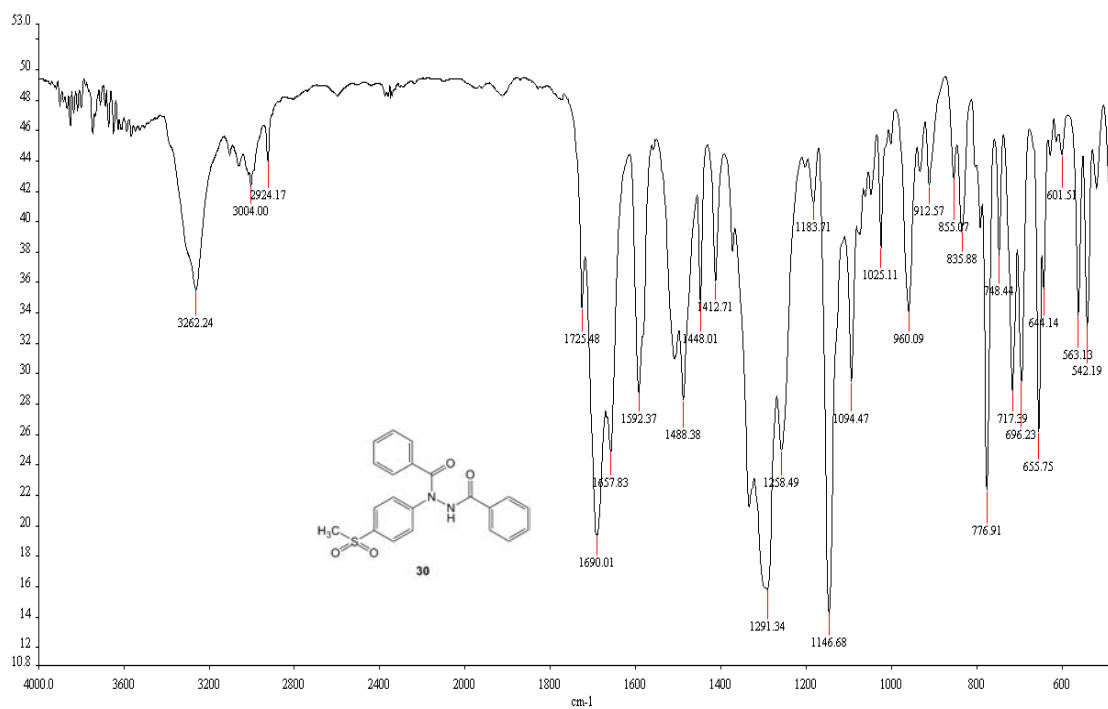


Figure 86 IR spectrum (KBr) of *N'*-benzoyl-*N*-(4-(methylsulfonyl)phenyl)benzohydrazide (**30**)

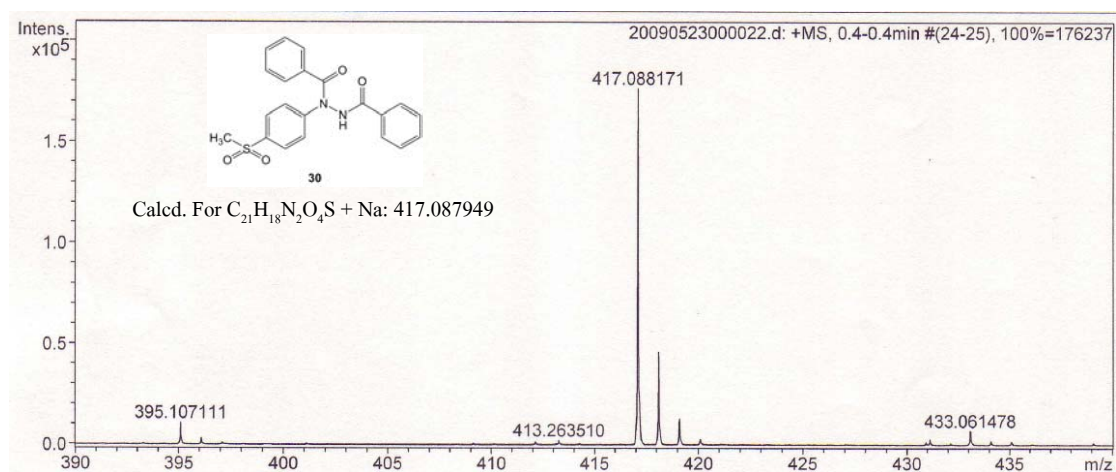


Figure 89 The mass (HR-MS; ESI) spectrum of *N'*-benzoyl-*N*-(4-(methylsulfonyl)phenyl)benzohydrazide (**30**)

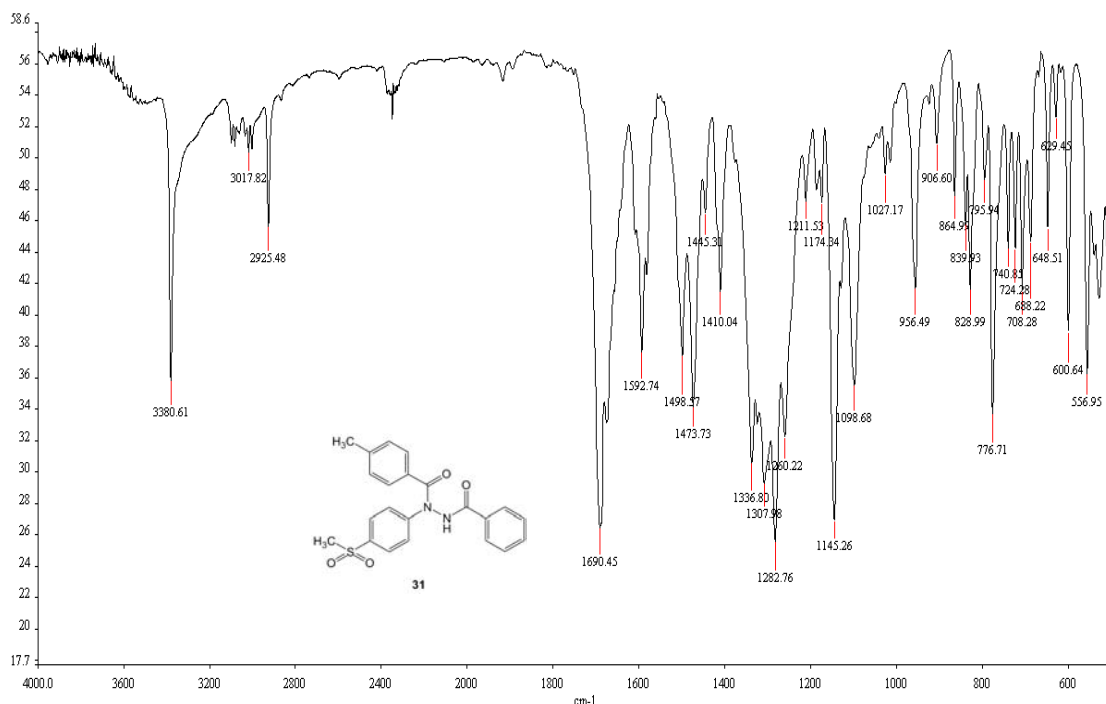


Figure 90 IR spectrum (KBr) of *N'*-benzoyl-4-methyl-*N*-(4-(methylsulfonyl)phenyl)benzohydrazide (**31**)

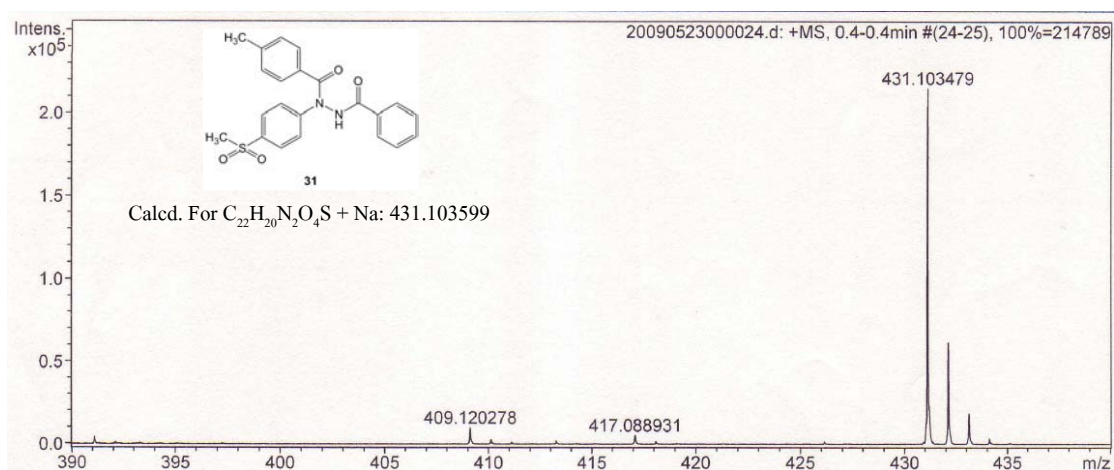


Figure 93 The mass (HR-MS; ESI) spectrum of *N'*-benzoyl-4-methyl-*N*-(4-(methylsulfonyl)phenyl)benzohydrazide (**31**)

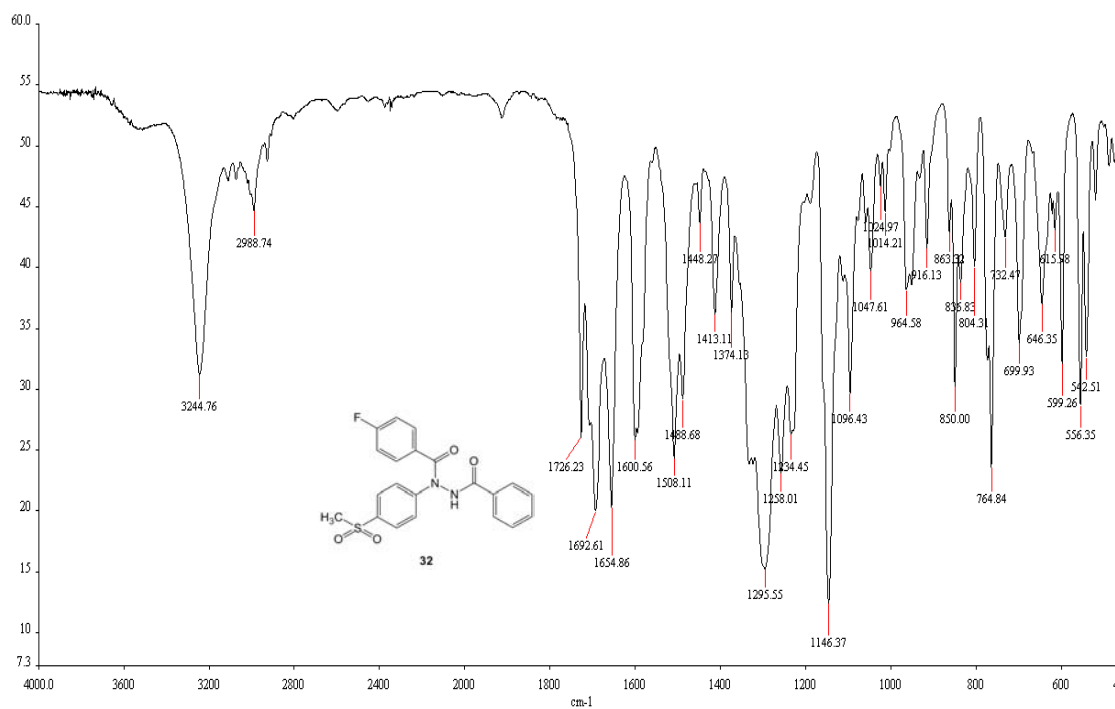


Figure 94 IR spectrum (KBr) of *N'*-benzoyl-4-fluoro-*N*-(4-(methylsulfonyl)phenyl)benzohydrazide (**32**)

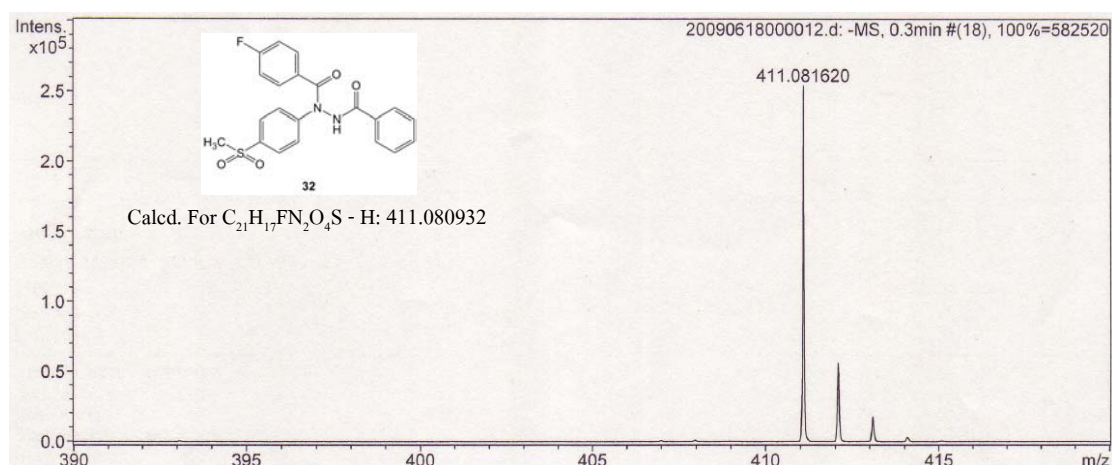
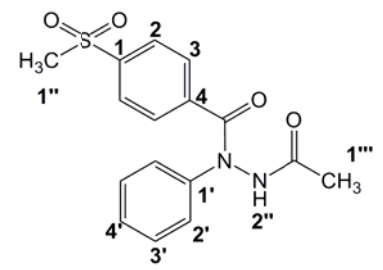


Figure 97 The mass (HR-MS; ESI) spectrum of *N'*-benzoyl-4-fluoro-*N*-(4-(methylsulfonyl)phenyl)benzohydrazide (**32**)



No.	ppm	Assignment
2	7.72	(d, $J = 8.3$ Hz, 2H)
3	7.93	(d, $J = 8.3$ Hz, 2H)
2'	7.35	(d, $J = 8.3$ Hz, 2H)
3'	7.38	(d, $J = 7.3$ Hz, 2H)
4'	7.24	(d, $J = 6.6$ Hz, 1H)
1''	3.19	(s, 3H)
1'''	1.74	(s, 3H)
2''	10.7	(br, s, 1H)

Note: 2.49 (DMSO), 3.06 (H₂O)

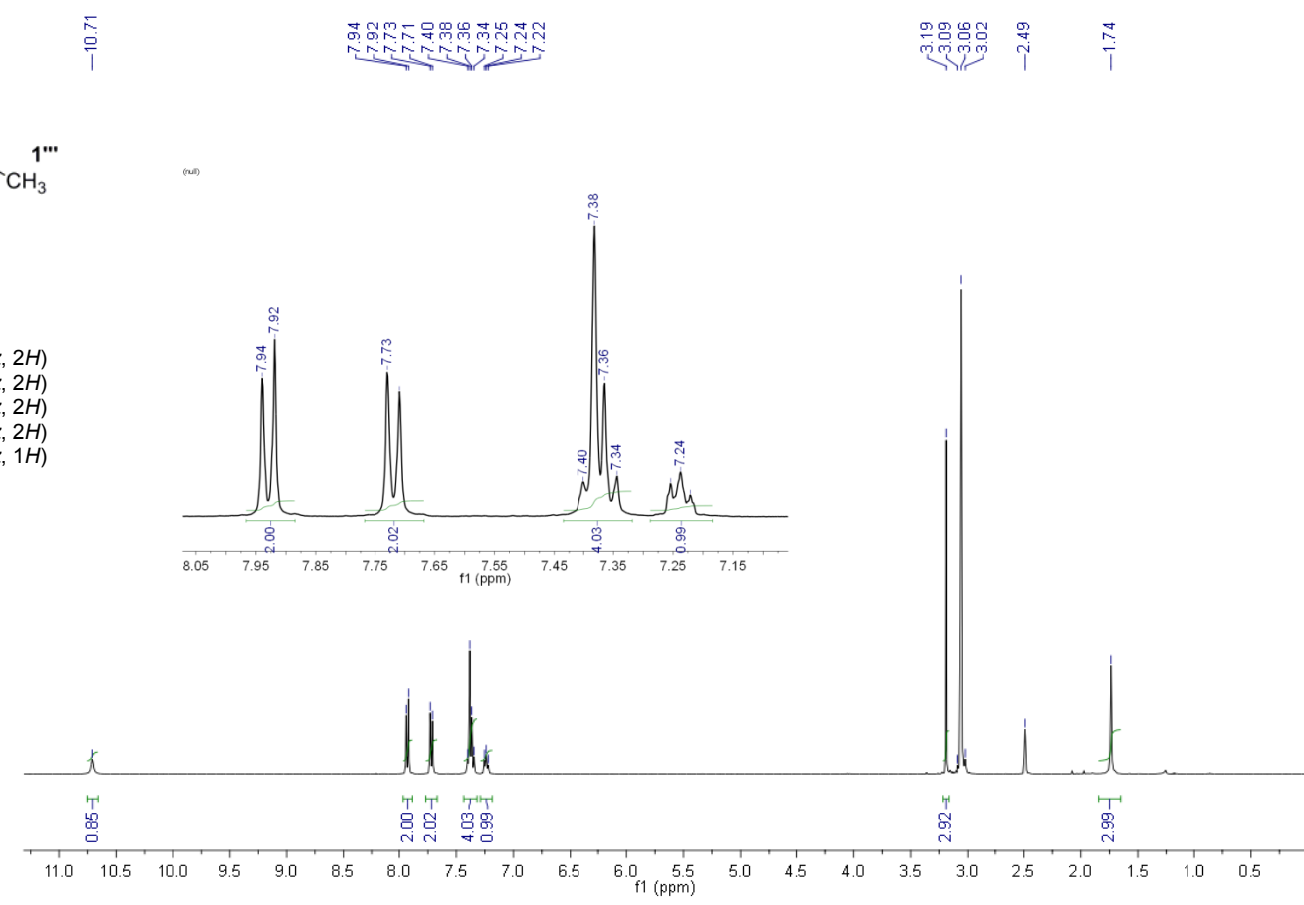


Figure 41 ¹H-NMR (400MHz, DMSO-*d*₆, 90 °C) spectrum of *N'*-acetyl-4-(methylsulfonyl)-*N*-phenylbenzohydrazide (16)

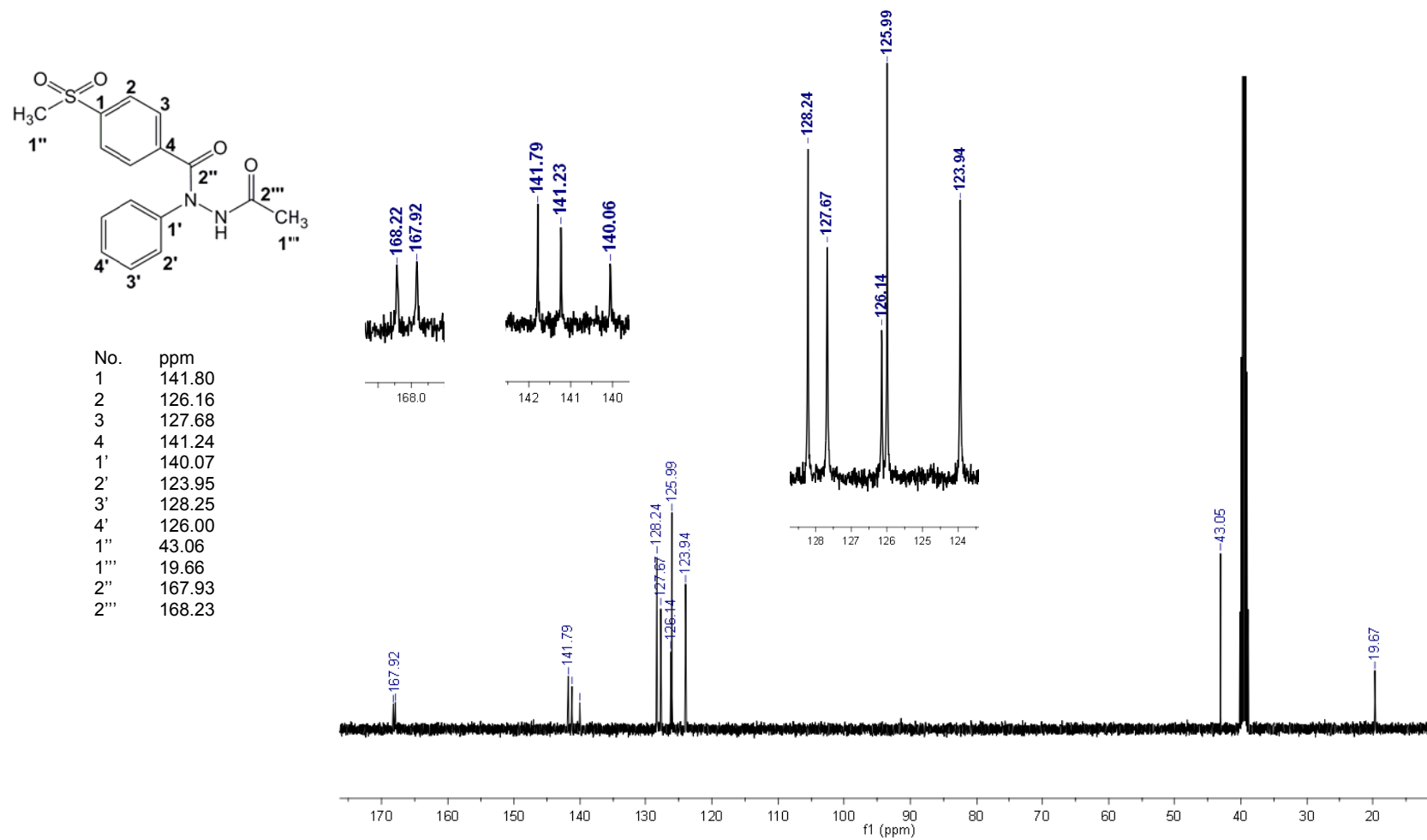
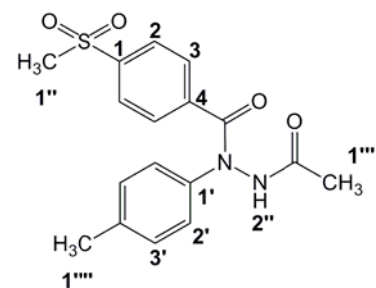


Figure 42 ^{13}C -NMR (400MHz, $\text{DMSO-}d_6$, 90 °C) spectrum of *N*-acetyl-4-(methylsulfonyl)-*N*-phenylbenzohydrazide (**16**)



No.	ppm	Multiplicity
2	7.63	(d, J = 7.8 Hz, 2H)
3	7.80	(d, J = 8.3 Hz, 2H)
2'	7.04	(d, J = 7.8 Hz, 2H)
3'	7.09	(d, J = 8.3 Hz, 2H)
1''	2.98	(s, 3H)
1'''	2.02	(s, 3H)
1''''	2.28	(s, 3H)
2''	9.91	(br, s, 1H)

Note: 7.24 (CDCl₃), 1.53 (H₂O)

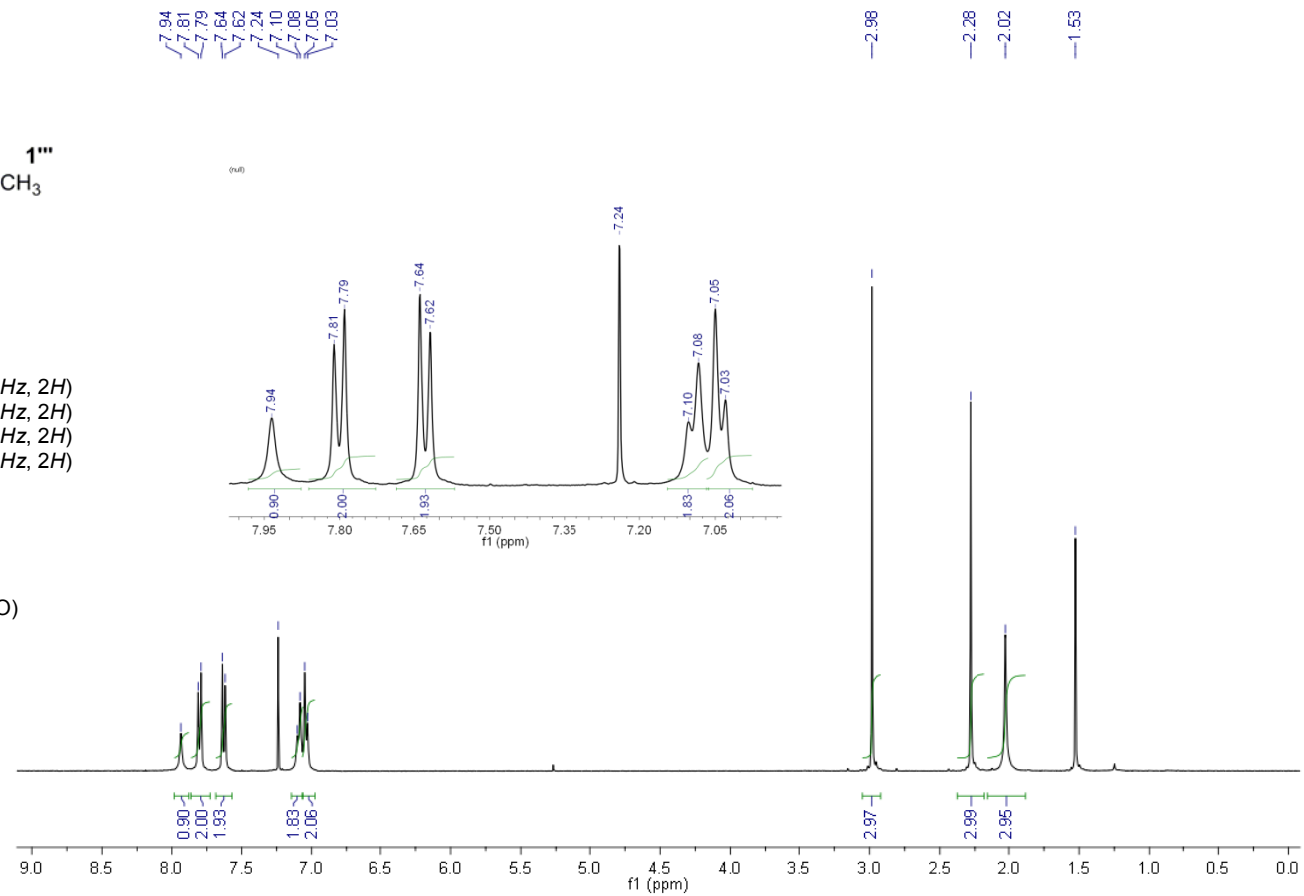
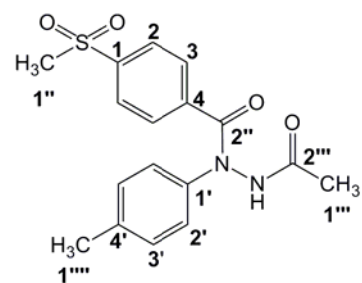


Figure 45

¹H-NMR (400MHz, CDCl₃, 52 °C) spectrum of *N'*-acetyl-4-(methylsulfonyl)-*N*-*p*-tolylbenzohydrazide (17)



No.	ppm
1	142.20
2	127.13
3	129.41
4	139.96
1'	139.39
2'	126.17
3'	129.97
4'	138.18
1''	44.31
1'''	20.79
2''	168.30
2'''	169.42
1''''	21.00

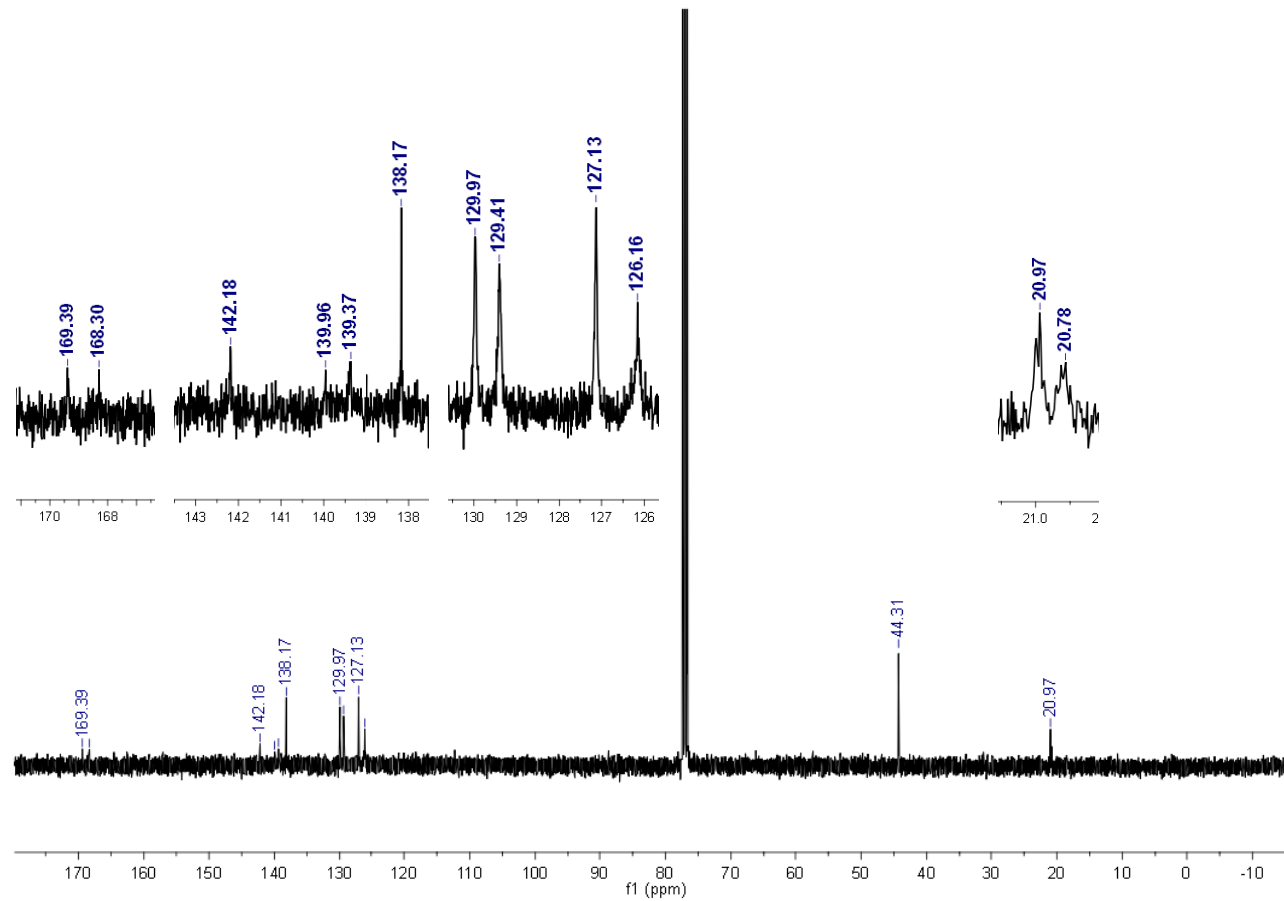


Figure 46

¹³C-NMR (400MHz, CDCl₃, 52 °C) spectrum of *N'*-acetyl-4-(methylsulfonyl)-*N-p*-tolylbenzohydrazide (**17**)

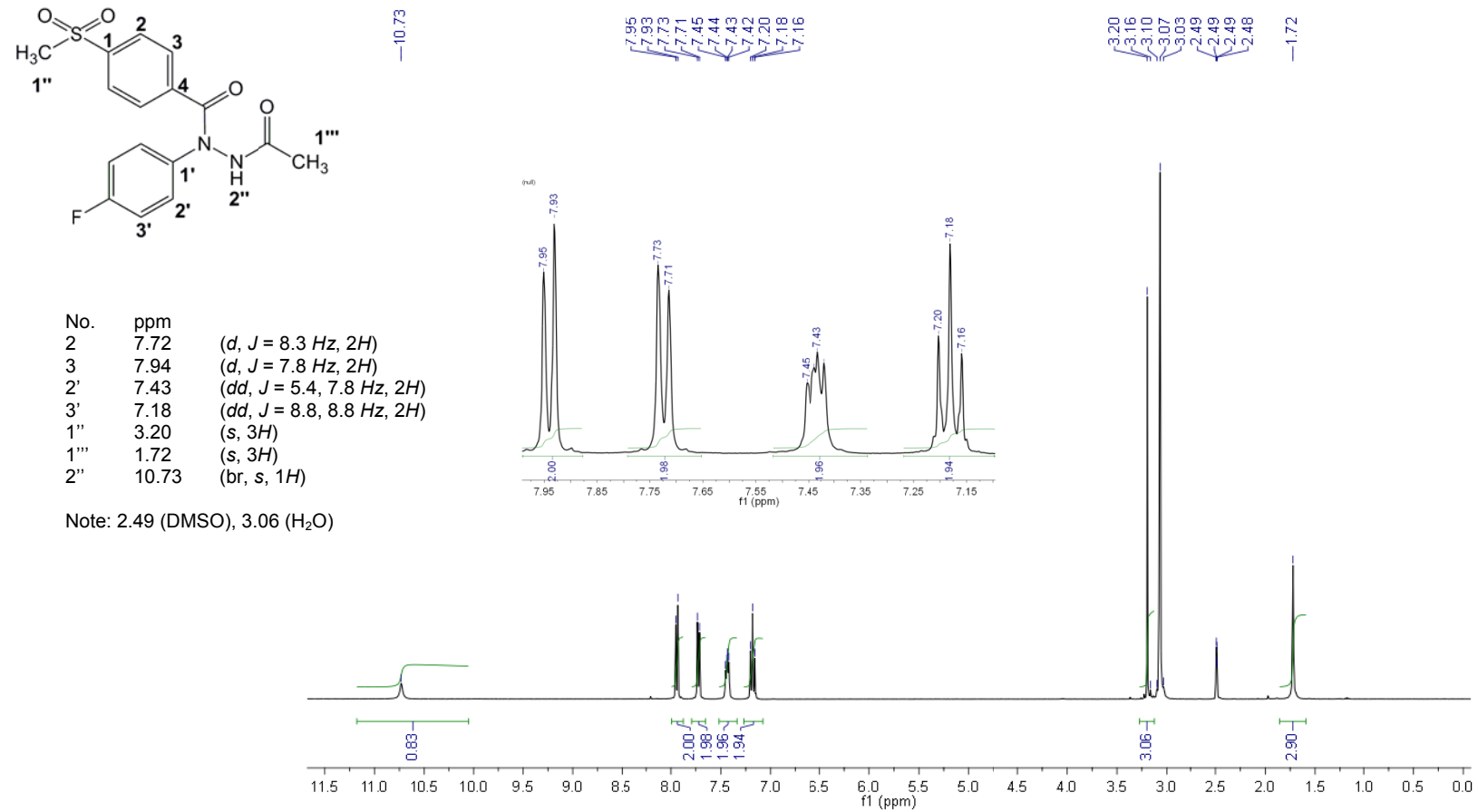
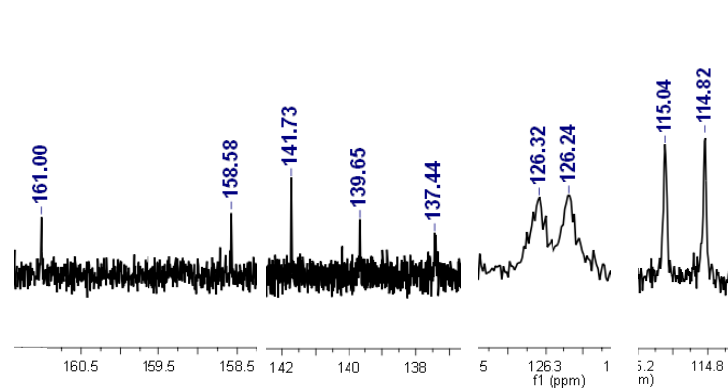
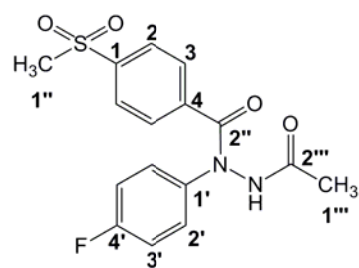


Figure 49

¹H-NMR (400MHz, DMSO-*d*₆, 90 °C) spectrum of *N'*-acetyl-*N*-(4-fluorophenyl)-4-(methylsulfonyl)benzohydrazide (**18**)



No.	ppm
1	141.74
2	125.94
3	127.57
4	139.66
1'	137.44
2'	126.28 (<i>d</i> , $J_{F-C-C} = 8.3$ Hz)
3'	114.93 (<i>d</i> , $J_{F-C-C} = 23.2$ Hz)
4'	159.80 (<i>d</i> , $J_{F-C} = 247.9$ Hz)
1''	43.05
1'''	19.70
2''	167.89
2'''	167.89

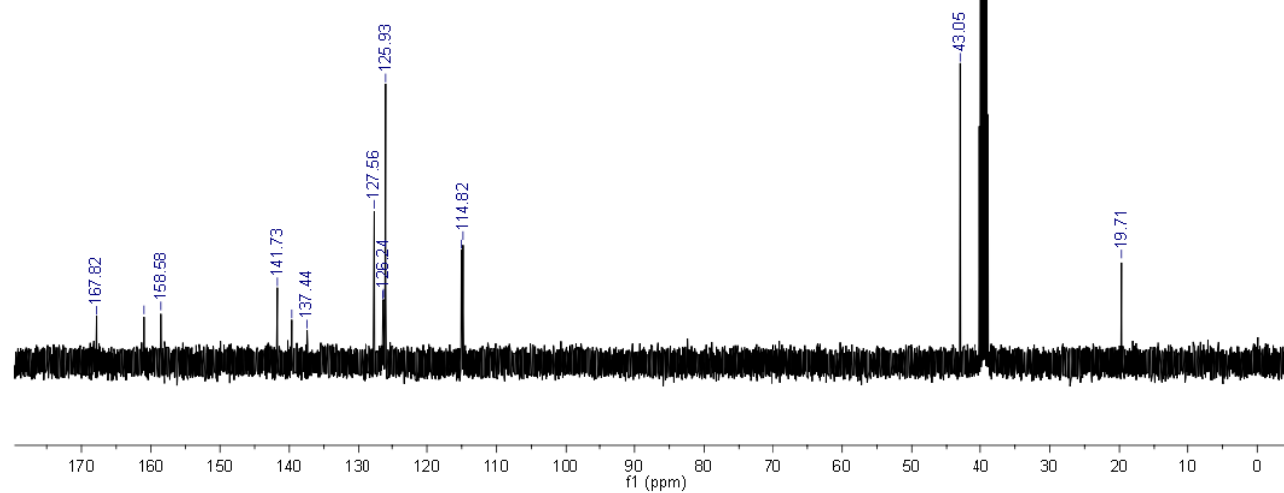
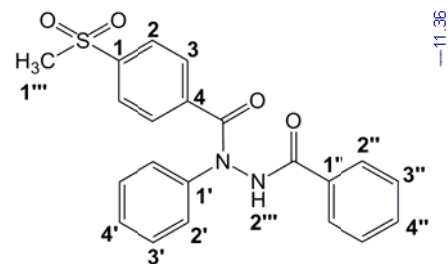


Figure 50

¹³C-NMR (400MHz, DMSO-*d*₆, 90 °C) spectrum of *N*-acetyl-*N*-(4-fluorophenyl)-4-(methylsulfonyl)benzohydrazide (**18**)



No.	ppm	
2	7.80	(d, $J = 8.3$ Hz, 2H)
3	7.92	(d, $J = 8.3$ Hz, 2H)
2'	7.49	(d, $J = 7.8$ Hz, 2H)
3'	7.40	(t, $J = 7.8$ Hz, 2H)
4'	7.26	(t, $J = 7.3$ Hz, 1H)
2''	7.65	(d, $J = 7.8$ Hz, 2H)
3''	7.43	(t, $J = 7.8$ Hz, 2H)
4''	7.54	(t, $J = 7.3$ Hz, 1H)
1'''	3.14	(s, 3H)
2'''	11.39	(br, s, 1H)

Note: 2.49 (DMSO), 3.06 (H₂O)

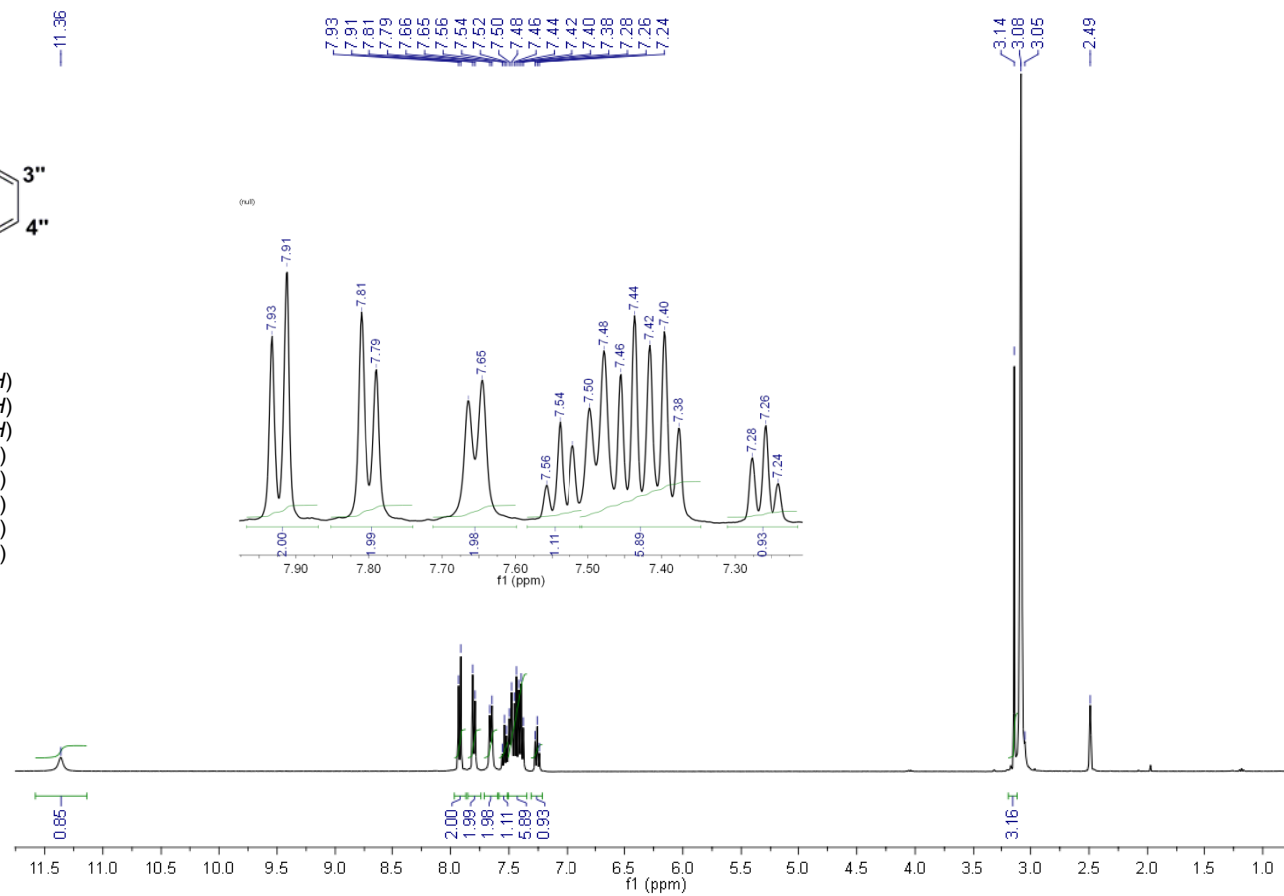


Figure 53

¹H-NMR (400MHz, DMSO-*d*₆, 90 °C) spectrum of *N*-benzoyl-4-(methylsulfonyl)-*N*-phenylbenzohydrazide (**19**)

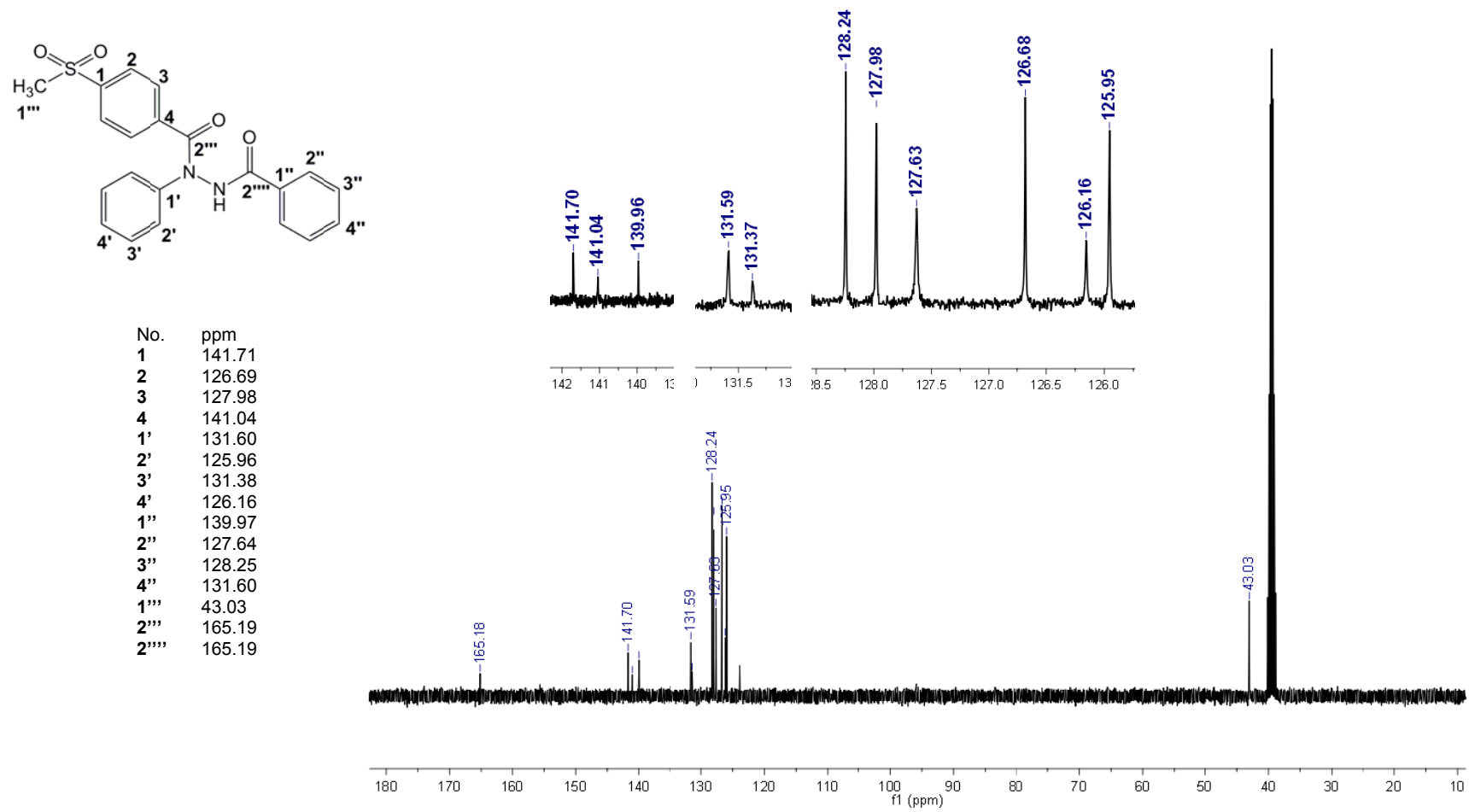
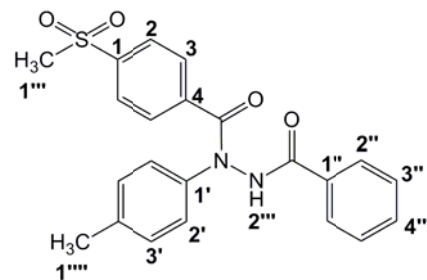


Figure 54

¹³C-NMR (400MHz, DMSO-*d*₆, 90 °C) spectrum of *N*-benzoyl-4-(methylsulfonyl)-*N*-phenylbenzohydrazide (19)



No.	ppm	
2	7.76	(d, J = 7.3 Hz, 2H)
3	7.80	(d, J = 8.8 Hz, 2H)
2'	7.06	(d, J = 8.3 Hz, 2H)
3'	7.19	(d, J = 8.3 Hz, 2H)
2''	7.69	(d, J = 8.3 Hz, 2H)
3''	7.40	(t, J = 7.8 Hz, 2H)
4''	7.52	(t, J = 7.3 Hz, 1H)
1'''	2.97	(s, 3H)
1''''	2.29	(s, 3H)
2'''	8.62	(s, 1H)

Note: 7.24 (CDCl₃), 1.51 (H₂O)

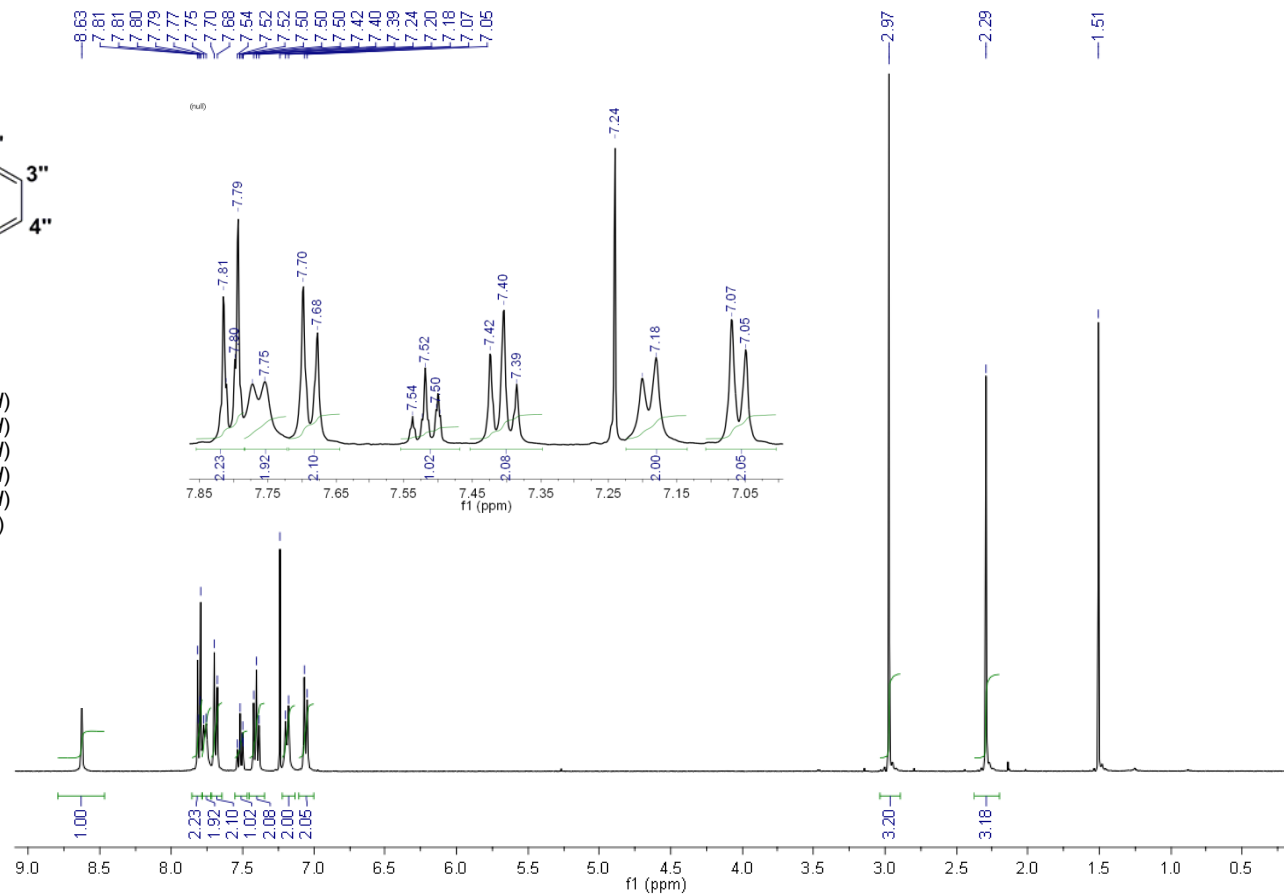


Figure 57

¹H-NMR (400MHz, CDCl₃, 50 °C) spectrum of *N'*-benzoyl-4-(methylsulfonyl)-*N-p*-tolylbenzohydrazide (**20**)

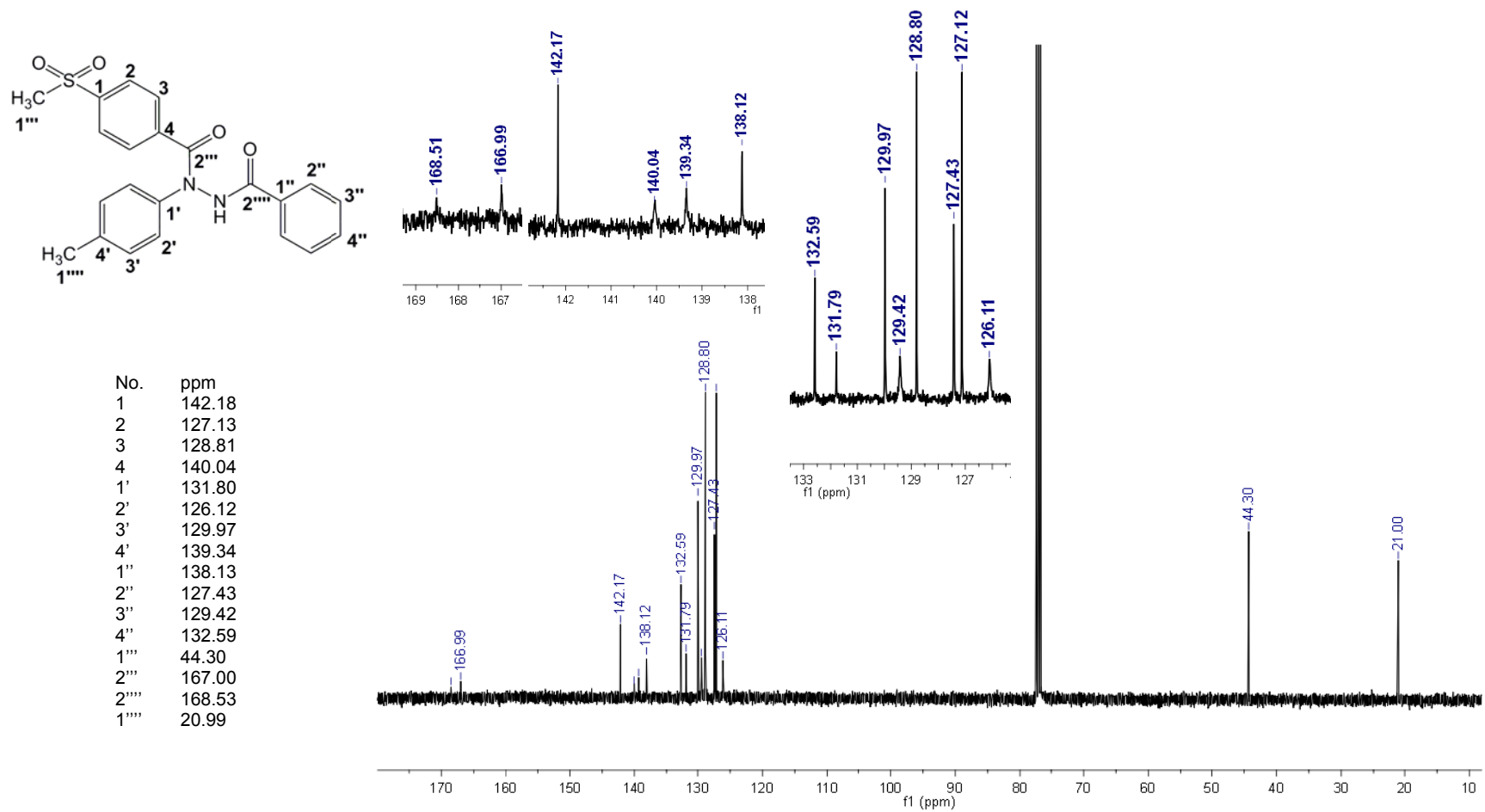
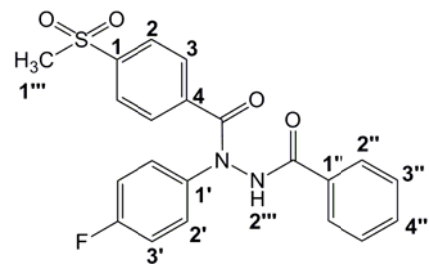


Figure 58

^{13}C -NMR (400MHz, CDCl_3 , 50 °C) spectrum of *N*-benzoyl-4-(methylsulfonyl)-*N*-*p*-tolylbenzohydrazide (**20**)



No.	ppm	Multiplicity and Coupling
2	7.73	(d, J = 7.3 Hz, 2H)
3	7.83	(d, J = 8.8 Hz, 2H)
2'	7.34	(dd, J = 4.6, 8.5 Hz, 2H)
3'	6.97	(dd, J = 8.5, 8.5 Hz, 2H)
2''	7.69	(d, J = 8.3 Hz, 2H)
3''	7.41	(t, J = 7.8 Hz, 2H)
4''	7.53	(t, J = 7.6 Hz, 1H)
1'''	2.98	(s, 3H)
2'''	8.63	(s, 1H)

Note: 7.24 (CDCl₃), 1.50 (H₂O)

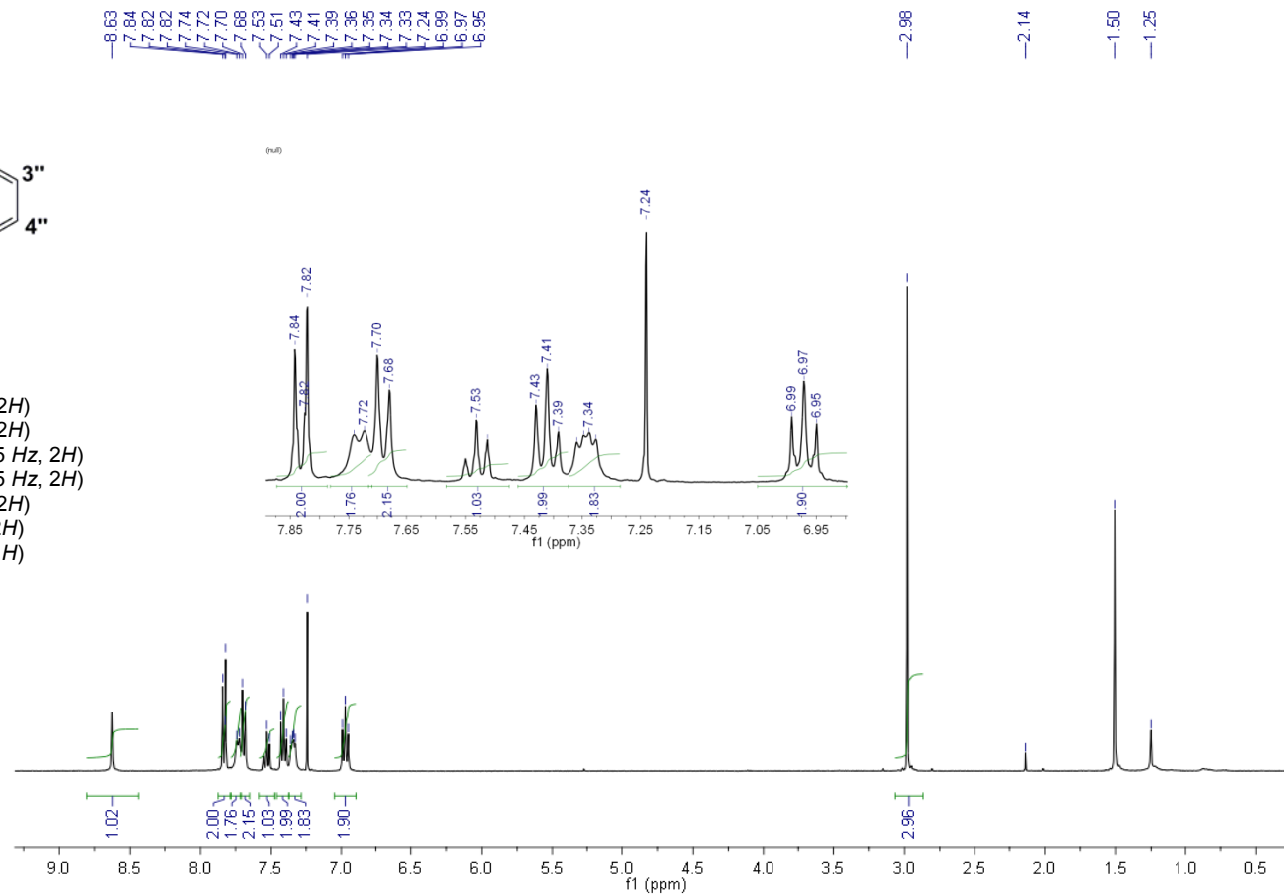


Figure 61

¹H-NMR (400MHz, CDCl₃, 50 °C) spectrum of *N'*-benzoyl-*N*-(4-fluorophenyl)-4-(methylsulfonyl)benzohydrazide (**21**)

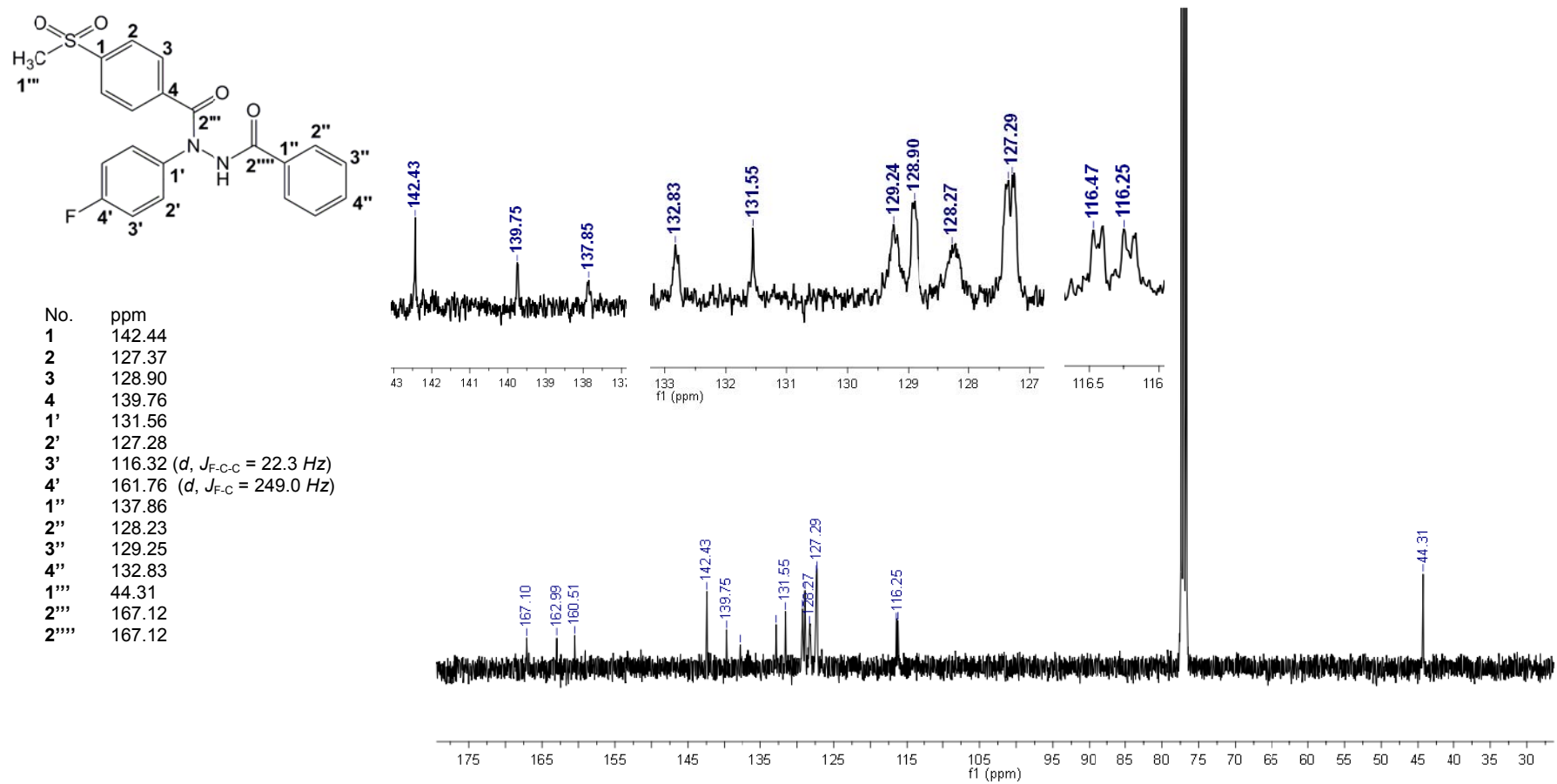
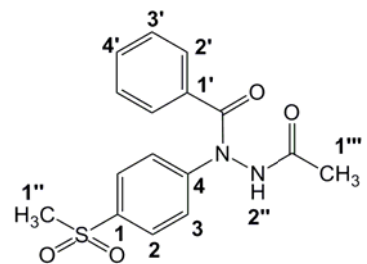


Figure 62

^{13}C -NMR (400MHz, CDCl_3 , 50 °C) spectrum of *N*-benzoyl-*N*-(4-fluorophenyl)-4-(methylsulfonyl)benzohydrazide (21)



No.	ppm	
2	7.69	(d, $J = 8.8$ Hz, 2H)
3	7.36	(d, $J = 8.8$ Hz, 2H)
2'	7.51	(d, $J = 7.3$ Hz, 2H)
3'	7.32	(t, $J = 7.6$ Hz, 2H)
4'	7.42	(t, $J = 7.6$ Hz, 1H)
1''	3.00	(s, 3H)
1'''	1.92	(s, 3H)
2''	8.59	(s, 1H)

Note: 7.24 (CDCl₃), 1.62 (H₂O)

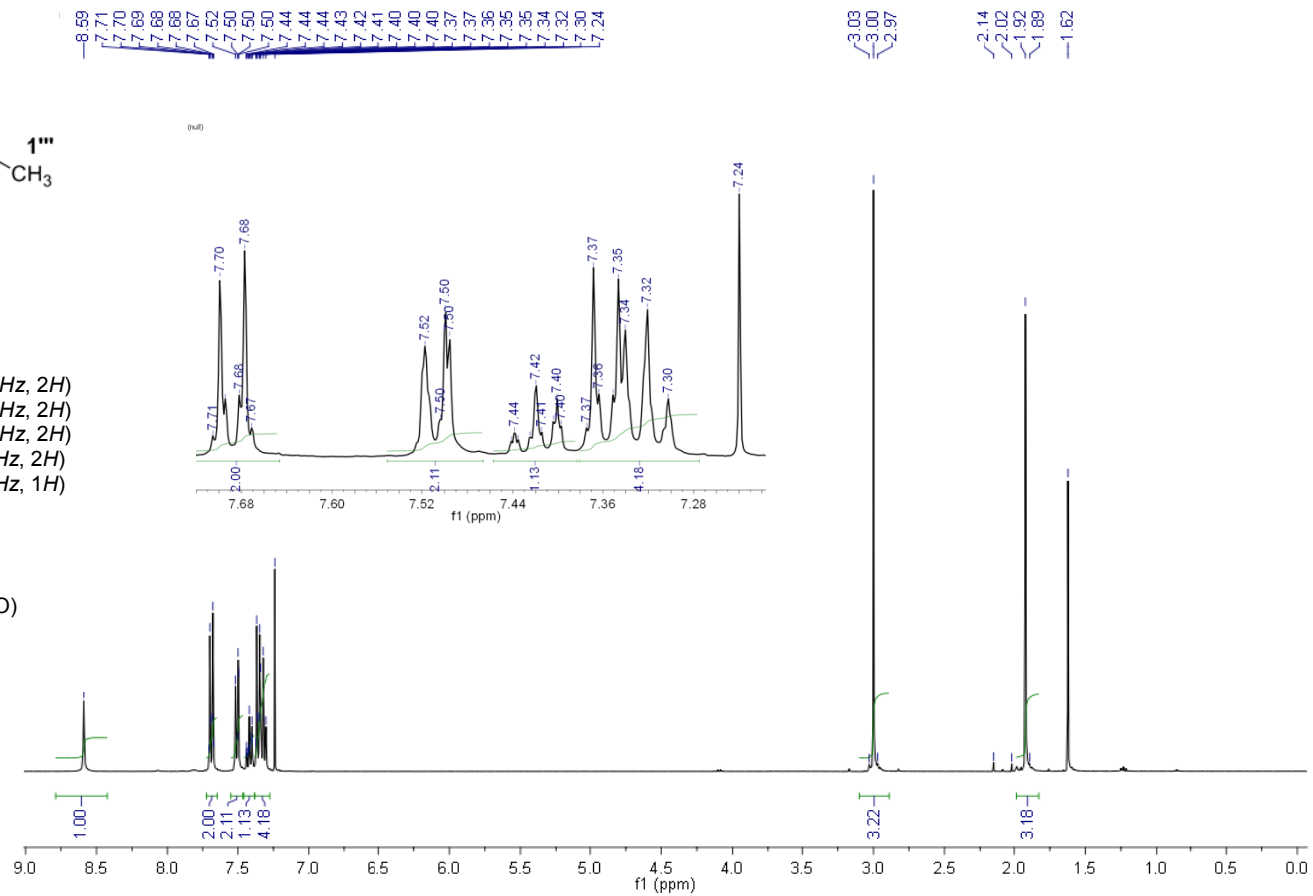
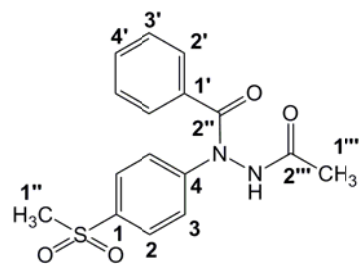


Figure 75

¹H-NMR (400MHz, CDCl₃) spectrum of *N'*-acetyl-*N*-(4-(methylsulfonyl)phenyl)benzohydrazide (27)



No.	ppm
1	136.98
2	128.26
3	124.11
4	146.61
1'	133.77
2'	128.00
3'	131.23
4'	128.06
1''	44.60
1'''	20.67
2''	169.43
2'''	170.50

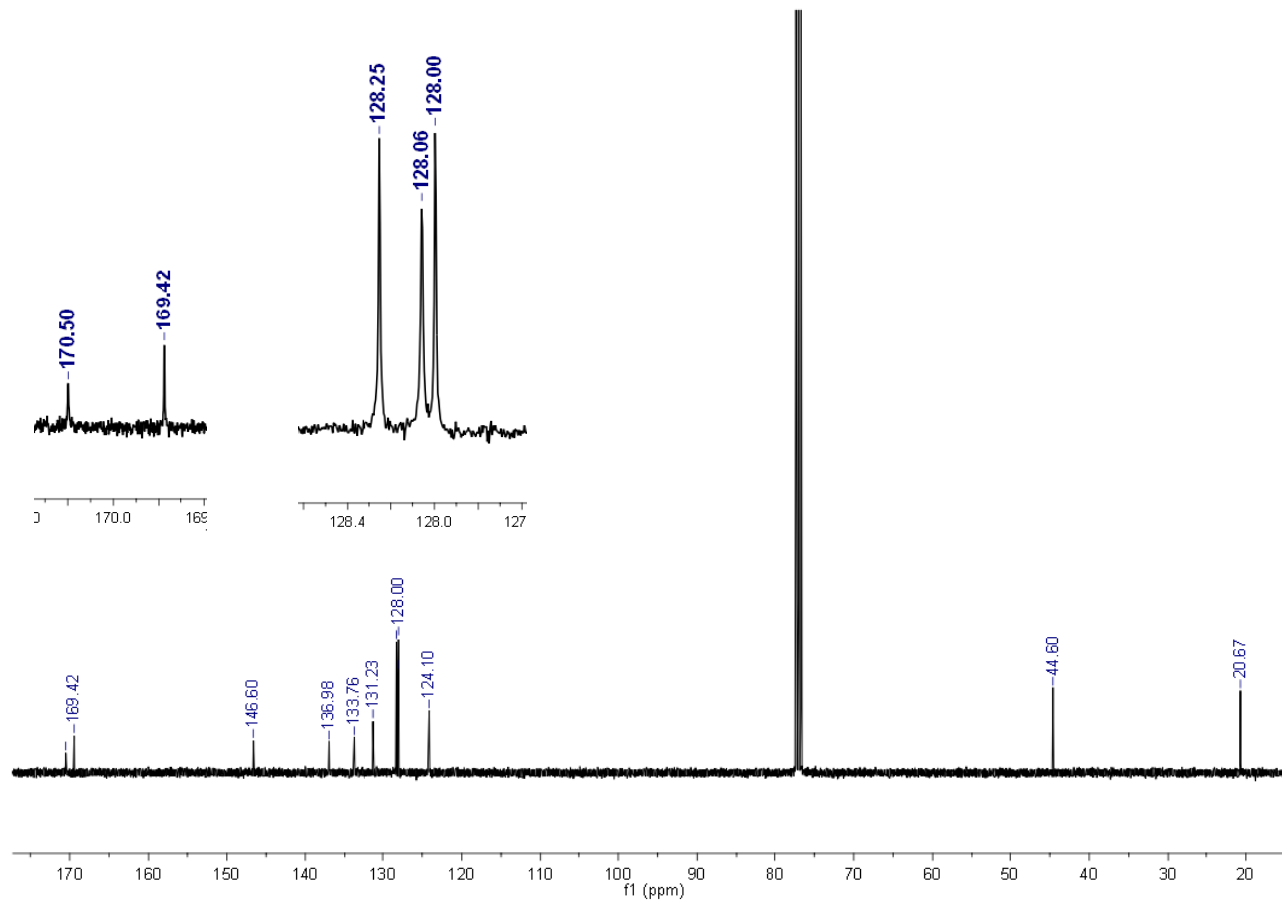
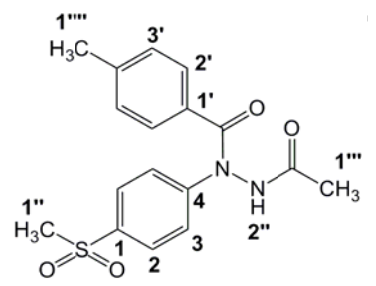


Figure 76

¹³C-NMR (400MHz, CDCl₃) spectrum of *N*-acetyl-*N*-(4-(methylsulfonyl)phenyl)benzohydrazide (27)



No.	ppm	Assignment
2	7.71	(d, $J = 8.8$ Hz, 2H)
3	7.33	(d, $J = 8.8$ Hz, 2H)
2'	7.39	(d, $J = 8.3$ Hz, 2H)
3'	7.10	(d, $J = 7.8$ Hz, 2H)
1''	3.00	(s, 3H)
1'''	1.61	(s, 3H)
1''''	2.33	(s, 3H)
2''	8.44	(s, 1H)

Note: 7.24 (CDCl₃), 1.61 (H₂O)

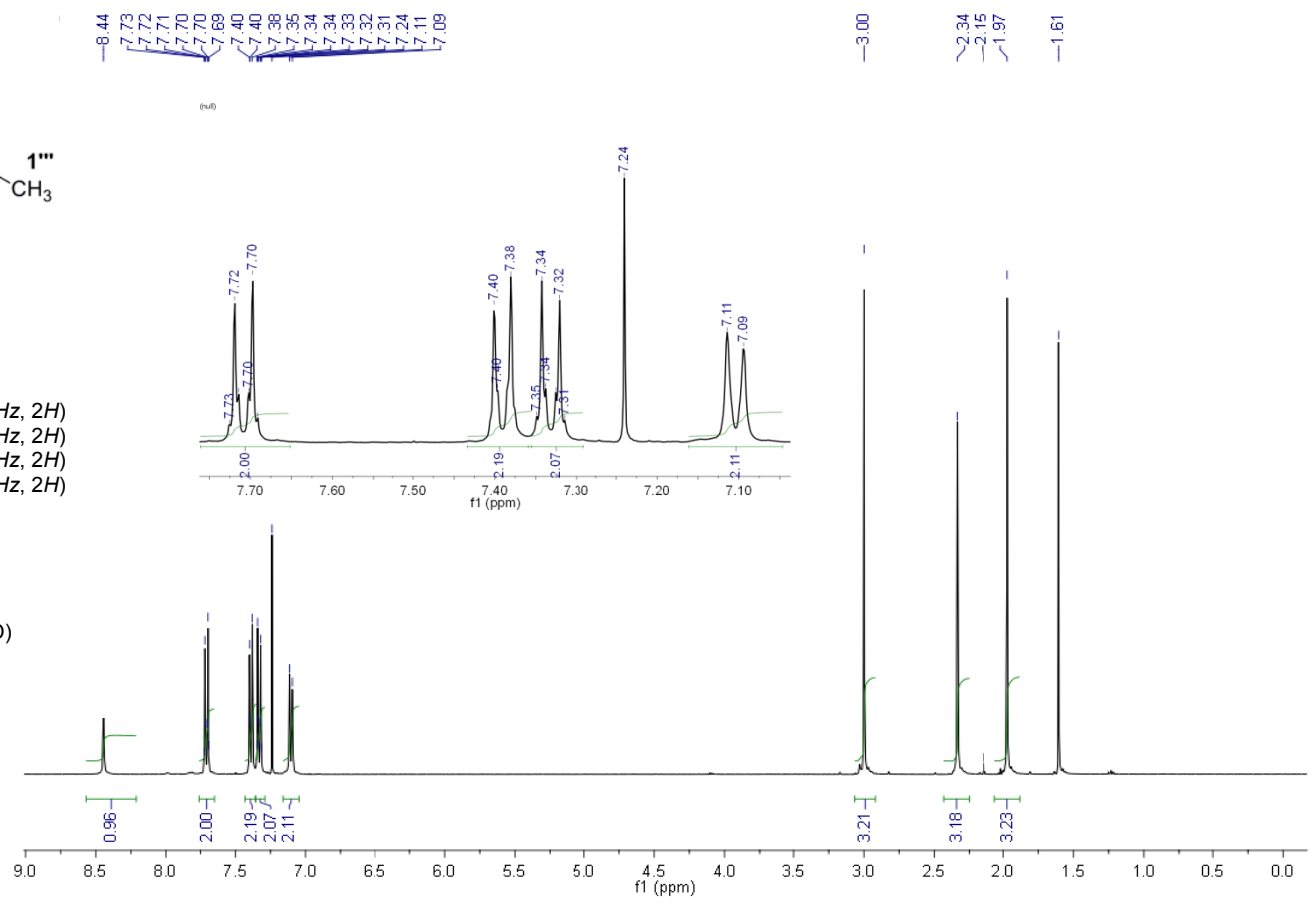


Figure 79

¹H-NMR (400MHz, CDCl₃) spectrum of *N'*-acetyl-4-methyl-*N*-(4-(methylsulfonyl)phenyl)benzohydrazide (28)

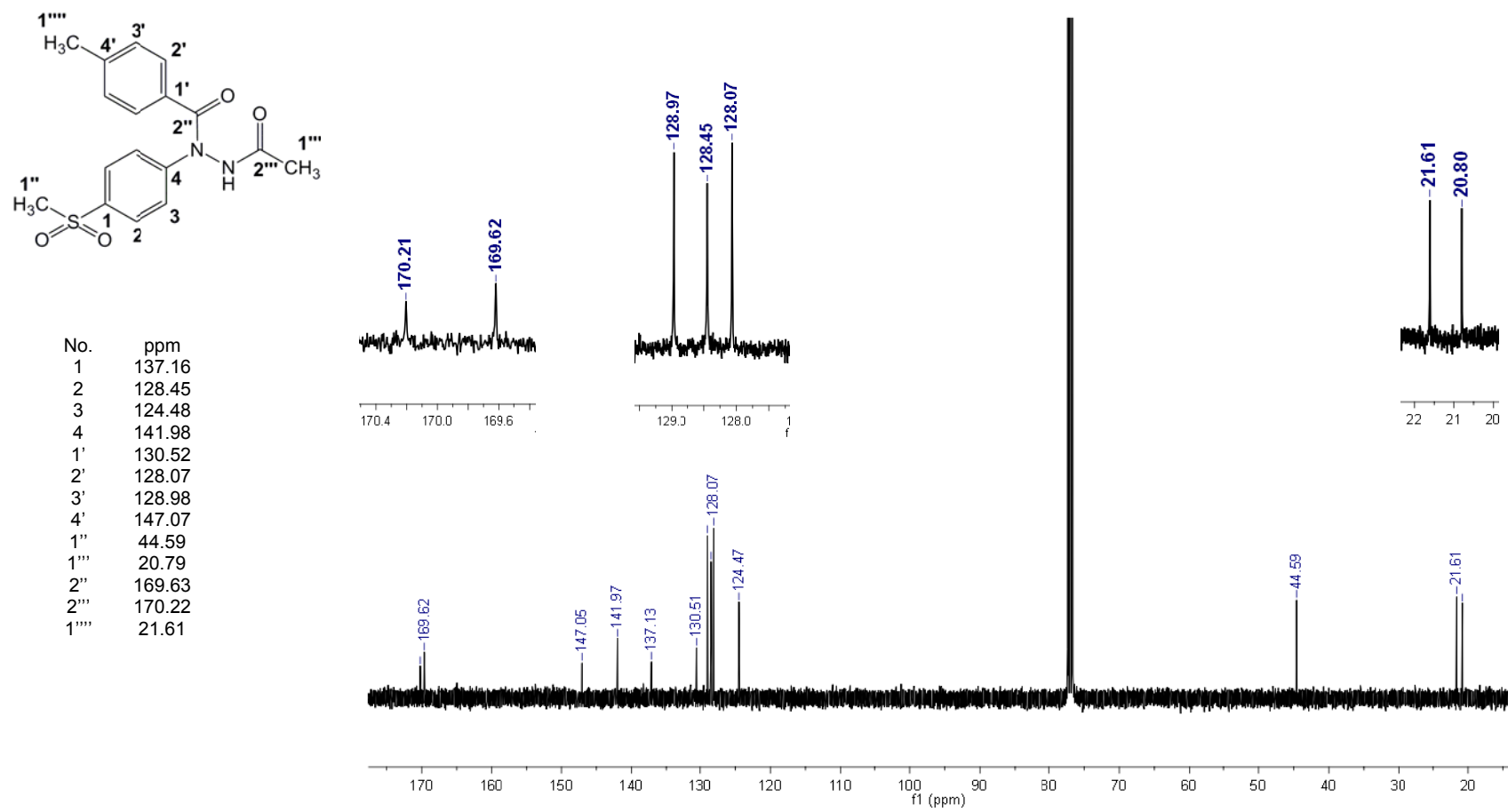


Figure 80

¹³C-NMR (400MHz, CDCl₃) spectrum of *N*-acetyl-4-methyl-*N*-(4-(methylsulfonyl)phenyl)benzohydrazide (28)

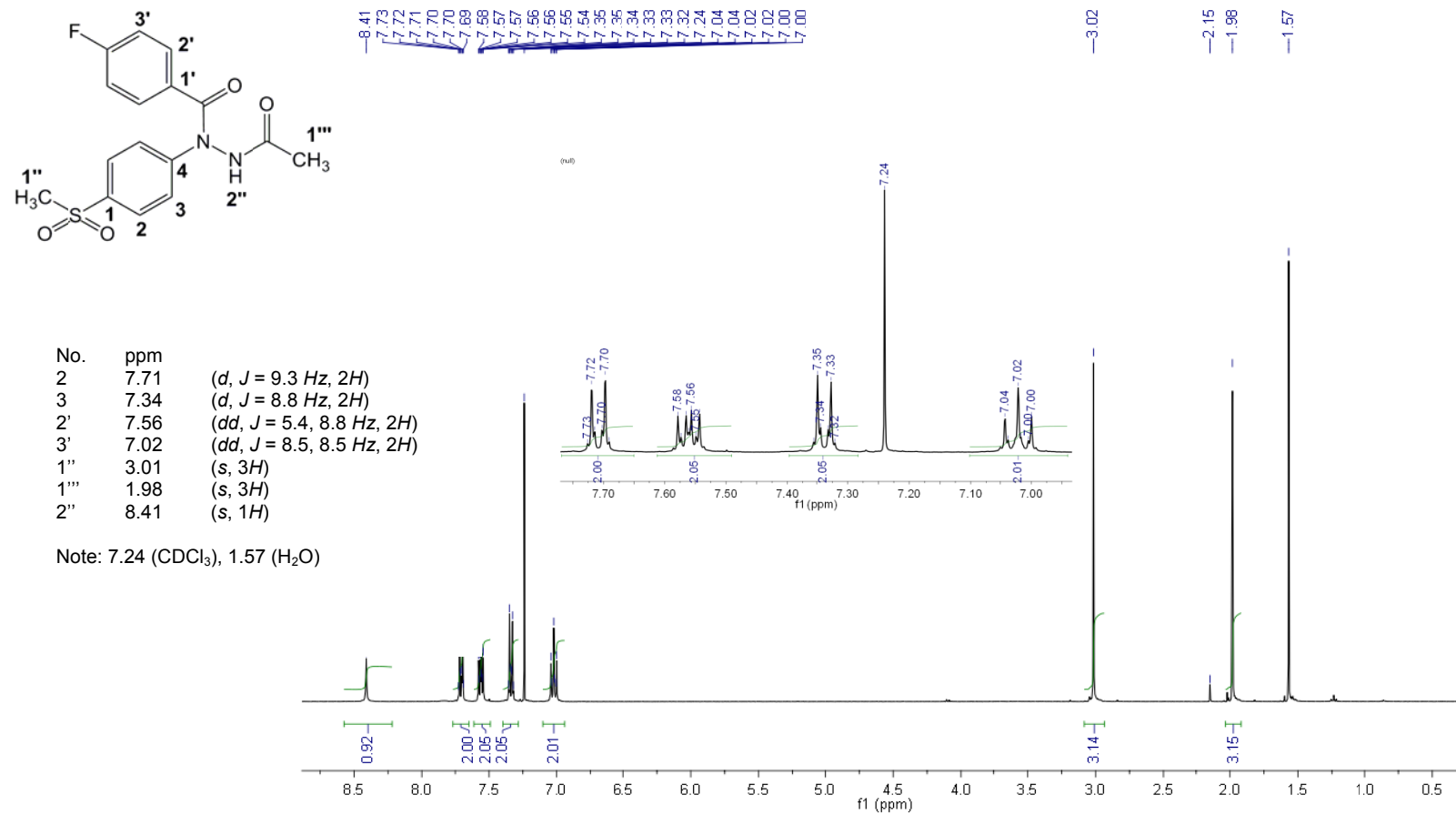
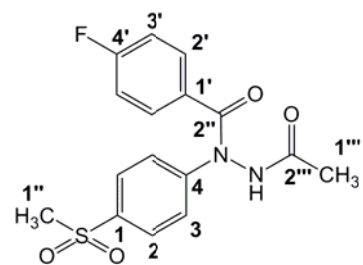


Figure 83

¹H-NMR (400MHz, CDCl₃) spectrum of *N'*-acetyl-4-fluoro-*N*-(4-(methylsulfonyl)phenyl)benzohydrazide (**29**)



No.	ppm
1	137.04
2	128.06
3	124.04
4	146.55
1'	130.72
2'	130.63
3'	115.52 (<i>d</i> , $J_{F-C-C} = 22.0$ Hz)
4'	164.19 (<i>d</i> , $J_{F-C} = 255.0$ Hz)
1''	44.61
1'''	20.69
2''	169.38
2'''	169.48

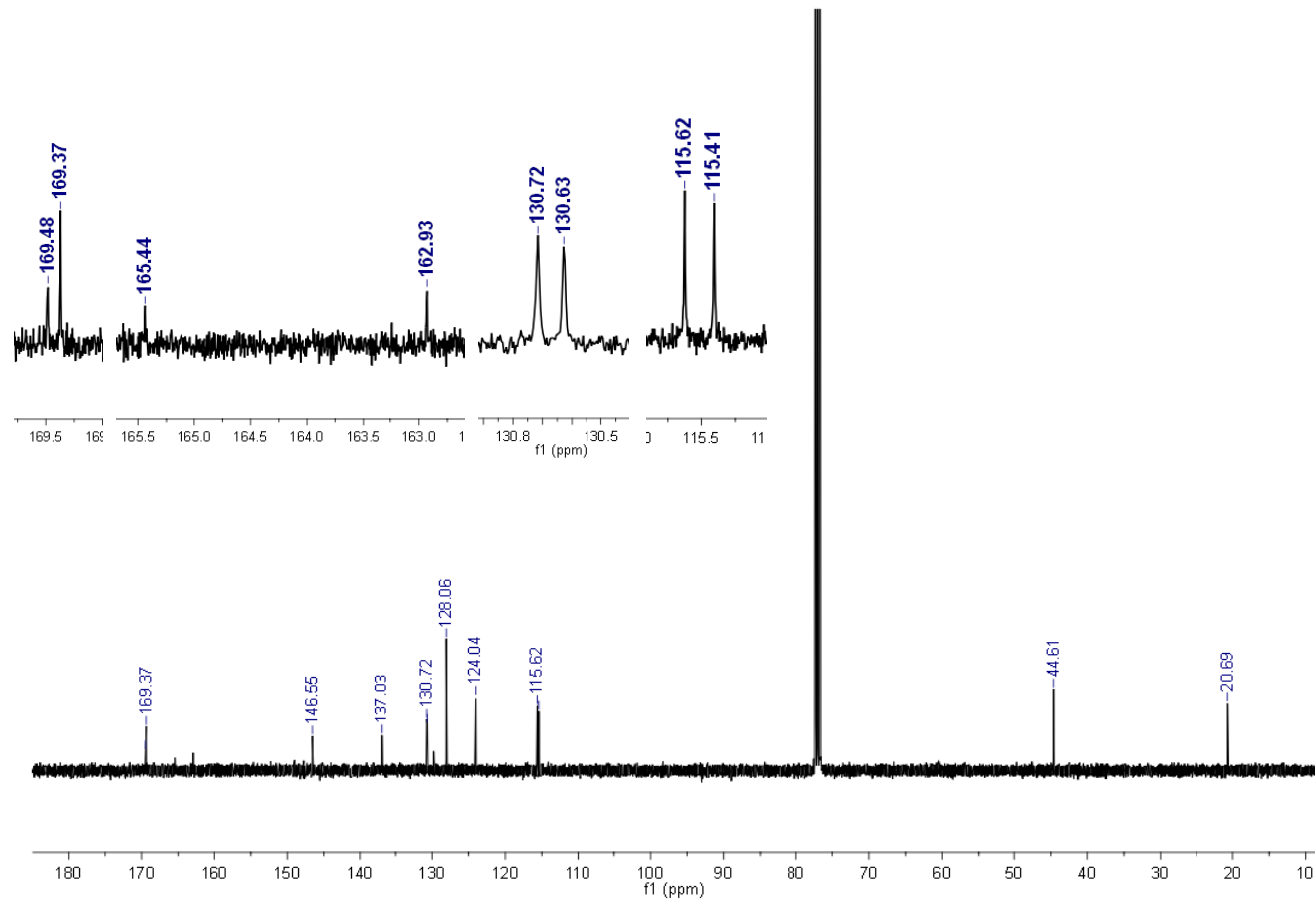
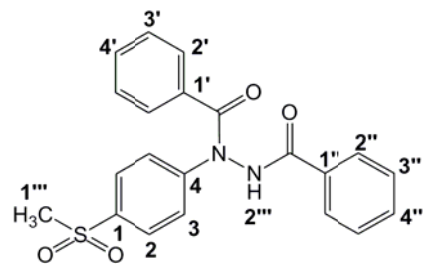


Figure 84

¹³C-NMR (400MHz, CDCl₃) spectrum of *N*-acetyl-4-fluoro-*N*-(4-(methylsulfonyl)phenyl)benzohydrazide (**29**)



No.	ppm	
2	7.71	(d, $J = 8.8$ Hz, 2H)
3	7.43	(d, $J = 8.8$ Hz, 2H)
2'	7.70	(d, $J = 8.3$ Hz, 2H)
3'	7.40	(t, $J = 7.8$ Hz, 2H)
4'	7.52	(t, $J = 7.3$ Hz, 1H)
2''	7.57	(d, $J = 6.8$ Hz, 2H)
3''	7.30	(t, $J = 7.6$ Hz, 2H)
4''	7.38	(m, 1H)
1'''	3.00	(s, 3H)
2'''	9.13	(s, 1H)

Note: 7.24 (CDCl₃), 1.57 (H₂O)

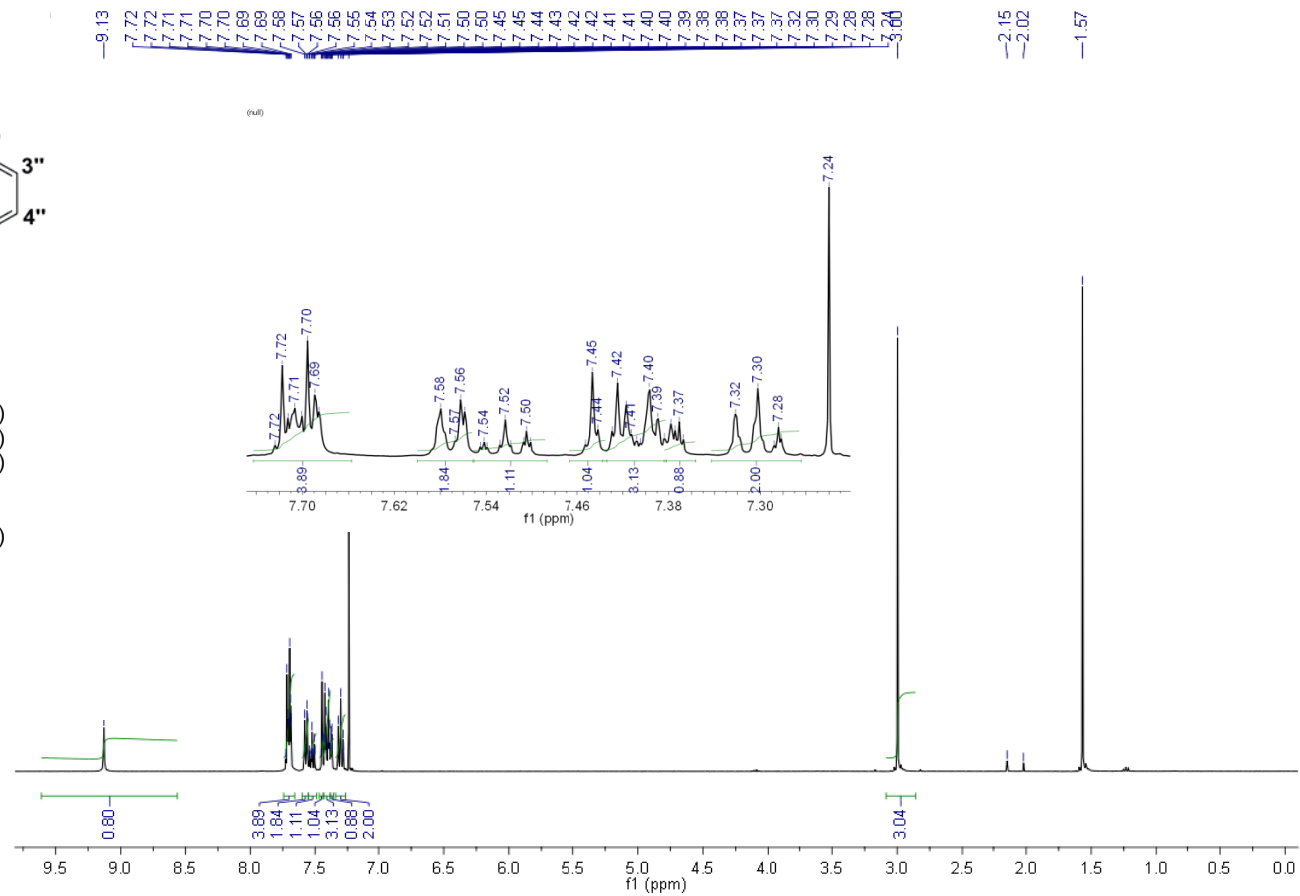
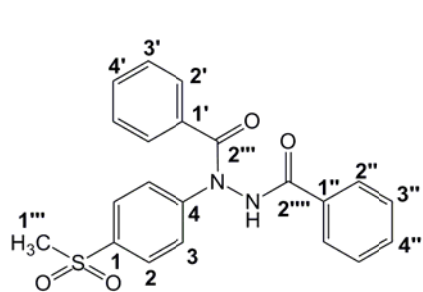


Figure 87

¹H-NMR (400MHz, CDCl₃) spectrum of *N'*-benzoyl-*N*-(4-(methylsulfonyl)phenyl)benzohydrazide (**30**)



No.	ppm
1	131.05
2	128.13
3	124.13
4	146.63
1'	137.02
2'	128.08
3'	128.28
4'	132.73
1''	131.25
2''	127.29
3''	128.79
4''	133.81
1'''	44.62
2'''	166.74
2'''	170.66

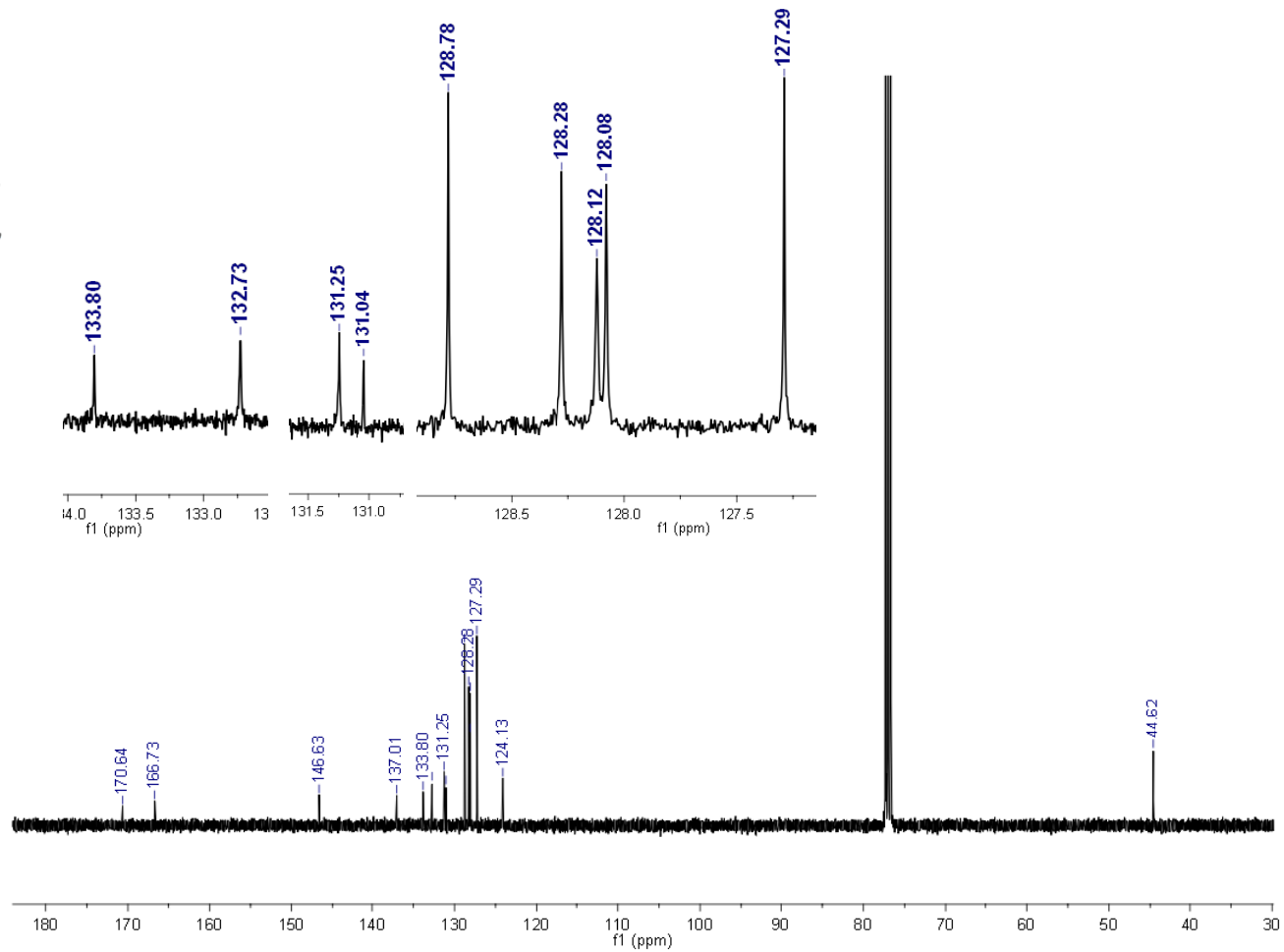
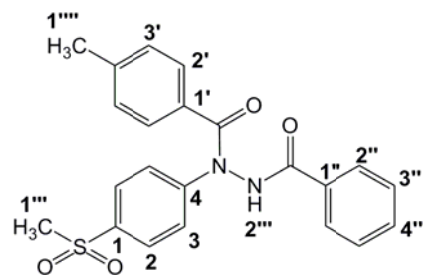


Figure 88

^{13}C -NMR (400MHz, CDCl_3) spectrum of *N*-benzoyl-*N*-(4-(methylsulfonyl)phenyl)benzohydrazide (**30**)



No.	ppm	Assignment
2	7.72	(d, $J = 8.3$ Hz, 2H)
3	7.40	(d, $J = 6.8$ Hz, 2H)
2'	7.41	(d, $J = 8.3$ Hz, 2H)
3'	7.09	(d, $J = 7.8$ Hz, 2H)
2''	7.44	(d, $J = 7.8$ Hz, 2H)
3''	7.73	(t, $J = 8.3$ Hz, 2H)
4''	7.52	(t, $J = 7.6$ Hz, 1H)
1'''	3.00	(s, 3H)
1''''	2.31	(s, 3H)
2'''	9.08	(s, 1H)

Note: 7.24 (CDCl₃), 1.57 (H₂O)

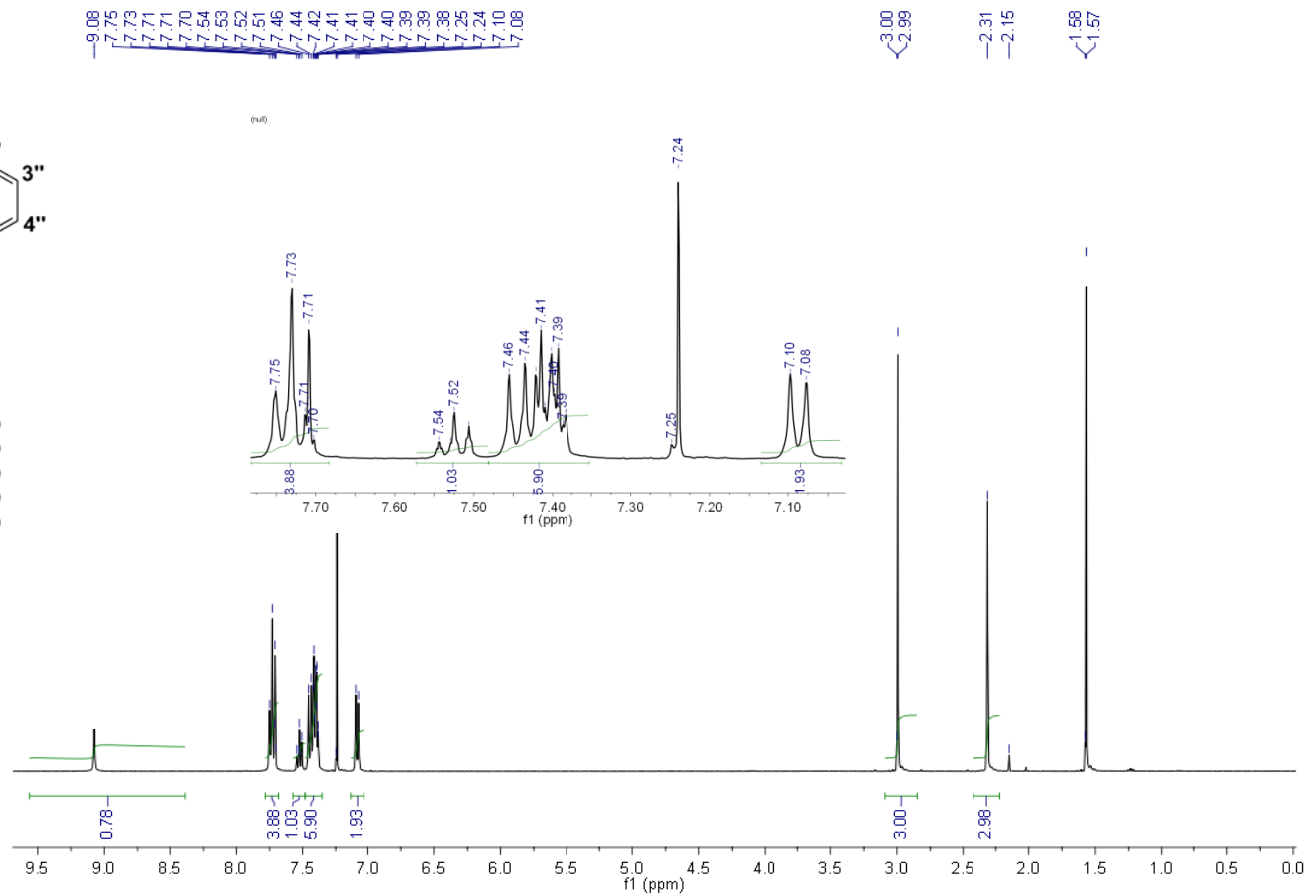
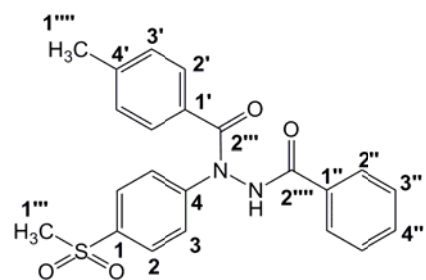


Figure 91

¹H-NMR (400MHz, CDCl₃) spectrum of *N'*-benzoyl-4-methyl-*N*-(4-(methylsulfonyl)phenyl)benzohydrazide (**31**)



No.	ppm
1	130.57
2	128.50
3	124.45
4	141.99
1'	131.13
2'	127.35
3'	128.99
4'	147.04
1''	137.09
2''	128.12
3''	128.78
4''	132.71
1'''	44.60
2'''	166.86
2''''	170.45
1''''	21.60

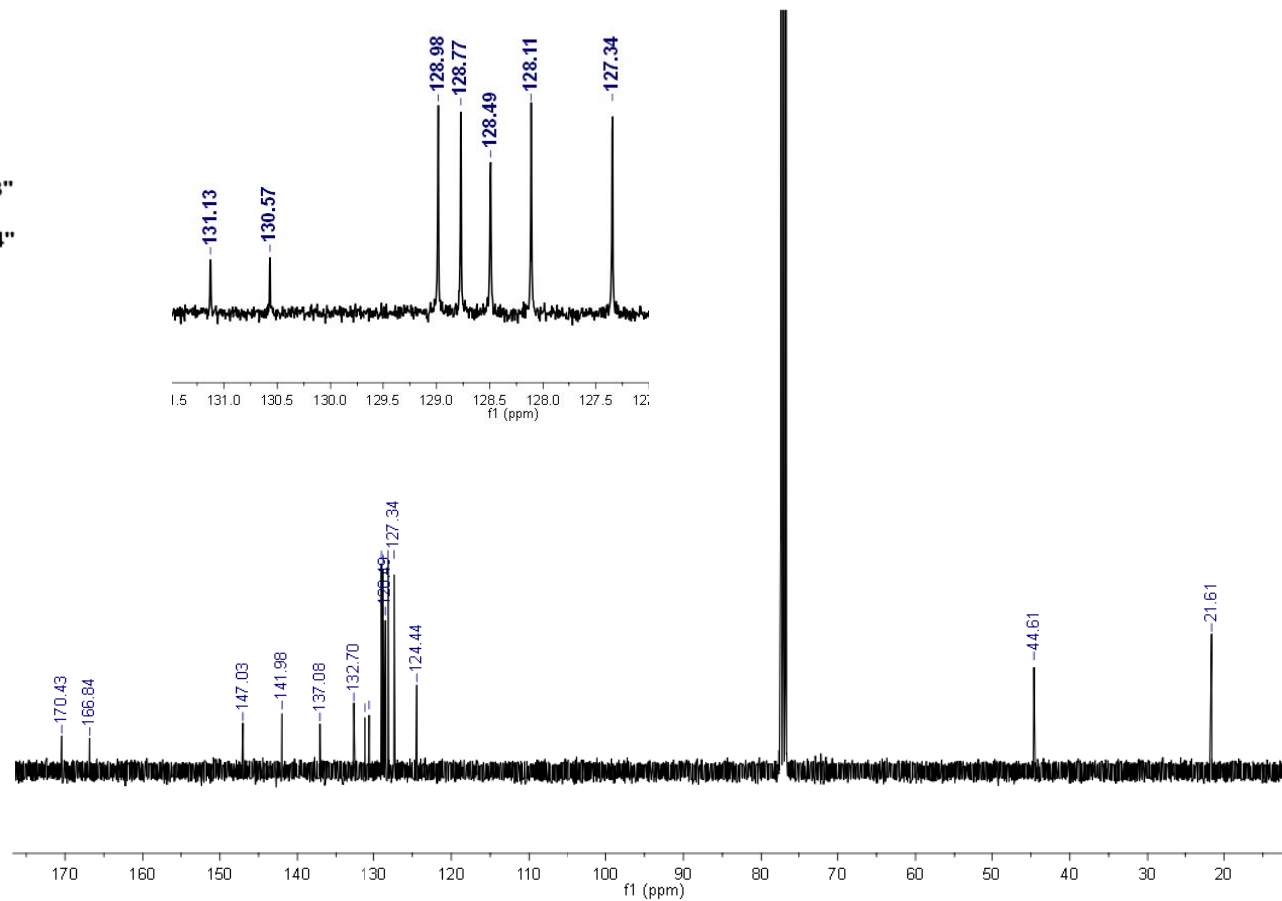
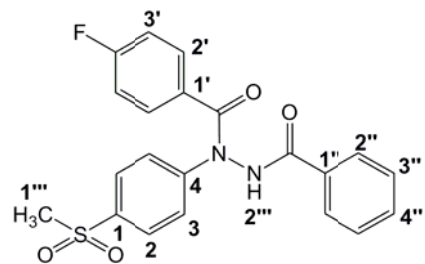


Figure 92

¹³C-NMR (400MHz, CDCl₃) spectrum of *N*-benzoyl-4-methyl-*N*-(4-(methylsulfonyl)phenyl)benzohydrazide (31)



No.	ppm	Assignment
2	7.74	(d, $J = 6.3$ Hz, 2H)
3	7.43	(d, $J = 8.8$ Hz, 2H)
2'	7.74	(d, $J = 8.8$ Hz, 2H)
3'	7.01	(dd, $J = 8.5, 8.5$ Hz, 2H)
2''	7.63	(dd, $J = 4.9, 8.8$ Hz, 2H)
3''	7.44	(t, $J = 8.1$ Hz, 2H)
4''	7.56	(t, $J = 7.3$ Hz, 1H)
1'''	3.01	(s, 3H)
2'''	8.97	(s, 1H)

Note: 7.24 (CDCl₃), 1.54 (H₂O)

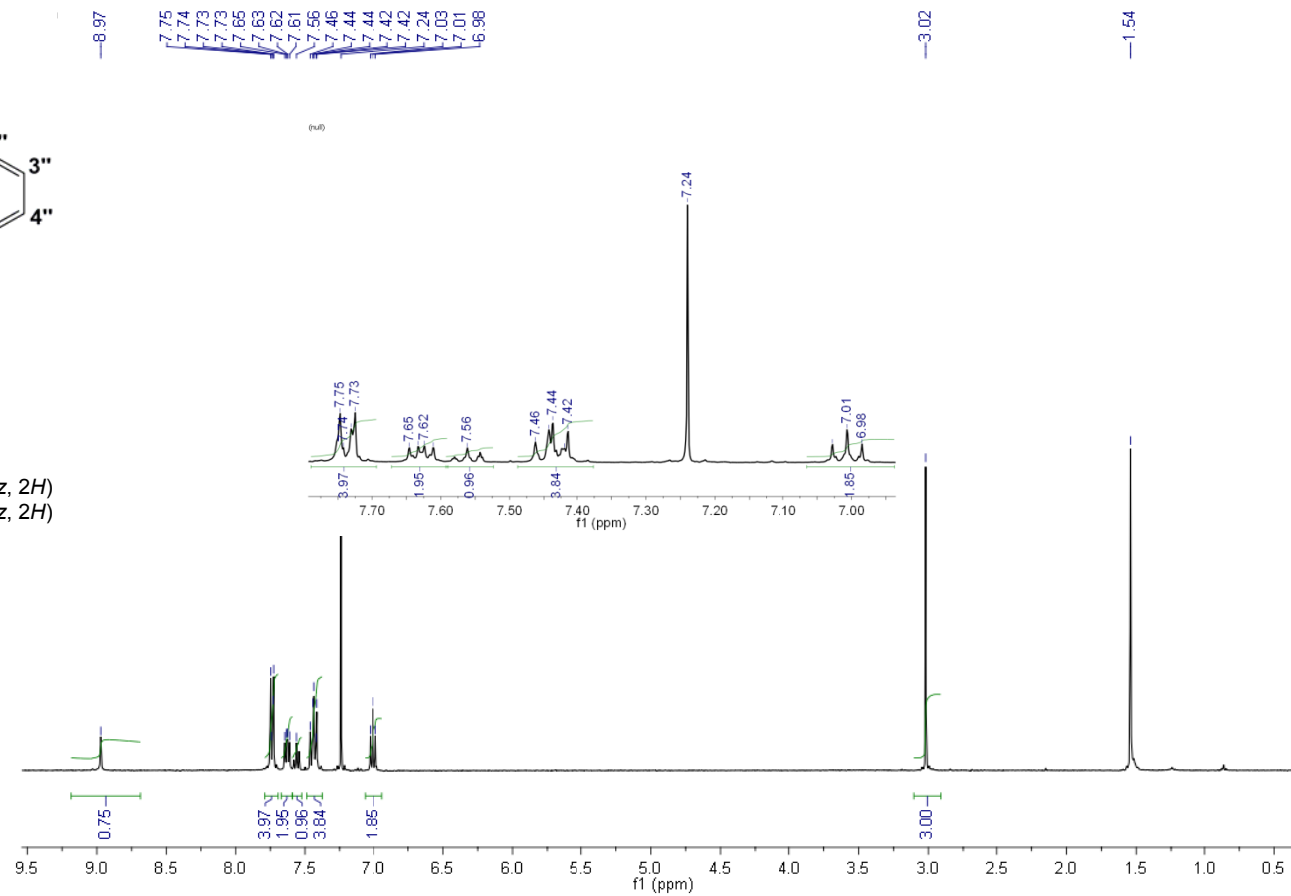


Figure 95

¹H-NMR (400MHz, CDCl₃) spectrum of *N'*-benzoyl-4-fluoro-*N*-(4-(methylsulfonyl)phenyl)benzohydrazide (**32**)

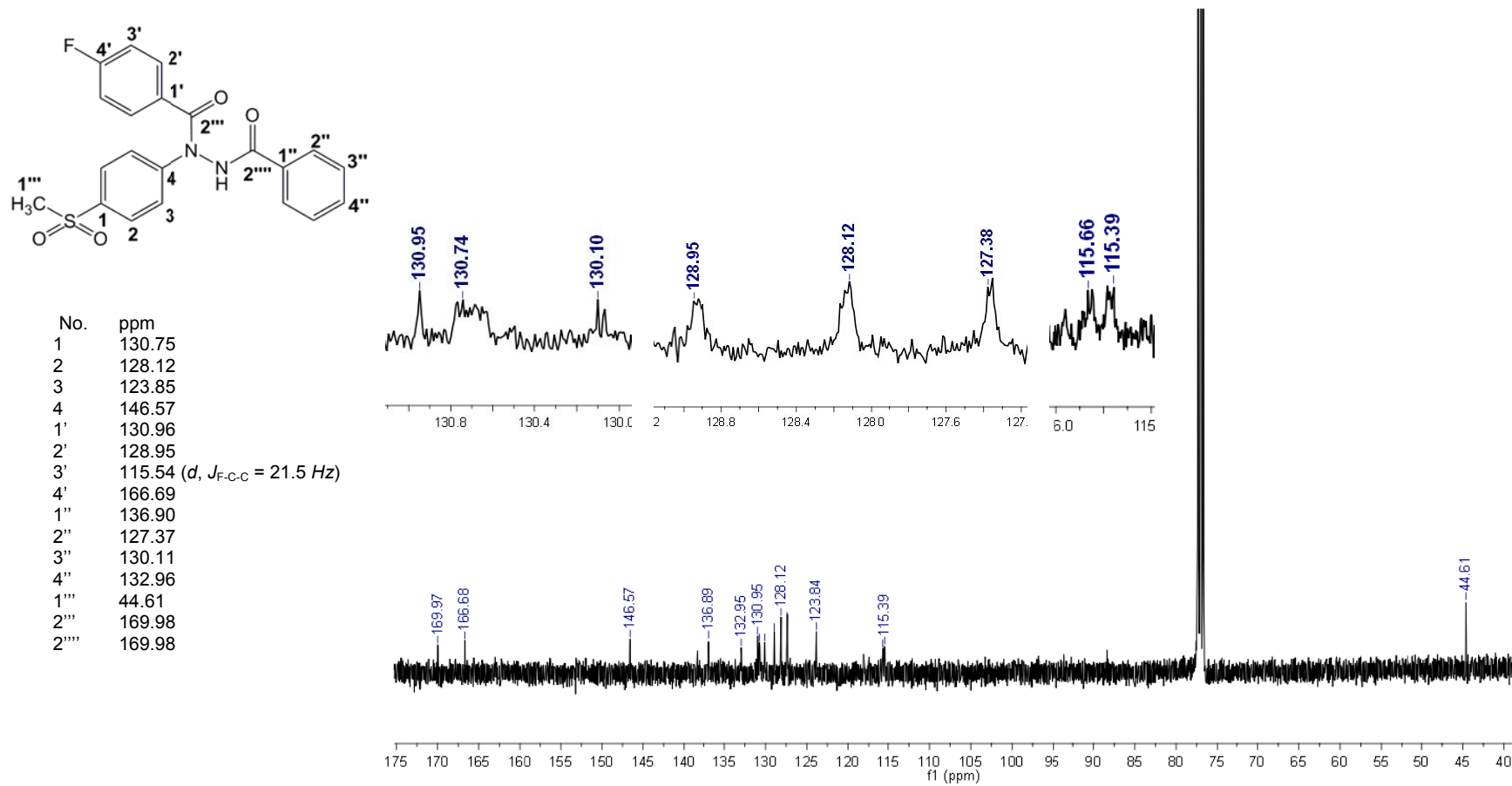


Figure 96

^{13}C -NMR (400MHz, CDCl_3) spectrum of *N*-benzoyl-4-fluoro-*N*-(4-(methylsulfonyl)phenyl)benzohydrazide (32)

VITAE

Name Miss Watcharin Diloknawarit

Student ID 5010720034

Education Attainment

Degree	Name of Institution	Year of Graduation
Bachelor of Pharmacy (First class honor)	Prince of Songkla University	2007

Scholarship Award during Enrollment

This project is supported by research funds from Graduate School and Faculty of Pharmaceutical Sciences, Prince of Songkla University, Hat-Yai, Songkhla, 90112, THAILAND

List of Publication and Proceeding

Diloknawarit, W., Tanatani, A., Kagechika, H., and Songkram, C. Synthesis and cyclooxygenase inhibitory properties of *N*'-acetyl-*N*-phenylbenzohydrazide derivatives possessing methylsulfonyl pharmacophore. 2009. In proceedings of The Fifteenth National Graduate Research Conference 2009. Nakhon Ratchasima Rajabhat University. 14-15 December 2009.